CLASS VI PERMIT APPLICATION NARRATIVE
LAC 43:XVII.3607(C)

Project Name: Live Oak CCS Hub

Facility Information

Facility Contact: Live Oak CCS, LLC
14302 FNB Parkway
Omaha, Nebraska 68154
402-691-9500

OOC Code No.: L1135

Well locations:

Well Name	Latitude (WGS84)	Longitude (WGS84)	Parish	State
LO-01 M[1]	Claimed as PBI	[redacted]	West Baton Rouge	Louisiana
LO-01 F[1]	Claimed as PBI	[redacted]	West Baton Rouge	Louisiana
LO-02 M	Claimed as PBI	[redacted]	West Baton Rouge	Louisiana
LO-03 M	Claimed as PBI	[redacted]	Iberville	Louisiana
LO-04 F-M	Claimed as PBI	[redacted]	Iberville	Louisiana
LO-05 M	Claimed as PBI	[redacted]	Iberville	Louisiana
LO-06 M[1]	Claimed as PBI	[redacted]	Iberville	Louisiana
LO-06 F[1]	Claimed as PBI	[redacted]	Iberville	Louisiana

[1] For shared well pads, surface hole location spacing is set to a minimum of 15 feet.

Table of Contents

List of Figures[1]

[1] See Appendix G for Expanded Size Figure Reference

List of Tables

List of Appendices

List of Acronyms

amsl	Above mean sea level
ANSI	American National Standards Institute
ANSS	Advanced National Seismic System
ASME	American Society of Mechanical Engineers
AOI	Area of Interest
AoR	Area of Review
AP	Artificial Penetrations
bgs	Below ground surface
BH	Bottom Hole
BVW	Bulk Volume Water
CCS	Carbon Capture and Storage
CO_2	Carbon Dioxide
CI	Casing Inspection
CBL	Cement Bond Log
CM	Central Mississippi Dispersal Axis
COCORP	Consortium for Continental Reflection Profiling
DAS	Distributed Acoustic Sensing
DTS	Distributed Temperature Sensing
DH	Downhole
EM	East Mississippi Dispersal Axis
ERRP	Emergency and Remedial Response Plan
EPA	Environmental Protection Agency
ft	Feet

GS	Geologic Sequestration
gm	Gram
H_2S	Hydrogen Sulfide
HN	Houston Dispersal Axis
LA	Louisiana
LaDOTD	Louisiana Department of Transportation and Development
LDENR	Louisiana Department of Energy and Natural Resources
LMIC	Lower Miocene Injection Complex
Ma	Mega annum, Million years ago
MICP	Mercury Injection Capillary Pressure
MIT	Mechanical Integrity Test
MMI	Modified Mercalli Intensity
MMt	Million Metric Tonnes
MMt/y	Millions of Metric Tonnes per year
mol%	Percentage of Total Moles in a Mixture made up by One Constituent
MRA	Mississippi River Alluvial
Mt/y	Thousand Metric Tonnes per year
NACE	National Association of Corrosion Engineers
OFIC	Oligocene Frio Injection Complex
OC	Louisiana Department of Energy and Natural Resources' Office of Conservation
PHIE	Effective Porosity
PHIT	Total Porosity
PISC	Post-Injection Site Care
ppmv	Parts per million volume
psi	Pounds per Square Inch
psia	Pounds per Square Inch, Absolute
P/T	Pressure-Temperature
PNC	Pulsed Neutron Capture
QASP	Quality Assurance and Surveillance Plan
RD	Red River Dispersal Axis
RL	Reporting Limit
SAPT	Standard Annulus Pressure Test
SGR	Shale Gouge Ratio
SHAS	Southern Hills Aquifer System
SP	Spontaneous Pontential
SIC	Standard Industrial Classification
SEM	Static Earth Model
SLA	South Louisiana Allochthon
SSF	Shale Smear Factor
SSTVD	Sub-Sea True Vertical Depth

Sw	Water Saturation
Swe	Effective Water Saturation
t/d	Tons per day
TD	Total Depth
TDS	Total Dissolved Solids
UIC	Underground Injection Control
USDW	Underground Source of Drinking Water
VSP	Vertical Seismic Profile
XRD	X-Ray Diffraction Analysis

Certification of Professional Geologist:

Sections of the permit application that represent geologic work shall be sealed, signed, and dated by a licensed professional geologist as required by LAC 43:XVII.3603(H)(2).

The geologic interpretations, cross-sections, maps, hydrologic studies, modeling inputs and results that are included in this application were all completed under the responsible charge or direct supervision of the licensee, who has reviewed this work and certified that it is prepared according to the highest standards of Professional Geology.

STAMP BY	APPLICABLE SECTIONS
Robin Swank, PG	**1. Narrative Application (LAC 43:XVII.3607(C))** a. Reviewed all document text, figures, tables, and appendices **2. Area of Review and Corrective Action Plan (LAC 43:XVII.3615)** a. Reviewed modeling inputs and results, all document text, figures, tables, and appendices **3. Post-Injection Site Care and Site Closure Plan (LAC 43:XVII.3633)** a. Reviewed all document text, figures, tables, and appendices

X Robin L. Swank
Robin L. Swank, PG (printed name)

X
P.G. Number (SEAL)

X Robin L Swank
Robin L. Swank, PG (signature)

X 10/04/2024
Date Signed

Certification of Professional Engineer:

Sections of the permit application that represent engineering work shall be sealed, signed, and dated by a licensed professional engineer as required by LAC 43:XVII.3603(H)(3).

I, Bryan K. Bell, the undersigned state: As an employee of Terra Dynamics Incorporated that these documents (Construction Details and Injection Well Plugging Plan) were prepared under my supervision and direction. All facts stated herein are true, correct and complete to the best of my knowledge. The specifications and recommendations attested to in these documents (Construction Details and Injection Well Plugging Plan) were prepared in accordance with generally and currently accepted engineering principles and practices. The information specifically covered by this seal relates to the Class VI Well Permit Application. The engineering drawings, specifications and other related documents referenced herein are subject to revision based on the drilling and completion of LO-01 M, LO-01 F, LO-02 M, LO-03 M, LO-04 F-M, LO-05 M, LO-06 M and LO-06 F.

STAMP BY	APPLICABLE SECTIONS
Bryan Bell, PE	**1. Construction Details (LAC 43:XVII.3617)** a. Reviewed all text, figure and tables of the Construction Details documents for wells LO-01 M, LO-01 F, LO-02 M, LO-03 M, LO-04 F-M, LO-05 M, LO-06 M, and LO-06 F **2. Injection Well Plugging Plan (LAC 43:XVII.3631)** a. Reviewed all text, figure and tables of the Injection Well Plugging documents for wells LO-01 M, LO-01 F, LO-02 M, LO-03 M, LO-04 F-M, LO-05 M, LO-06 M, and LO-06 F

X Bryan Bell

Bryan Bell, PE (printed name)

X

Licensed P.E. #41052 State of Louisiana
Terra Dynamics Inc. P.E. Firm EF6140

X

Bryan Bell, PE (signature)

X 10/15/2024

Date Signed

Application Certification (LAC 43:XVII.3605(G)):

I certify under penalty of law that this document and all attachments were prepared under my direction or supervision in accordance with a system designed to assure that qualified personnel properly gather and evaluate the information submitted. Based on my inquiry of the person or persons who manage the system, or those persons directly responsible for gathering the information, the information submitted is, to the best of my knowledge and belief, true, accurate, and complete. I am aware that there are significant penalties for submitting false information, including the possibility of fine and imprisonment for knowing violations.

X Larry Carlson

Larry Carlson (printed name)
VP Environmental Affairs - Live Oak CCS, LLC

X

Larry Carlson (signature)
VP Environmental Affairs - Live Oak CCS, LLC

X 10/15/24

Date Signed

1. Project Background and Contact Information

Live Oak CCS, LLC is proposing development of an industrial scale carbon capture and storage (CCS) hub in Iberville and West Baton Rouge parishes, Louisiana (LA) (the "project"; Figure 1). The Live Oak CCS Hub envisions the development of several CO_2 injection wells with the capability of storing over 450-million metric tonnes (MMt) with injection taking place over 30 years.

The hub will be used to provide the region's emitters with a safe and secure subsurface storage solution. Potential CO_2 sources are agrochemical, petrochemical, power plant, inorganic chemical, polymer, hydrogen production, and gas processing facilities, and refineries near the Live Oak CCS Hub. These sources could provide up to 38.4 MMt/y of CO_2 injection, though initial plans are to provide up to 12.65 MMt/y of CO_2 injection for 30 years (379.5 MMt total). The eight injection wells will be capable of storing an average of 34,650 t/d.

This narrative is provided in support of the Class VI Underground Injection Control (UIC) permit applications for the project and covers the proposed development and operation of eight injection wells (LO-01 M, LO-01 F, LO-02 M, LO-03 M, LO-04 F-M, LO-05 M, LO-06 M, and LO-06 F). Additionally, the project will include seven in-zone observation wells (IOB-01, IOB-02, IOB-03, IOB-04, IOB-05, IOB-06, and IOB-07), three above-zone observation wells (AOB-01, AOB-04, and AOB-06), three lowermost underground source of drinking water (USDW) observation wells (UOB-01, UOB-04, and UOB-06), and one shallow groundwater monitoring well that are within the project area (Figure 2). The Application Narrative is for proposed wells LO-01 M, LO-01 F, LO-02 M, LO-03 M, LO-04 F-M, LO-05 M, LO-06 M, and LO-06 F.

Live Oak CCS, LLC is a subsidiary of Greenbridge Land II, Inc. and an affiliate of Tenaska Energy, Inc. (Tenaska) who has made major, corporate-level commitments toward development of the hub. Tenaska is a privately held, independent power company based in Omaha, Nebraska. Established in 1987, Tenaska has a generating fleet over 7,500 MW, is one of the largest gas marketing companies in North America and has balance sheet equity of $2.9 billion. Live Oak CCS, LLC will serve as the project owner and will assume liability for project development, finance, and operation.

The key project contacts are:

Ryan Choquette
Live Oak CCS, LLC
14302 FNB Parkway
Omaha, Nebraska 68154
Claimed as PBI

Andrew Becker, PMP
Projeo Corporation
1700 S Mount Prospect Rd.
Des Plaines, Illinois 60018
Claimed as PBI

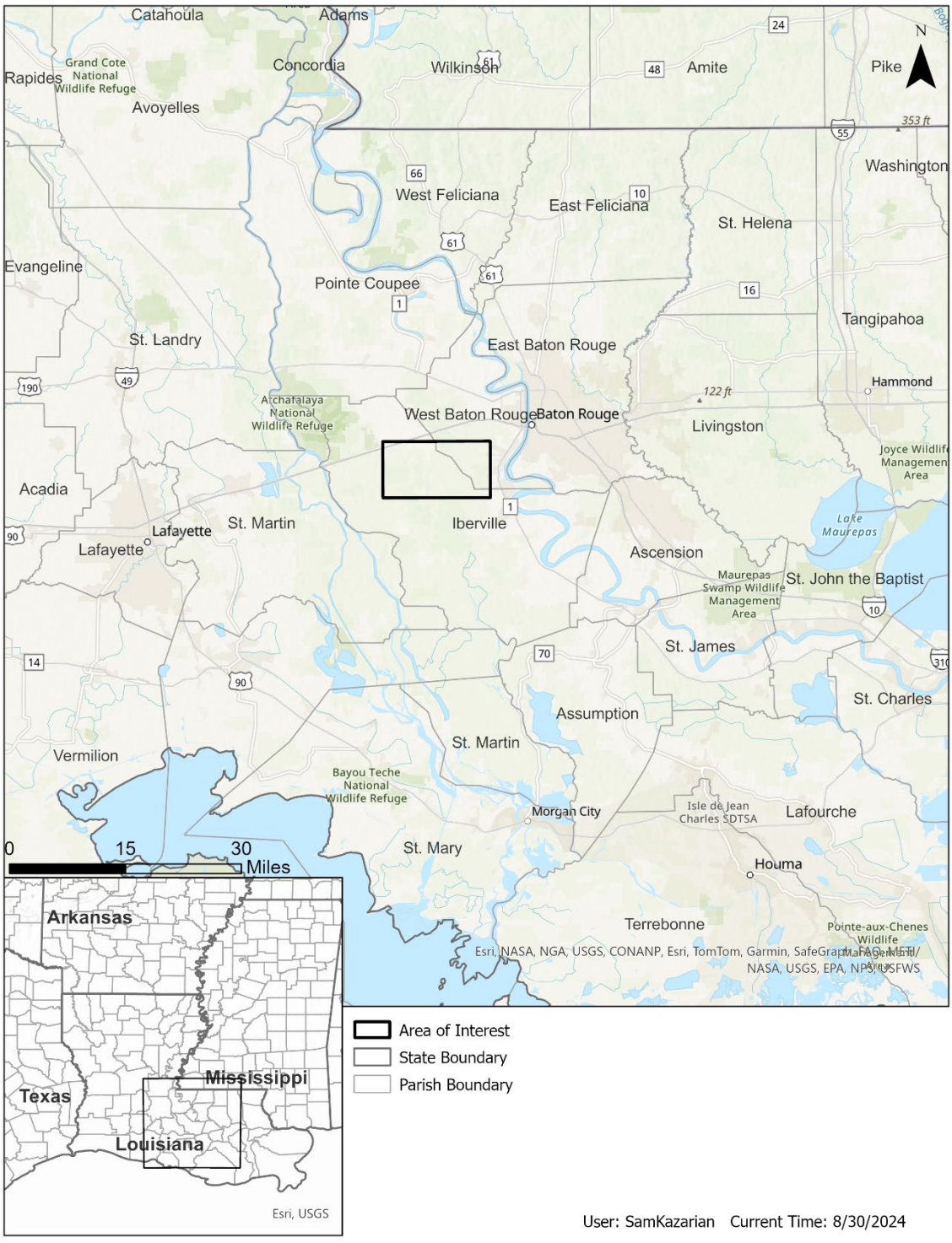

Figure 1: Location of the Live Oak CCS Hub.

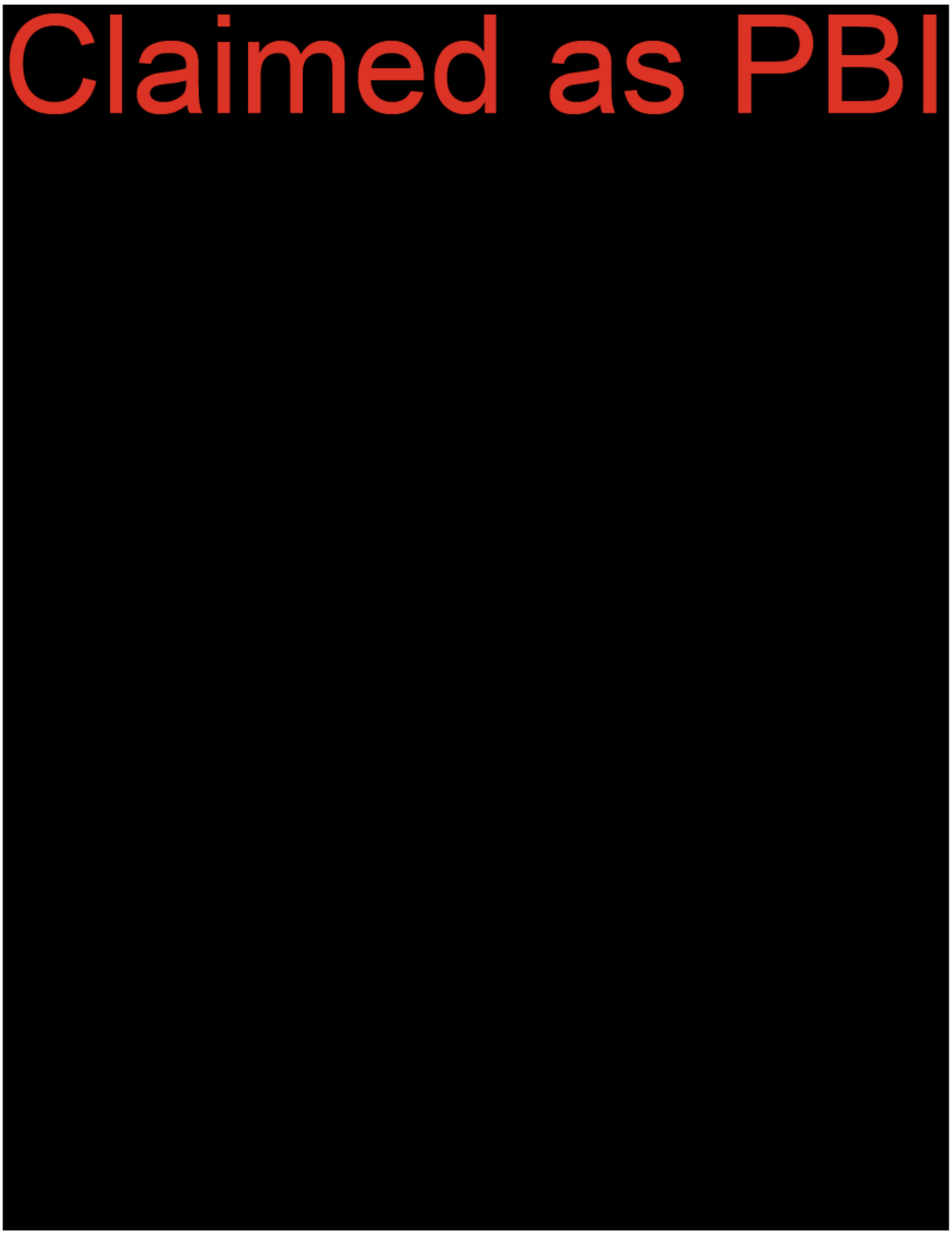

Figure 2: Locations of proposed injection (e.g., LO-01 M), in-zone (e.g., IOB-01), above-zone (e.g., AOB-01) and lowermost USDW observation (e.g., UOB-01) wells, oil and gas wells in the AoR, water wells within the AoR and a half mile buffer (blue), and the project Area of Review (red). Location and detailed information for each water well is included in Figure 99 and Table 15.

With this application, Live Oak CCS, LLC is requesting permits to construct for LO-01 M, LO-01 F, LO-02 M, LO-03 M, LO-04 F-M, LO-05 M, LO-06 M, and LO-06 F. After issuance of the permits by the Louisiana Department of Energy and Natural Resources' Office of Conservation (OC), Live Oak CCS, LLC plans to start construction of the injection wells within 2 years but additionally requests two options to extend the permit term by 2 years. The reason for this request is that the project relies on the installation of capture equipment at the emitter and construction of pipeline infrastructure to the emitter, both of which may be delayed for reasons outside the control of Live Oak CCS, LLC. After submittal of required documentation to the OC and receiving authorization to inject and once the emitter is ready to operate their CO_2 capture equipment, Live Oak CCS, LLC will initiate injection. This application assumes that the 30-year injection period will start in approximately 2026, end in 2057, and be followed by a 50-year post-injection site care period, taking the project to 2106. Start of injections could vary by 1 to 5 years. The projected drilling schedule for the project is provided in Appendix F.

The project is not requesting an injection depth waiver or an expansion of aquifer exemptions with this application.

There are no federally recognized Native American tribal lands or territories within the proposed Area of Review (AoR) (LAC 43:XVII.3607(B)(10)).

The SIC codes applicable to the project are identified below (LAC 43:XVII.3607(B)(8)):

- 49530300 Nonhazardous waste disposal sites – primarily engaged in collection and disposal of refuse by processing or destruction or in operation of incinerators/waste treatment plants/landfills/other sites for disposal of such materials;
- 51690203 Carbon Dioxide – primarily engaged in wholesale distribution of CO_2; and
- 4619 Pipelines, not elsewhere classified – primarily engaged in pipeline transportation of commodities except petroleum and natural gas.

State and local contacts with jurisdictions within the proposed AoR include the following (LAC 43:XVII.3607(C)(2)(s)):

U.S. Environmental Protection Agency, Region 6
1201 Elm Street, Suite 500
Dallas, TX 75270
Brandon Maples
maples.brandon@epa.gov
214-665-7252

Louisiana Department of Energy and Natural Resources
Office of Conservation, Injection & Mining Division
617 North Third Street, LaSalle Building, 8th Floor
Baton Rouge, LA 70802
Holton Hinchliffe
Holton.hinchliffe@la.gov
225-342-8936

West Baton Rouge Parish, Community Planning and Development
880 N. Alexander Avenue, Governmental Building
Port Allen, LA 70767
224-336-1840
Jason Manola, Parish President
Jason.Manola@wbrcouncil.org
225-354-6592

Iberville Parish
59705 Bayou Road
Plaquemine, LA 70764
225-687-5148
Chris Daigle, Iberville Parish President
225-776-4122

The names and addresses of all property owners within the AoR are included in Appendix B to this Application Narrative (LAC 43:XVII.3607(B)(12)).

The permits and authorizations that will likely be required for the project, the permit/authorization jurisdictions, and the associated project development activities are provided in Table 1 (LAC 43:XVII.3607(B)(9)). Live Oak CCS, LLC has not received or applied for these permits/authorizations to date, excepting this Class VI UIC application process for permits to construct.

Table 1: Permits and Authorizations necessary for the development of Live Oak CCS Hub.

Permit/Authorization	Activity	Jurisdiction
Greenhouse Gas Rule Subpart RR Monitoring, Reporting, and Verification Plan Approval	Injecting CO_2	Federal
UIC Class VI Permit to Construct	Drilling of Injection Wells	Louisiana Department of Energy and Natural Resources' Office of Conservation
UIC Class VI Authorization to Inject	Injecting CO_2	
Class V Well Permit	Drilling and operating in-zone and above-zone observation wells	
Section 404 Permit	Temporary and permanent impacts to jurisdictional waters	Federal/State
Construction Stormwater General Permit	Management of stormwater during construction	Louisiana Department of Environmental Quality
Notification of Water Well and Registration	Lowermost USDW and shallow groundwater monitoring well construction	Louisiana Department of Energy and Natural Resources
Site Plan Review and Floodplain Development Permit	To ensure compliance with parish development regulations	Iberville Parish; West Baton Rouge Parish

Four figures were created (Figure 3, Figure 4, Figure 5, Figure 6) to address requirements at LAC 43:XVII.3607(C)(1) for a map of the area, with features shown or absent as noted below:

- Wells: Subsection 4.1.1 of the Area of Review and Corrective Action Plan further discusses oil and gas wells, including available well data and the plan for obtaining information on wells that do not have records.
  - Injection wells: There are no records of currently active injection wells in the AoR.
  - Producing wells: There are no records of producing wells in the AoR.
  - Abandoned wells: There are four wells with the status "completed," "inactive," or "unknown" in the AoR, shown as part of the oil and gas wells in Figure 2.
  - Plugged wells or dry holes: There are 18 known plugged and abandoned wells in the AoR, shown as part of the oil and gas wells in Figure 2.
  - Deep stratigraphic boreholes: There are no records of deep stratigraphic boreholes in the AoR.
  - Water wells: There are 36 known water wells in the AoR, of which 22 are active as of June 2024, as shown in Figure 2. See subsection 2.7 for more information on water wells.
- State or U.S. EPA-approved subsurface cleanup sites: There are no records of state voluntary remediation cleanup sites or federal Brownfield, Superfund, EPA facility cleanup, or RCRA subsurface cleanup sites in the AoR.
- Surface bodies of water: The following named surface bodies of water are in the mapped area, as shown in Figure 4: Choctaw Bayou, Intracoastal Waterway, Smith Lake, Bear Bayou, Trinity Drainage Canal, Bayou Bogan, King Ditch, Green Lake, Catfish Canal, Bayou Hopper, Halfway Lake, Port Allen Lock, Grand Bayou, Bayou Maringouin, and Bayou Bourbeaux . There are various unnamed tributaries and ponds in the AoR as well.
- Springs: There are no records of springs in the mapped area.
- Surface and subsurface mines: There are no records of surface or subsurface mines in the AoR. Mining operations in the mapped area are shown in Figure 5.
- Quarries: There are no records of quarries in the AoR.
- Section, township, and range and state, tribal, parish, city, and municipality boundaries: There are no tribal boundaries in the AoR or 2-mile radius. Other boundaries are shown in Figure 6.
- Roads: U.S. Interstate 10, Highway 77, and various county and town roads are in the AoR, as shown in Figure 3.
- Other pertinent surface features: Structures, natural gas pipelines, railroads, and cemeteries are shown on Figure 3. The municipalities of Baton Rouge (west), Brusly, Addis, Plaquemine, Crescent, Rosedale and Grosse Tete are nearby and are shown in Figure 6.

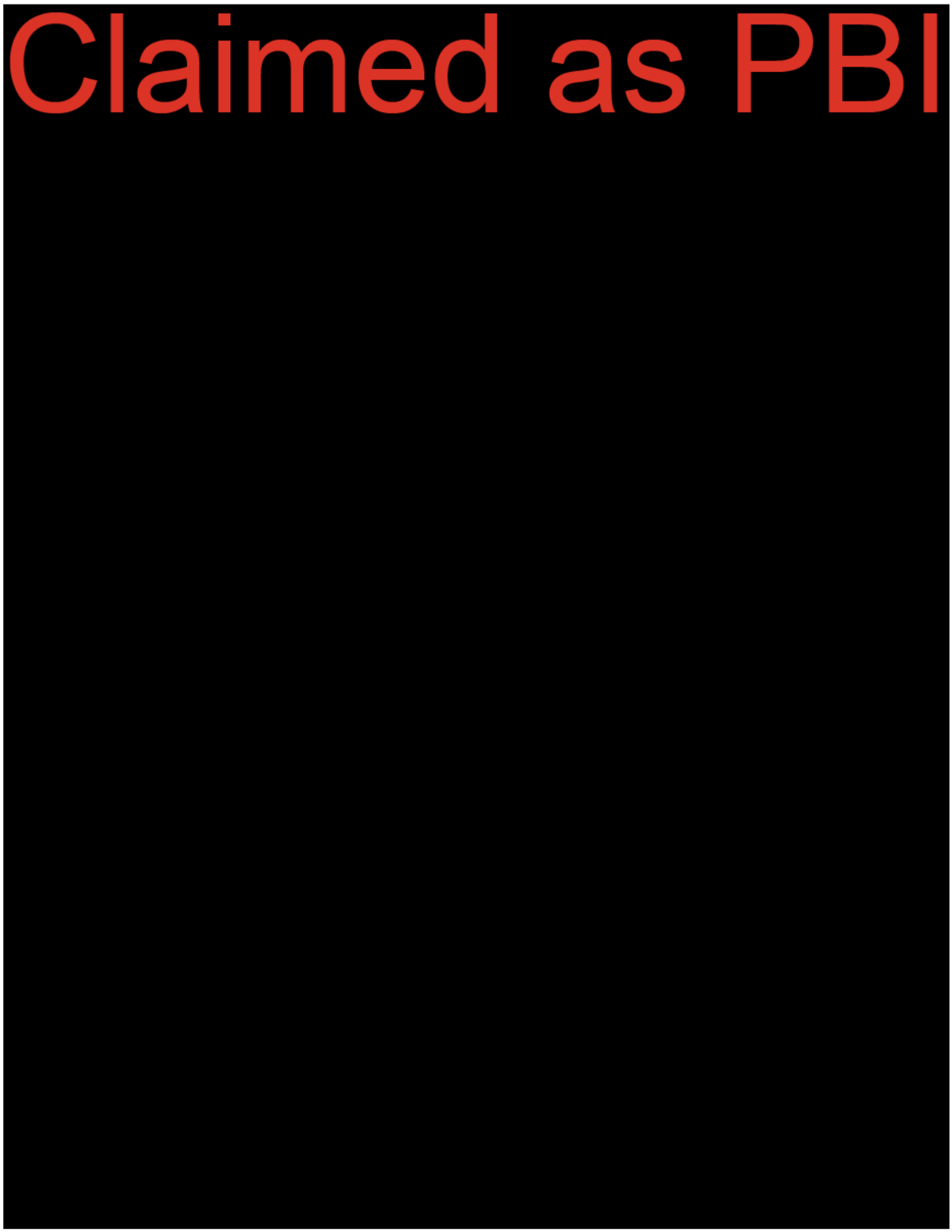

Figure 3: Infrastructure near proposed injection and observation wells.

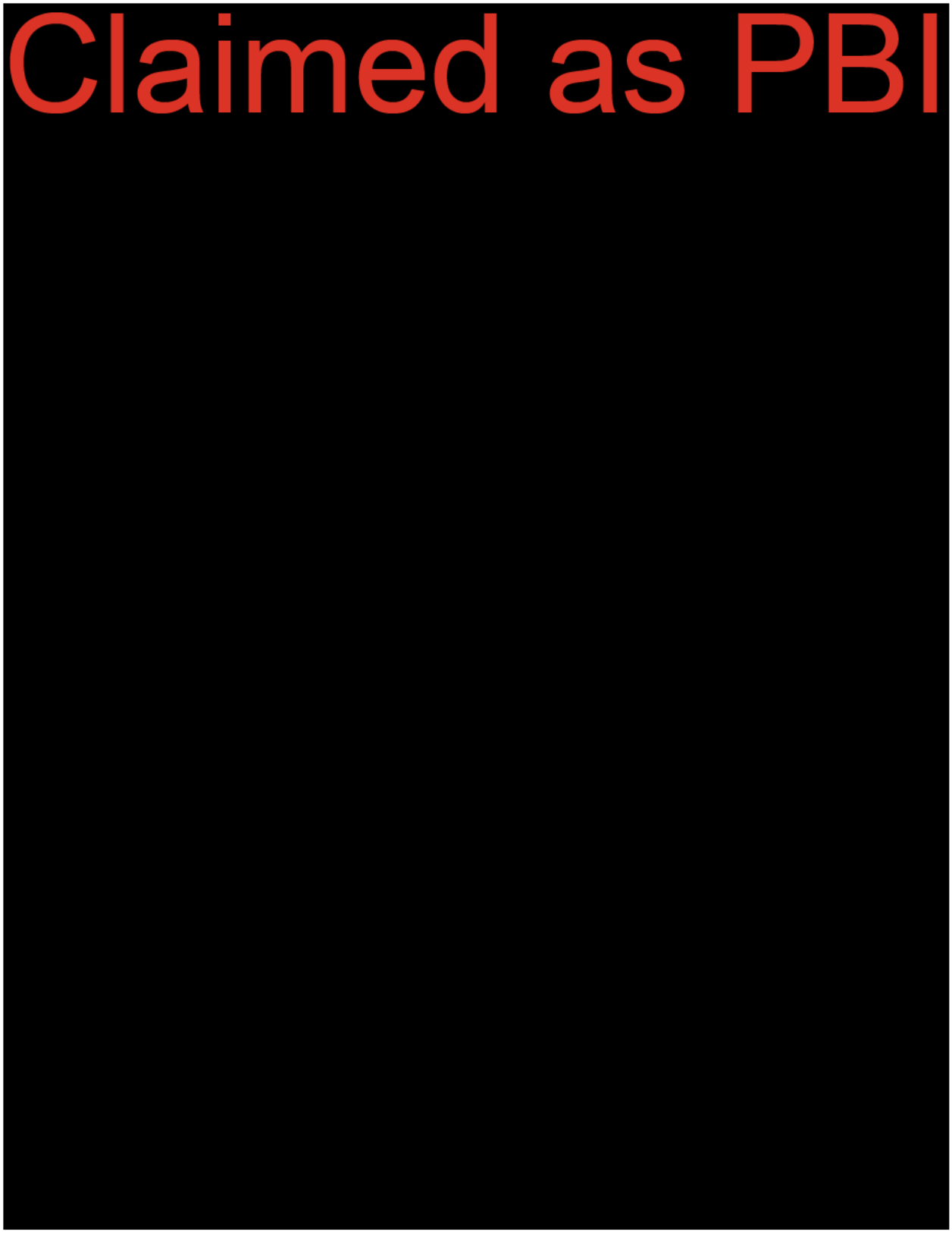

Figure 4. Surface water and conservation areas near proposed injection and observation wells.

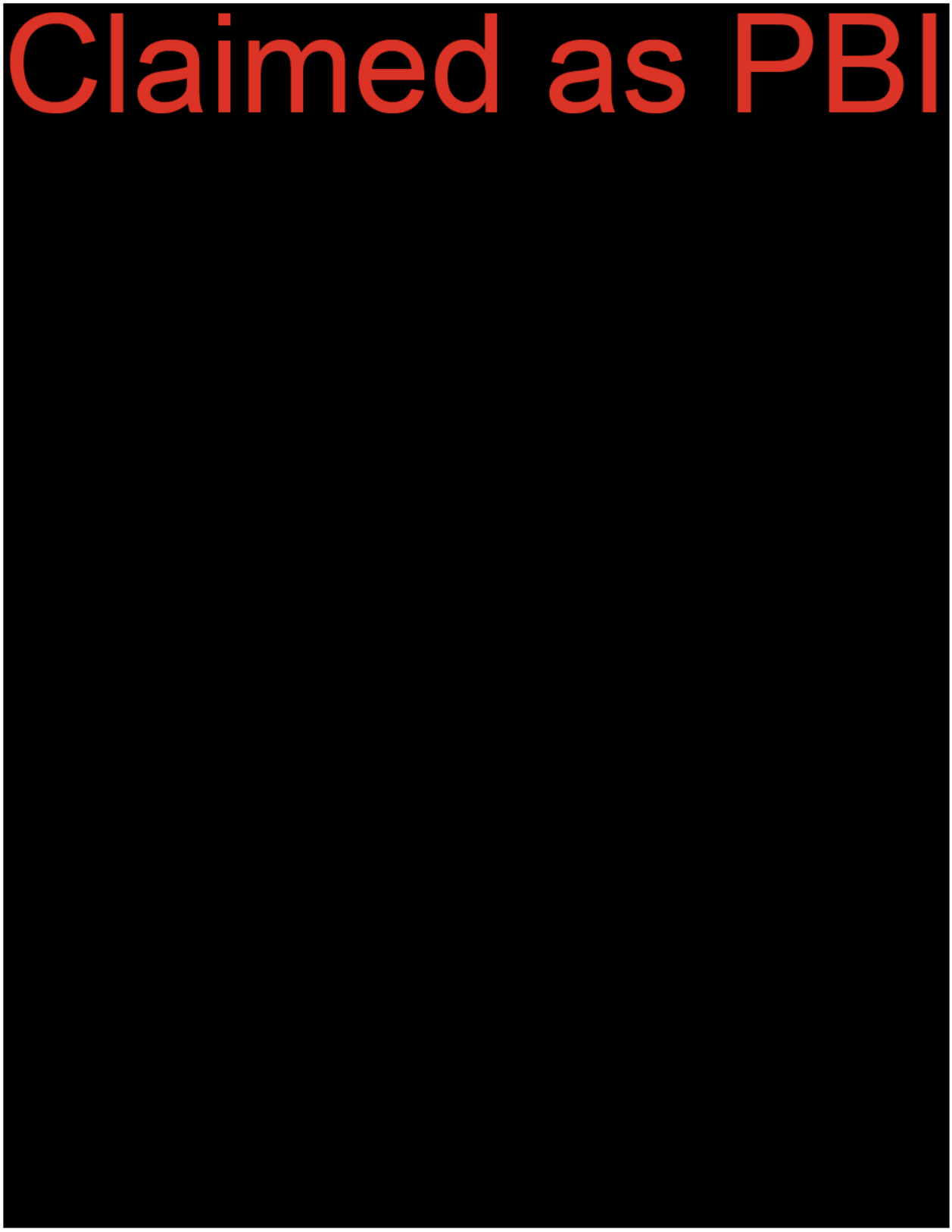

Figure 5: Mineral tracts near proposed injection and observation wells.

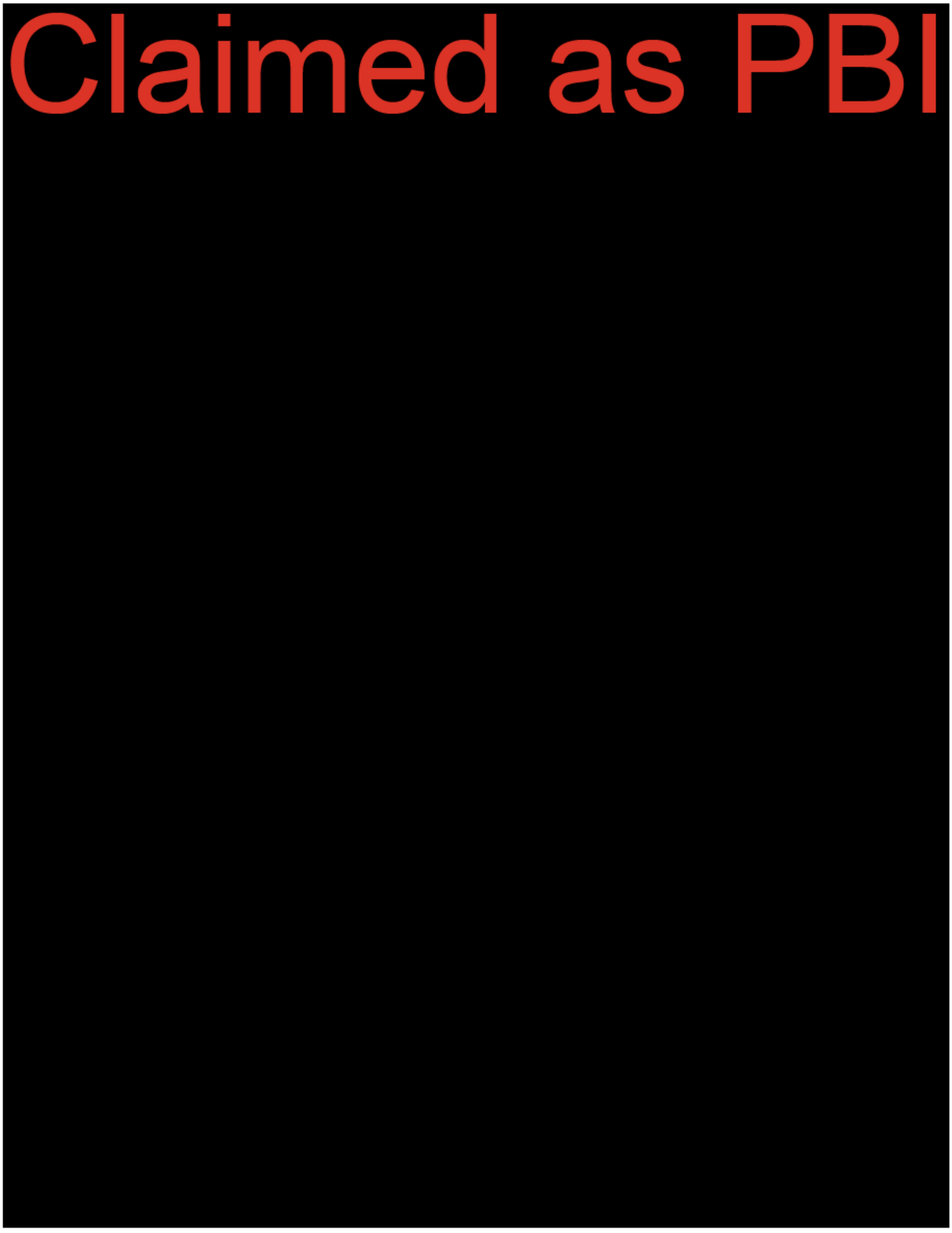

Figure 6: Map of the AoR and 2-mile buffer, injection and observation wells, township, range, and section lines, and municipal boundaries. Each set of injection and observation wells includes facility boundaries of a 1-acre well pad and associated access roads.

2. Site Characterization

2.1. Regional Geology, Hydrogeology, and Local Structural Geology

2.1.1 Geographic Overview

The project is located along the northern Gulf of Mexico in southern Louisiana, west of Baton Rouge, and falls within the Central Louann salt rift basin (Figure 7). On the North American plate, the northern limit of the Gulf of Mexico basin is delineated by the now buried Paleozoic Ouachita-Marathon-Appalachian orogenic front and extends southward to the abyssal plain in the deepwater Gulf of Mexico (Filina et al., 2022). The project area is situated on the Gulf Coast at the northern edge of the basin, where the modern Mississippi River delta system has governed deposition and landscape evolution since the Pliocene (Snedden et al. 2020).

The remainder of this page intentionally left blank.

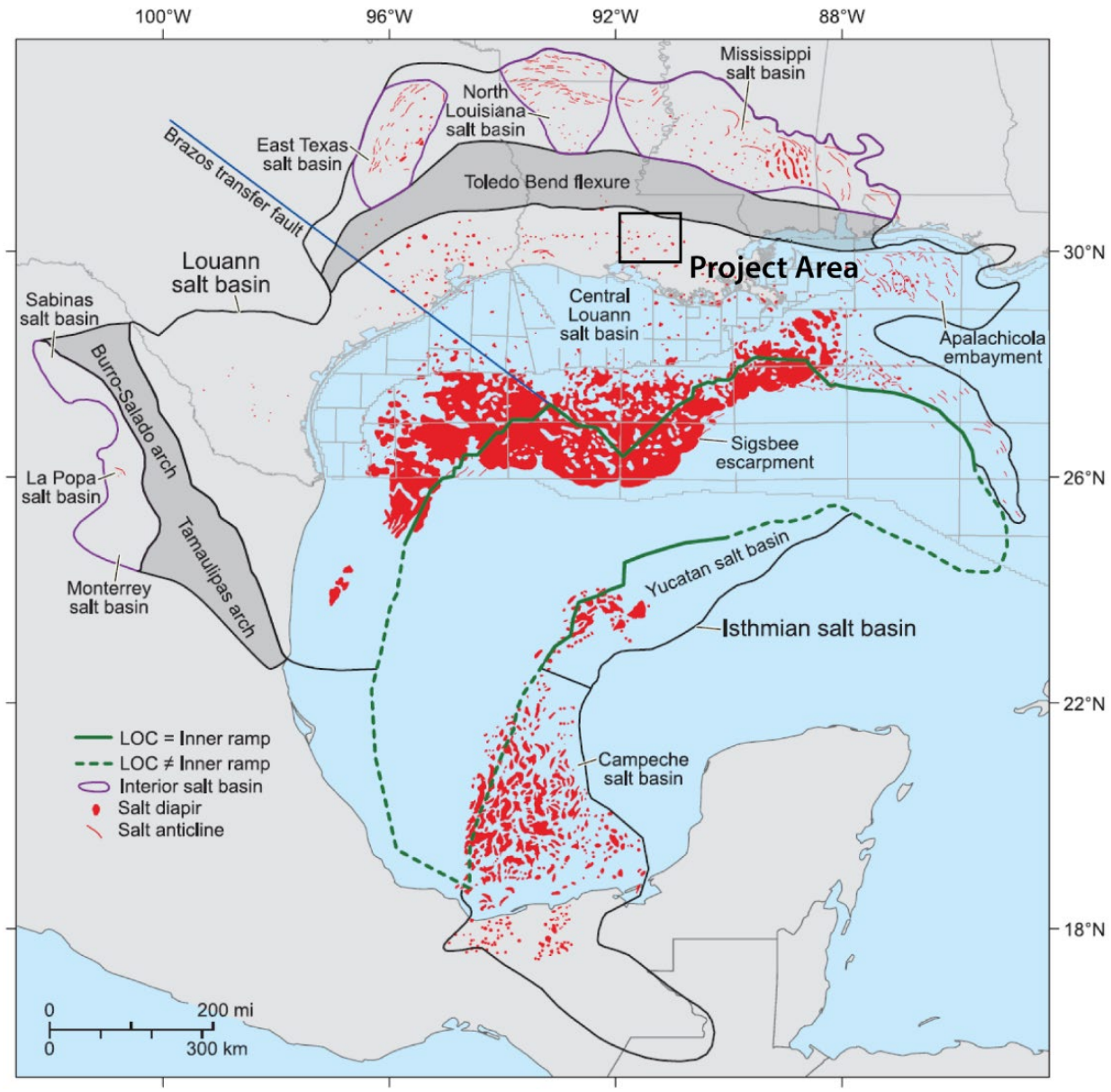

Figure 7: Salt basins in the Gulf of Mexico region, showing locations of salt structures and the interpreted limit of normal oceanic crust in the basin. Project area is marked with a black box. (Figure from Hudec et al., 2013b)

A notable subsurface feature in the Gulf of Mexico is the regional presence of evaporitic sediments comprised mostly of halite, which in lithologic context is referred to as salt. The Jurassic Louann salt is the most significant salt formation in the Gulf of Mexico, reaching thicknesses up to 4 km (Figure 8; Hudec et al., 2013b). Salt is buoyant relative to most sedimentary rocks and behaves as a fluid at geologic strain ratios (Hudec and Jackson, 2007). Regionally, salt deposits have migrated over time, creating salt domes (e.g., the Bayou Choctaw) and extensional faulting (e.g., the Baton Rouge fault system) in the project area even in the absence of active plate tectonic forces.

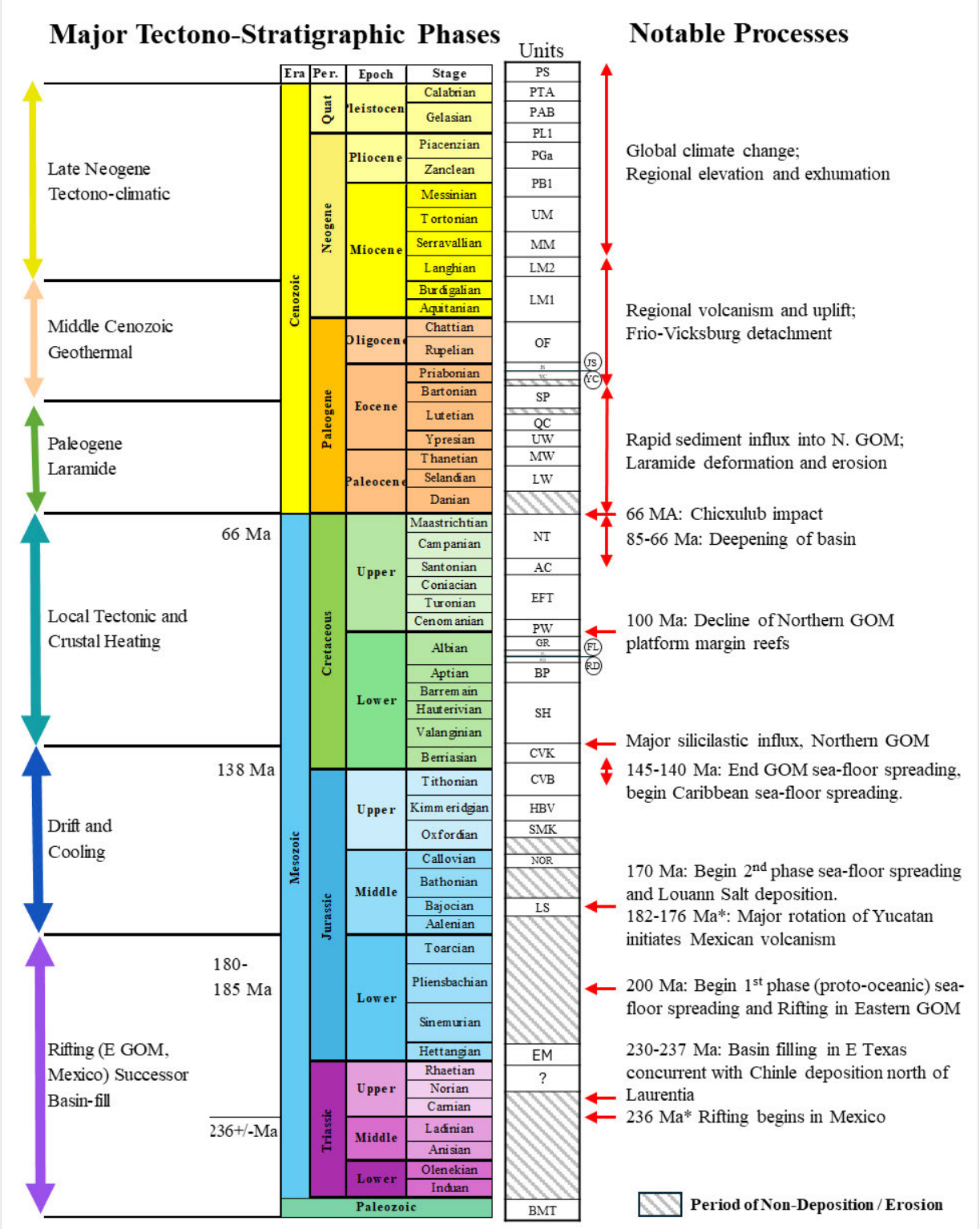

Figure 8: Major tectono-stratigraphic phases of the Gulf of Mexico basin and predecessors. AC = Austin Chalk; BMT = basement; BP = Bexar–Pine Island Shale; CVB = Cotton Valley–Bossier; CVK = Cotton Valley–Knowles; E = eastern; EFT = Eagle Ford–Tuscaloosa; EM = Eagle Mills; FL = Ferry Lake Anhydrite; GR = Glen Rose; HVB = Haynesville–Buckner; JS = Jackson–Yazoo; LM1 = lower

Miocene 1; LM2 = lower Miocene 2; LS = Louann Salt; LW = lower Wilcox; MM = middle Miocene; MW = middle Wilcox; N. = northern; NOR = Norphlet; NT = Navarro–Taylor; OF = Frio Vicksburg; PAB = Pleistocene- Angulogerina B; PB1 = Miocene–Pliocene-Buliminella 1; PGa = Pliocene Globigerina altespira; PL1 = Pliocene–Pleistocene-Lenticulina 1; PS = Pleistocene; PTA = Pleistocene Trimosina A; PW = Paluxy–Washita; QC = Queen City; Quat = Quaternary; RD = Rodessa; SH = Sligo–Hosston; SMK = Smackover; SN = Smackover–Norphlet; SP = Sparta; UM = upper Miocene; UW = upper Wilcox; YC = Yegua–Cockfield. (Figure from Snedden and Galloway, 2019). *Lawton et al., (2018); Barboza-Gudina et al., (2016); Umbarger 2018; LV Ray well palynology analysis.

2.1.2 Tectonic History

The geology of the Gulf Coast region largely reflects progressive passive margin development preceded by continental rifting during the late Triassic breakup of Pangea (~200 Ma, Filina et al., 2022). The transition from continental rifting to a passive margin occurred when sea floor spreading began sometime between 190 – 150 Ma (Filina et al., 2022). One of the first basin-wide depositional events was accumulation of the Jurassic Louann salt (timing uncertain, estimates range from 170 to 155 Ma; Filina et al., 2022) which has subsequently acted as a regional detachment for salt tectonic deformation of the overlying Mesozoic and Cenozoic sedimentary sequences. Since the Gulf of Mexico basin reached its present size around the mid-Mesozoic (145-140 Ma; Snedden et al., 2019), it has continuously accumulated sediment into the present day, resulting in a thick sedimentary package that locally exceeds 14 km (Filina et al., 2022).

2.1.3 Mesozoic Basin History: Basin Opening and Passive Margin Development

The geologic processes that governed the early evolution of the Gulf of Mexico at the project area began with Triassic basin opening (~236 Ma) and continental rifting, followed by middle Mesozoic passive margin development as sea floor spreading initiated to the south, and transitioned into thermal subsidence and sediment loading in the late Mesozoic (Snedden et al., 2019).

2.1.4 Permo-Triassic Pre-Rift to Late Triassic Rifting

The rocks and basement structures recording the pre-rift history of the Gulf of Mexico have largely been obscured by the substantial Mesozoic and Cenozoic sedimentary section that has accumulated since the basin opened. As a result, the pre-rift geologic configuration and timing of basin opening is still debated (Filina et al., 2022). It is generally agreed that basin opening followed the late Paleozoic assemblage of Pangea, post-dating the Ouachita-Marathon-Appalachian orogeny at the Laurentia-Gondwana suture zone. The orogeny represents the modern limit of continental extension on the North American plate and is the northern margin of the Gulf of Mexico (Figure 9). Snedden and Galloway (2019) argue for the presence of a “post-orogenic successor basin” based on the absence of pre-salt extensional features in the northern Gulf of Mexico, whereas Stern and Dickinson (2010) interpret the East Texas basin to be a late Jurassic rift feature. Regardless, initial opening of the basin occurred during the late Triassic breakup of Pangea as the Yucatan block and South American plate separated from North America (Figure 10). The Triassic Eagle Mills (EM) Formation red beds and equivalents (Figure 8) were deposited at this time, possibly within grabens along the developing basin margin (Salvador, 1991).

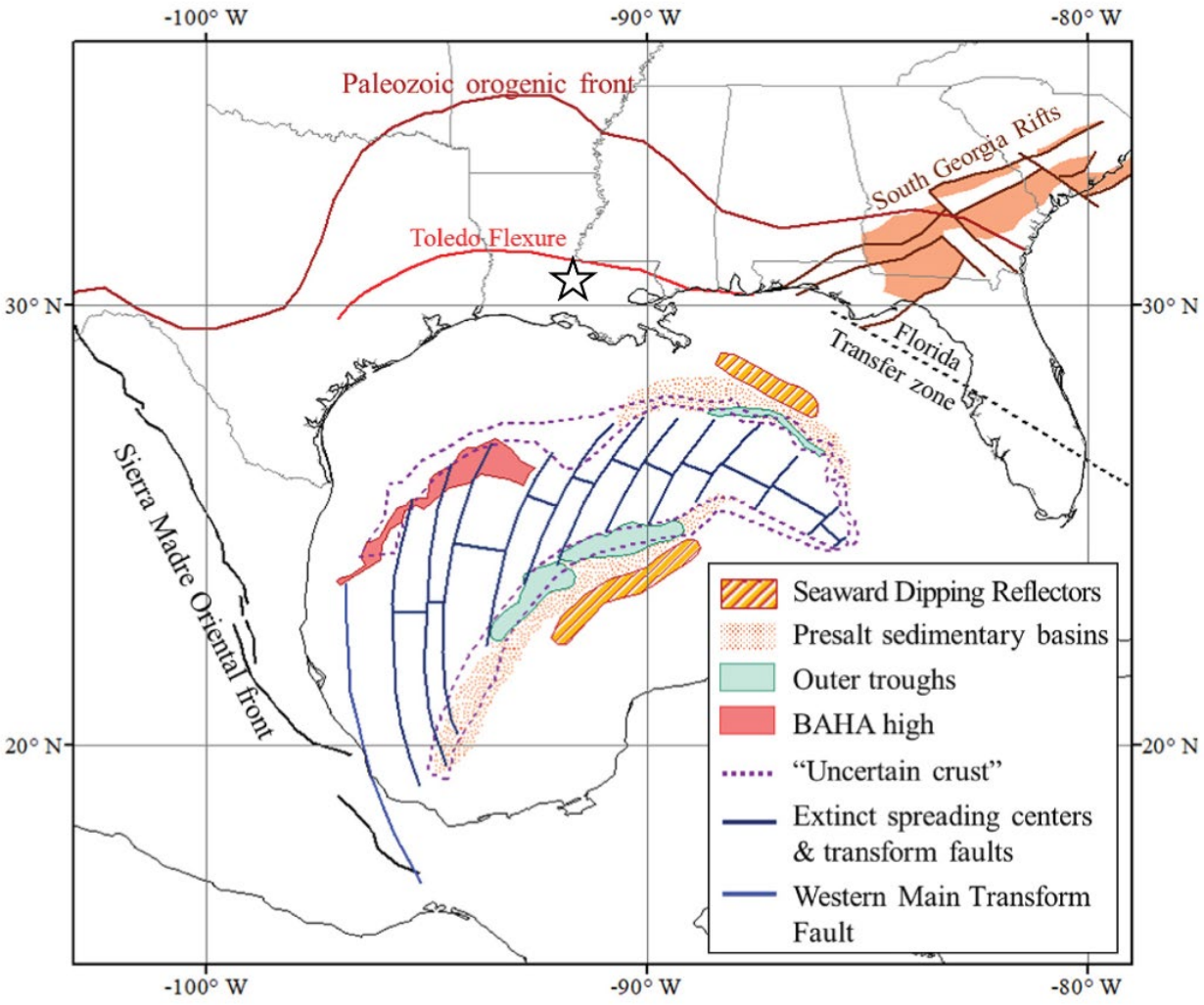

Figure 9: Key tectonic features in the Gulf of Mexico. The approximate location of the AoR is marked with a star. (Figure from Filina et al., 2022)

The remainder of this page intentionally left blank.

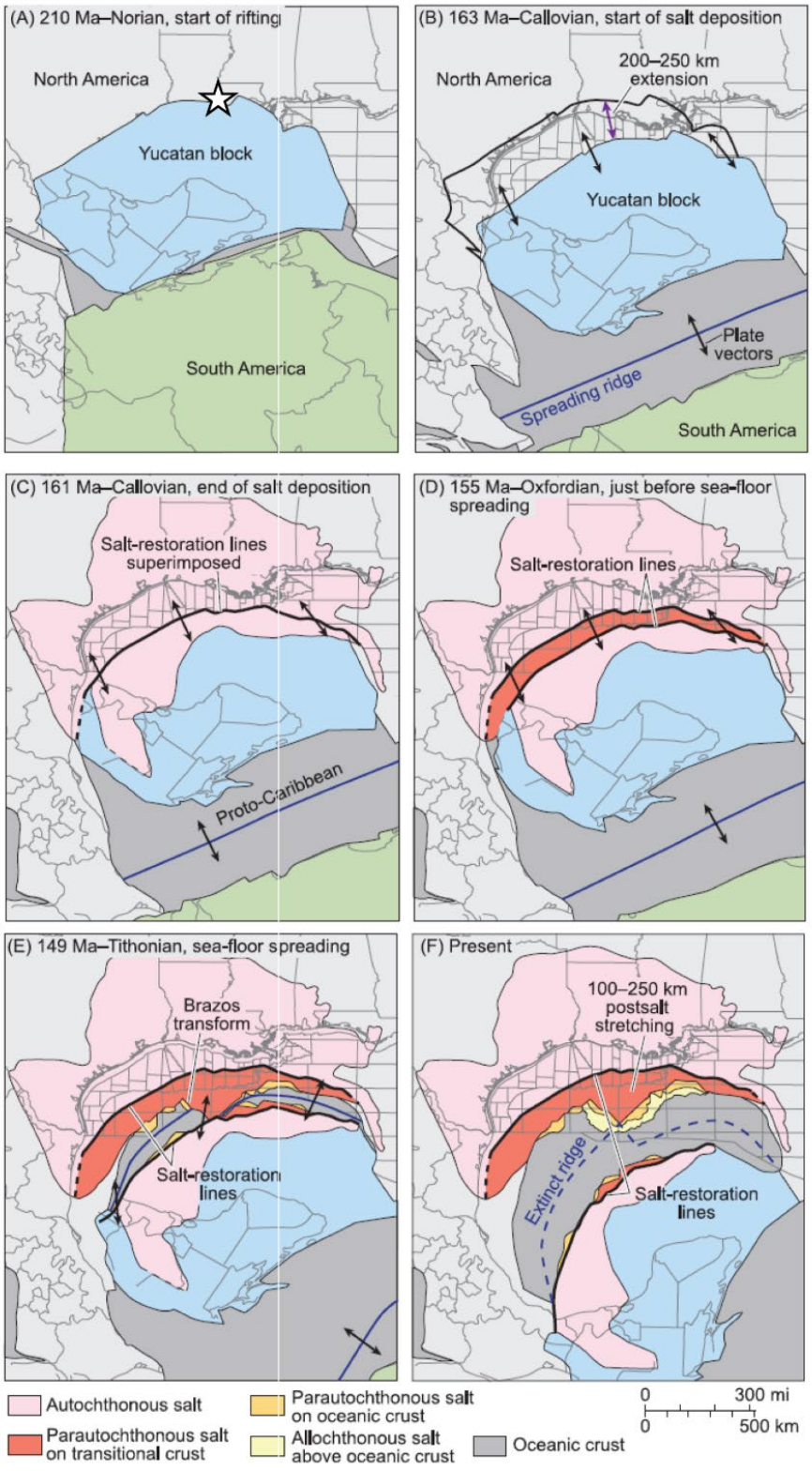

Figure 10: Sequential plate restoration of rifting, salt deposition, and seafloor spreading in the Gulf of Mexico. The approximate location of the AoR is marked with a star. (Figure from Hudec et al., 2013b)

2.1.5 Middle Mesozoic: Drift, Cooling, and Louann Salt Deposition

Initiation of seafloor spreading in the mid-Mesozoic marks the transition from continental rift to passive margin development in the northern Gulf of Mexico. As with the continental rift phase, the timing of seafloor spreading is also uncertain, largely due to poor quality marine magnetic anomaly in the basin. Published ages for the start of seafloor spreading range from 190 to 150 Ma, but there is a general consensus that the final phase of spreading began between 170 and 162 Ma as the Yucatan block rotated away from North America (Figure 10; Filina et al., 2022).

At the same time, the Jurassic Louann salt was deposited across the growing Gulf of Mexico basin. The Louann and its equivalents in Mexico (Figure 7; the Yucatan and Campeche salt basins, Hudec et al., 2013b) are generally interpreted to mark the beginning of sediment accumulation in the Gulf of Mexico as they span the entire basin and are found on both sides of the oceanic spreading center (Figure 10; Galloway, 2008). However, the exact timing of Louann salt deposition is not well established, with recent age estimates spanning 170 – 158 Ma (Filina et al., 2022). It is also uncertain if the salt was marine in origin or if the developing basin was entirely isolated from global oceans (Hudec et al., 2013b). In either case, salt progressively accumulated as water within the basin evaporated due to the hotter, dryer climatic conditions found within the sub-sea level depressions created by rifting and subsidence (Figure 11). Areas such as the Toledo bend flexure (Figure 7) are characterized by substantially less salt and have been interpreted to be topographic highs underlain by basement arches created during rifting (Figure 11). These basement highs separate the perched, onshore salt basins (e.g., East Texas, North Louisiana, and Mississippi salt basins) from the main Central Louann salt basin in the Gulf of Mexico (Figure 7 and Figure 11). The project area location on the southern flank of the Toledo bend flexure means that salt in the area is relatively thin but still present.

Following Louann deposition, continued arid climatic conditions in the Middle Mesozoic favored subaerial deposition, generating a large aeolian sand sea in the northeast Gulf of Mexico that became the Norphlet sandstone (Figure 8; Snedden et al., 2020). By the late Jurassic, limited water circulation preserved organics that comprise the Smackover and Haynesville-Buckner source rocks.

The remainder of this page intentionally left blank.

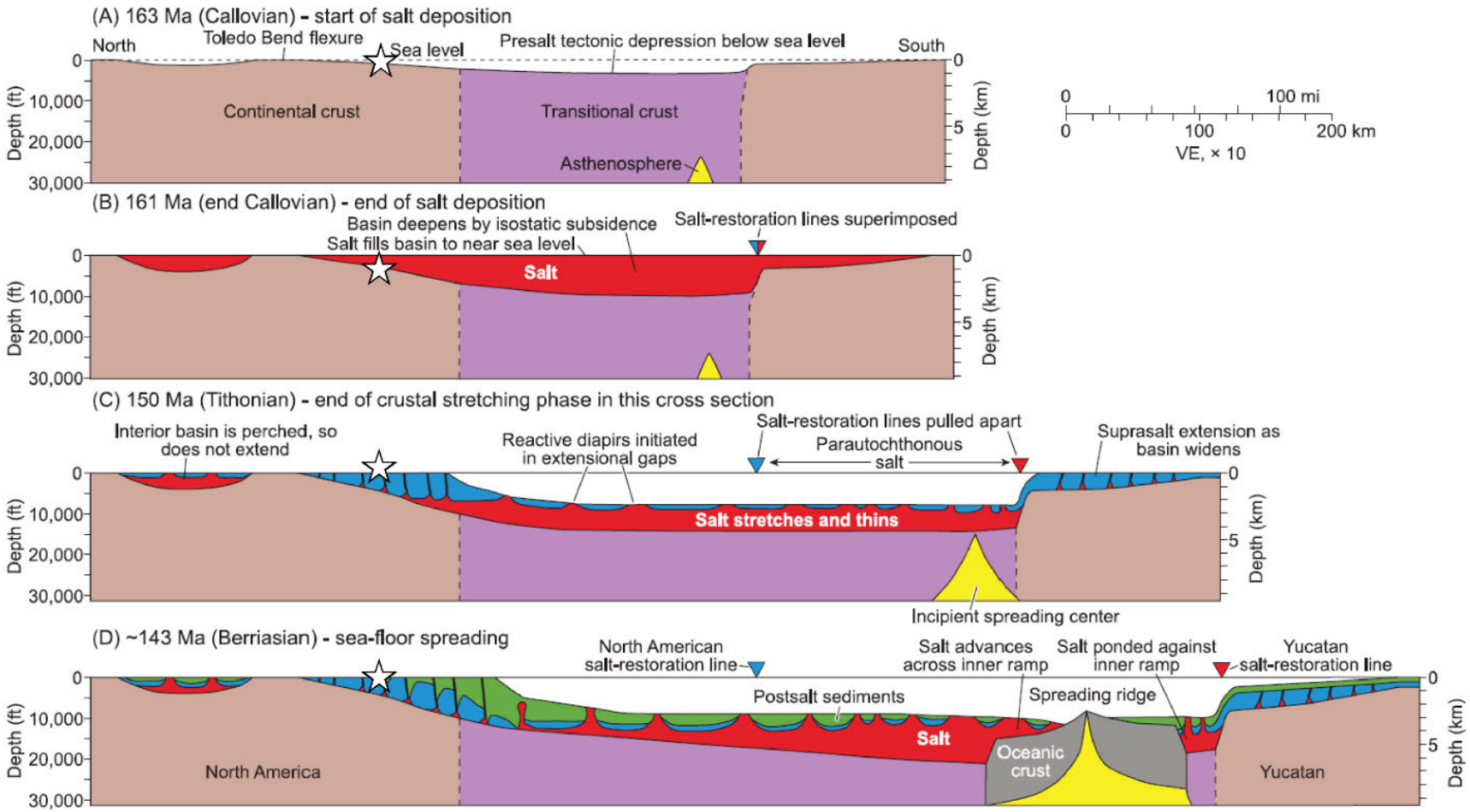

Figure 11: Schematic section restoration of basin evolution, emphasizing salt and its overburden. Internal structures in the crust are not shown. Line of section passes through the Walker Ridge salient, where seafloor spreading began relatively late. The approximate location of the AoR is marked with a star. VE = vertical exaggeration. (Figure from Hudec et al. 2013b)

2.1.6 Late Mesozoic Local Tectonic and Crustal Heating

The Gulf of Mexico basin reached its present size in the late Mesozoic. Seafloor spreading within the Gulf ceased between 145 and 140 Ma (Snedden et al., 2020), marking the transition to the thermal subsidence and sediment loading phase of basin development. Deposition of the early Cretaceous Sligo-Hosston Formation records an initial siliciclastic influx from older source terranes such as the Appalachian orogen (Snedden et al., 2020). This was followed by a transition into carbonate deposition, starting with local grainstone shoals and progressing into full platform margin and shelf reef systems (Mancini et al., 2004). Reef formation peaked around 100 Ma in the late Albian and then abruptly terminated, demarcated by a major influx of sand and deepwater submarine fan building in the upper Cretaceous (e.g., Tuscaloosa Formation in Figure 8; Snedden et al., 2020). Immediately following Tuscaloosa deposition, global sea level rise inundated the basin, shifting facies to deep shelf and basinal carbonate deposition in the late Mesozoic.

The end of the Cretaceous is punctuated by the Chicxulub impact at 66 Ma. The impact significantly modified the bathymetry and land surface of the Gulf region, setting the stage for significant sedimentation and basin loading during the Cenozoic (Snedden et al., 2020).

2.1.7 Cenozoic Basin History: Sediment Fill Derived from Climatic and Distant Tectonic Processes

The Cenozoic basin fill in the Gulf of Mexico is characterized by sediment input from processes affecting the continental interior, including Laramide, Appalachian, and Rocky Mountain uplifts; re-organization of continental drainage; icehouse and hothouse climatic periods; and glaciation. Sediment produced by these processes was carried into the Gulf of Mexico via large river systems, bypassing the shelf edge and building submarine fans that would ultimately cover the basin floor. Snedden and Galloway (2019) organize these events into three phases: Paleogene Laramide phase, middle Cenozoic geothermal phase, and the Neogene tectono-climatic phase.

2.1.8 Paleogene Laramide Phase: Sedimentation from Orographic Development

At the western margin of the North American plate, Laramide orogeny mountain building and concomitant erosion sent an influx of siliciclastic sediment into the Gulf of Mexico. These orogenic sediments filled and then bypassed Rocky Mountain basins, reaching the western Gulf of Mexico via continental-scale river systems (DeCelles, 2004; Snedden and Galloway, 2019). Consequent deposition of the Paleocene-Eocene age Lower, Middle, and Upper Wilcox successions occurred in paleoenvironments ranging from fluvial to abyssal plain settings (Figure 12; Galloway et al., 2000). This massive influx of sediment provided a sufficient gravitational load to mobilize the underlying Jurassic Louann salt, effectively displacing the salt towards the basin and deforming the overlying Mesozoic and Cenozoic sediments in the process. At the distal seaward edges of the passive margin, the salt formed extensive allochthonous salt canopies as salt was expelled towards the depositional surface. At the landward edge of the basin margin, where the project area is located, salt migration resulted in the development of extensional growth faults such as the precursor to the Baton Rouge Fault system (Figure 11).

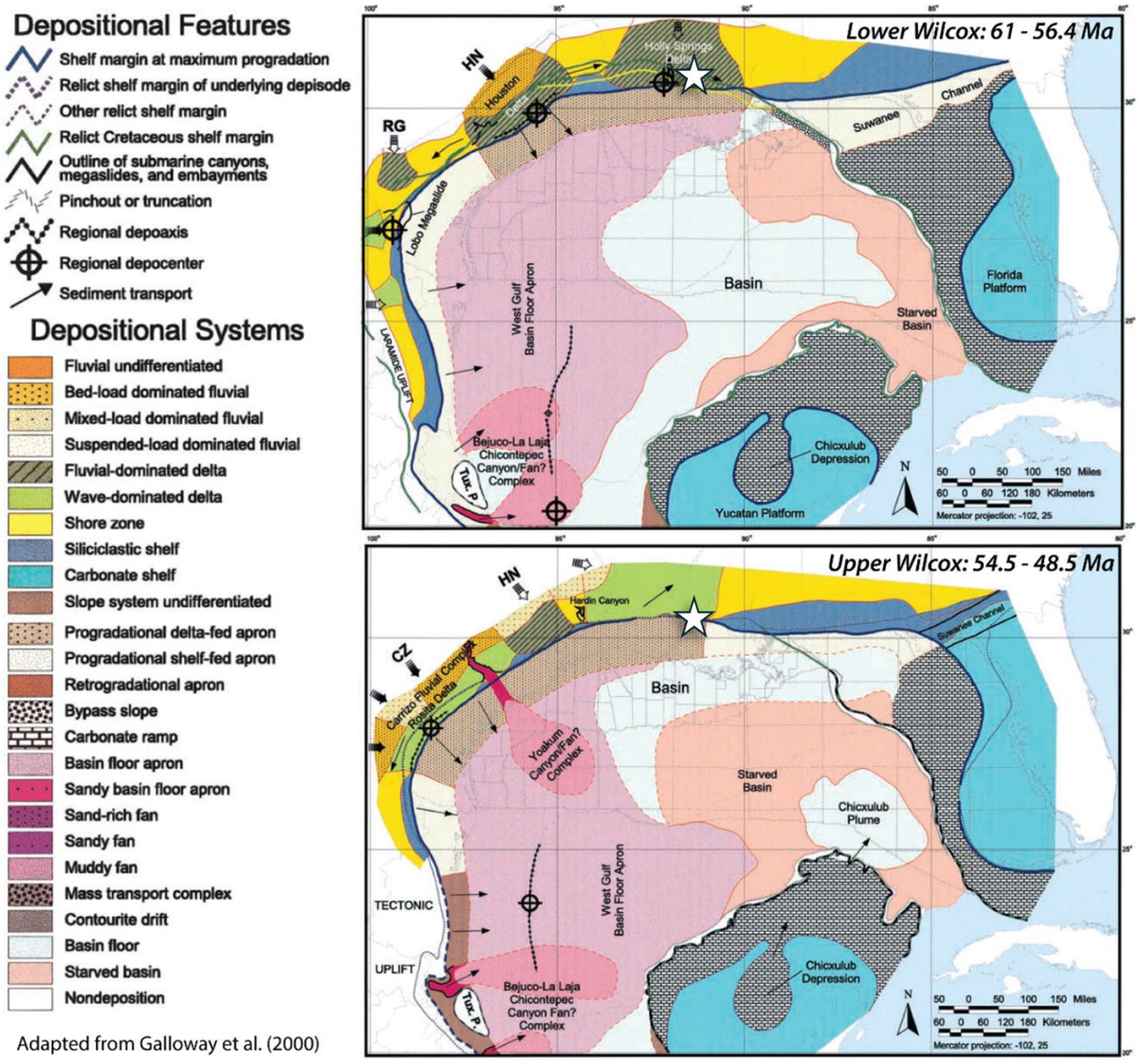

Figure 12: Paleogeography of the Lower Wilcox (LW-B, 61–56.4 Ma) (top) and the Upper Wilcox (UW-C, 48.5–54.5 Ma) (bottom) depisodes. The approximate location of the AoR is marked with a star. (Figure adapted from Galloway et al., 2000)

2.1.9 Middle Cenozoic Geothermal Phase: Sediment Inputs from Volcanic Sources and Crustal Uplift

The Oligocene and Miocene sediment fill was influenced by widespread volcanic activity and crustal uplift in the southwest of North America. In the western Gulf of Mexico, onshore basin accommodation space controlled by the Vicksburg-Frio fault system was filled, routing Oligocene Frio sequence sediment towards the deep basin. Conversely, Oligocene sedimentation in the eastern Gulf of Mexico continued to be limited compared to the western Gulf (Figure 13; Galloway et al., 2000). Throughout the Miocene, sedimentation shifted eastwards away from the Rio Grande River system towards the Mississippi drainage (Figure 14; Galloway et al., 2000). Regionally, the North American craton was undergoing uplift related to deeper mantle processes, accentuating the

basin-ward tilt of the northern Gulf of Mexico margin. This tilt provided the gravitational potential necessary to maintain seaward salt migration and associated growth faulting at the northern basin margin (Figure 11D. On the Baton Rouge fault system in the project area, active extensional fault slip during this period is recorded by expanded Oligocene – Miocene stratigraphic thicknesses in the hanging wall of the fault (Hanor, 1982).

The remainder of this page intentionally left blank.

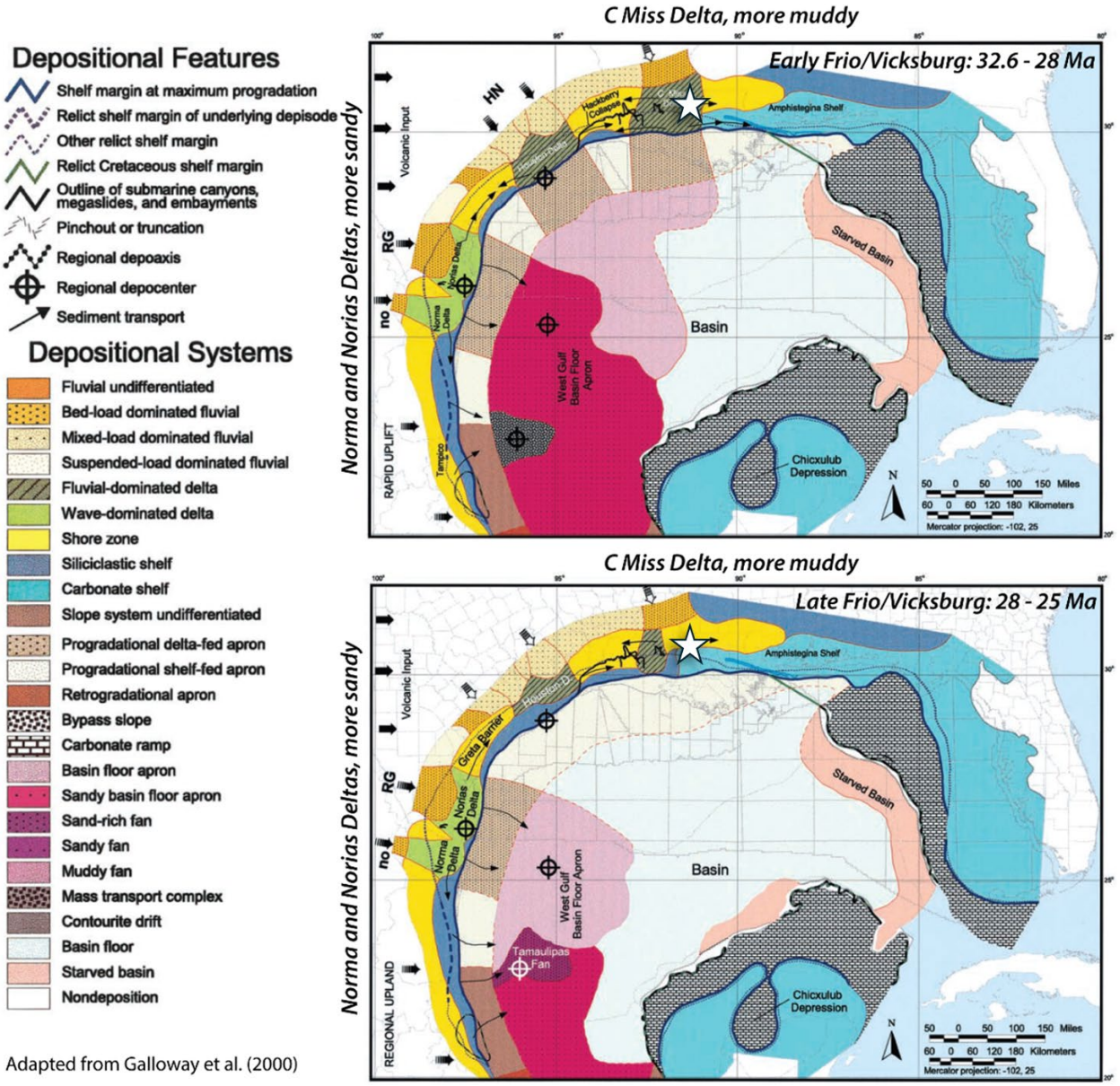

Figure 13: Paleogeography of the early Frio/Vicksburg (OF-E, 32.6–28 Ma) (top) and the late Frio/Vicksburg (OF-F, 28–25 Ma) (bottom) depisodes. The approximate location of the AoR is marked with a star. (Figure adapted from Galloway et al., 2000)

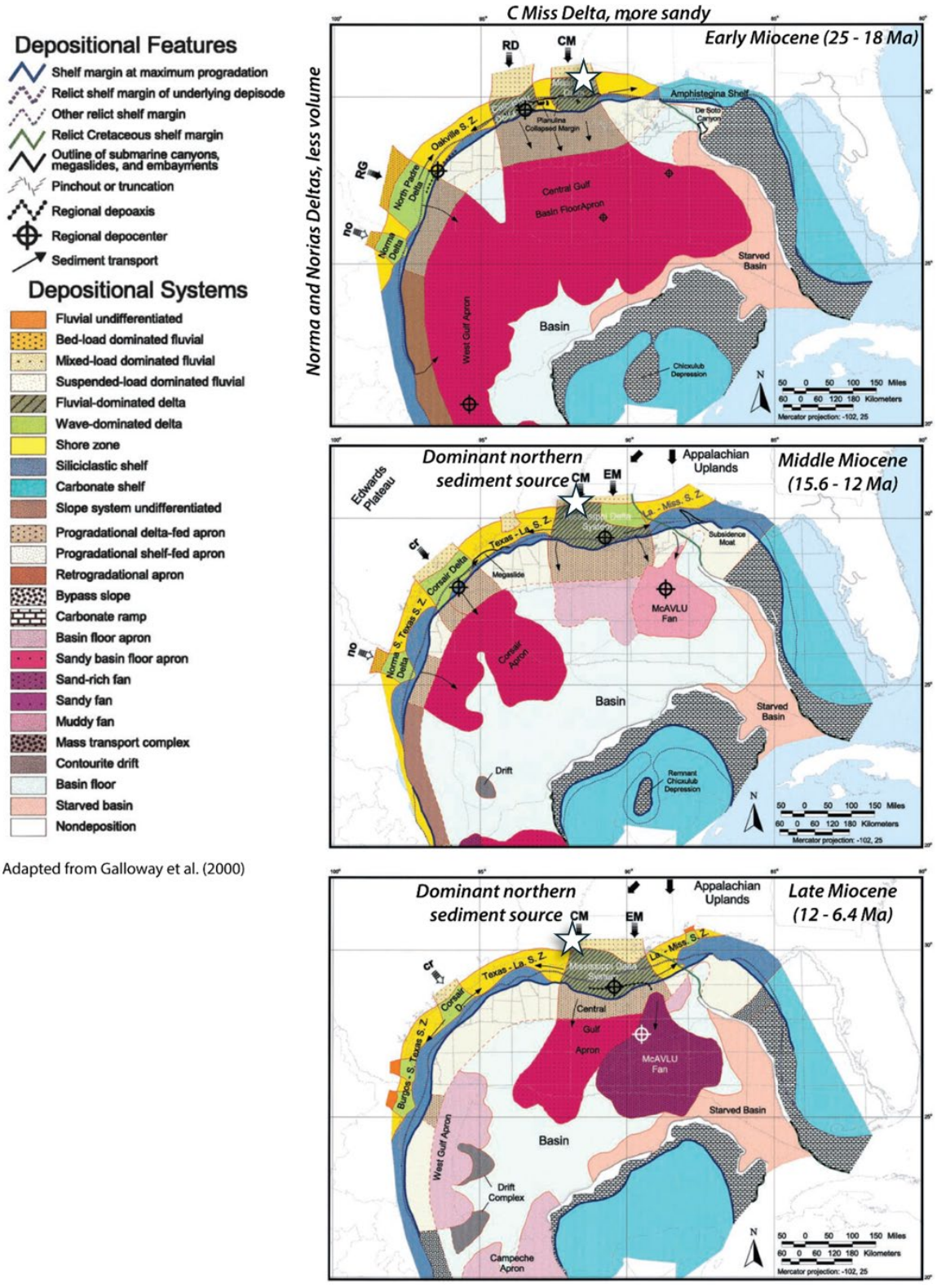

Figure 14: Paleogeography of the early Miocene (LM1-G, 25–18 Ma) (top), the middle Miocene (MM-I, 15.6–12 Ma) (middle), and the late Miocene (UM-K, 12–6.4 Ma) (bottom) depisodes. The approximate location of the AoR is marked with a star. (Figure adapted from Galloway et al., 2000)

2.1.10 Late Neogene Tectono-Climatic Phase: Appalachian Uplift, Mississippi River Formation, and Glaciation

By the early Pleistocene, sediment input into the Gulf of Mexico generally declined relative to the Oligocene – Miocene but remained significant (Figure 15; Galloway et al., 2000; Snedden et al., 2020). The bulk of sedimentation was focused in the eastern Gulf due to a new phase of Appalachian uplift driven by deep crustal processes. Early Pleistocene sediments largely accumulated within salt-controlled minibasins that formed above the allochthonous salt canopies emplaced during the Oligocene-Miocene (Figure 15; Galloway et al., 2000; Snedden et al., 2020). By the Pliocene, a series of river systems draining western and Appalachian regions coalesced into the precursor of the modern Mississippi River drainage. Sediment derived from Pleistocene ice sheets to the north was carried south through the proto-Mississippi into the Gulf of Mexico, building the Mississippi fan that now covers about half of the northern Gulf of Mexico margin (Late Pleistocene in Figure 15; Galloway et al., 2011). Pleistocene sediment accumulation was relatively limited at the landward limits of the Gulf basin but was sufficient to drive further salt tectonic activity and a renewed phase of growth faulting on the Baton Rouge fault system that continues today (Gagliano et al., 2003a). At present, the sedimentary package overlying the Jurassic Louann salt reaches thicknesses up to 12-13 km (Sawyer et al., 1991; Salvador et al., 1991).

The remainder of this page intentionally left blank.

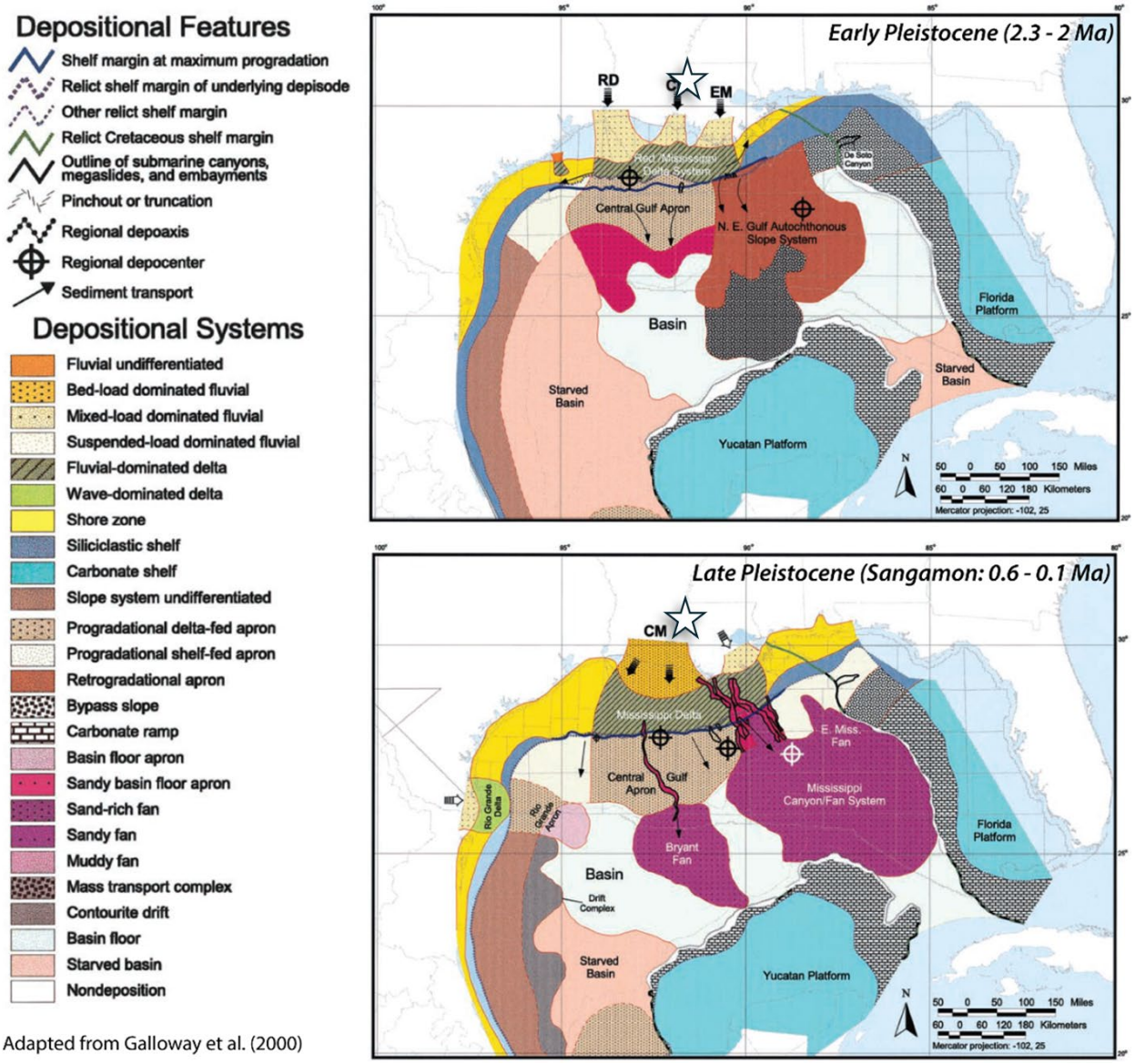

Figure 15: Paleogeography of the early phase of the Angulogerina B (PAB-P, 2.3–2) (top) and the Sangamon (PS-R, 0.6–0.1 Ma) (bottom) depisodes. The approximate location of the AoR is marked with a star. (Figure adapted from Galloway et al., 2000)

2.1.11 Summary

Sediments deposited beginning in the Oligocene and ending in the Miocene are the intended injection complexes for the project. They include from oldest to youngest: Vicksburg Shale (OFIC lower confining zone), Frio Formation (OFIC lower injection zone), Anahuac Formation (OFIC upper confining zone and LMIC lower confining zone), Lower Miocene Sand (LMIC injection zone), and Middle Miocene Confining Zone (LMIC upper confining zone). Characterization, lateral continuity, and remaining uncertainties are discussed in Section 2.5 of this Application Narrative.

2.1.12 Hydrogeology

Aquifers in the Baton Rouge region are characterized by sand bodies interspersed within the Miocene Hattiesburg through Quaternary Citronelle formations and shallow Pleistocene section (Figure 86; see subsection 2.7 of the Application Narrative). The aquifer sands below the shallow Mississippi River alluvial aquifer are named based on depths in West Baton Rouge parish. They are grouped into regional equivalents: the Chicot equivalent system contains the "400-foot" and "600-foot" sands; the Evangeline system contains the "800-foot", "1,000-foot", "1,200-foot", "1,500-foot", and "1,700-foot" sands; and the Jasper system contains the "2,000-foot", "2,400-foot", and "2,800-foot" sands (Griffith, 2003). The Baton Rouge fault appears to influence hydraulic conductivity across all the aquifers, with the base of freshwater being significantly deeper north of the fault than within the footwall of the fault to the south (Griffith, 2003). Precipitation to the north of the project area is the primary source of recharge for the aquifers (Griffith, 2003).

2.1.13 Local Structural Geology

The major geologic features in the project area are related to the architecture of the Central Louann salt basin and the salt tectonic system that has been active since the Mesozoic (Figure 7).

The primary components of the salt tectonic system at the project area are:

- Toledo Bend Flexure: a basement high formed during rifting and limit of salt deposition;
- Salt Domes: salt diapirs distributed throughout the region that deform surrounding strata; and
- Growth faults (e.g., Baton Rouge Fault): southward dipping normal faults related to salt migration.

In the project area, both basinward-dipping growth faults and salt domes are salt tectonic structures that deform the overlying Mesozoic and Cenozoic stratigraphy (Figure 11 and Figure 16). Salt tectonics refers to rock deformation that occurs due to the mobility of evaporites comprised mostly of halite (NaCl) within a sedimentary section (Hudec and Jackson, 2007). Under geologic strain rates, salt flows like a fluid and has negligible yield strength, making it mechanically weaker than surrounding rocks (Hudec and Jackson, 2007). Salt (acting as a fluid) flows in response to hydraulic head gradients. A head gradient in geologic settings can be produced by rock overburden weight (e.g., sedimentation over salt) and gravitational body forces within salt (regional tilting within a basin). During the development of the Gulf of Mexico basin, major depositional events (e.g., Paleocene-Eocene Wilcox formations) had negligible yield strengths, making them mechanically weaker than surrounding rocks (Hudec and Jackson, 2007). Salt (acting as a fluid) flows in response to hydraulic head gradients. A head gradient in a geologic setting can be produced by the weight of rock overburden (e.g., sedimentation over salt) and gravitational body forces within salt (regional tilting within a basin). During the development of the Gulf of Mexico basin, major depositional events (e.g., Paleocene-Eocene Wilcox formations in Figure 12, Oligocene Vicksburg Shale/Frio Formation in Figure 13) provided enormous sediment loads. In addition, regional uplift of the North American craton (proposed to begin ~30 Ma, accelerated in mid Miocene ~15 Ma; Jackson et al., 2011) further increased basinward tilt along the northern

Gulf of Mexico. Both loading and tilting of the passive margin are reflected by periods of active, syn-sedimentary extensional faulting and salt diapir emplacement in the northern Gulf of Mexico where the project area is located (Figure 16).

The remainder of this page intentionally left blank.

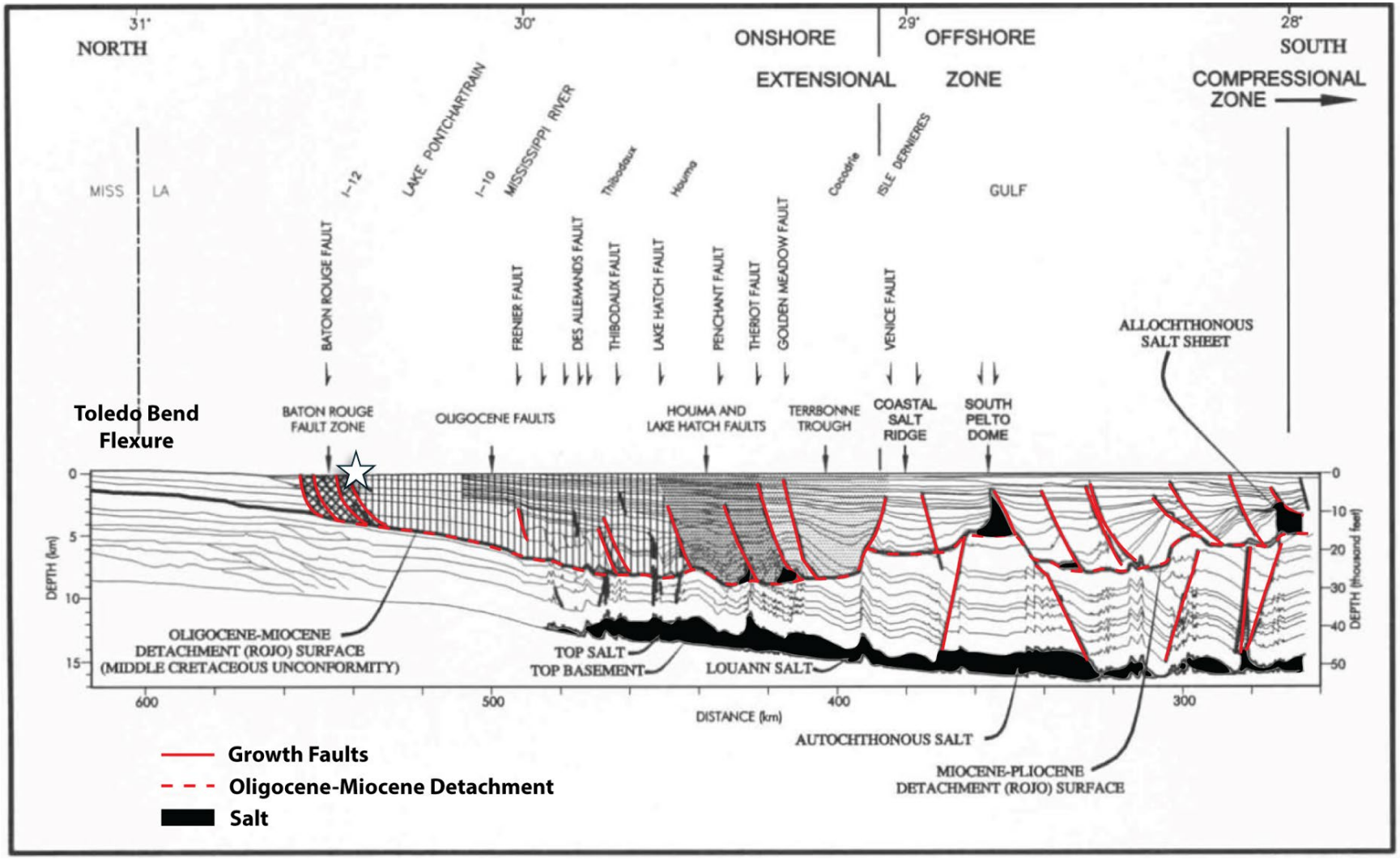

Figure 16: Segment of north-south megaregional cross-section through southeastern Louisiana showing the location of the Baton Rouge fault zone (red dashed box) in relation to the larger gravitationally-driven deformation system at the Gulf Coast. The growth faults within the Baton Rouge fault zone merge into the regional Oligocene-Miocene detachment at 3-5km depth. (Figure adapted from Gagliano et al., 2003b)

2.1.13.1 Toledo Bend Flexure

The Toledo Bend flexure is a regional basement high that separates the Central Louann salt basin from the onshore North Louisiana and Mississippi salt basins at the northern limit of the Gulf of Mexico basin (Figure 7 and Figure 16; Anderson, 1979; Hudec et al., 2013b). The Toledo Bend developed during the late Triassic opening of the Gulf of Mexico as crustal extension created a series of grabens (i.e., the future North Louisiana and Mississippi salt basins) and horst blocks along the edge of the nascent Gulf of Mexico basin (Salvador, 1991). The grabens became depocenters that accumulated substantial Louann salt thicknesses, while salt is largely absent over the structural high along the modern Toledo Bend (Hudec et al., 2013a). As a result, the Toledo Bend marks the northern limit of salt domes and growth faults associated with the Central Louann salt basin. Growth fault systems such as the Baton Rouge and Tepetate faults are the northernmost faults in the Central Louann salt basin at its border with the Toledo Bend flexure. The Toledo Bend is thought to have reactivated as a tectonic hinge line during Cenozoic uplift of the North American craton, possibly starting in the early Oligocene and continuing today (Jackson et al., 2011). Cratonic uplift has sustained the basin-ward tilt of the Gulf of Mexico margin, driving ongoing faulting and folding of the Cenozoic passive margin strata involved in the Gulf Coast salt tectonic system.

2.1.13.2 Salt Domes

The project area is located south of the Toledo Bend flexure and at the northern limit of the Central Louann salt basin. As such, the region is characterized by numerous 1- to 5-mile diameter salt domes scattered along the salt basin limit (Figure 7). In the immediate area, studies of the Choctaw (Rautman and Stein, 2004; Rautman et al., 2010), Darrow (Cook, 1938), and White Castle (Hulsey, 2016) fields have used well and seismic data to characterize the domes to depths of 15,000 ft (Figure 18). Where constrained, the domes feature vertical, cylindrical salt stocks through the Miocene – Oligocene strata with dome roofs near the Pliocene level (e.g., Rautman and Stein, 2004; Hulsey, 2016). The stratigraphic bases of the salt domes near the project area are unconstrained in the published seismic sections, but the salt stocks extend down to at least the Oligocene Frio Formation level (Figure 17, Figure 18B and Figure 18C; Rautman et al., 2010). Approximately 45 miles southwest of the project area, alkalic igneous xenoliths from the Jefferson, Avery, and Weeks salt domes have been dated to the late Jurassic, indicating that the base of those domes is well below the Cenozoic section (Stern et al., 2011). This raises the possibility that the salt domes adjacent to the project area reach stratigraphic depths below the Oligocene.

The remainder of this page intentionally left blank.

Figure 17: Map for Figure 16A west-to-east 2-D seismic profile (A-A') through the approximate center of the Bayou Choc-taw salt dome, extracted and interpreted from the 3-D seismic volume (adapted from Rautman et al., 2010). The approximate project AoR boundary in shown in black.

The remainder of this page intentionally left blank.

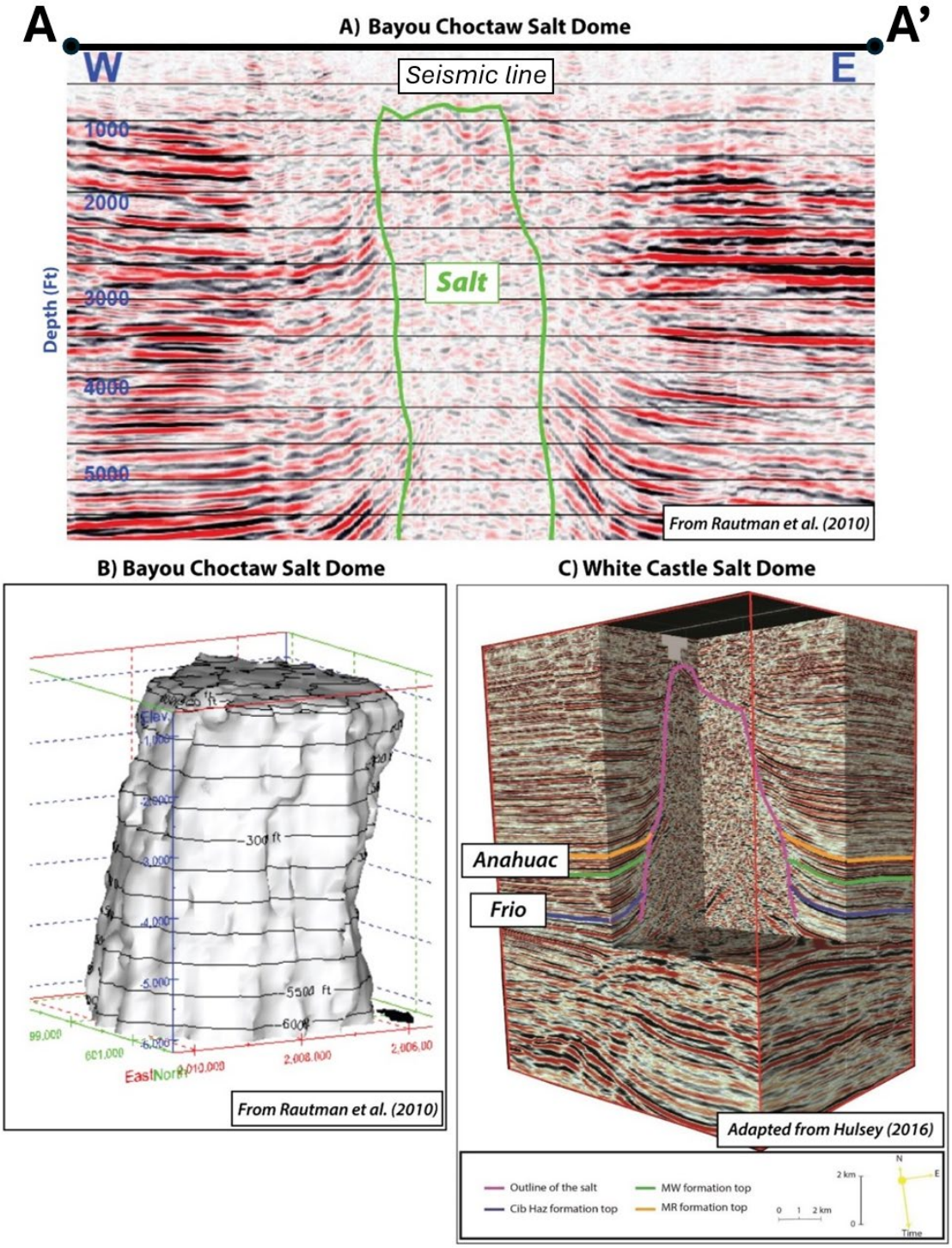

Figure 18: A) West-to-east 2-D seismic profile through the approximate center of the Bayou Choctaw salt dome, extracted and interpreted from the 3-D seismic volume (map in Figure 17). Horizontal lines are 100 msec timing lines. Numbers indicate approximate depth, in feet. B) Low-angle perspective view of the three-dimensional model of the Bayou Choctaw salt dome, incorporating interpretation of the 3-D seismic survey. C) The White Castle Salt Dome shown in the middle of a 3-D seismic volume. (Figure 18A and Figure 18B adapted from Rautman et al., 2010; Figure 18C adapted from Hulsey, 2016)

Structurally, seismic imaging of the salt dome flanks shows unconformities, sedimentary wedging, and drag folding in the Oligocene and Miocene section, indicative of active diapirism during that time (Figure 18; Rautman et al., 2010; Hudec and Jackson, 2007; Hulsey, 2016). Active diapirs grow at or just below the depositional surface; as sediment is deposited around the salt body, it subsides, forming flanking minibasins. The relatively buoyant salt body rises relative to the minibasins, progressively folding and faulting the flanking strata (Hudec and Jackson, 2007). As is typical for these types of salt diapirs, there are local radial faults in the overlying cap rock over the crest of the dome as well as faults running tangentially to the flanks of the diapir at depth (Rautman et al., 2010; Hulsey, 2016). Based on the literature reviewed here, the salt domes near the project area have not been directly tied to regional growth fault systems such as the Baton Rouge Tepetate fault system.

2.1.13.3 Baton Rouge – Tepetate Fault System

The principal faults in the project area are the west – east striking, south-dipping listric growth faults that comprise the Baton Rouge and Tepetate fault system (Figure 38). Growth faults are extensional faults that form concurrently with sedimentation. This results in stratigraphic thicknesses that increase from footwall to hanging wall across the fault and increasing stratigraphic separation with depth (Figure 19). Individual fault segments have been mapped based on surficial observations (e.g., terraces, fault scarps, and geomorphic indicators; e.g., Gagliano et al., 2003a) and subsurface datasets (e.g., well logs and seismic data; Lopez et al., 1997; Gagliano et al., 2003a; Frank, 2017). Adjacent to the project area, seismic data from western Lake Pontchartrain shows listric growth faults featuring dips between 65 and 68 degrees that gradually flatten towards 14,000 ft but are unresolved at greater depths (Figure 19; Frank, 2017). Published regional cross sections constrained by industry seismic data show the growth faults merging into the regional Oligocene-Miocene detachment at 20,000 – 30,000 ft (Figure 16; Gagliano et al., 2003a; McBride, 1998). The detachment is related to a currently absent allochthonous salt sheet that is thought to have been gradually evacuated further downslope to the south at the Terrebonne Trough (Figure 16; McBride, 1998). While salt is still present in the subsurface at the project area, as evidenced by numerous salt domes, published cross sections do not show a direct relationship between the Baton Rouge – Tepetate faults and the salt domes. Elsewhere in the Gulf Coast salt tectonic system, salt domes and major growth faults are genetically related to salt rising along the extending fault planes (c.f., Raceland salt dome; Gagliano et al., 2003a).

The remainder of this page intentionally left blank.

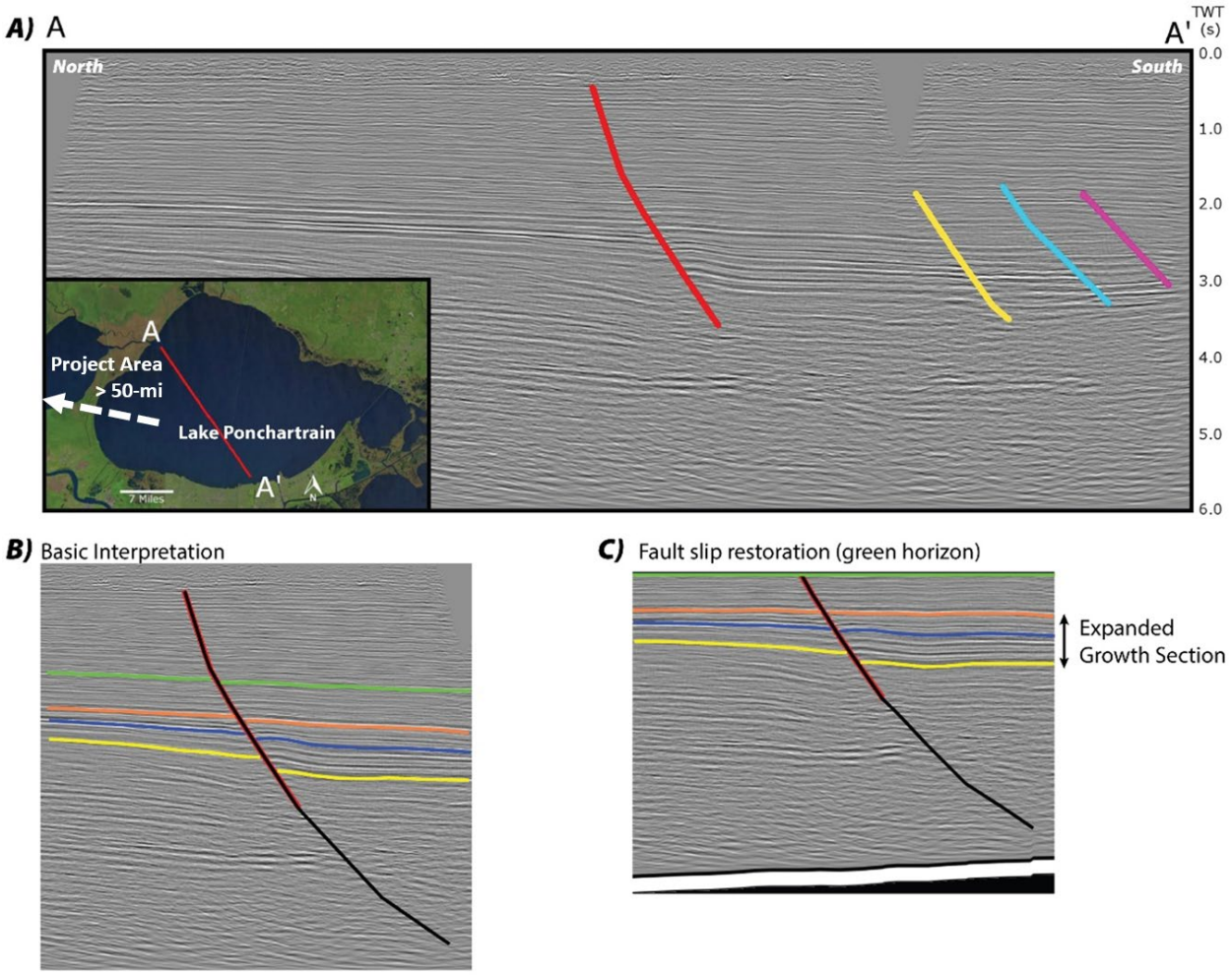

Figure 19: Interpreted 2-D seismic line of faults in Lake Pontchartrain. Project area is greater than 50 miles from Lake Pontchartrain study location. (Figure adapted from Frank, 2017)

Depth-displacement relationships and cross sections constrained by well and seismic data indicate the Baton Rouge and Tepetate growth faults systems were active from the Paleocene through Oligocene during Wilcox deposition (Hanor, 1982; McBride, 1998; McCulloh and Heinrich, 2012). By the Mid-Oligocene and Frio deposition, there was a period of relative quiescence until growth faulting resumed in the late Pliocene (Hanor, 1982; McCulloh and Heinrich, 2012). Shallow, high resolution seismic data from eastern Lake Ponchartrain show segments of the Baton Rouge fault have expanded Pleistocene and younger stratigraphic intervals indicating growth into the present (Lopez et al., 1997; Frank, 2017).

2.1.13.4 Data Used for Geologic Characterization

The data used to develop the geologic model for the project includes drilled well information and two-dimensional (2-D) and three-dimensional (3-D) seismic data. Drilled well information includes location, deviation surveys, well logs, hydrocarbon production, and wastewater injection rates. The well logs include Measured Depth, Gamma Ray (GR), Neutron Porosity Sandstone,

Density Porosity Sandstone, Bulk Density, Spontaneous Potential (SP), Caliper, Shallow, Medium and Deep Resistivity, and Sonic. In addition, historic core analyses from 30 wells along with literature analyses from other core were used to characterize the injection complexes (Table 2).

Digital well logs from 19 legacy wells were licensed and loaded into Petrel geologic interpretation software (Petrel is trademarked by and licensed from Schlumberger (SLB) Corporation) and used for picking tops for the two CCS Systems' reservoirs and confining units. Well log cross sections, shown later in this Application Narrative, were created using a subset of these logs. Subsets of these data sets were used to build the petrophysical model and calculate the porosity and permeabilities for the injection complexes (further discussed in subsection 2.7 of the Application Narrative). The locations of wells, cores, and type logs used to build the geologic model are outlined in Figure 20, Figure 21, and Figure 22. See Table 2 to match well numbers with API numbers, latitudes, and longitudes.

The remainder of this page intentionally left blank.

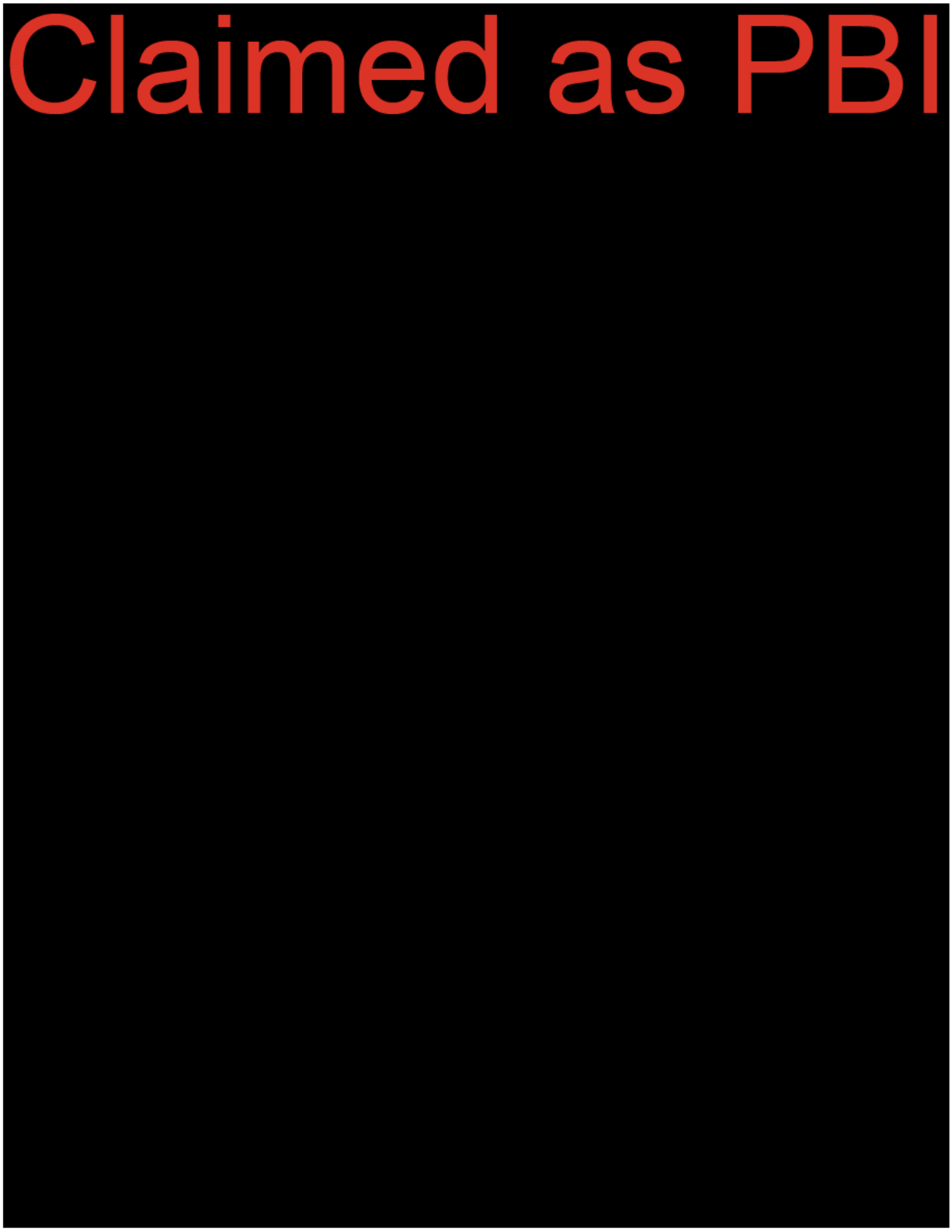

Figure 20: Location of wells used to characterize the Lower Miocene Injection Complex petrophysics. See Table 2 to match well numbers with API numbers, latitudes, and longitudes.

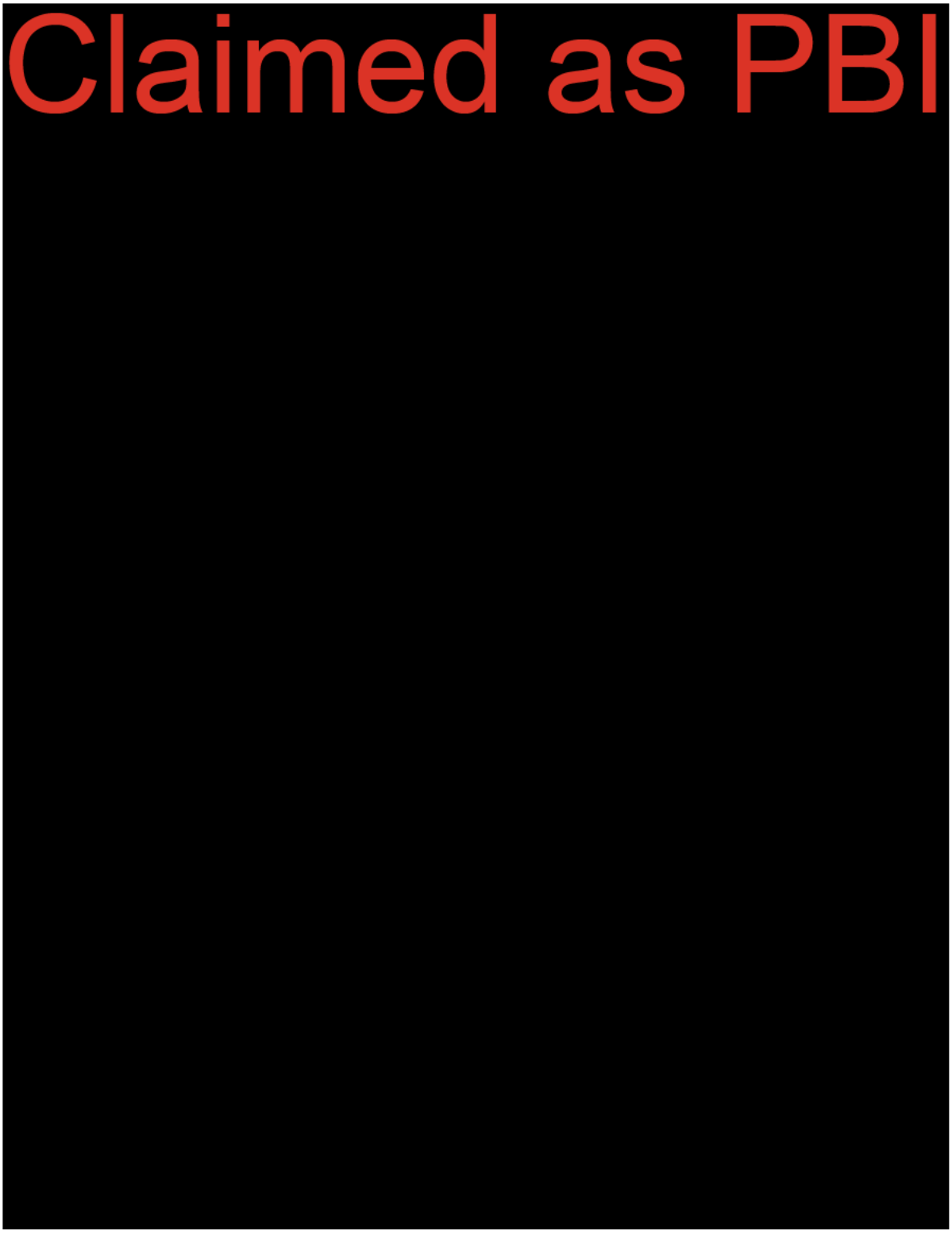

Figure 21: Location of wells used to characterize the Oligocene Frio Injection Complex petrophysics. See Table 2 to match well numbers with API numbers, latitudes, and longitudes.

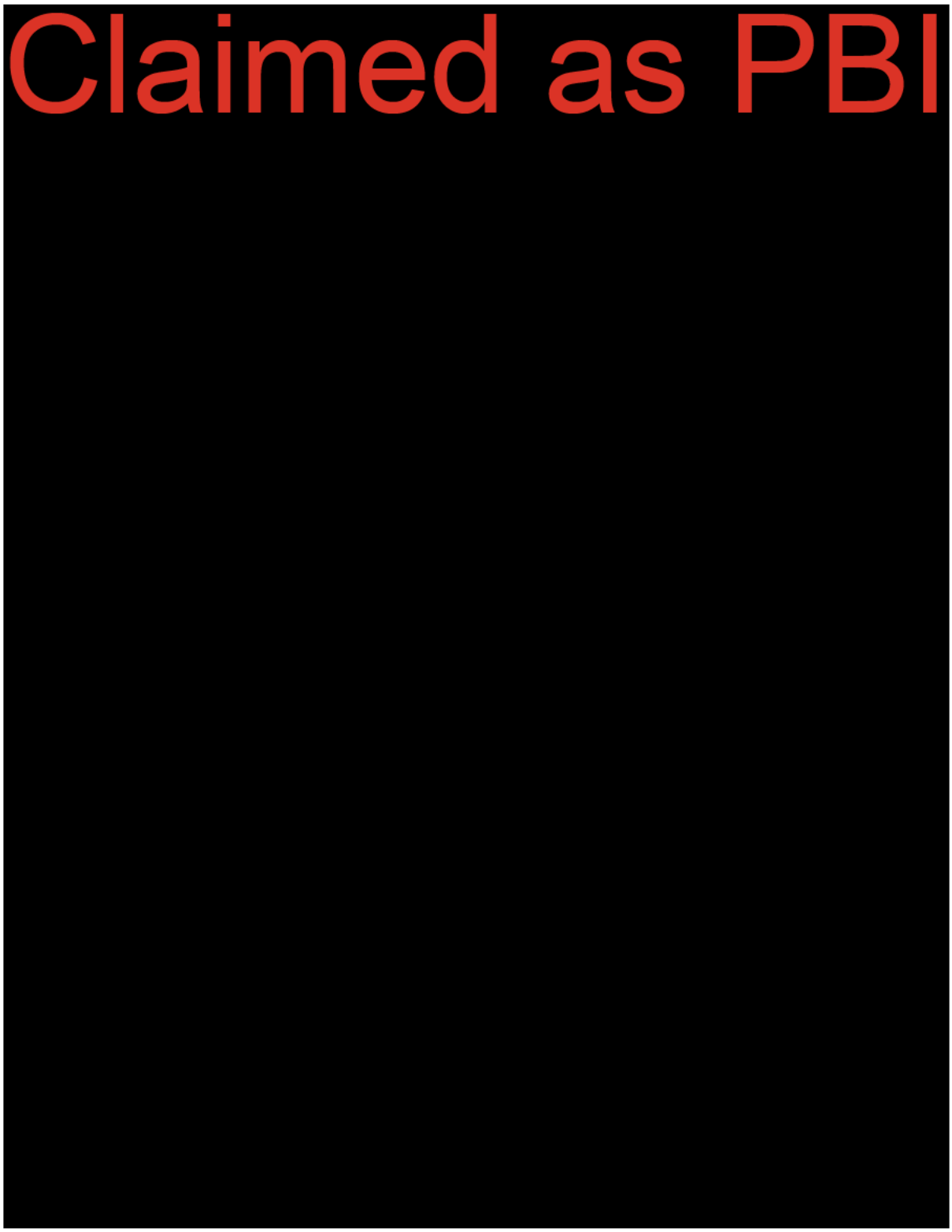

Figure 22: Location of wells with core used to characterize the injection complexes (pink). See Table 2 to match well numbers with API numbers, latitudes, and longitudes.

Table 2: List of well names, API numbers, latitude and longitudes for core, type logs, literature core studies, and petrophysical model logs used to build the geologic model. [1]Unknown wells furnished by Shreveport Petroleum Data Associated without identifying information (SPDA, https://www.spdalogs.org/data).

Well Name and Number	Serial #	API	Operator	Lat (WGS84)	Long (WGS84)	TD (MD, ft)	Reference Datum (ft)	Map #
LMIC Core Analysis Wells								
Claimed as PBI								
OFIC Core Analysis Wells								
	Claimed as PBI							

Well Name and Number	Serial #	API	Operator	Lat (WGS84)	Long (WGS84)	TD (MD, ft)	Reference Datum (ft)	Map #
Claimed as PBI	[redacted]	[redacted]	[redacted]	[redacted]	[redacted]	[redacted]	[redacted]	[redacted]
[redacted]	[redacted]	[redacted]	[redacted]	[redacted]	[redacted]	[redacted]	[redacted]	[redacted]
[redacted]	[redacted]	[redacted]	[redacted]	[redacted]	[redacted]	[redacted]	[redacted]	[redacted]
[redacted]	[redacted]	[redacted]	[redacted]	[redacted]	[redacted]	[redacted]	[redacted]	[redacted]
[redacted]	[redacted]	[redacted]	[redacted]	[redacted]	[redacted]	[redacted]	[redacted]	[redacted]
[redacted]	[redacted]	[redacted]	[redacted]	[redacted]	[redacted]	[redacted]	[redacted]	[redacted]
[redacted]	[redacted]	[redacted]	[redacted]	[redacted]	[redacted]	[redacted]	[redacted]	[redacted]
[redacted]	[redacted]	[redacted]	[redacted]	[redacted]	[redacted]	[redacted]	[redacted]	[redacted]
[redacted]	[redacted]	[redacted]	[redacted]	[redacted]	[redacted]	[redacted]	[redacted]	[redacted]
[redacted]	[redacted]	[redacted]	[redacted]	[redacted]	[redacted]	[redacted]	[redacted]	[redacted]
[redacted]	[redacted]	[redacted]	[redacted]	[redacted]	[redacted]	[redacted]	[redacted]	[redacted]
[redacted]	[redacted]	[redacted]	[redacted]	[redacted]	[redacted]	[redacted]	[redacted]	[redacted]
[redacted]	[redacted]	[redacted]	[redacted]	[redacted]	[redacted]	[redacted]	[redacted]	[redacted]
Live Oak Area Type Log								
[redacted]	[redacted]	[redacted]	Claimed as PBI [redacted]	[redacted]	[redacted]	[redacted]	[redacted]	[redacted]
LMIC Petrophysical Wells								
[redacted]	[redacted]	[redacted]	Claimed as PBI [redacted]	[redacted]	[redacted]	[redacted]	[redacted]	[redacted]
[redacted]	[redacted]	[redacted]	[redacted]	[redacted]	[redacted]	[redacted]	[redacted]	[redacted]
[redacted]	[redacted]	[redacted]	[redacted]	[redacted]	[redacted]	[redacted]	[redacted]	[redacted]
[redacted]	[redacted]	[redacted]	[redacted]	[redacted]	[redacted]	[redacted]	[redacted]	[redacted]
[redacted]	[redacted]	[redacted]	[redacted]	[redacted]	[redacted]	[redacted]	[redacted]	[redacted]
[redacted]	[redacted]	[redacted]	[redacted]	[redacted]	[redacted]	[redacted]	[redacted]	[redacted]

Well Name and Number	Serial #	API	Operator	Lat (WGS84)	Long (WGS84)	TD (MD, ft)	Reference Datum (ft)	Map #
Claimed as PBI								
OFIC Petrophysical Wells								
			Claimed as PBI					

Well Name and Number	Serial #	API	Operator	Lat (WGS84)	Long (WGS84)	TD (MD, ft)	Reference Datum (ft)	Map #
Claimed as PBI								

The remainder of this page intentionally left blank.

Live Oak CCS, LLC licensed a total of ~73.7 linear miles of existing 2-D seismic lines from Seismic Exchange Inc. and ~25 square miles of existing 3-D seismic as part of the Interdomal Bayou Ges Glaises seismic survey from Seitel Inc. that transect the project area (Figure 23). These data were used to interpret site-specific and regional geologic structure, to determine lateral continuity, and build the geologic inputs used for computational modeling. The seismic data included seven 2-D lines and one 3-D survey that provided data to refine the structural interpretation of the project area. Additionally, seismic data were used to confirm the lateral continuity of the geometry and lateral continuity of the injection and confining zones.

The remainder of this page intentionally left blank.

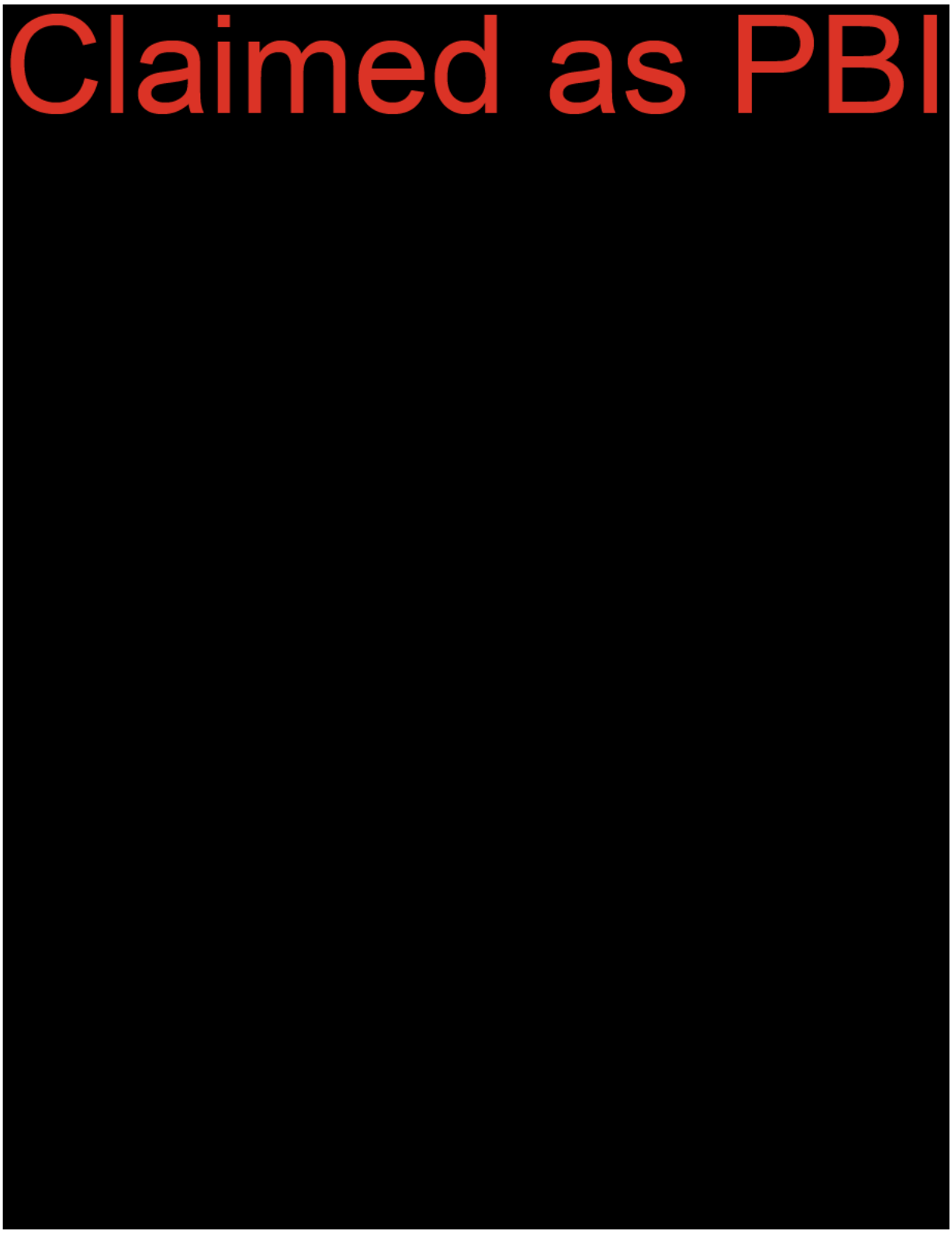

Figure 23: Location of the seven 2-D seismic lines and one 3-D seismic survey used in the Live Oak CCS Hub subsurface assessments. Note: 2-D seismic data were licensed from Seismic Exchange Inc. and 3-D from Seitel Inc.

Geologic formations were then mapped on the 2-D and 3-D seismic data (Figure 23), and structure and isopach maps were created using both the well log tops and seismic data. Together, these data sets were used to build a 3-D Static Earth Model (SEM) in the Petrel geological modeling software suite representative of the geologic and petrophysical characteristics within the Live Oak CCS Hub. The areal extent of the 3-D SEM is shown in Figure 28 and discussed in subsection 2.2 of this Application Narrative**.**

2.2. Maps and Cross Sections of the AoR

The project consists of two injection complexes: the Lower Miocene Injection Complex (LMIC) and the Oligocene Frio Injection Complex (OFIC). The regional cross-sections in Figure 24 and Figure 25 show the regional structural character schematically illustrated by Dokka et al. (2006). The regional cross-sections in Figure 26 and Figure 27 show the stratigraphy as presented by Bebout and Guitierrez (1983). The location map and cross-sections confined to the injection complexes and model domain in Figure 28 through Figure 35 highlight the regional and local lateral continuity and thickness of both the Frio Formation and the Lower Miocene depisode defined by Galloway et al., 2000. In addition, the Middle Miocene Confining Zone, the LMIC upper confining zone, and the Anahuac Formation and Vicksburg Shale confining zones also exhibit regional and local lateral continuity and consistent thickness. Further discussion of the regional geology, seal thicknesses and lateral extents, injection zone thicknesses and lateral extents, and other site-specific geologic characteristics is in subsection 2.1 and subsection 2.4, respectively, of this Application Narrative.

The gamma ray and petrophysical character of both the Frio Formation and the Lower Miocene Depositional Episode in the SEM domain is consistent in both the strike and dip direction. There are few wells that penetrate the entire Frio Formation and encounter the Vicksburg Shale lower confining zone; thus, there is limited petrophysical analysis and uncertainty in characterizing this interval. The lowermost USDWs, in the Jasper Equivalent Aquifer System, are Upper Miocene sands ranging in depth from 2,300 to 2,500 feet below sea level. These sands are approximately 3,000 feet above the top of the Middle Miocene Confining Zone and are shown in Figure 53 in subsection 2.4 of this Application Narrative. Further discussion of USDWs is in subsection 2.7.4 of this Application Narrative. Further discussion of the petrophysics of the OFIC and the LMIC is in subsection 2.5 of this Application Narrative.

The Baton Rouge fault system is an east-west trending, south-dipping growth fault located north of the AoR. A similar fault is inferred to the south of the AoR based on regional mapping of Gagliano (2005); however, seismic transects across this area do not show evidence of a fault in this location. The Baton Rouge fault system does not pose a risk to containment for this project as it does not intersect any of the injection or confining zones within the AoR or within more than 4.5 miles of the proposed injection wells.

Detailed information concerning these fault systems, associated fractures, and their spatial relation to the injection wells is further discussed in subsection 2.3 of this Application Narrative. The mitigation of project risk associated with the Baton Rouge Fault system is discussed in detail in subsection 2.3.4 of this Application Narrative.

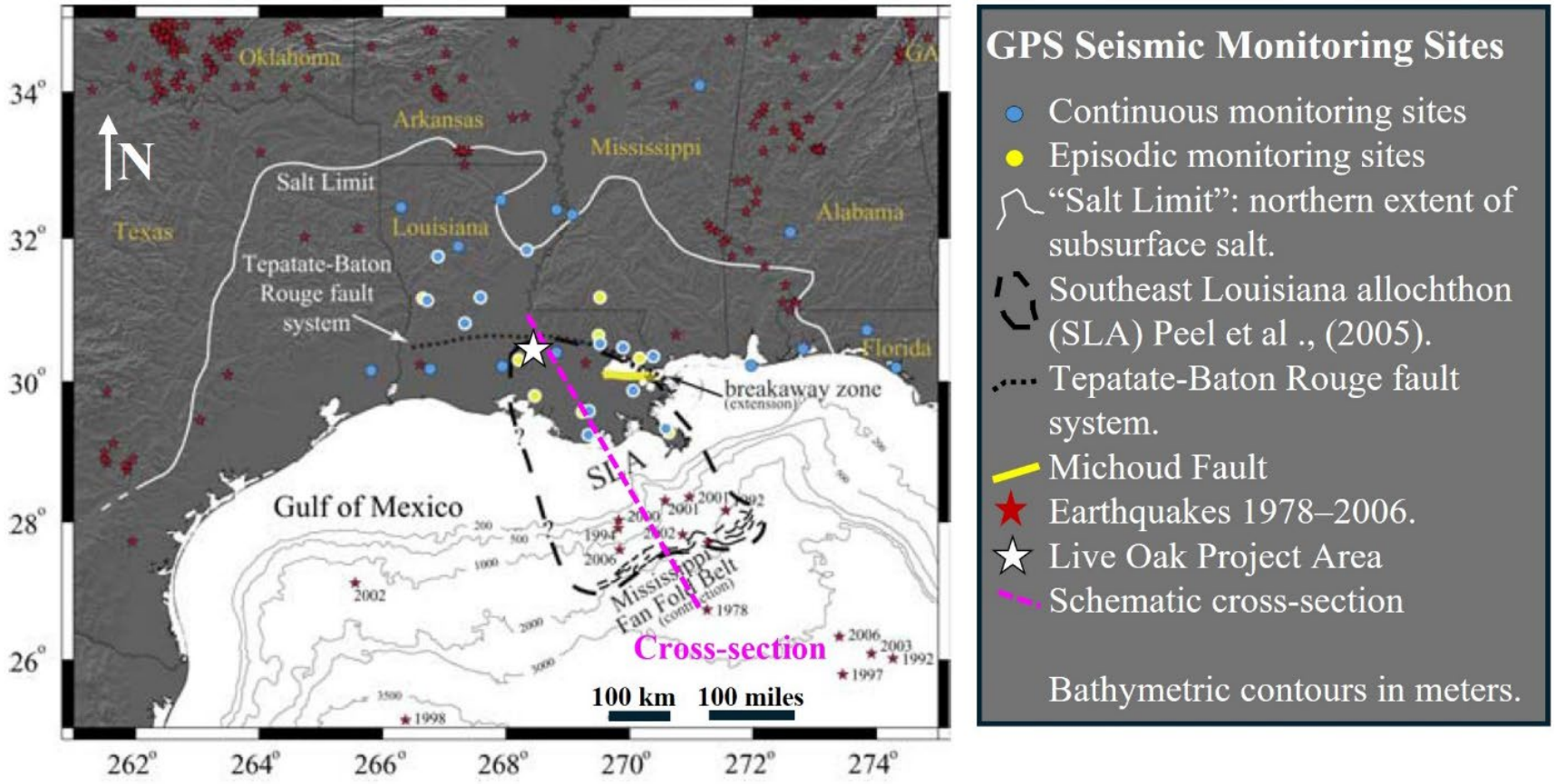

Figure 24: Shaded relief map modified from Dokka et al. (2006) showing the location of the Tepatate-Baton Rouge fault system in a complex breakaway zone with the Michoud fault at the north extent of the Southeastern Louisiana allochthon (SLA) (Peel et al., 2005), the approximate north edge of lithosphere thinned by Jurassic rifting (Worrall and Snelson, 1989). The Mississippi Fan Fold Belt, the southern extent of the SLA, is in contraction due to SLA extension. GPS sites in Louisiana are used to interpret fault slip and magnitude (Dokka et al., 2006). U.S. Geological Survey earthquakes https://earthquake.usgs.gov/earthquakes/search/.

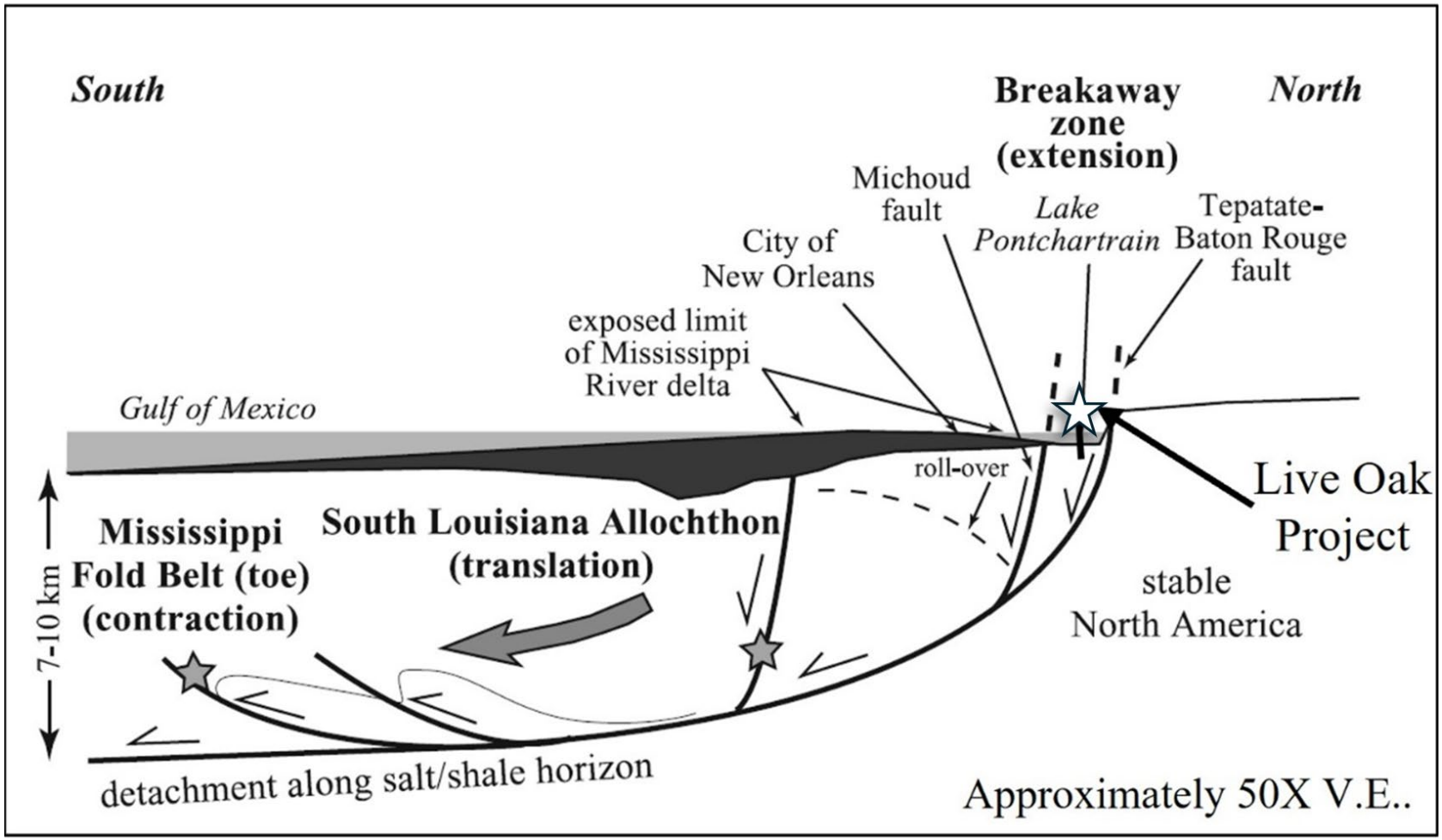

Figure 25: Schematic diagram of SLA (Peel et al., 1995) detachment driven by Quaternary Mississippi Delta sediment loading and sea level rise (Dokka et al., 2006). The listric, down-to-the south Tepatate-Baton Rouge fault system is at the north limit of the breakaway zone of a partially intact allochthon where faulting is composed of downward hanging wall motion and local reverse drag (Dokka et al., 2006). The project area is labeled and shown with a white star.

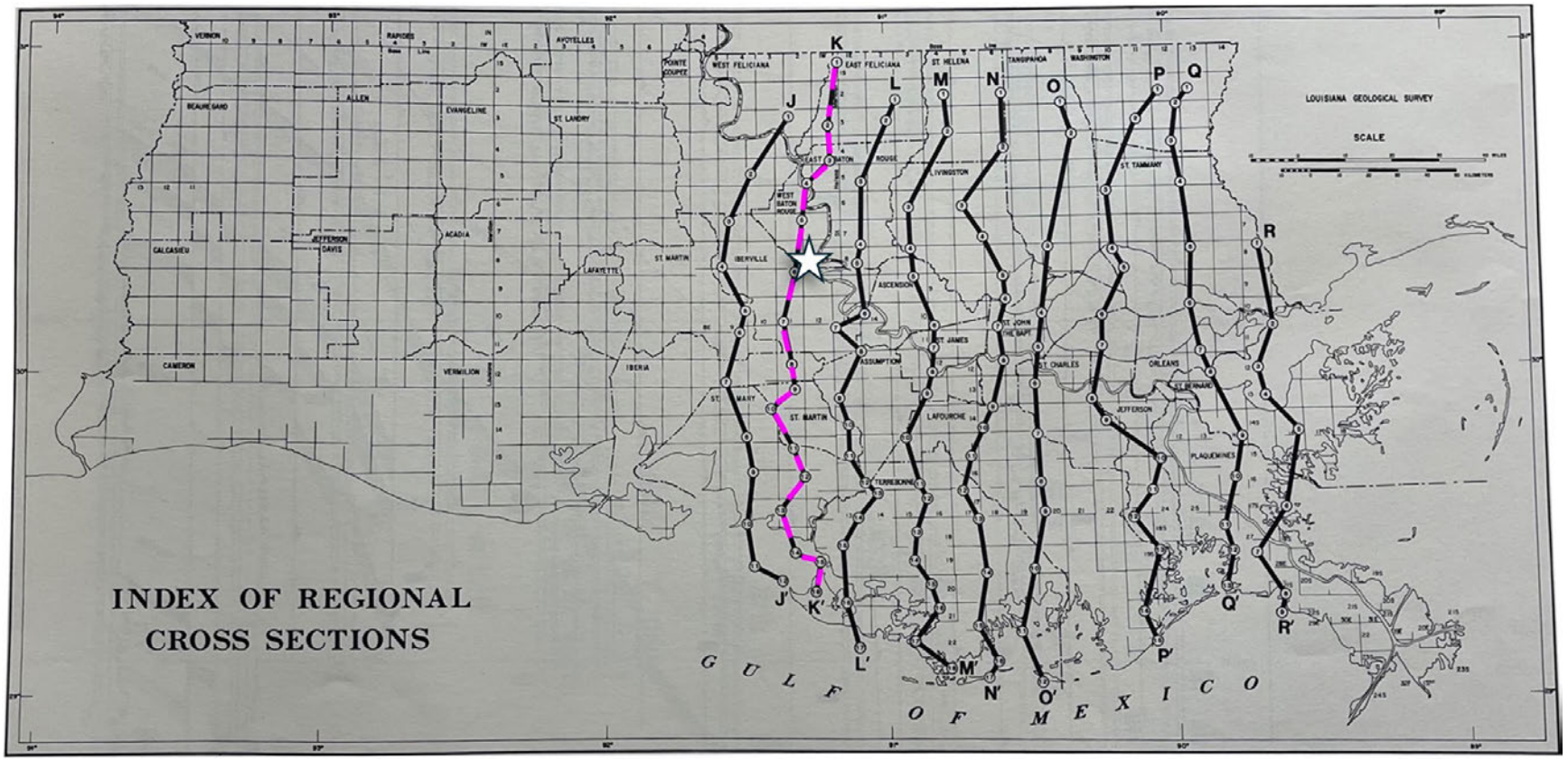

Figure 26: Location map for cross section in Figure 27. Cross section location is shown with a pink dashed line. The Live Oak Project area is shown with a star. (Figure adapted from Bebout and Guitierrez, 1983)


Claimed as PBI

Figure 27: (above) Structural cross section K-K' modified from Bebout and Guitierrez (1983). Vertical exaggeration is 40X. Shallow Miocene, Deep Miocene and Frio Formation injection zone tops are highlighted in yellow. Miocene Upper, Deep Miocene sub-confining zones as well as Anahuac and Vicksburg Shale confining zones are highlighted in blue. Bebout and Guitierrez (1983) place the top of the Lower Miocene lower than Galloway et al. (2000). The portion of the cross section crossing West Baton Rouge and Iberville parishes is labeled, and the approximate project area is indicated by a star and arrow. Interpreted down-to-the-south listric normal faults interpreted by Bebout and Guitierrez (1983) are highlighted in red.

The remainder of this page intentionally left blank.

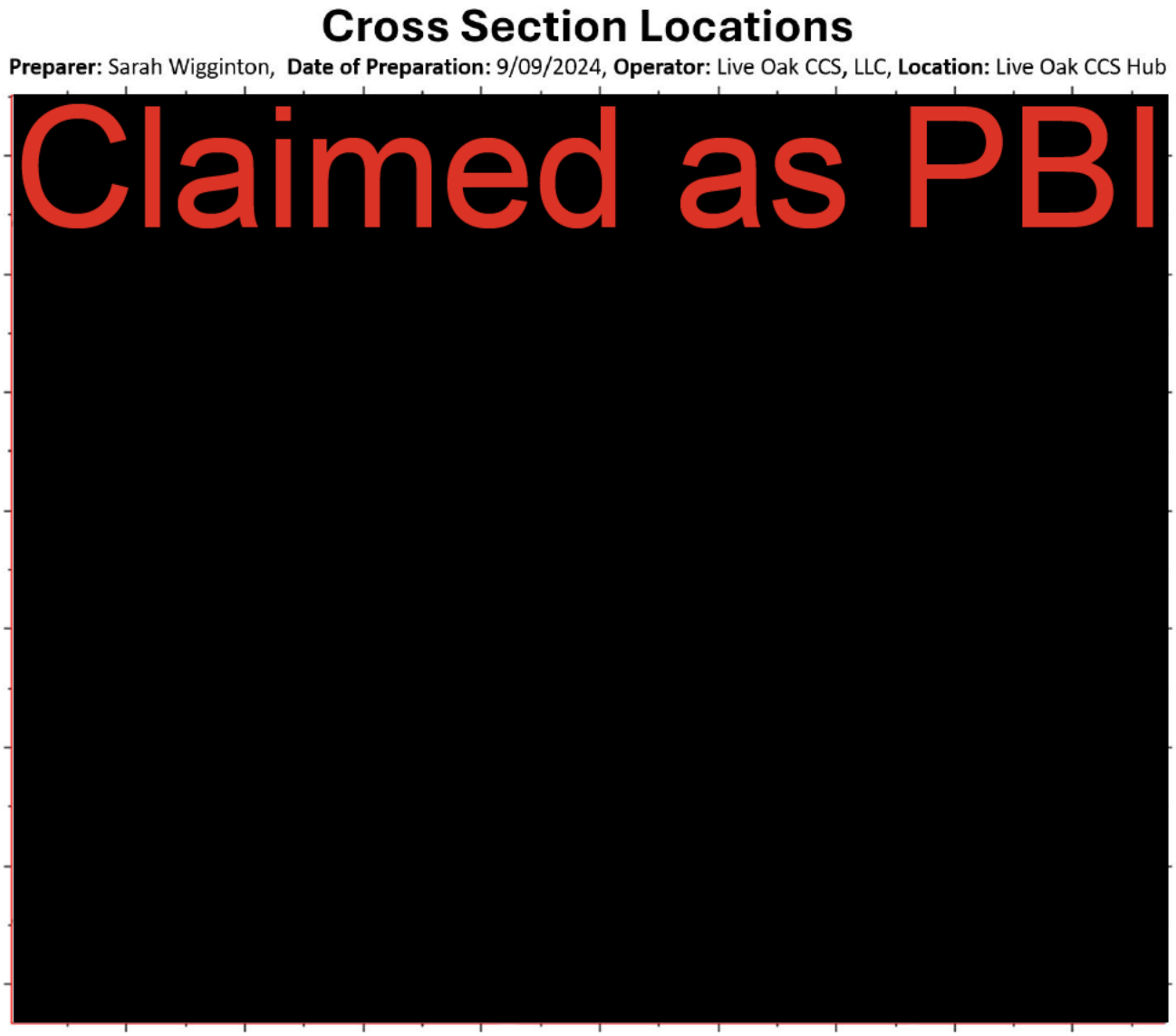

Figure 28: Base map of the project model domain and petrophysical wells included in the SEM build for the project AoR (red) with LMIC cross sections along the A-A' (Figure 29) strike cross section, and the B-B' and C-C' dip cross sections (Figure 30 and Figure 31).

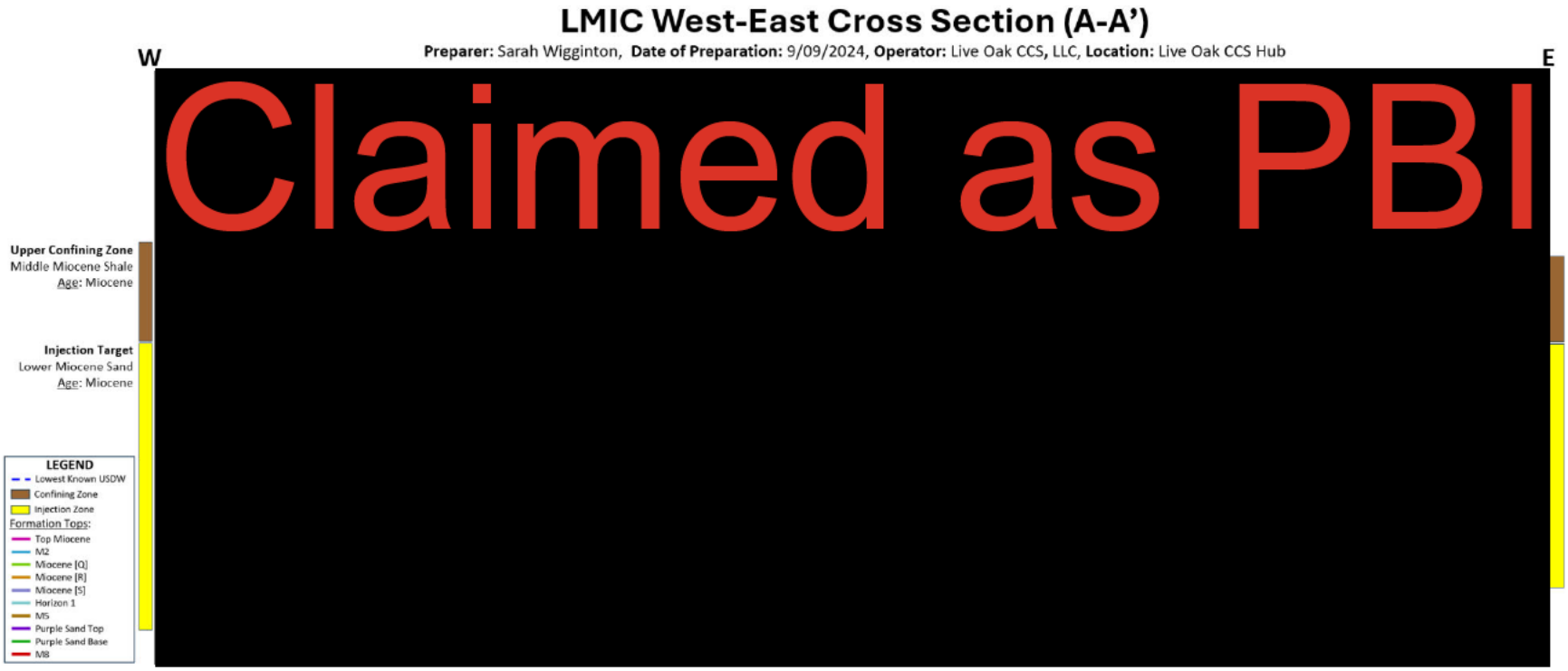

Figure 29: Strike cross section A-A' through the project model domain (see map Figure 28) with the depth track in feet measured depth (far left), normalized gamma ray, the spontaneous potential, and the porosity. Crossing of AoR boundary indicated in red. For detailed discussions on the petrophysical model and the specific wells used in this analysis, refer to subsection 2.5 of this Application Narrative. For associated well data see Appendix A.

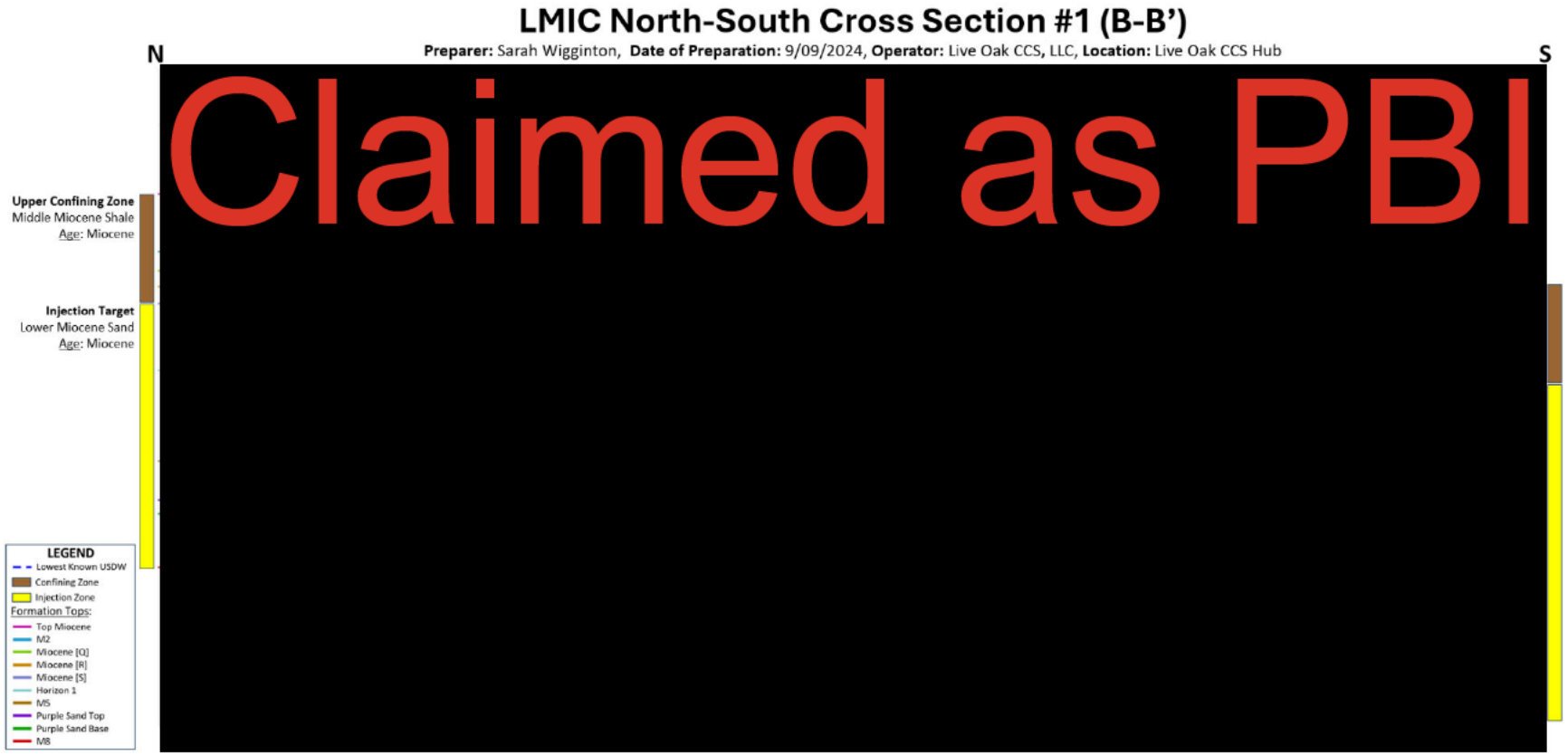

Figure 30: Dip cross section B-B' through the project model domain (see map Figure 28) with the depth track in feet measured depth (far left), normalized gamma ray, the spontaneous potential, and the porosity. For detailed discussions on the petrophysical model and the specific wells used in this analysis, refer to subsection 2.5 of this Application Narrative. For associated well data see Appendix A.

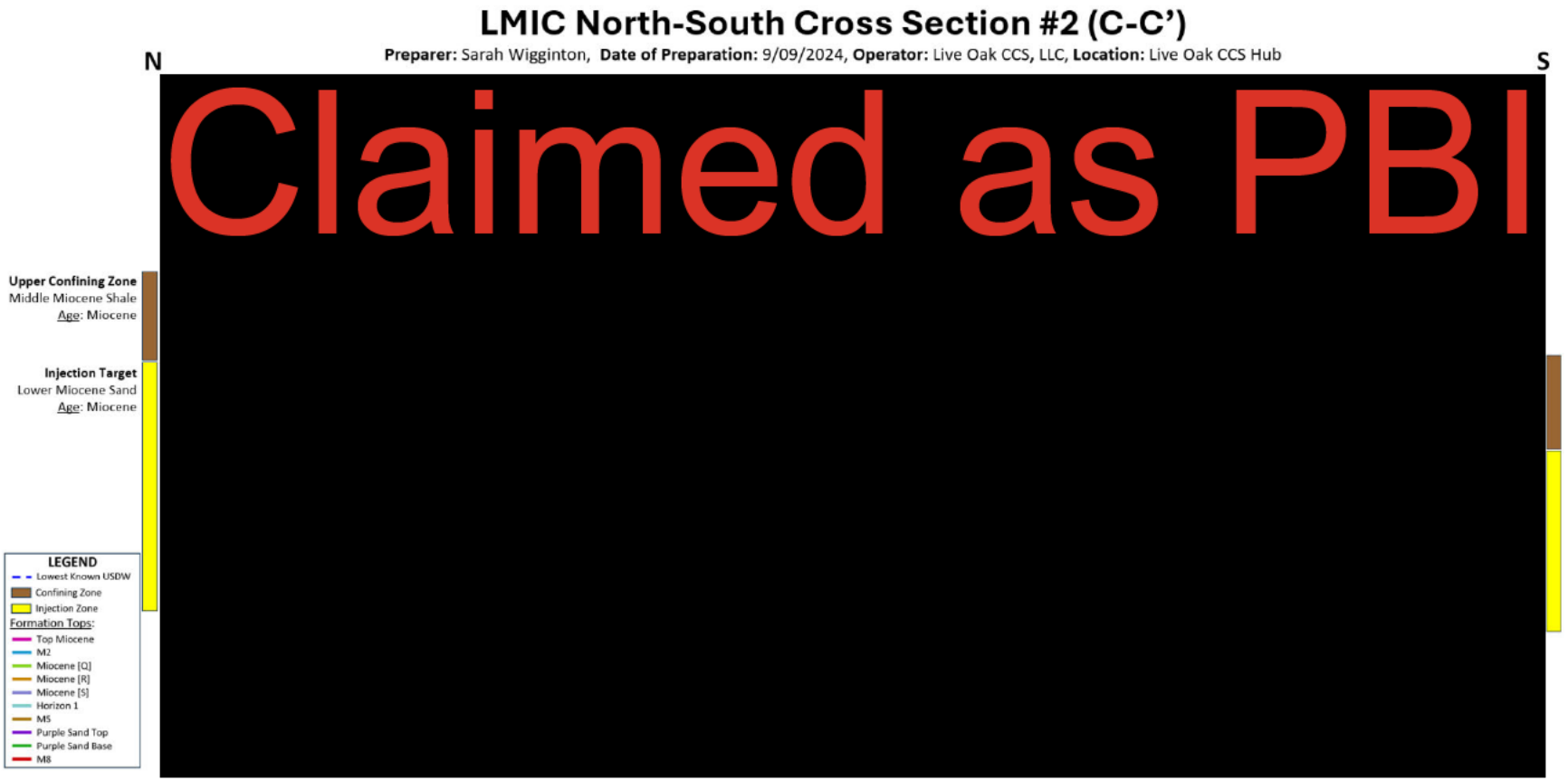

Figure 31: Dip cross section C-C' through the project model domain (see map Figure 28) with the depth track in feet measured depth (far left), normalized gamma ray, the spontaneous potential, and the porosity. Crossing of AoR boundary indicated in red and inferred fault with black-dashed line. For detailed discussions on the petrophysical model and the specific wells used in this analysis, refer to subsection 2.5 of this Application Narrative. For associated well data see Appendix A.

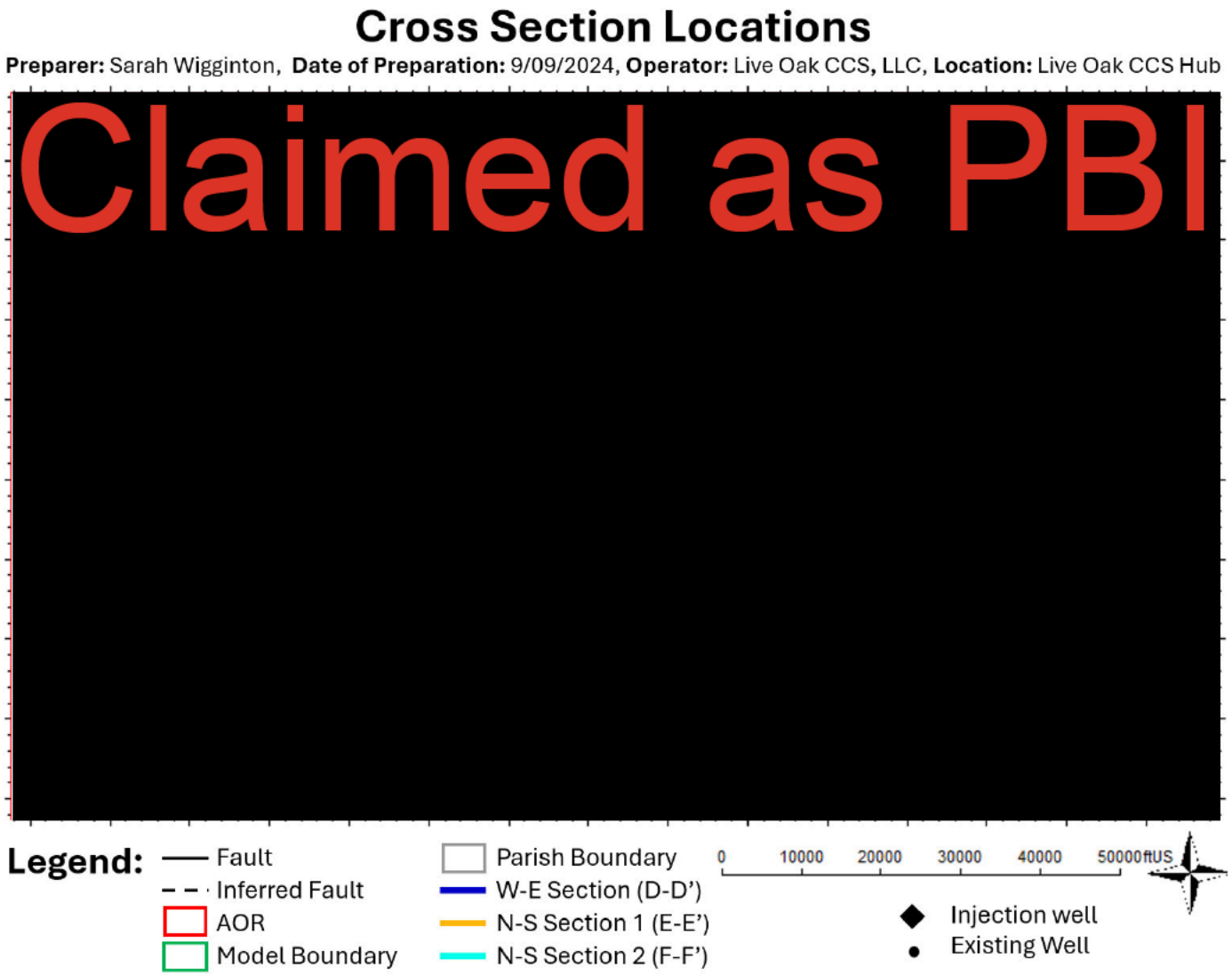

Figure 32: Base map of the project model domain and petrophysical wells included in the SEM build for the project AoR (red) with the OFIC cross section along the D-D' strike cross section (Figure 33), and the E-E' and F-F' dip cross sections (Figure 34 and Figure 35).

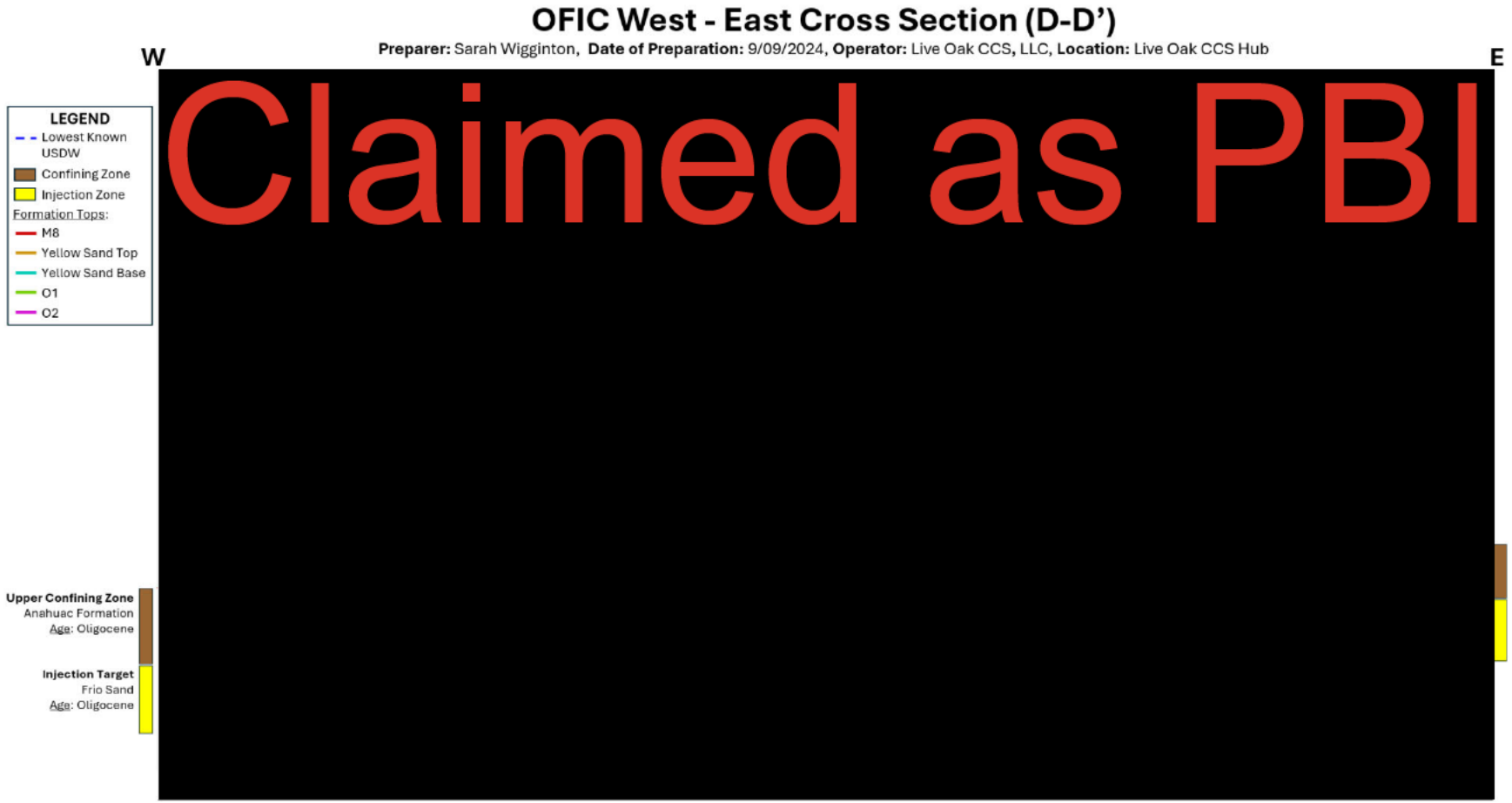

Figure 33: Dip cross section D-D' through the project model domain (see map Figure 32) with the depth track in feet measured depth (far left), normalized gamma ray, the spontaneous potential, and the porosity. For detailed discussions on the petrophysical model and the specific wells used in this analysis, refer to subsection 2.5 of this Application Narrative. For associated well data see Appendix A.

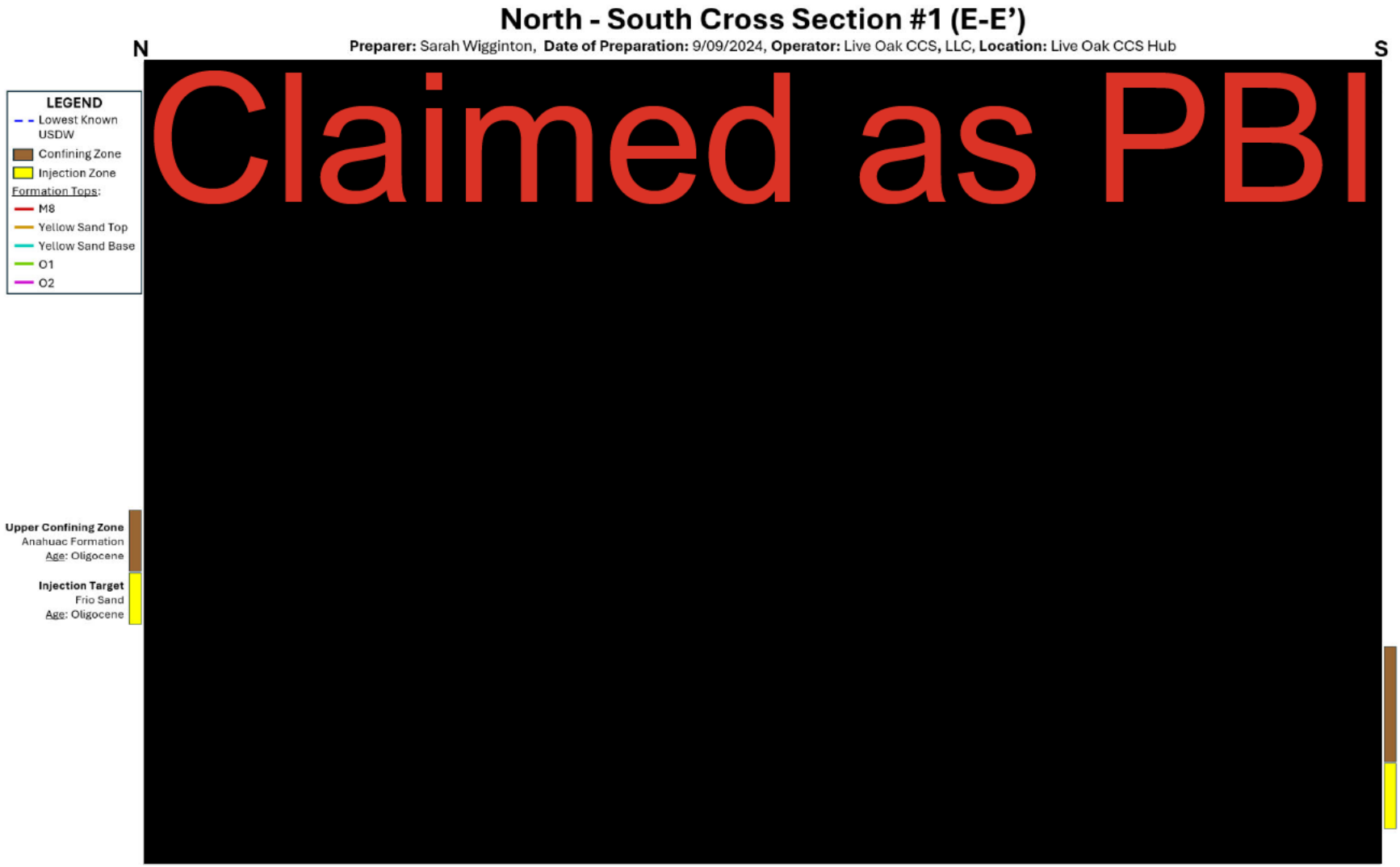

Figure 34: Dip cross section E-E' through the project model domain (see map Figure 32) with the depth track in feet measured depth (far left), normalized gamma ray, the spontaneous potential, and the porosity. For detailed discussions on the petrophysical model and the specific wells used in this analysis, refer to subsection 2.5 of this Application Narrative. For associated well data see Appendix A.

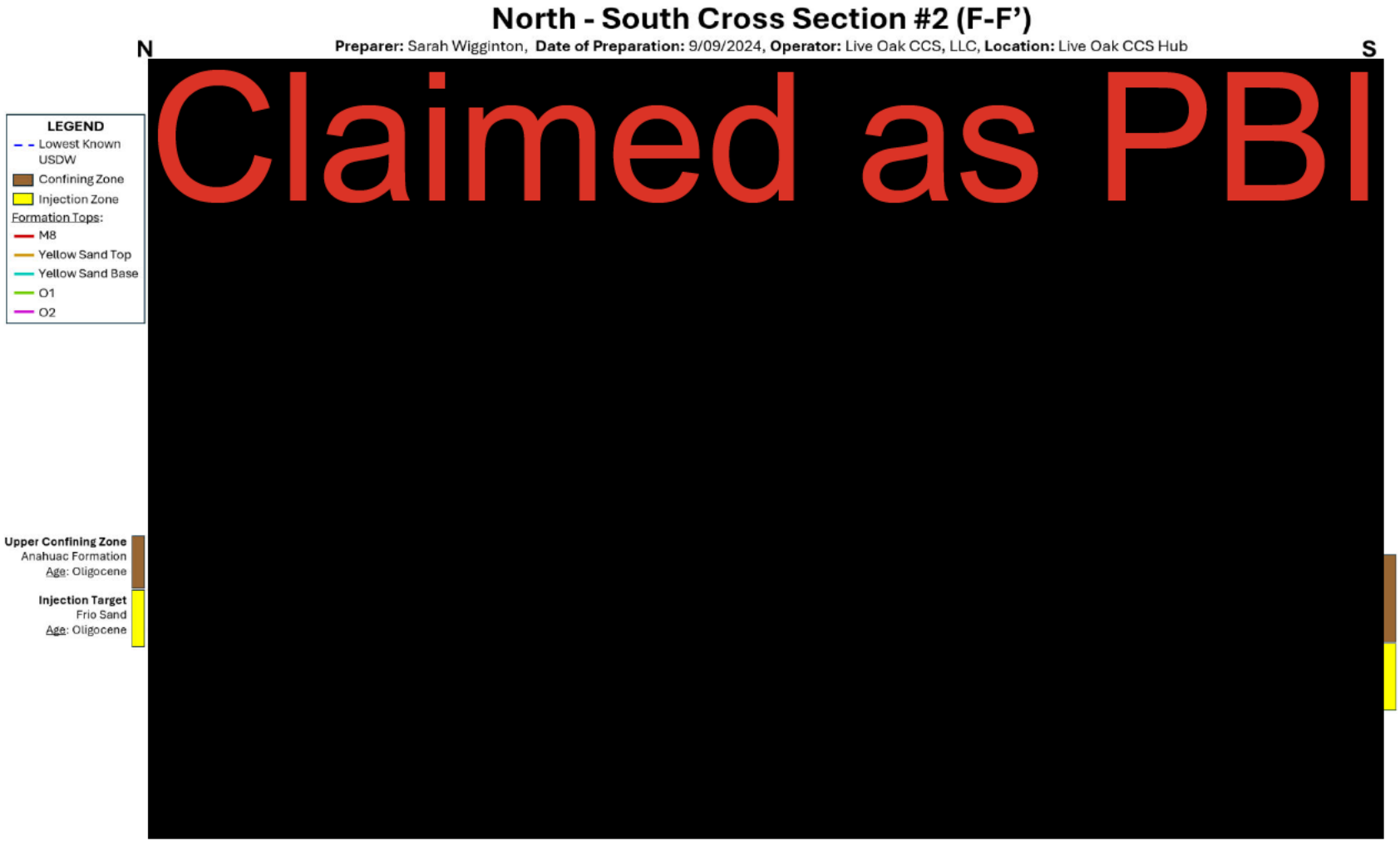

Figure 35: Dip cross section F-F' through the project model domain (see map Figure 32) with the depth track in feet measured depth (far left), normalized gamma ray, the spontaneous potential, and the porosity. Crossing of AoR boundary indicated in red and inferred fault with black-dashed line. For detailed discussions on the petrophysical model and the specific wells used in this analysis, refer to subsection 2.5 of this Application Narrative. For associated well data see Appendix A.

2.3. Faults and Fractures

2.3.1 Known and Suspected Faults

Adjacent to the project area, there is one known and one suspected listric normal fault that is part of a larger east-west trending regional growth fault system spanning the Louisiana Gulf coast (Figure 36). Of the two faults, the known northern fault is part of the Baton Rouge Fault zone, whereas the southern fault is suspected but not observed. The northern Baton Rouge Fault zone is observed both at the surface and in 2-D seismic data which shows an east-west trending listric normal fault system that dips to the south. The southern fault is suspected based on regional mapping of Gagliano (2005) but is not observed in 2D seismic that transects the mapped location of the fault. The Baton Rouge Fault cuts and offsets the proposed injection and confining zones north of the project AOR at a variable distance, ranging from 1.4 mi to greater than 3 mi (Figure 36).

The remainder of this page intentionally left blank.

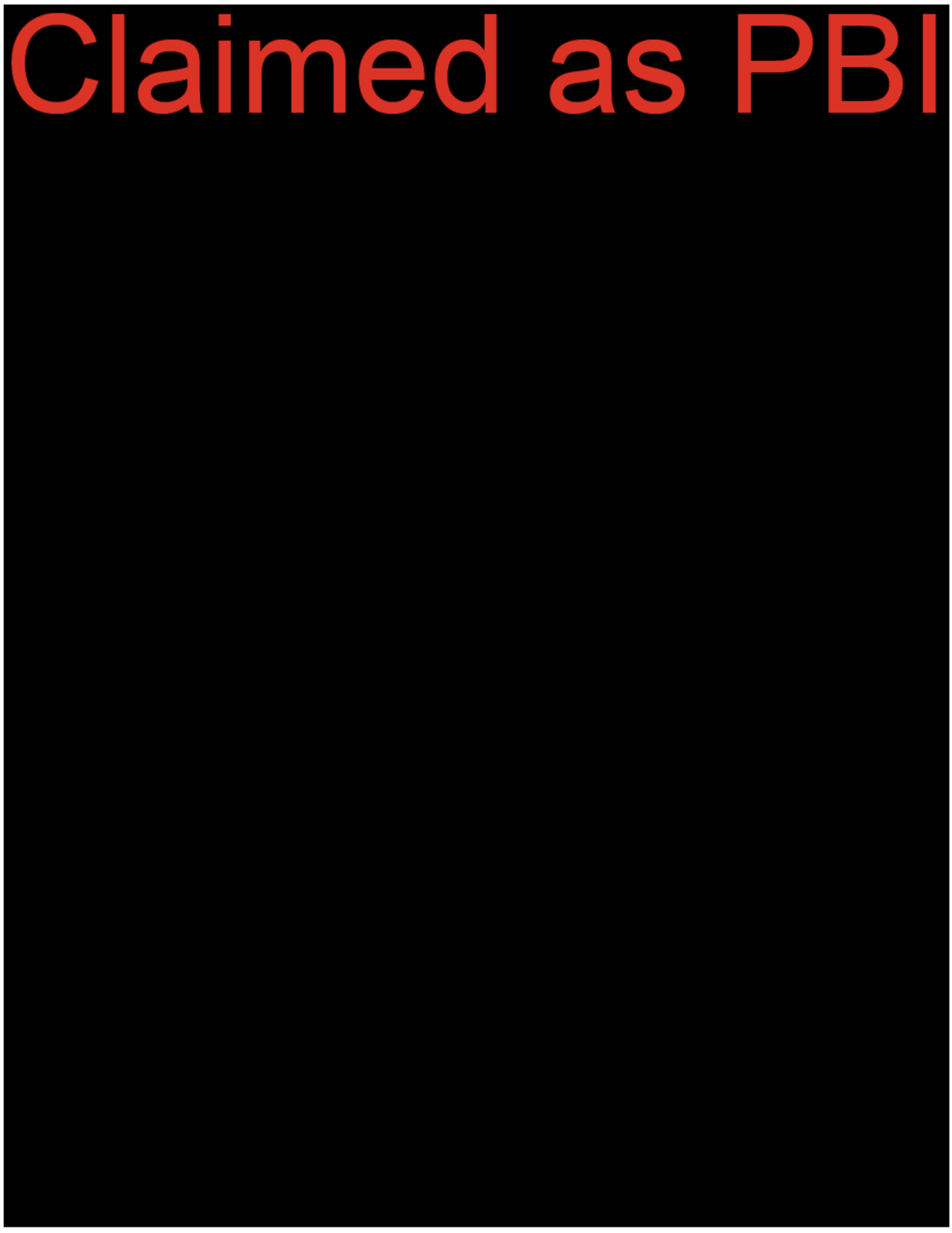

Figure 36: Location map of faults for the Baton Rouge Fault (black with ticks), inferred faults (dashed black), and salt diapirs (cross-hatched black fill). The project AoR is delineated by the thicker black outline.

2.3.2 Seismic Data and Structural Transects

Both 2-D and 3-D seismic data are used to interpret the subsurface geology of the project area. A 25 square mile portion of the Interdomal Bayou Des Glaises 3-D seismic survey was selected to delineate the stratigraphy and geometry of the confining and injection zones in a core area of the project. Eight 2-D seismic lines were used to extend the subsurface interpretation and were strategically chosen to investigate structural complexity (faults, salt diapirs) near the project area (Figure 37, Table 3). All 2-D seismic lines tie to both the 3-D survey and one another allowing for continuous and correlated interpretation across the project area.

Table 3: 2-D Seismic Dataset utilized for project.

Line Name	Line UID	Length (mi)	Channel	Fold	Year Shot	Year Reprocessed
Claimed as PBI	[redacted]	10.5	48	12	1977	2011
Claimed as PBI	[redacted]	27.5	48	12	1976	2011
Claimed as PBI	[redacted]	4.9	24	6	1967	2011
Claimed as PBI	[redacted]	5	48	12	1977	2011
Claimed as PBI	[redacted]	14.4	48	12	1977	2011
Claimed as PBI	[redacted]	4.6	48	12	1978	1978
Claimed as PBI	[redacted]	6.8	24	6	1972	1972

The remainder of this page intentionally left blank.

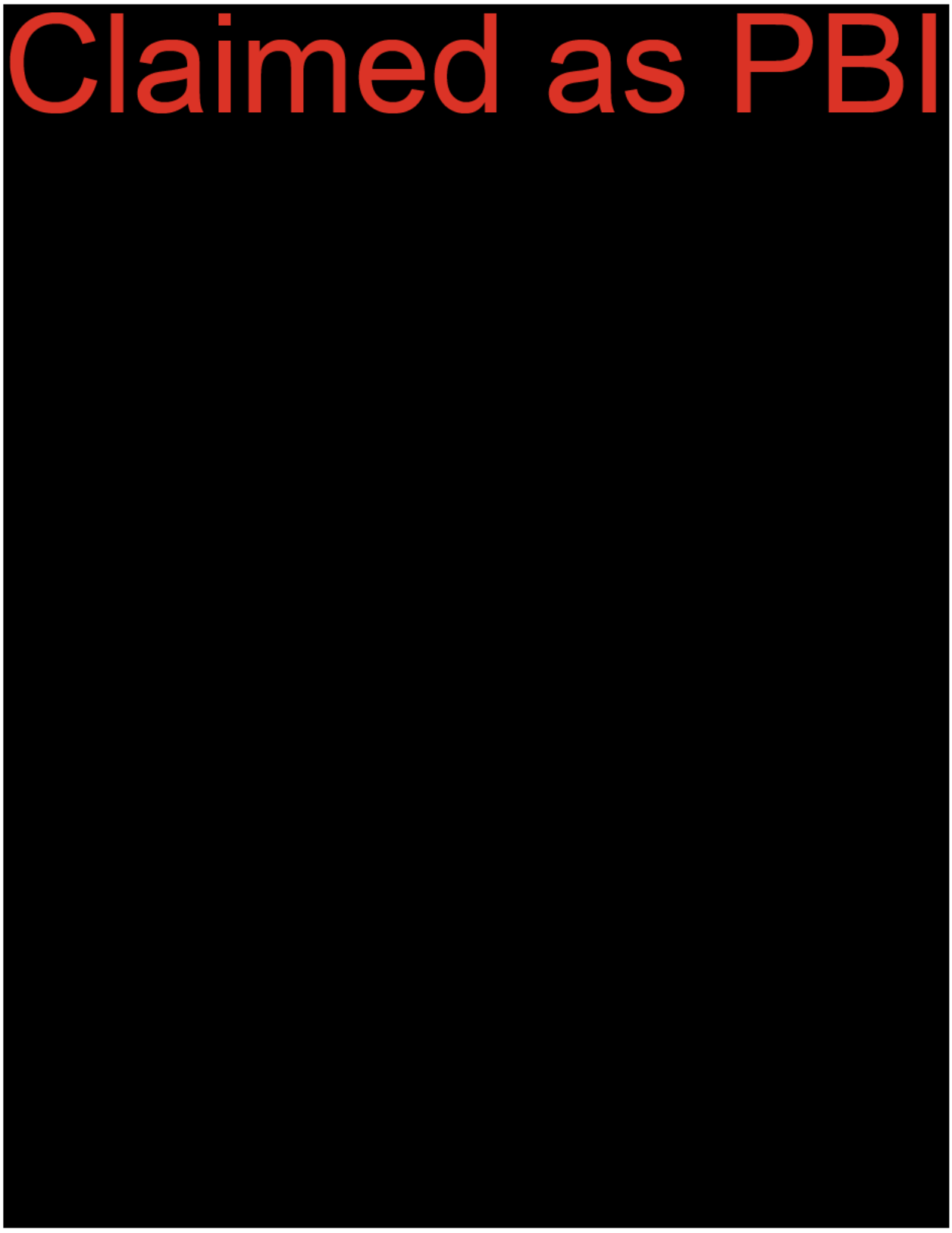

Figure 37: Structural Transects A-E used for kinematic fault analysis of the Baton Rouge Fault system. 2-D seismic lines (green) projected to the transects.

To develop a series of structural transects across the Baton Rouge Fault system, the orientation of the seismically interpreted fault planes was considered relative to the direction of tectonic transport (Figure 38).

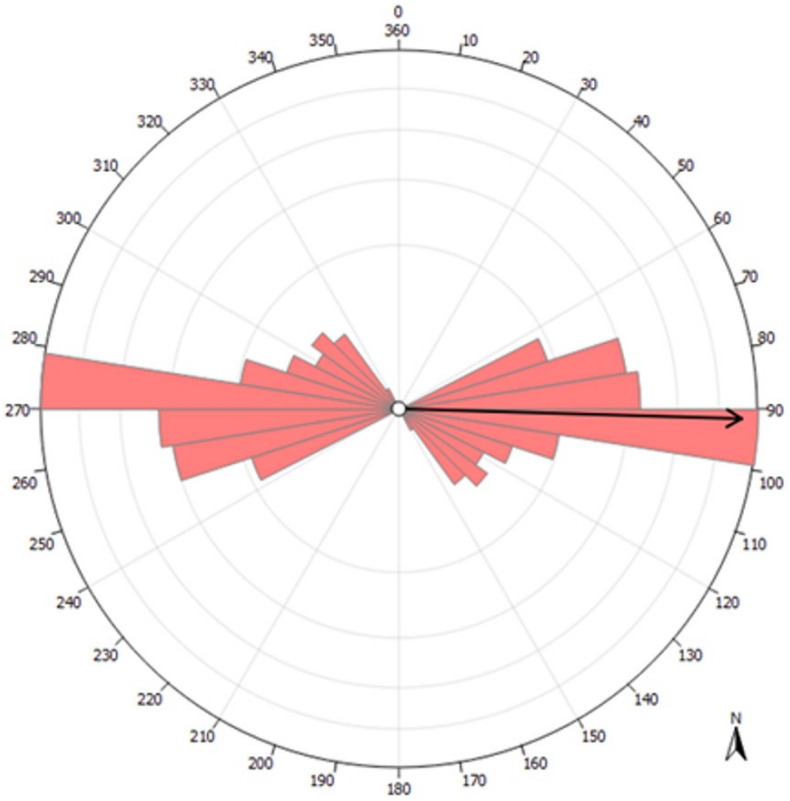

Figure 38: Baton Rouge fault and splay orientations as interpreted from 2-D seismic. The fault system strikes nearly east-west where seismically observed.

A series of four north-south orientated structural transects (parallel to tectonic transport) were developed across the Baton Rouge Fault system to investigate the geometry and character of the fault system (Figure 37, Transects A-D). A fifth, east-west orientated structural transect (Transect E on Figure 37), provides a strike interpretation that ties the dip-normal transects A-D. 2-D seismic data and interpretations were projected normal to the transect to allow for structural and kinematic interpretations in the true dip and strike directions.

2.3.3 Baton Rouge Fault

The geologic history of the Baton Rouge Fault system and details on regional deformation related to salt tectonics near the project area are discussed in subsection 2.1.

2-D seismic data imaging across the Baton Rouge Fault shows listric growth fault geometry with a steeply dipping upper segment that asymptotically flattens and merges with the regional detachment at the Cretaceous/Jurassic level at ~22,500 ft below the surface (Figure 39).

Figure 39: Structural Transect A, 2-D seismic projected from 2-D line [redacted] (see Figure 37 for location). Approximate location of project AoR boundary indicated in red.

The fault geometry is kinematically forward modeled using simple shear with a shear angle of 67° normal to the fault plane. The simple shear geometry is based on the interpreted fold geometry of the hanging wall strata.

The westernmost structural transects, A (Figure 39) and B (Figure 40), show the Baton Rouge Fault as a single fault plane whereas the easternmost transects, C (Figure 41) and D (Figure 42), show two distinct fault planes. As the major listric growth fault systems along the Gulf Coast are often composed of multiple arcuate fault strands that overlap and merge at the ends of the individual fault planes, this is likely an indication of overlapping individual fault strands that merge between structural transects B and C (Figure 37). The structural transects also delineate an older listric normal fault to the north of the Baton Rouge Fault system. This fault was likely active until sometime in the late Eocene based on the offset of stratigraphic horizons and development of growth strata across the fault (Figure 39 through Figure 43). This fault merges into and shares the same detachment level as the Baton Rouge Fault strands.

The remainder of this page intentionally left blank.

Figure 40: Structural Transect B, seismic projected from 2-D line Claimed as PBI (see Figure 37 for location). Approximate location of project AoR boundary indicated in red.

Figure 41: Structural Transect C, seismic projected from 2-D line Claimed as PBI (see Figure 37 for location). Approximate location of project AoR boundary indicated in red.

The remainder of this page intentionally left blank.

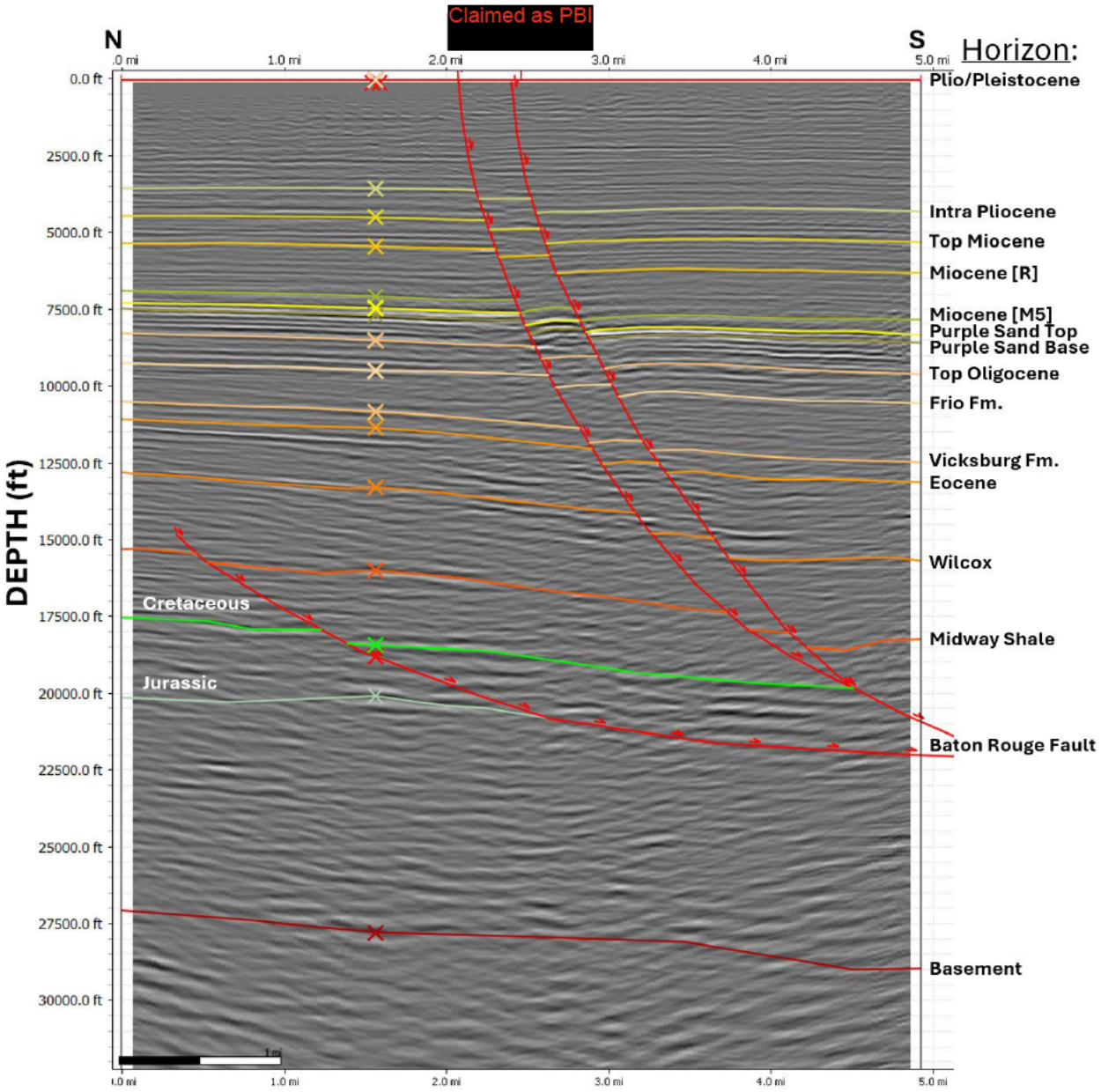

Figure 42: Structural Transect D, seismic projected from 2-D line Claimed as PBI (see Figure 37 for location). Seismic section does not cross project AoR boundary.

The remainder of this page intentionally left blank.

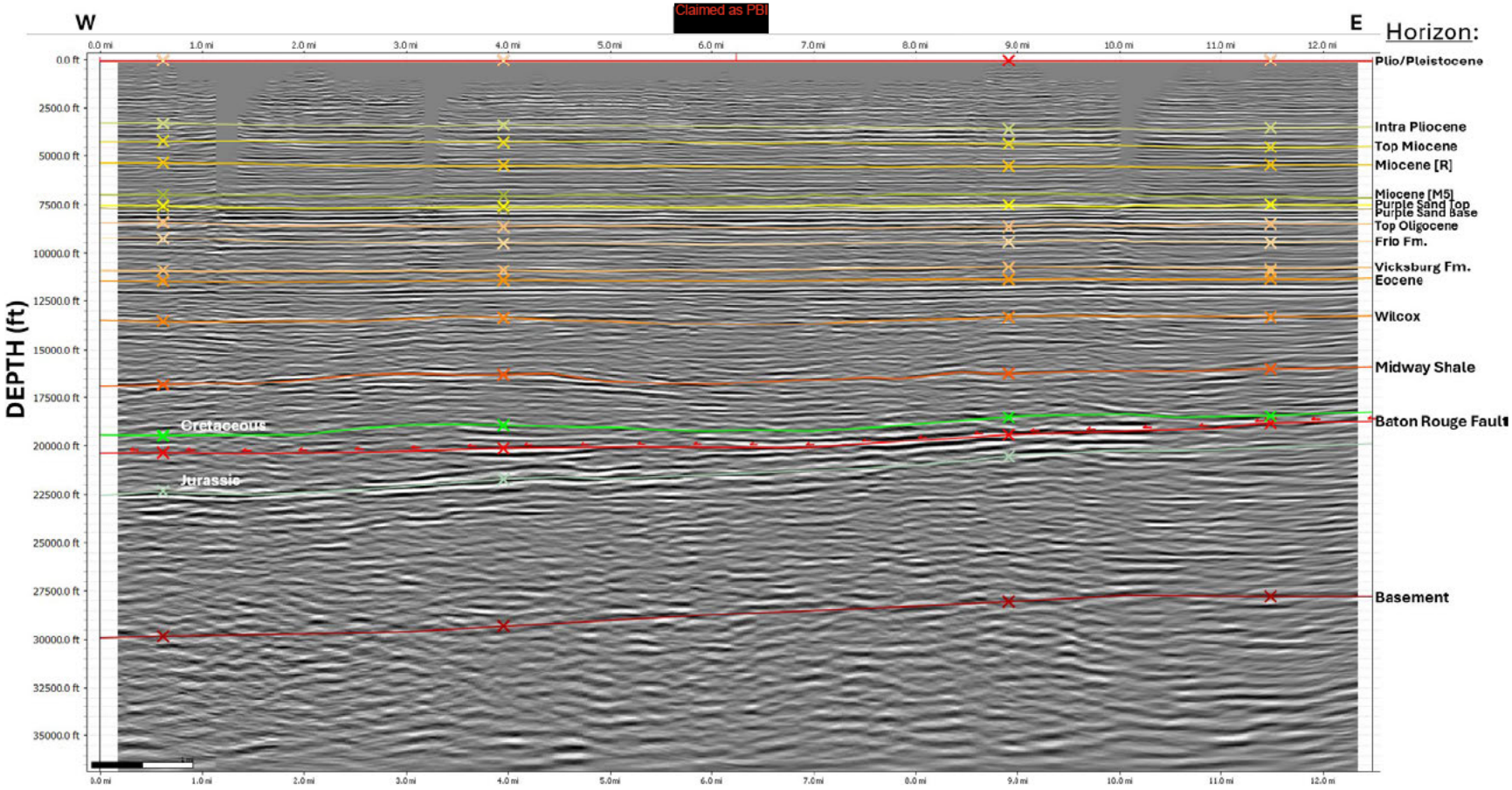

Figure 43: Structural Transect E, seismic projected from 2-D line Claimed as PBI (see Figure 37 for location map). Seismic section does not cross project AoR boundary.

As interpreted from seismic, the Baton Rouge Fault system has been active at various stages throughout the Cenozoic with stratigraphic offset and throw generally increasing with depth and age (Figure 44). Structural sections show smaller amounts of throw throughout the Pleistocene-Pliocene stratigraphic sections (Figure 39) with increasing throw throughout the Miocene, Oligocene, and Eocene sections respectively (Figure 39). The amount of throw of mapped stratigraphic horizons ranges from ~300 to 1250 feet, with generally larger amounts of throw observed where the fault is a single strand along the western side of the project area and smaller amounts of throw where the fault is comprised of two fault strands to the east (Figure 44).

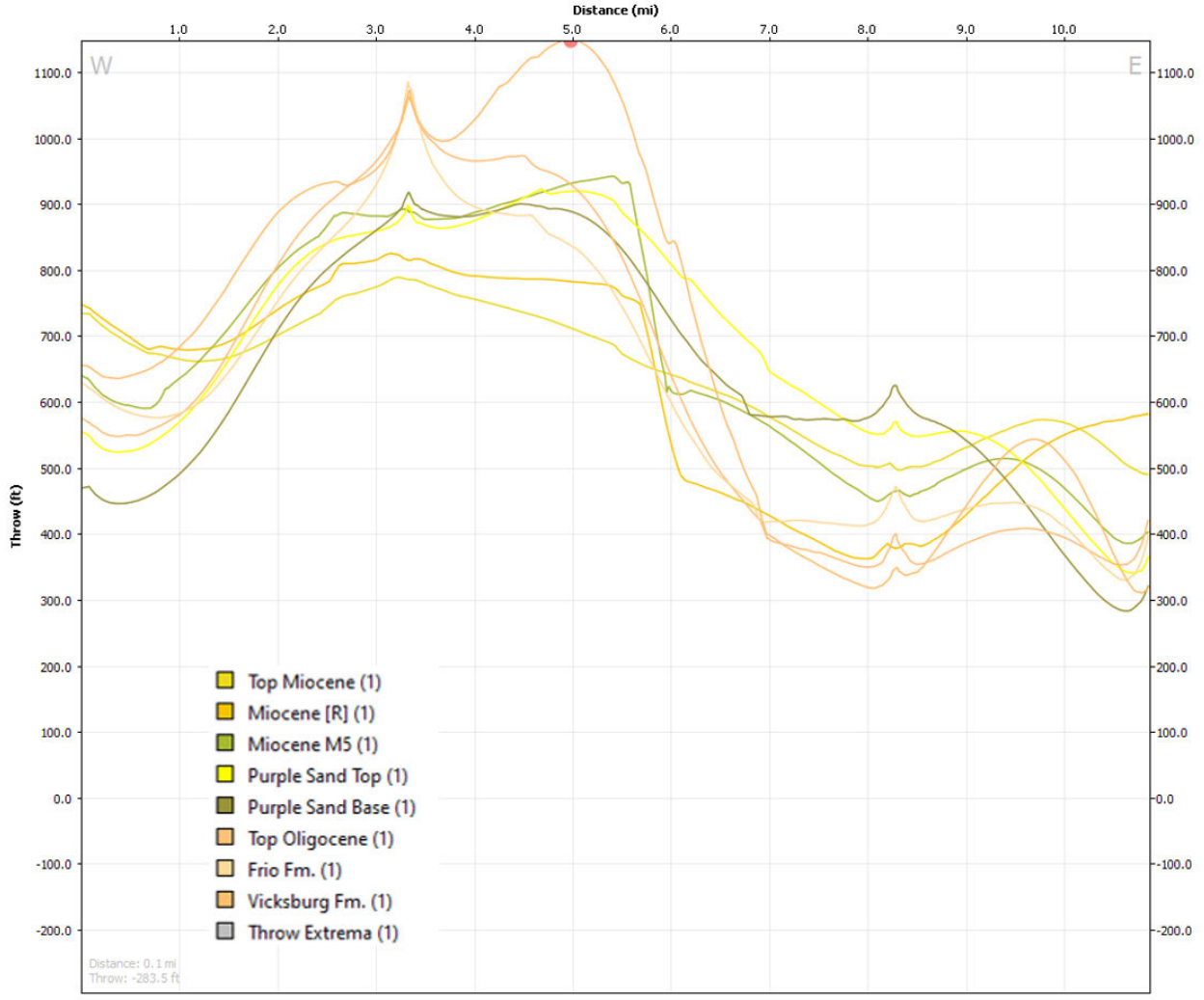

Figure 44: Diagram of fault throw versus distance from west to east along the interpreted structural transects of the Baton Rouge Fault.

Episodic slip on the Baton Rouge Fault system is related to time-varying sedimentation along the Gulf Coast: when sediment loading is sufficiently high, gravitationally driven sliding occurs on the underlying Jurassic Louann salt (Figure 39 through Figure 43). Slip on the Louann detachment is then accommodated by extensional faulting in the overlying Cenozoic sediments. Growth on the

Baton Rouge Fault is also recorded by stratigraphic thicknesses that increase from the footwall to hanging wall resulting from increased accommodation in the hanging wall. Seismic sections from the project area show that both the Miocene and Oligocene injection and confining zones all expand on the hanging wall side of the Baton Rouge Fault system by 300-1000' and display moderate rollover anticline development (Figure 39 through Figure 42).

Overall, the Baton Rouge Fault system is expressed as either a single fault plane or two discrete fault planes that are well defined by seismic and structural transects north of the AoR. Both the fault plane(s) and representative geometry of the hanging wall were used in simulation and modelling, and both the pressure and CO_2 plume for all injection zones remain approximately 1 mile or more away from the fault for 150 years post-injection (see subsection 3.2 of the Area of Review and Corrective Action Plan). Simulation indicates neither pressure or CO_2 plumes would interact with the Baton Rouge Fault system throughout the lifetime of the project and, therefore, do not pose a risk to containment. A fault seal analysis for the Baton Rouge Fault system is presented below.

2.3.4 Baton Rouge Fault Sealing Capacity and Fluid Flow

The sealing capacity of the Baton Rouge Fault in the project area is examined both through fault seal analysis and observations of fault-fluid interactions from aquifers and hydrocarbon fields. Several observations from both aquifer and hydrocarbon systems along the fault system provide some evidence for the sealing capacity of the fault system. These observations include changes in groundwater aquifer salinity across the fault and demonstrated fault seal at the Port Arthur and Lobdell fields indicating that the Baton Rouge Fault can act as a barrier to fluid flow, discussed in further detail below.

In addition to observational data on the fault-fluid interaction along the Baton Rogue Fault system, a fault juxtaposition and fault seal analysis investigation of the Baton Rouge Fault system was completed along the kinematically modeled structural transects presented above to better understand the fault's sealing capacity and capability.

2.3.4.1. Observations of fault-fluid interactions

In the case of the Baton Rouge aquifers, the locally named 400 to 2,800 foot sands are offset by the Baton Rouge Fault and generally contain fresh water in the footwall north of the fault but saline water in the hanging wall south of the fault (Figure 45; Nasreen 2003; Tomaszewski, 1996). The 2,400 and 2,800 foot sands are part of the Miocene Hattiesburg formation within the proposed injection and confining zone. While some saline intrusion into the shallower aquifers has occurred into the footwall of the Baton Rouge Fault due to pumping, the 2,400 foot sand aquifer is entirely fresh in the footwall. The 2,800 foot sand aquifer is naturally saline in the immediate footwall of the Baton Rouge Fault, possibly due to incomplete flushing by freshwater recharge to the north (Whiteman, 1979; Tomaszewski, 1996). Consistent with growth fault behavior, the 2,400 and 2,800 foot sands show greater offset than the shallower aquifers (hundreds of feet, Figure 45). This may indicate that lithologic juxtaposition across the Baton Rouge Fault plays an important role in the transmissibility of fluids across the fault.

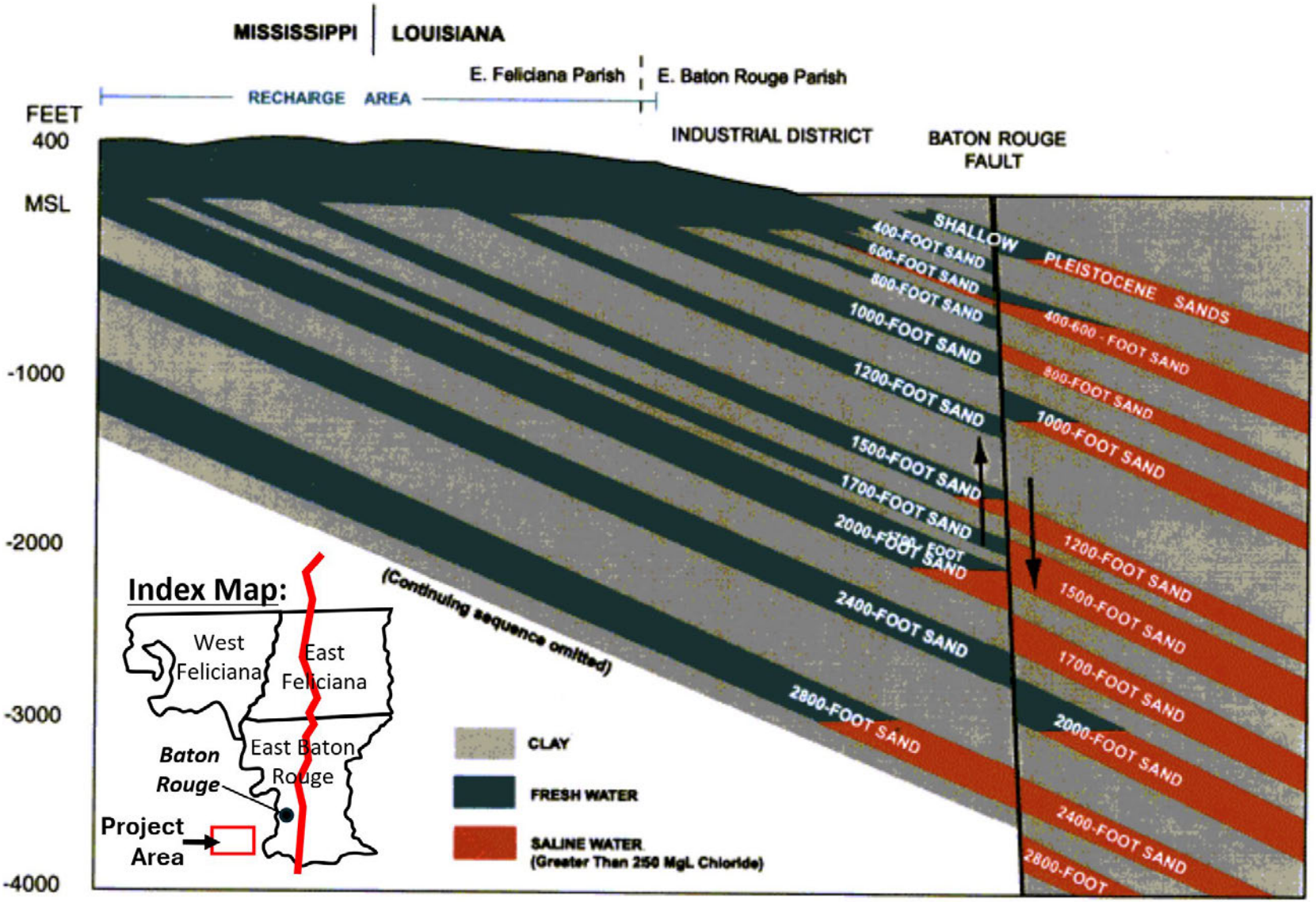

Figure 45: From Nasreen (2003): "Hydrologic cross section including saline water intrusion in the East Baton Rouge Parish and the surrounding region" (adopted from Tomaszewski, 1996).

Structural hydrocarbon traps in the nearby Port Arthur and Lobdell fields also provide evidence for viable fault seals on growth faults similar to the Baton Rouge fault system. Both fields produce from various levels within the Frio Formation. The reservoirs, located in the hanging walls of high angle, are east-west trending growth faults that dip to the south, similar to the Baton Rouge Fault system (Figure 46; Goddard et al., 2005). The Lobdell field to the north contains water in the Upper Frio and hydrocarbons in the lower Frio zone. Crossing a growth fault to the south, the Port Allen field produces hydrocarbons from both the Upper and Lower Frio zones. Notably, a key biostratigraphic marker horizon within the Frio shows only 50 feet of throw across the Lobdell field fault, whereas the Port Allen fault has an average of 500 feet of throw for the same marker. The variation in fluid contacts across the Port Allen and Lobdell field faults suggests some level of sealing capacity on the growth faults that is potentially related to fault throw and stratigraphic juxtaposition.

The remainder of this page intentionally left blank.

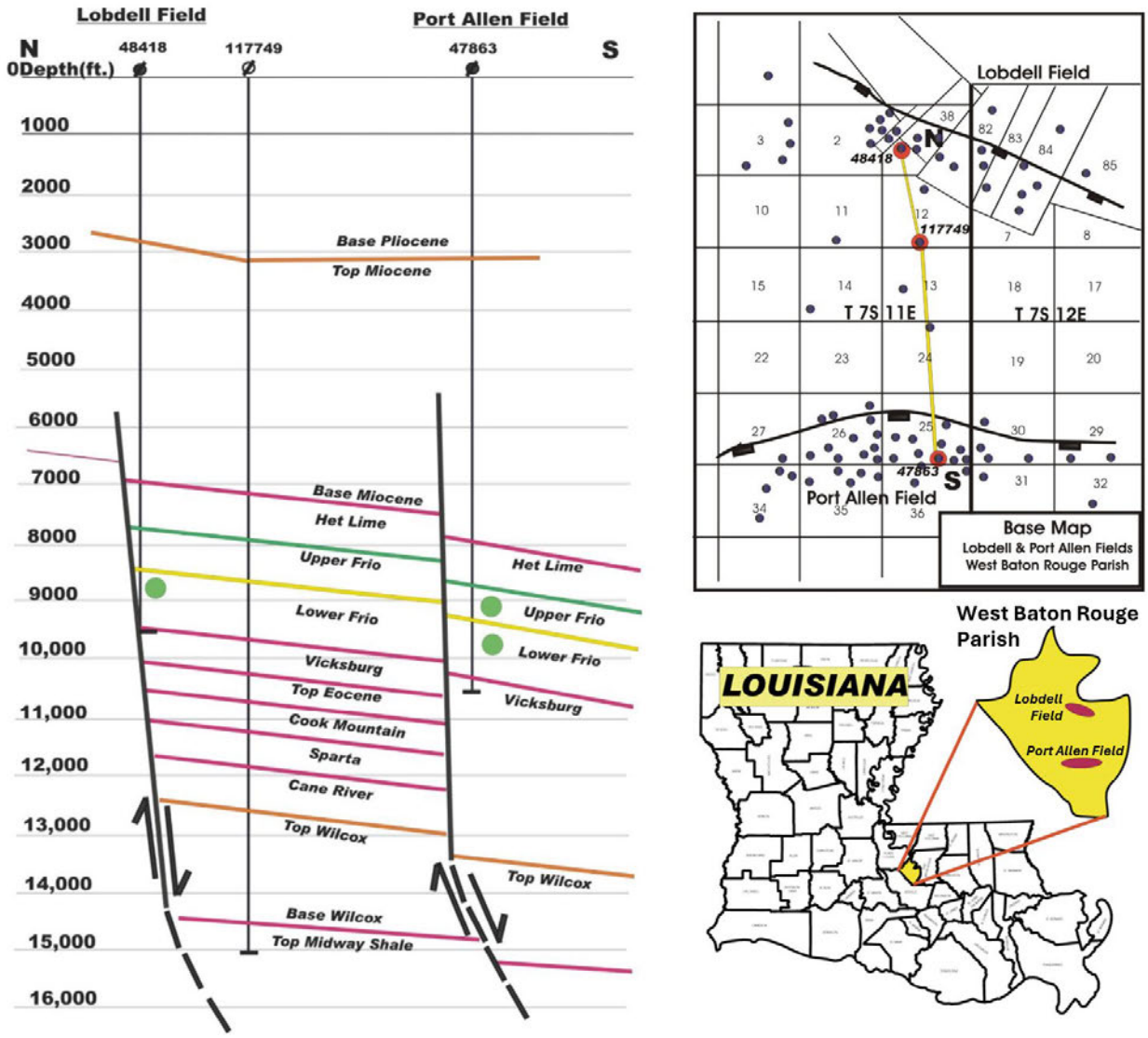

Figure 46: Structural cross section of Lobdell and Port Allen fields. (Figure adapted from Goddard et al., 2005)

2.3.4.2. Fault Juxtaposition and Fault Seal Analysis Methodology

Faults can act as either a conduit for vertical and across-fault fluid migration or as a baffle or seal to these same fluid flow processes (Childs et al., 2002; Yielding et al., 2010). Whether a fault acts as a conduit or barrier to migration depends on several factors (Figure 47):

- Lithologic Juxtaposition: Across-fault seal results from the geometric juxtaposition of reservoir rocks in the hanging wall against non-reservoir rocks in the foot wall (Allan, 1989).

- Membrane or Cataclasis Seal: The mechanical breakdown (cataclasis) of rocks within the fault zone (fault gouge) develops a barrier to fluid flow (Knipe et al., 1998, Yielding et al., 1997).

- Shale or Clay Smear: Where the incorporation of fine-grained material (clay-rich sediments) into the fault zone through 'smearing' during fault displacement increases the sealing potential of the fault (Lindsay et al., 1993).

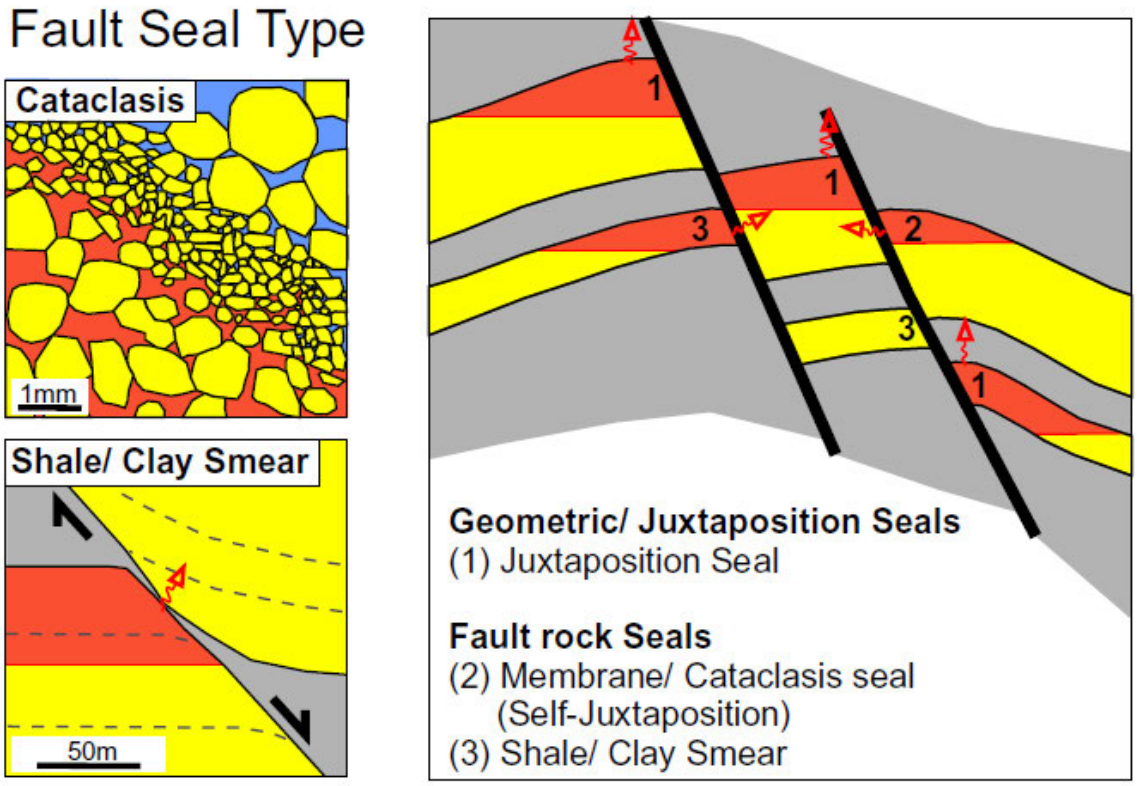

Figure 47: Types of fault seal from Oligvie et al., 2020.

The lithologic juxtaposition of reservoir and non-reservoir rocks across the fault is a geometric description of general rock lithology across the fault (Figure 47) that is developed from seismic interpretations and prescribed lithologic properties from petrophysical studies (see subsection 2.4 of this Application Narrative). The probability of the fault sealing or being a conduit to fluid-flow is displayed through an Allan diagram or map (Allan, 1989), where a shale-on-shale contact would have the greatest likelihood of providing an effective seal and a sand-on-sand contact would have the least likelihood of preventing cross-fault fluid migration.

While juxtaposition diagrams can be used to assess the geometric sealing capacity of a fault system, the overall sealing capacity of the fault system can be influenced by the incorporation of clay-rich content into the fault zone, either through mechanical incorporation during cataclasis (Shale Gouge Ratio, SGR), or 'smearing' of low permeability clays across the fault surface (Shale Smear Factor, SSF).

Both SGR and SSF are quantitatively determined through the following algorithms from Yielding et al. (1997):

$$SGR = \frac{\sum[(zone\ thickness)x(clay\ content)]}{fault\ throw} \quad \text{Eq 1}$$

To assist with interpretation of the results from SGR calculations, Childs et al. (2009) demonstrated that fault seal can occur at SGR values of 0.2 or greater by using migration modeling.

The following equation from Lindsay et al. (1993) was used to analyze approximately 80 faults, where it was found that SSF values greater than 7 resulted in incomplete or ineffective shale smear:

$$SSF = \sum \frac{fault\ throw}{thickness\ of\ clay\ zone} \quad \text{Eq 2}$$

Total clay content for both SGR and SSF calculations can be determined from petrophysics (*Vshale*) or estimated based on general rock lithology. For the purposes of this study the overall clay content for each lithologic unit was estimated from the petrophysical study presented in subsections 2.4 and 2.5 of this Application Narrative.

2.3.4.3. Results of Fault Juxtaposition and Fault Seal Analysis

Allan maps and diagrams describing the lithologic juxtaposition of geologic units across the Baton Rouge Fault system were developed from the four structural transects presented above (Figure 37). Figure 48 shows the resulting lithologic juxtaposition across the fault plane interpreted from seismic and kinematically modeled.

The remainder of this page intentionally left blank.

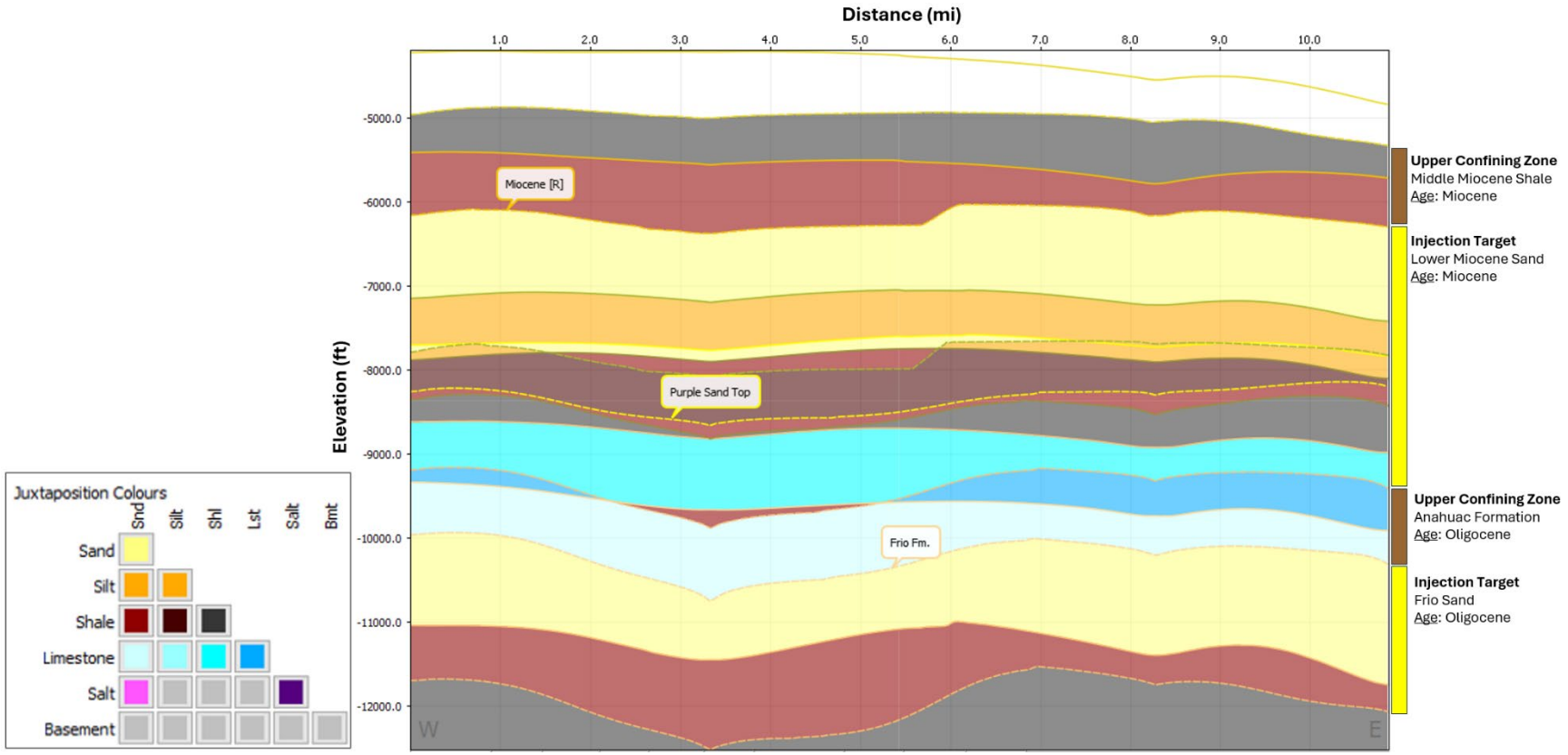

Figure 48: Allan diagram showing the lithologic juxtaposition of stratigraphic units on the W-E cross-section across the Baton Rouge Fault system north of the AoR. Solid lines indicate foot wall cutoffs of stratigraphic units, whereas dashed lines indicate hanging wall cutoffs of the same units. Several key stratigraphic zones are noted, these include the Miocene [R], the Purple Sand Top, and the Frio Formation.

The Middle Miocene Confining Zone (above Miocene [R]) exhibits a shale-on-sand juxtaposition (Figure 48 and Figure 49) and is therefore more likely sealing. The upper reservoir interval below the Miocene [R] has a sand-on-sand contact (Figure 48 and Figure 49), which from a purely geometric standpoint could allow across-fault fluid flow. Therefore, fault sealing capability of the Lower Miocene Sand injection zone would require fault membrane sealing should it encounter fluids This scenario is discussed below for both the SGR and SSF calculations.

Both the Middle Miocene Confining Zone and Lower Miocene Sand injection zones exhibit lithologic juxtapositions that are likely fault sealing, with these being shale-on-silt, shale-on-shale, and shale-on-sand juxtapositions (Figure 48 and Figure 49).

The OFIC confining zone shows a limestone-on-sand juxtaposition, whereas the injection zone has a sand-on-sand lithologic juxtaposition (Figure 48 and Figure 49).

SGR was calculated using Equation 1 above for each structural transect (Figure 37) and mapped to the Baton Rouge Fault plane (Figure 50 and Figure 51).

The remainder of this page intentionally left blank.

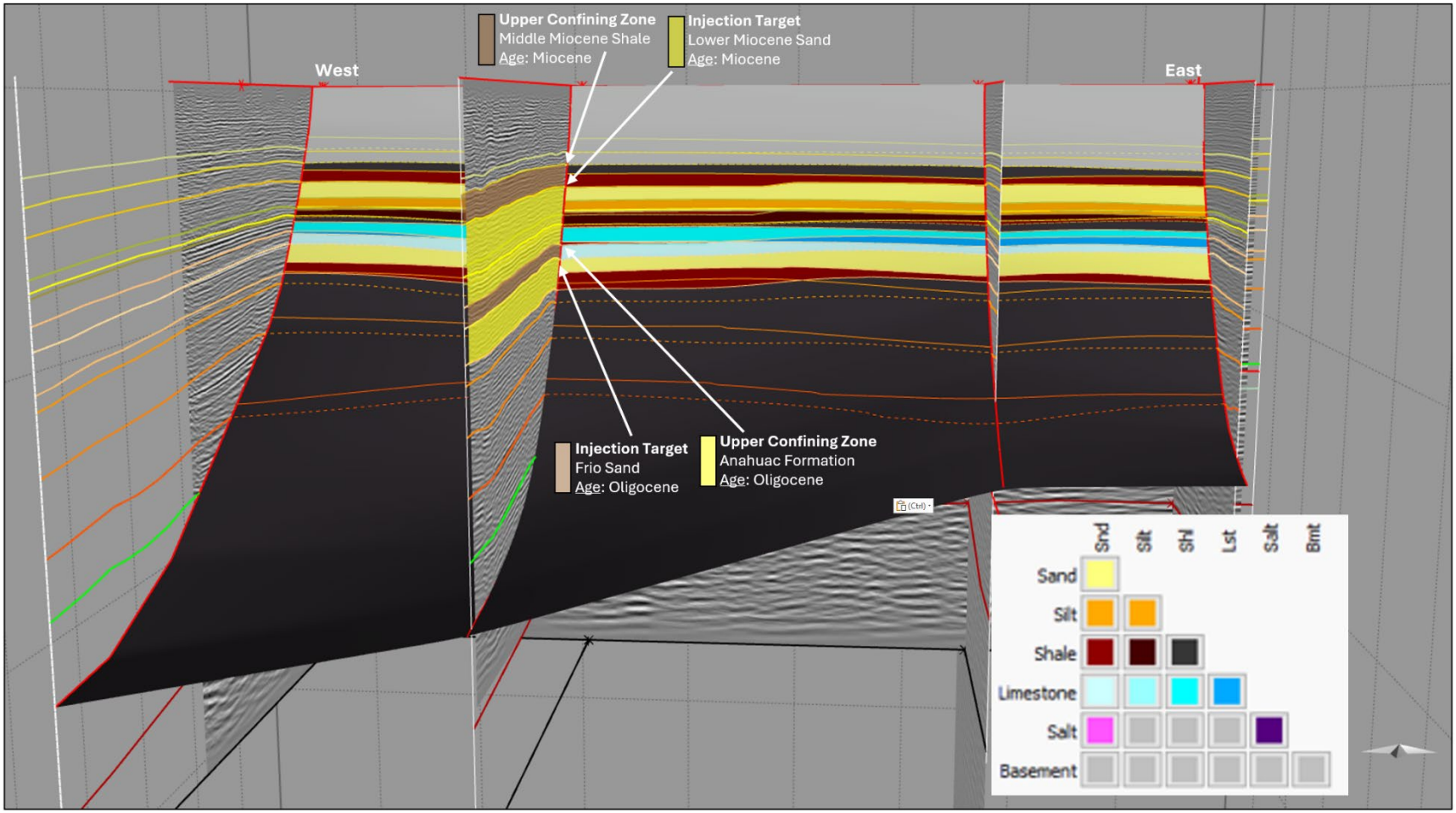

Figure 49: Three-Dimensional view of the Baton Rouge Fault plane modelled from structural transects A-E, viewed from the south looking to the north. The lithologic juxtapositions across the hanging wall and foot wall of the fault system are projected onto the Baton Rouge Fault plane. Solid lines projected onto the fault plane represent the foot wall cutoffs for respective stratigraphic horizons, whereas dashed lines projected onto the fault plane represent the respective stratigraphic hanging wall cutoffs.

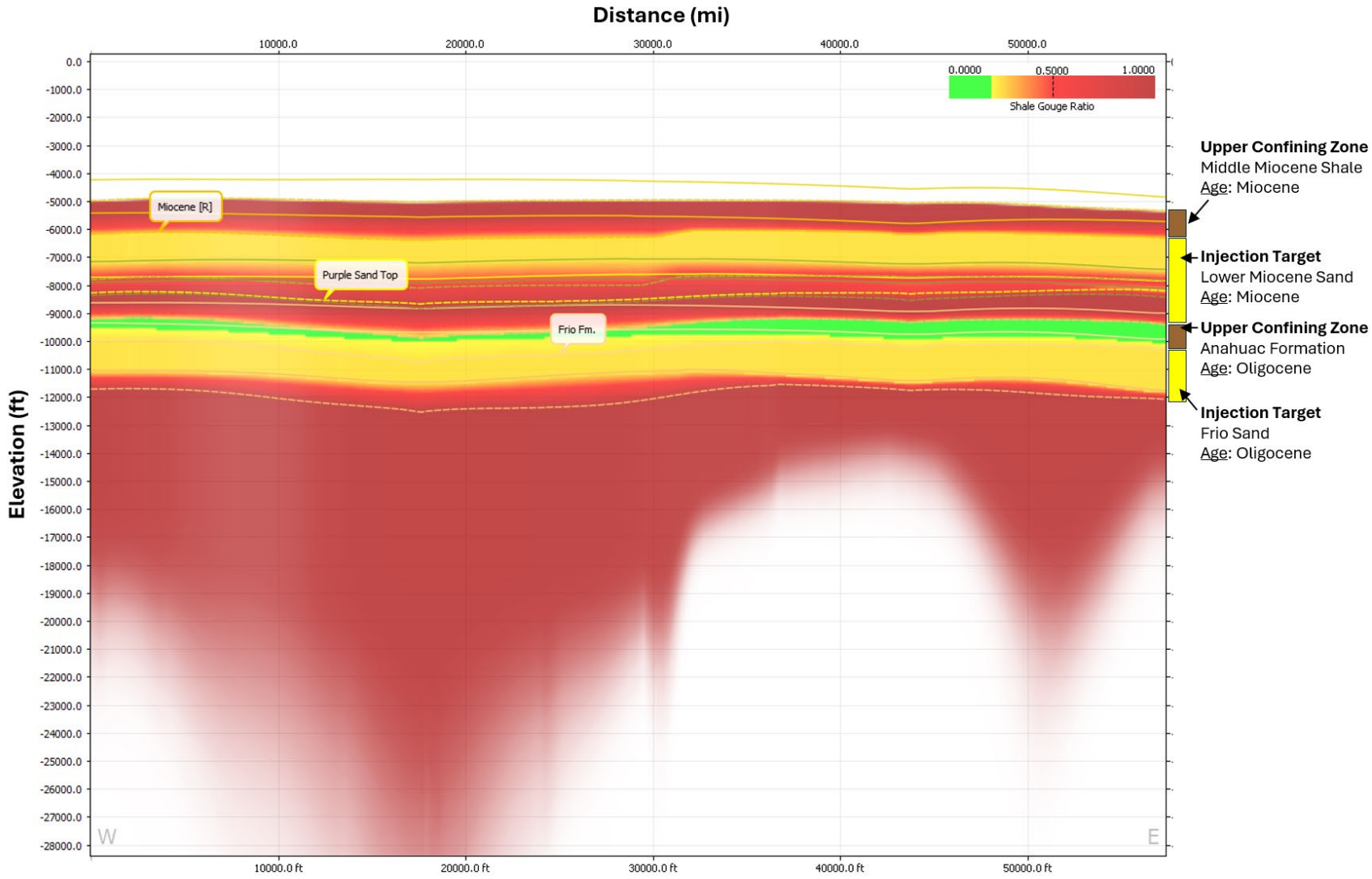

Figure 50: Shale gouge ratio calculated on the W-E cross-section across the Baton Rouge Fault. Solid lines indicate foot wall cutoffs of stratigraphic units, whereas dashed lines indicate hanging wall cutoffs of the same units. Several key stratigraphic zones are noted, these include the Miocene [R], the Purple Sand Top, and the Frio Formation. Shale gouge ratios less than 0.2 are shown in green and may represent an ineffective seal. See Figure 37 for location of the Baton Rouge Fault system relative to the project AoR.

SGRs calculated across the Baton Rouge Fault suggest that in almost all stratigraphic and geographic locations, the fault may act as an effective seal. There is one distinct interval of SGR < 0.2 that is above the OFIC injection and confining zones. It should be noted that the proxy of SGR for this interval suggests that all of the Frio Formation injection zone should have a SGR > 0.2, and within the confining zone, there is an interval of several hundred feet (at a minimum) that has an SGR of greater than 0.2 (Figure 50 and Figure 51).

The remainder of this page intentionally left blank.

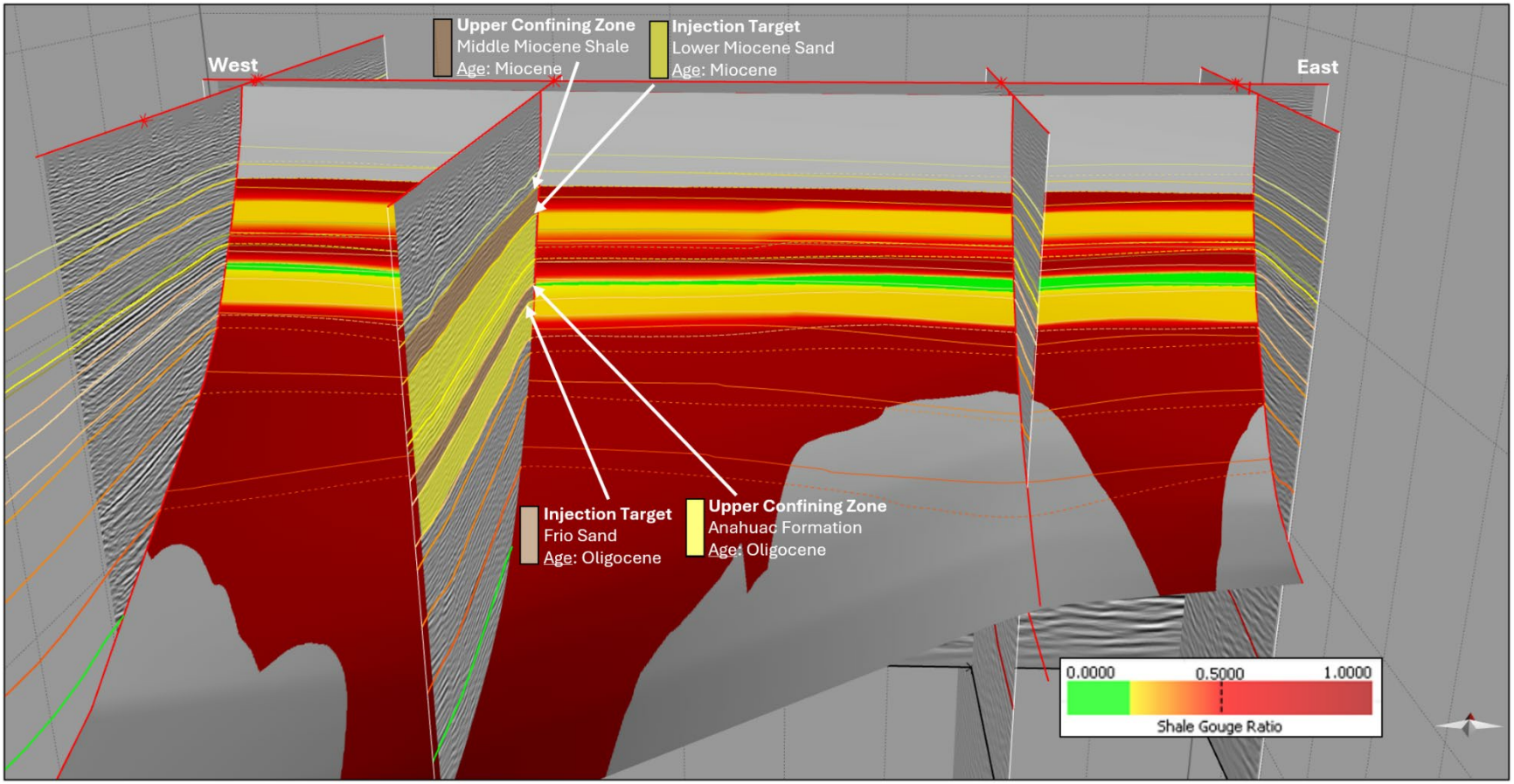

Figure 51: Three-Dimensional view of the Baton Rouge Fault plane modelled from structural transects A-E, viewed from the south looking to the north. The calculated shale gouge ratio (SGR) is projected onto the Baton Rouge Fault plane. Solid lines projected onto the fault plane represent the foot wall cutoffs for respective stratigraphic horizons, whereas dashed lines projected onto the fault plane represent the respective stratigraphic hanging wall cutoffs. SGR values < 0.2 are shown in green, whereas values 0.2 and greater are shown in yellow to red and likely represent ratios of shale gouge that could be an effective fault seal.

SSF was calculated using Equation 2 presented above for each structural transect (Figure 37) and mapped to the Baton Rouge Fault plane (Figure 47). Both the upper Miocene and Frio Formation injection zones and portions of the confining zone have shale smear factors greater than 7, indicating that the amount of shale smear is likely inadequate to present an effective seal on its own (Figure 52). The Middle Miocene Confining Zone and Lower Miocene Sand injection zone both have a SSF < 7 and are likely an effective seal based on shale smear factor alone (Figure 52).

Overall, when lithologic juxtaposition and fault membrane sealing parameters are considered holistically across the Baton Rouge Fault system, it appears that one or more of the sealing mechanisms is likely adequate for the fault system to act as a barrier to fluid flow. Given the integration of the quantitative assessment of the fault's sealing capacity with observational data related to both aquifer and hydrocarbon systems, the Baton Rouge Fault system is not likely a conduit for vertical or across-fault fluid migration. Furthermore, reservoir simulation and modeling efforts demonstrate that neither the pressure nor CO_2 plumes should migrate northward to and interact with the Baton Rouge Fault system.

The remainder of this page intentionally left blank.

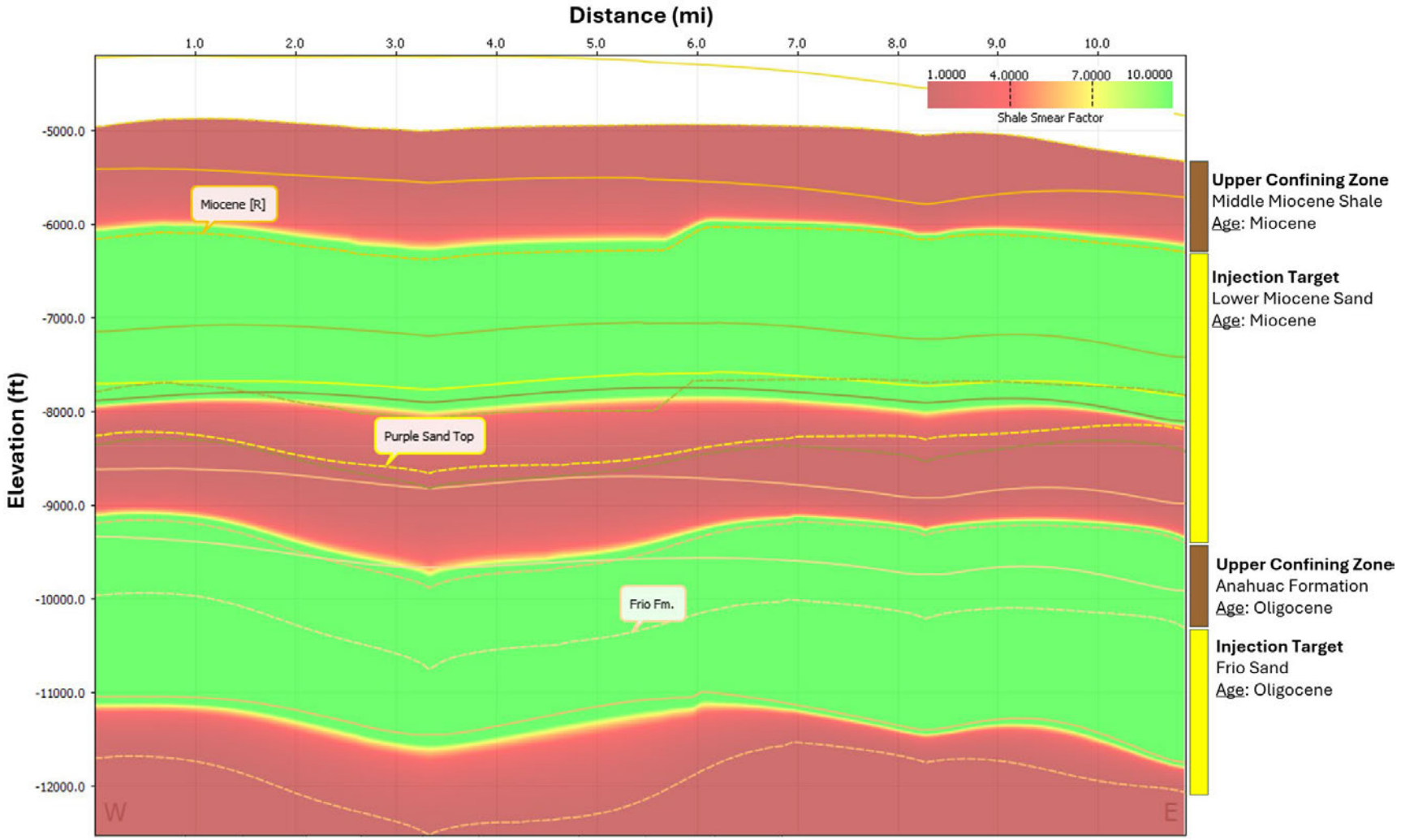

Figure 52: Shale smear factor calculated on the W-E cross-section across the Baton Rouge Fault system. Solid lines indicate foot wall cutoffs of stratigraphic units, whereas dashed lines indicate hanging wall cutoffs of the same units. Several key stratigraphic zones are noted, these include the Miocene [R], the Purple Sand Top, and the Frio Fm. Shale smear factors greater than 7 (yellow to green) suggest that the clay content in the fault zone is inadequate to provide an effective seal. See Figure 37 for location of the Baton Rouge Fault system relative to the project AoR.

2.3.5 Fault Stability

In terms of stability, the Baton Rouge Fault is considered active in present time as it has geomorphic surface expression and offsets Holocene to recent sediments in well and seismic data (Frank, 2017; Gagliano et al., 2003; Lopez et al. 1997). The detachment level for the Baton Rouge Fault and associated growth faults in the area is within the Louann Salt (see subsection 2.1.5 above). At temperatures over 100˚C (reached at approximately 3.2 kilometers in the general area), salt deformation is ductile rather frictional, implying that any slip on the detachment at 7 to 10 kilometers will likely be aseismic (Dokka et al., 2006). The few documented earthquakes in the project area likely occurred on smaller faults or were limited to shallow sections of the main Baton Rouge fault system (see subsection 2.6 below for more discussion of seismic history).

2.4. Injection and Confining Zone Details

The stratigraphic column in the project area is shown in Figure 53. There are an estimated 10-12 kilometers of sediments (Sawyer et al., 1991) deposited on top of mid-Jurassic Louann Salt in the project area (Figure 53). Many stratigraphers consider the relatively unexplored sediments below the Louann Salt as basement due to their lack of economic oil and gas potential and depths (Sawyer et al., 1991), which in the project area far exceed the 13,000 foot hypothetical depth of technical ability to inject CO_2 defined by Burruss et al. (2009), Brennan et al. (2010), and Blondes et al. (2013). There are freshwater aquifers found in Plio-Pleistocene age rocks and oil and gas production in the Upper Cretaceous through Middle Miocene strata (Goddard, 2015).

Dedicated subsurface mapping and analyses in the project area identified two intervals of stacked siliciclastic, porous saline reservoir targets that have sufficient upper and lower confining zones for CO_2 sequestration and occur below 3000 ft depth for super-critical CO_2 storage (Burruss et al., 2009; Brennan et al., 2010; and Blondes et al., 2013). The target zones within the AoR are greater than a mile laterally and greater than 1,000 vertical feet from existing oil and gas accumulations. Two potential injection complexes, each composed of an upper confining zone, a lower confining zone, and an injection zone, have been identified (Figure 53). The two injection complexes are: (1) CCS System 1: Lower Miocene Injection Complex (LMIC) and (2) CCS System 2: Oligocene Frio Injection Complex (OFIC). Throughout this permit, when referring to the entire injection complex, the nomenclature outlined above will be used, and when describing or indicating specific intervals, the Group, Formation, or appropriate formal interval (i.e., “Shale”) name will be used.

The remainder of this page intentionally left blank.

Era	Period	Epoch	Series	Group or Formation	Aquifer, Confining Zone or Reservoir	Oil Gas Prod.	Average Depth (ft)	Average Thickness (ft)	LO-01 M	LO-01 F	LO-02 M	LO-03 M	LO-04 F-M	LO-05 M	LO-06 M	LO-06 F
Cenozoic	Quatern.	Holo.		Alluvium	Freshwater Aquifers		0	550								
		Pleis.					550	450								
	Tertiary	Plio.		Undifferentiated			1,000	1,300								
		Mio-Plio			Base Lowermost USDW: 2,300-2,500'		2,300	1,865								
		Miocene	Upper	Upper Miocene	*Seal (Shale)*		4,165	735								
			Middle	Middle Miocene Confining Zone	Confining Zone		4,800	1,340	5,241 / 854	5,241 / 854	4,782 / 1,071	4,275 / 1,517	4,275 / 1,560	4,238 / 1,357	3,940 / 1,263	3,940 / 1,263
			Lower	Lower Miocene Sand (1 LMIC)	Injection Zone	●●	5,506	3,140	6,095 / 2,822	6,095 / 2,822	5,852 / 2,959	5,793 / 3,546	5,834 / 3,655	5,595 / 3,779	5,203 / 3,663	5,203 / 3,663
		Oligocene	Upper	Anahuac Form.	Confining Zone	●●	8,580	1,492	8,917 / 1,814	8,917 / 1,814	8,811 / 1,384	9,339 / 1,115	9,489 / 1,353	9,374 / 977	8,867 / 698	8,867 / 698
			Middle	Frio Formation (OFIC 2)	Injection Zone	●●	9,506	877	10,731 / 1,152	10,731 / 1,152	10,195 / 1,014	10,454 / 816	10,842 / 867	10,351 / 860	9,565 / 776	9,565 / 776
			Lower	Vicksburg Shale	Confining Zone		10,383	500[1]	11,882 / ~500	11,882 / ~500	11,209 / ~500	11,269 / ~500	11,709 / ~500	11,212 / ~500	10,340 / ~500	10,340 / ~500
		Eocene	Late	Jackson	*Seal (Shale, limestone)*		10,883	700[2]								
			Middle	Claiborne Group: Cockfield, Cook Mtn, Sparta Sand, Cane River Fm, Carrizo Sand	*Seal (Shale)* / *Seal (Shale)*	●●	11,583	1,800[2]								
			Early	Wilcox Group	*Conventional Oil/Gas Reservoir (interbedded shale)*	●●	13,383	3,250[3]								
		Paleo.	Late													
			Early	Midway Group	*Seal (Shale)*		16,633	2,500[4]								
Mesozoic	Cretaceous	Upper		Navarro / Taylor Gp. / Austin Gp. / Tokio Fm. / Eutaw Fm.	*Conventional Oil/Gas Reservoirs*	●●	19,133	2,500[5]								
				Eagle Ford	*Seal (Shale)*											
		Lower		Woodbine / Tuscaloosa / Washita Group (Buda Limestone) / Fredericksburg Gp. (Edwards Ls./Paluxy) / Glen Rose (Rodessa Fm) / Pearsall Fm. – James Lm. / Sligo Fm. / Hosston Fm. – Travis Peak	*Conventional Oil/Gas Reservoirs* / *Seal (Shale)* / *Seal (Shale)* / *Seal (Shale)*	●●	21,633	2,200[6]								
	Jurassic	Up.		Cotton Valley / Bossier Fm. / Haynesville Fm. / Gilmer Lm. / Smackover Fm. / Norphlet Fm.	*Seal (Shale)*		23,833	6,900[7]								
		Mid.		Louann Salt / Werner Formation	*Seal (Salt / Shale)*		30,733	?								
Basement																

Figure 53: (above) Stratigraphic column in the project area. Proposed Injection Complexes: 1 – LMIC; 2 – OFIC. Depths to the top of stratigraphic units are noted with estimated thicknesses presented as average and for all injection wells. Figure modified from Swanson et al. (2013). with data from Goddard (2015), Goddard et al. (2005)[1], Roberts-Ashby et al. (2014)[2], Barker et al. (2000)[3], BeBout (1992)[4], Sohl et al. (1991)[5], McFarlen Jr. and Menes (1991)[6], Salvador (1991)[7]. USDW information from Buono (1983), Stuart et al. (1994) and discussed in subsection 2.6 of this Application Narrative.

The remainder of this page intentionally left blank.

The post-Mid-Jurassic sedimentary column (Figure 54) in the Gulf of Mexico is divided into twenty-nine 2-12 million years long "principle depositional episodes" separated by basin-wide boundaries (Galloway, 2008). Eighteen of the episodes are identified Basin Center Seismic Sequences in which there are Cenozoic Depositional Episodes of varying duration and magnitude (Galloway 2008; Galloway et al., 2000; Feng 1995; Winker and Buffler, 1988; Galloway, 1989; Morton and Ayers, 1992).

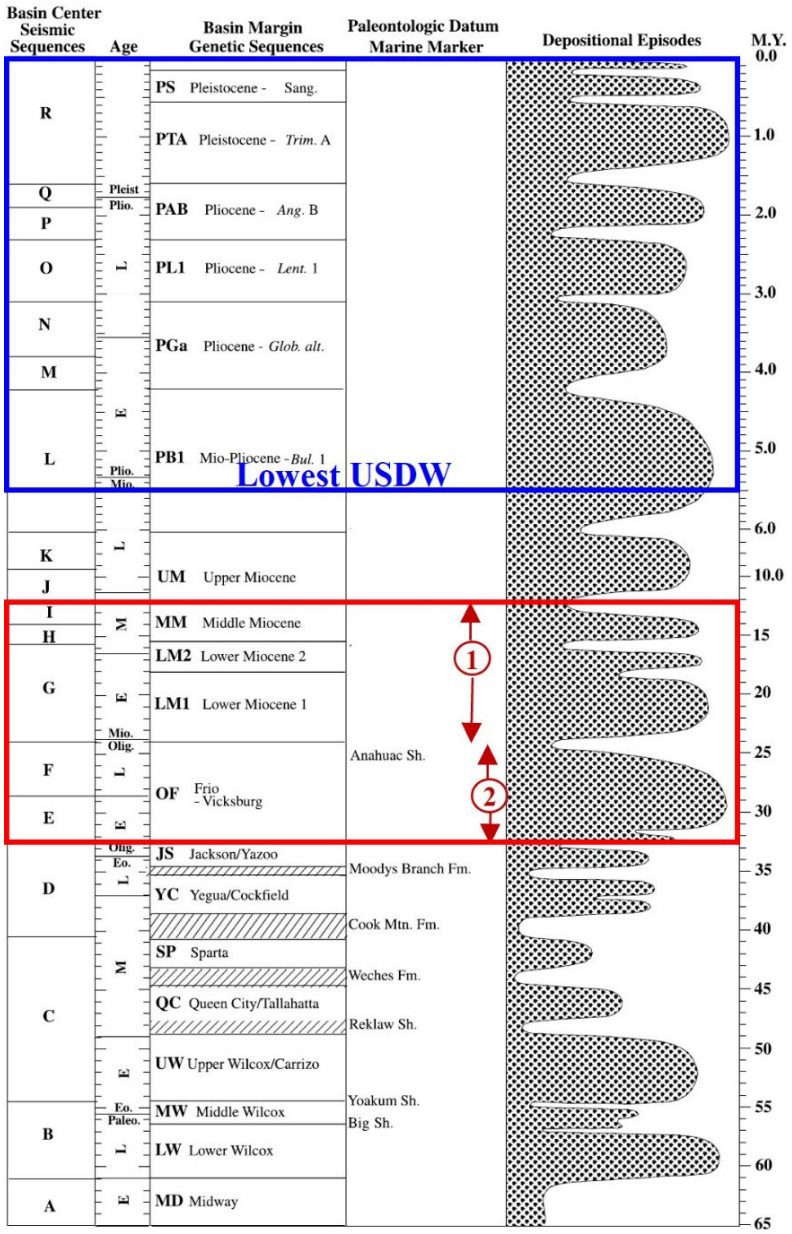

Figure 54: Regional Gulf of Mexico genetic sequences showing the volumetric contribution of each and bounding marine shale units. Freshwater and USDWs are shown in the blue box. Injection intervals are shown in the red outline. Proposed Injection Complexes; 1 – Lower Miocene Injection Complex; 2 – Oligocene Frio Injection Complex are labeled. (Figure modified from Galloway et al., 2000; Feng, 1995; Berggren et al., 1995. USDW information from Buono, 1983; Stuart et al., 1994)

Data for injection zone salinities directly measured from produced water and/or calculated using the Archie equation and resistivity logs indicate that Lower Miocene Sands and Frio Formation injection zone targets have a range of values from 85,000 ppm NaCl to >200,000 ppm NaCl and are not USDWs. The base of the lowest USDW in the project area is in the Upper Miocene Aquifer System, which equates to the Mio-Pliocene PB1 depisode designated by Galloway et a., (2000) as seen in Figure 54. The base of the lowest USDW is discussed in detail in subsection 2.7.5 of the Application Narrative.

2.4.1 CCS System 1: The Lower Miocene Injection Complex (LMIC)

The LMIC is composed from top to bottom of the Middle Miocene Confining Zone along with a shale sub-confining zone in the Middle and Lower Miocene, the Lower Miocene Sand injection zone, and the Anahuac Formation lower confining zone (Figure 53 and Figure 54). The Anahuac Formation is also the upper confining zone for the OFIC which will be addressed beginning in subsection 2.4.2 of this Application Narrative below. The upper confining zone and injection zone for the LMIC are Miocene in age.

Figure 14 shows paleogeographic reconstructions by Galloway et al. (2000) for the Lower, Middle and Upper Miocene Basin Margin Genetic Sequences, respectively. The figures show that through Miocene time, the largest sediment volume delivered to the Gulf of Mexico shifted away from the Rio Grande axis in the western Gulf of Mexico on the Texas Coast and toward the northeast. Thus, increasingly larger volumes of sediment were shed through the Red River (RD) dispersal axis/Calcasieu delta, then ultimately through the Central Mississippi (CM) dispersal axis/Mississippi Delta and the Eastern Mississippi (EM) dispersal axis (Galloway et al., 2000).

Figure 14 shows the paleogeography of the Lower Miocene depositional episode including the influx of more and sandier sediment from the Red River dispersal axis into the Calcasieu Delta in western Louisiana. The project area is in the Mississippi Delta area along the Central Mississippi axis, and deltaic and nearshore marine deposition is common (Galloway et al., 2000).

Figure 14 also shows the paleogeographic reconstruction of the Middle Miocene, during which the Mississippi Delta System was the main depocenter in southern Louisiana. The project area continues to receive a significant influx of fluvial deltaic sediments.

Finally, Figure 14 shows a paleogeographic reconstruction of the late Miocene, which looks much like the modern Gulf of Mexico. The Upper Miocene in the project area is now continental alluvium.

The Lower, Middle and Upper Miocene as presented in Figure 14 are separated by marine flooding surfaces offshore and equivalent nearshore marine to brackish fine-grained deposits closer to shore. Each of these episodes contains repeated stacked parasequences deposited from north to south containing distinct facies in order: continental sediments including massive sands with little to no shale; alternating nearshore and shallow marine sands and near shore marine shale; then moderately deep marine deposits containing offshore of sand, silt and shale including deep marine shales (Galloway et al., 2000; Rainwater, 1964; Limes and Stipe, 1959).

Rainwater (1964) presents schematic diagrams of Miocene deposition cycles through time in southern Louisiana, showing very sandy continental alluvial sediments in the northern shoreward

position with stratigraphically equivalent shallow marine then deep marine sediment furthest south in the deepest water (Figure 55). The top of the LMIC upper confining zone is at the *Bigenerina* (2) *nodosaria* var. faunal zone which Galloway et al. (2000) consider the top of the Middle Miocene Genetic Sequence (Figure 54).

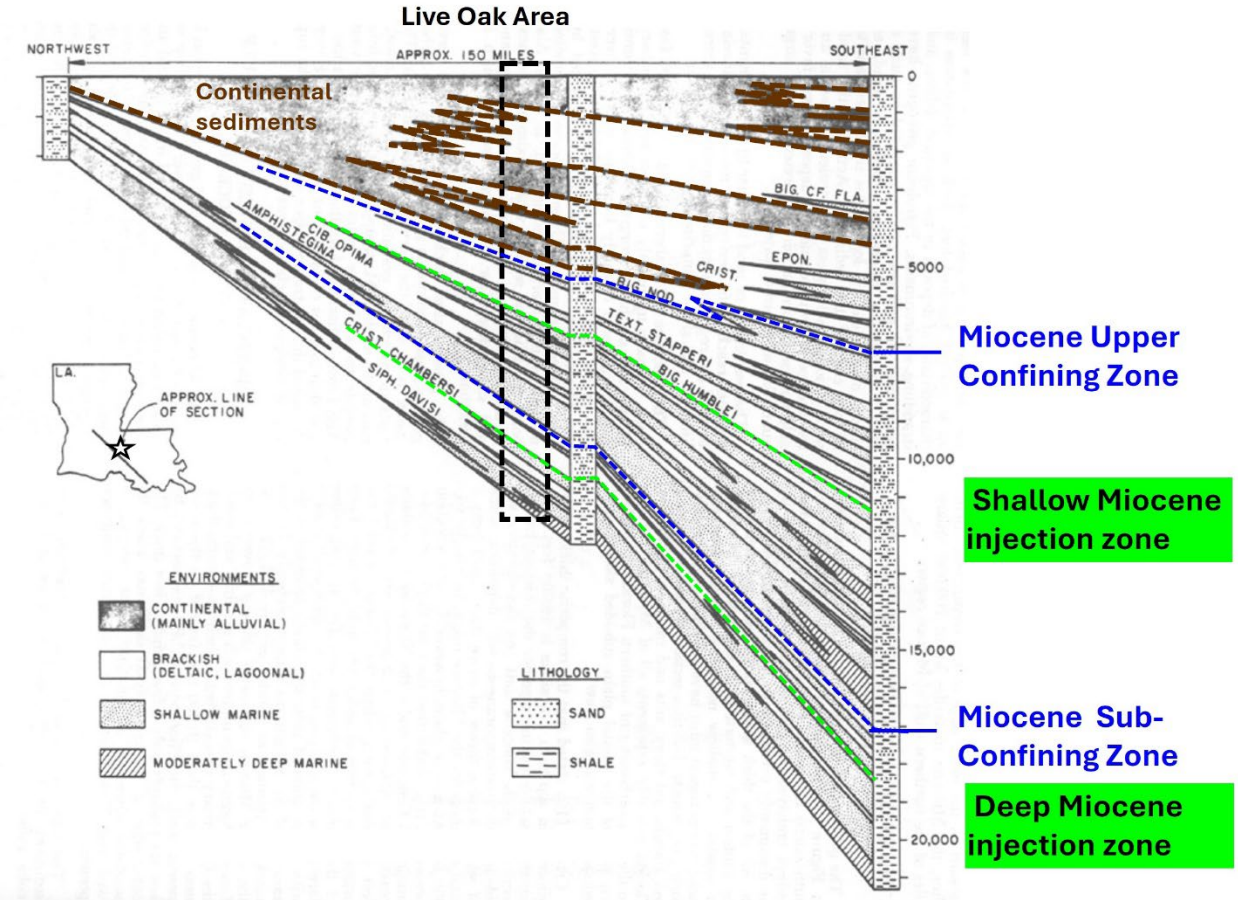

Figure 55: A Fence diagram showing the cyclical depositional pattern of Miocene strata through time in southern Louisiana. Repeated stacked sequences containing repeated lateral facies of continental, brackish, shallow marine and moderately deep marine sediments prograde seaward through time as the shoreline moves seaward. The dashed blue lines indicate the top of the Middle Miocene Confining Zone and Miocene sub-confining zone. The dashed bright green lines show the Shallow and Deep Miocene injection zones, and the brown dashed line indicates the base of continental alluvium. The project area is indicated on the location map with a star and on the fence diagram with a black dashed rectangle. Figure modified from Rainwater, 1964.

Major Miocene depocenters shifted from west to east and moved further south into the Gulf of Mexico Basin. Figure 14 and Figure 55 show the overall southward progression of younger continental sands through time. Smaller-scale north and south movements of the shoreline in Figure 48 are caused by shifts in near-shore marine deltaic lobe deposition rather than overall sea level rise and fall (Rainwater, 1964).

Abundant sediment deposition through dispersal axes in central Louisiana onto a muddy, unstable continental shelf caused collapses throughout the Miocene creating thick depocenters that received incredibly large volumes of sediment such as the Planulina Collapsed Margin, shown in Figure 14.

2.4.1.1. Middle Miocene Confining Zone: LMIC Upper Confining Zone

In the project area, the shale confining zone at the top of the Middle Miocene is ~12.5 million years old (Galloway et al., 2000).

Zulqarnian et al. (2013) describe a site selection workflow for CO_2 sequestration in Miocene sediments in southern Louisiana. A large-scale regional cross section (approximately 1" = 1,000' vertical scale) from this publication shows dominantly Lower Miocene with some Middle Miocene where the project area is projected (Figure 56). Lower, Middle and Upper Miocene are those designated by Galloway (1989), Galloway et al. (2000), Limes and Stipe (1959), and Olariu et al. (2019).

The remainder of this page intentionally left blank.

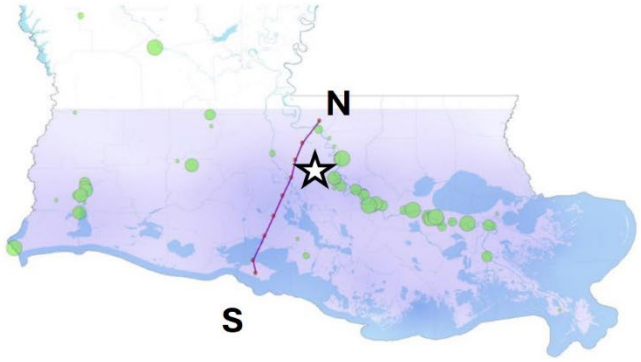

Projected Live Oak Area

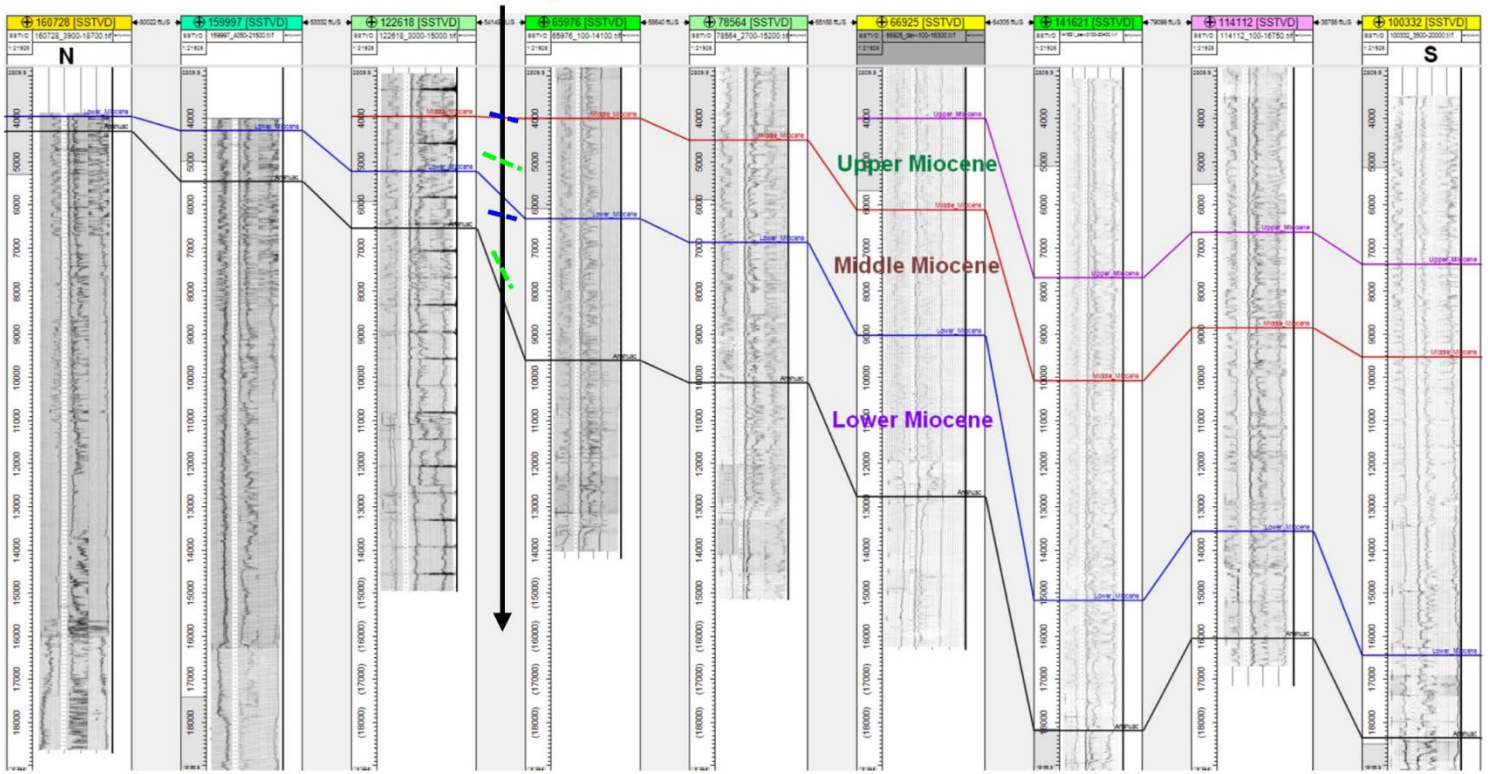

Figure 56: (above) A regional cross section through South Louisiana schematically showing the large-scale intervals of the Miocene. Modified from Zulqarnian et al., 2013. Project area shown with a star on the location map, the dashed blue lines are the Middle Miocene upper confining zone and Miocene sub-confining zone, and the bright green dashed lines are the Shallow and Deep Miocene injection zones. As indicated, Upper, Middle, and Lower Miocene are delineated by work in Galloway,1989; Galloway et al., 2000; Limes and Stipe, 1959; Olariu et al., 2019. Upper, Middle, and Lower Miocene are delineated by work in Galloway, 1989; Galloway et al., 2000; Limes and Stipe, 1959; Olariu et al., 2019.

The base of the upper confining zone can be seen on this cross-section and is at approximately 4,000 ft TVD at the project location. The visible part of the confining zone is composed of a largely shaley interval with interbedded thinner sands, though at this scale little detail can be seen.

This shaley upper confining zone is the regional seal for Miocene gas reservoirs in the Florida parishes area. The Florida parishes as described by Goddard and Zimmerman (2003) are West and East Feliciana, East Baton Rouge, Saint Helena, Livingston, Tangipahoa, Washington, and Saint Tammy parishes. In the Florida parishes area the aforementioned shaley confining zone is described as a 100 ft to 400 ft thick interdistributary bay shale containing lignite beds deposited in a lower delta plain setting (Figure 57).

The remainder of this page intentionally left blank.

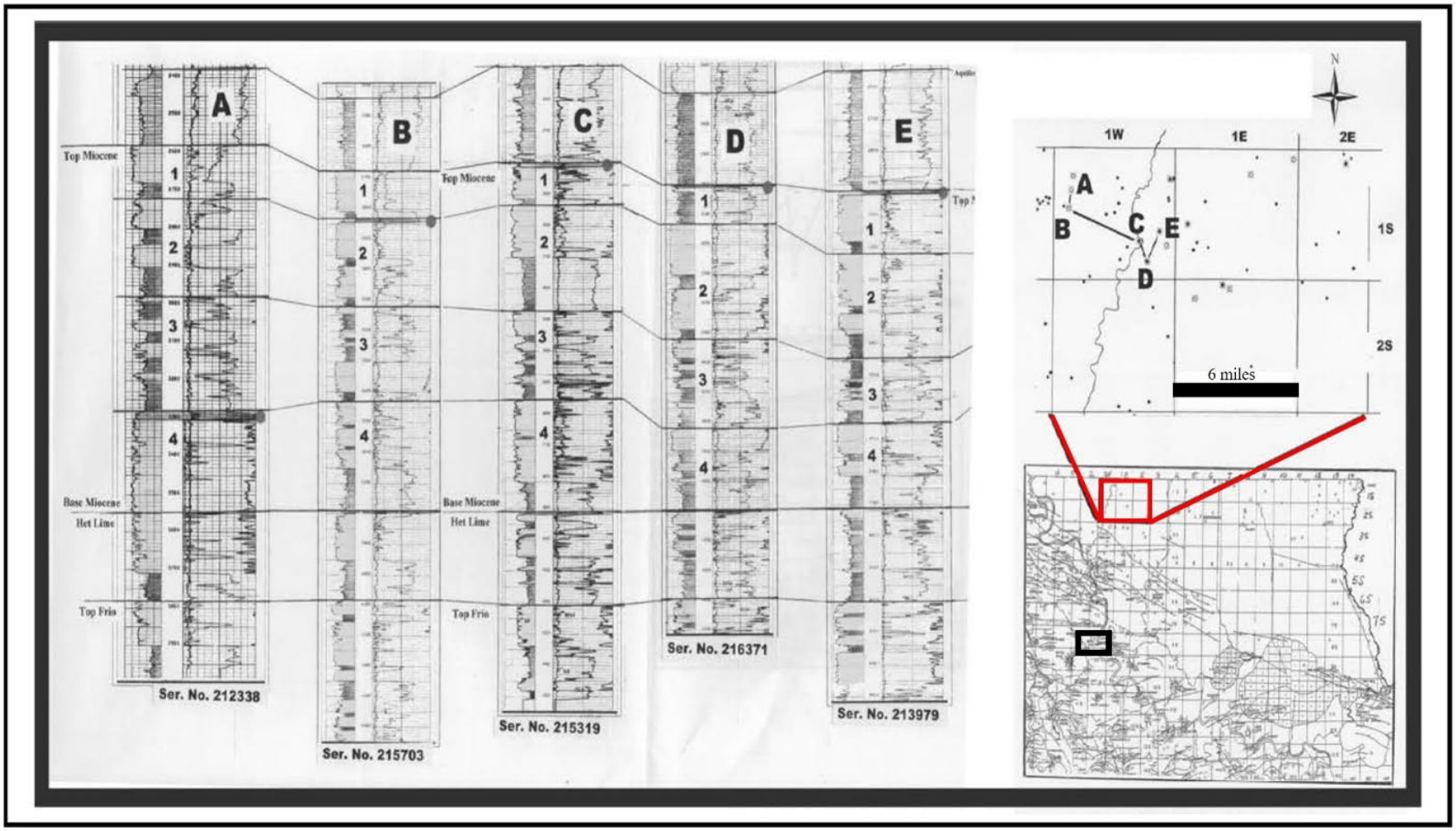

Figure 57: Cross section showing the Miocene and its upper confining zone across the West and East Feliciana parishes within the greater Florida parishes area. The black rectangle on the location map shows the project area. As indicated in the text, this is a regional top seal for the Miocene in this area. Modified from Goddard and Zimmerman, 2003.

The type log for the Claimed as PBI (API No. Claimed as PBI see well nos. 31, 32, and 49 in Figure 20, Figure 21, and Table 2) in West Baton Rouge parish shows that the top of the Middle Miocene Confining Zone shale would be encountered at approximately 4,800 feet TVD and would be approximately 1,315 feet thick (Figure 58). The Vshale curve in Figure 58 shows that there are thin sand and silt beds in this shale confining zone.

The remainder of this page intentionally left blank.

Figure 58: Type log for the LMIC and OFIC in the Claimed as PBI (API No. Claimed as PBI locations for well nos. 31, 32, and 49 in Figure 20, Figure 21, and Table 2) well in West Baton Rouge parish showing the Middle Miocene Confining Zone, Lower Miocene Sands injection zone, Anahuac Formation confining zone and Frio Formation injection zone.

Figure 59 shows a local structure and isopach map for the Middle Miocene Confining Zone in the project area. The Middle Miocene Confining Zone in this area is anticipated to be encountered at an average true vertical depth of approximately 4,200 feet and will average 1,315 feet in thickness.

Figure 59: Top structure (top) and isochore (bottom) of the Middle Miocene Confining Zone (structure C.I. = 250'; depths SSTVD; Isochore C.I. = 50') with the six potential LMIC injection sites shown. See information for LMIC petrophysical wells in Figure 20 and Table 2.

Five wells in Ascension parish to the south and east of the project area have cores and/or sidewall cores through the Miocene though none have sampled the upper confining zone for analysis of its properties. Core descriptions for the confining zone in these wells indicate a gray shale, firm, brittle, commonly silty, occasionally very silty with up to 10% fine sand, and occasionally calcareous and rarely containing shell fragments.

Published X-Ray Diffraction data (XRD) for confining zone mineral composition from Trevina et al. (2018) and Trevino and Meckel (2019) are summarized in Table 4 below.

Table 4: Confining zone mineralogy (XRD) for the top Miocene confining zone from West Cameron Block 205 Offshore Louisiana; OCS G-3496 #A-3 and OCS-G-4392 #C-4 wells. Table 4 data from Trevina and Meckel, 2019; and Trevino et al., 2018. Location map modified from Trevina et al 2018. The black box shows the approximate West Cameron Block well location, while the dark red triangle shows the approximate location of the High Island 24L No. 9 presented in Lu et al., 2017. A star shows the approximate location of the project area.

Confining Zone Mineralogy		
Component	**Range (%)**	**Average (%)**
Quartz	19.7-31.3	25.04
Calcite	0.2-7.1	3.59
Plagioclase	2.1-6.1	4.17
K-Feldspar	7-12.8	9.49
Total	**34.4-49.4**	**41.89**
Illite	29.3-41.3	35.42
Kaolinite	2.1-4.2	3.21
Chlorite	14-17.9	16.02
Total Clay	**48.1-61.1**	**54.66**
Anatase	1.3-1.9	1.53
Pyrite	0.5-1.5	0.74
Anydrite	1.3-1.9	0.55
Siderite	0.3-1.3	0.80
Dolomite	0.40	0.40
Total Other	**2.5-4.6**	**3.53**

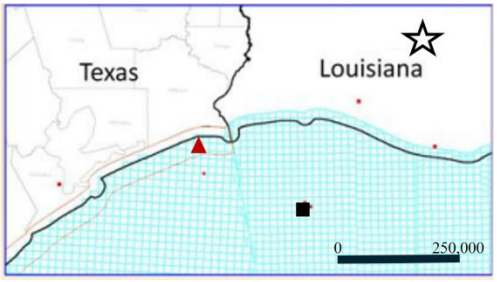

The compositional data in Table 4 shows that the Miocene confining zone in the West Cameron Block contains an average of ~55% clay which is dominated by illite. Quartz, plagioclase, and K-feldspar with calcite, mostly from shell fragments, make up most of the other ~42% of samples. Non-clay minerals are largely non-reactive to injected CO_2. Illite, kaolinite, and chlorite will adsorb CO_2, fixing it in place and aiding in sequestration efforts (Busch et al., 2016). There are no indications of smectite in these samples, likely due to their depths of 12,954.2 feet to 13,138 feet TVD. At these depths, all the smectite has converted to illite.

Lu et al. (2017) report XRD data for the same interval in the High Island 24L No. 9 (API No. 4270830316) in Texas State waters south of Jefferson County from samples at depths from 8,403.1 to 8,492 feet. This data is shown in Table 5, while the well location is shown on the map presented with Table 4.

Table 5: Confining zone mineralogy in the High Island 24L No. 9 in Texas State Waters (API No. 4270830316). Sample data from Lu et al., 2017. Location is shown on Table 4 map.

Confining Zone Mineralogy		
Component	**Range (%)**	**Average (%)**
Quartz	18.9-42.5%	29.42%
Calcite	2.4-19.4%	10.35%
Plagioclase	6.2-16.2%	10.42%
K-Feldspar	9.8-20.4%	13.78%
Total	**52.4-77.7%**	**63.96%**
2:1 Al Clay	15.2-33.9%	24.43%
Kaolinite	2.9-15.6%	11.62%
Chlorite	NR	NR
Total Clay	**22.4-49.5**	**36.05%**

The total clay percentage in the samples presented in Table 5 is 36% but is still dominantly illite or mixed layer illite/smectite with no chlorite reported. In the most favorable case, smectite will adsorb CO_2 fixing it in place. Busch et al. (2016) identify and discuss adverse cases in which certain smectite mineralogy can react unfavorably to injected CO_2 including the following examples. First, fully hydrated smectite exposed to dry or nearly dry CO_2 in a super-critical state could dehydrate, releasing interlayer-bound water and collapsing its crystal lattice, creating fractures and compromising the confining zone. Second, incompletely hydrated smectite can adsorb CO_2 and swell, creating shear fractures that compromise the confining zone. Busch et al. (2016) indicate that this process is incredibly slow: on the order of tens of thousands of years. Martin et al. (2022) conducted laboratory testing showing that smectite in mixed-layer illite-smectite converts to illite at an accelerated rate when exposed to dry super-critical CO_2. The incrementally higher porosity created by clay mineral volume loss is small due to the precipitation of carbonate cement in the form of calcite, dolomite, and siderite, which decrease porosity and lower permeability (Martin et al., 2022). Busch et al. (2016) and Martin et al. (2022) stress the importance of understanding confining zone mineralogy, particularly clay mineralogy. Confining zones or caprocks addressed by Busch et al (2016) are composed of greater than 50% clay mineralogy with variable percentages of smectite in mixed layer illite-smectite, averaging approximately 9%. A Formation Sensitivity Study for the Waste Disposal 8 well (API# 1709588008) indicates that even though there is possibly sensitive smectite clay in the Lower Miocene Sand injection zone, it is such a small component of the rock overall, 50% of the 2.75% total clay fraction, that it is not of great concern. Site-specific data will be needed to determine the mineralogical makeup of this zone in the project area, but it is notable that Lu et al. (2016), Trevino et al. (2018), and Trevina and Meckel (2019) indicate that this Lower Miocene Sand injection zone is an excellent confining zone for CO_2 sequestration.

There are no publicly available porosity and permeability data for the Middle Miocene Confining Zone, but Trevino and Meckel (2019) published calculated permeability data for the OCS-G-3496 #A-3 (API No. 1770040400) well from West Cameron Block 205 of offshore Louisiana, shown in Table 6. Permeability was calculated using a technique found in Swanson (1981).

Table 6: Calculated Mercury Injection Capillary Pressure (MICP) porosity and permeability values for OCS-G03496 #A-3 in West Cameron Block 205 from Trevino and Meckel 2019. Note: Values correspond to the mineralogy in Table 4.

Depth (ft)	MICP Porosity (%)	Calculated Permeability (mD)
12954.2	10.82	0.000866
12966.8	10.19	0.000754
12975.5	10	0.000947
12984.9	11.93	0.001115
12999.5	11.41	0.001049
13050.0	9.77	0.001211
13060.5	9.57	0.001502

The average permeability derived from this data set is approximately ~0.0011 mD, making it a good confining zone. Trevino and Meckel (2019) indicate that compaction and secondary mineralization has lessened primary porosity, though secondary pores forming from mineral dissolution are larger, accounting for the apparent increase in permeability with depth. The deepest value and most permeable in this trend is 0.0015 mD which is still indicative of an effective confining zone.

There is evidence supporting the Middle Miocene shale intervals as an effective long-term seal for CO_2 injection. As previously mentioned, Goddard and Zimmerman (2003) recognize the Middle Miocene Confining Zone as a regional top-seal for Miocene gas reservoirs in the Florida parishes area, where it also prevents fresh water in shallow Plio-Pleistocene aquifers above it from mixing with much higher salinity water in Miocene sandstone reservoirs below. It also satisfies the U.S. Geological Survey requirements as a confining zone for the Lower Miocene Storage Assessment Unit (Roberts-Ashby et al., 2014).

Site-specific data will be gathered for all intervals of the LMIC and OFIC in the project area utilizing an in-zone monitoring well which will be drilled first in the sequence of project wells (see subsection 2 of the Pre-Operational Testing Program).

2.4.1.2. LMIC Injection Zone: Lower Miocene Sands

A structure map at approximately the top of the Lower Miocene depositional episode and coinciding with the Miocene injection zone interval in the Claimed as PBI (API No. Claimed as PBI) well shows that the project area is gently dipping to the south, and the anticipated depth for the top of this injection interval would be at ~ 6,000 feet TVD (Figure 60; John et al., 1992).

The remainder of this page intentionally left blank.

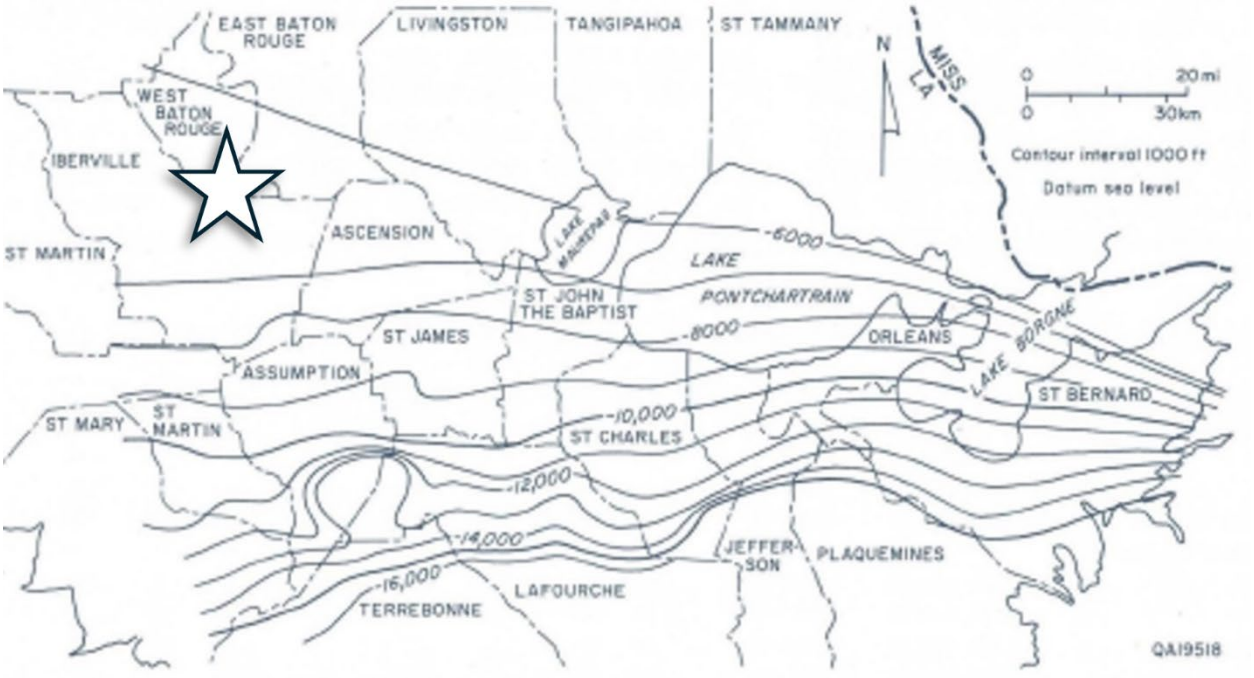

Figure 60: Approximate top Shallow Miocene injection interval structure map. The location of the project area is shown with a star. Modified from John et al 1992 and based on work completed by the New Orleans Geological Society Study Group (1962).

The Lower Miocene interval, composed of fluvial deltaic, marine shoreline and shoreface sandstones, and interstitial shales is the injection zone for this storage complex (Rainwater, 1964; John et al., 1992). Figure 59 shows that the anticipated total thickness of the Lower Miocene Sand injection zone will be almost 3,850 feet.

Lower Miocene sediments were deposited between approximately 25 and 16 Ma with a regional shale break at about 18 Ma. ago (Figure 54; Galloway et al., 2000; Berggren et al., 1995). Prolific depo-centers that were active in the western Gulf of Mexico during Oligocene Frio were abandoned, and the main sedimentary accumulation area shifted eastward to the RD and, ultimately, the CM dispersal axes (Figure 14; Galloway, 1986; Galloway et al., 2000). Mapping by the New Orleans Geological Society Study Group (1962) presented in John et al. (1992) shows that the Lower Miocene interval is approximately 50% to 60% sand in the southern part of West Baton Rouge Parish (Figure 61). This relatively sandy system of adjacent deltas and shoreline sands makes an attractive CO_2 sequestration target.

The remainder of this page intentionally left blank.

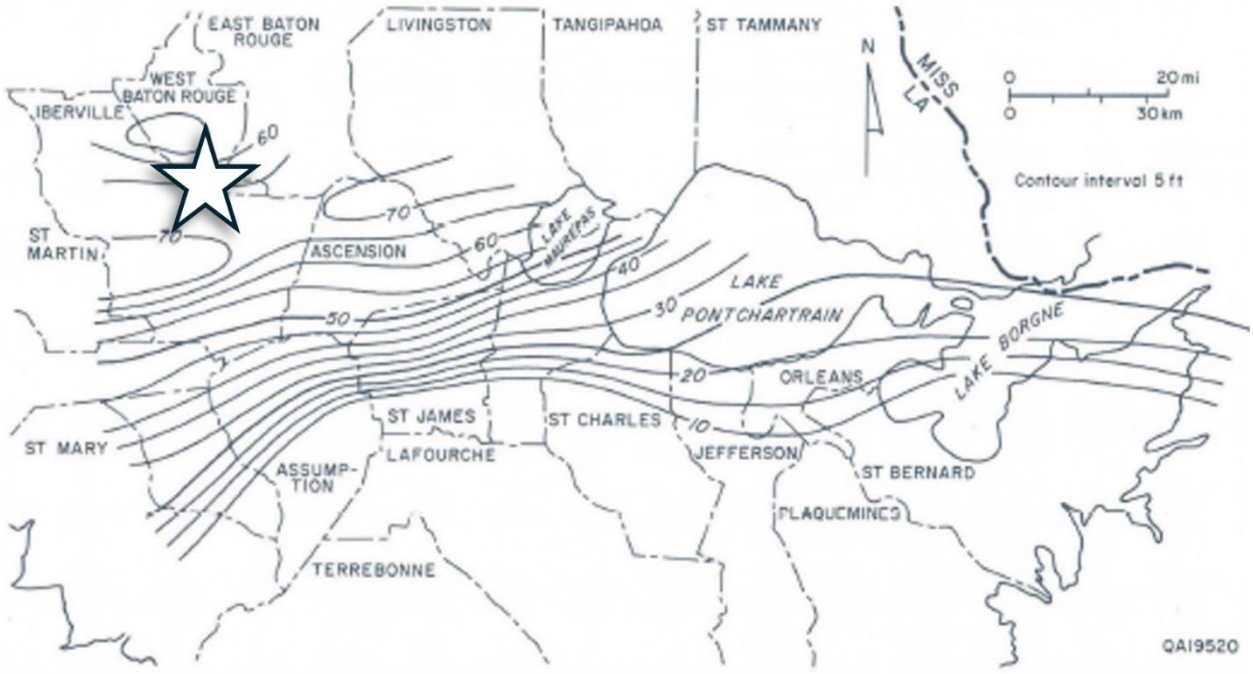

Figure 61: Approximate Miocene injection interval net to gross mapping showing an overall sandy interval in the project area which is highlighted by a star. Figure modified from John et al. (1992) after work by the New Orleans Geological Society Study Group (1962).

Goddard and Zimmerman (2015) also describe Miocene sandstone reservoirs as sand-rich (60% sand) fluvial-deltaic sands and distributary channels. Mapping in the immediate project area shows an average gross thickness of 3,140 feet for the Lower Miocene Sand injection interval and ~47% sand in formation at an average depth of 5,500 feet TVD in the project area, with an average of 1,590 feet of sand at the LMIC proposed injection well locations (Figure 62).

The remainder of this page intentionally left blank.

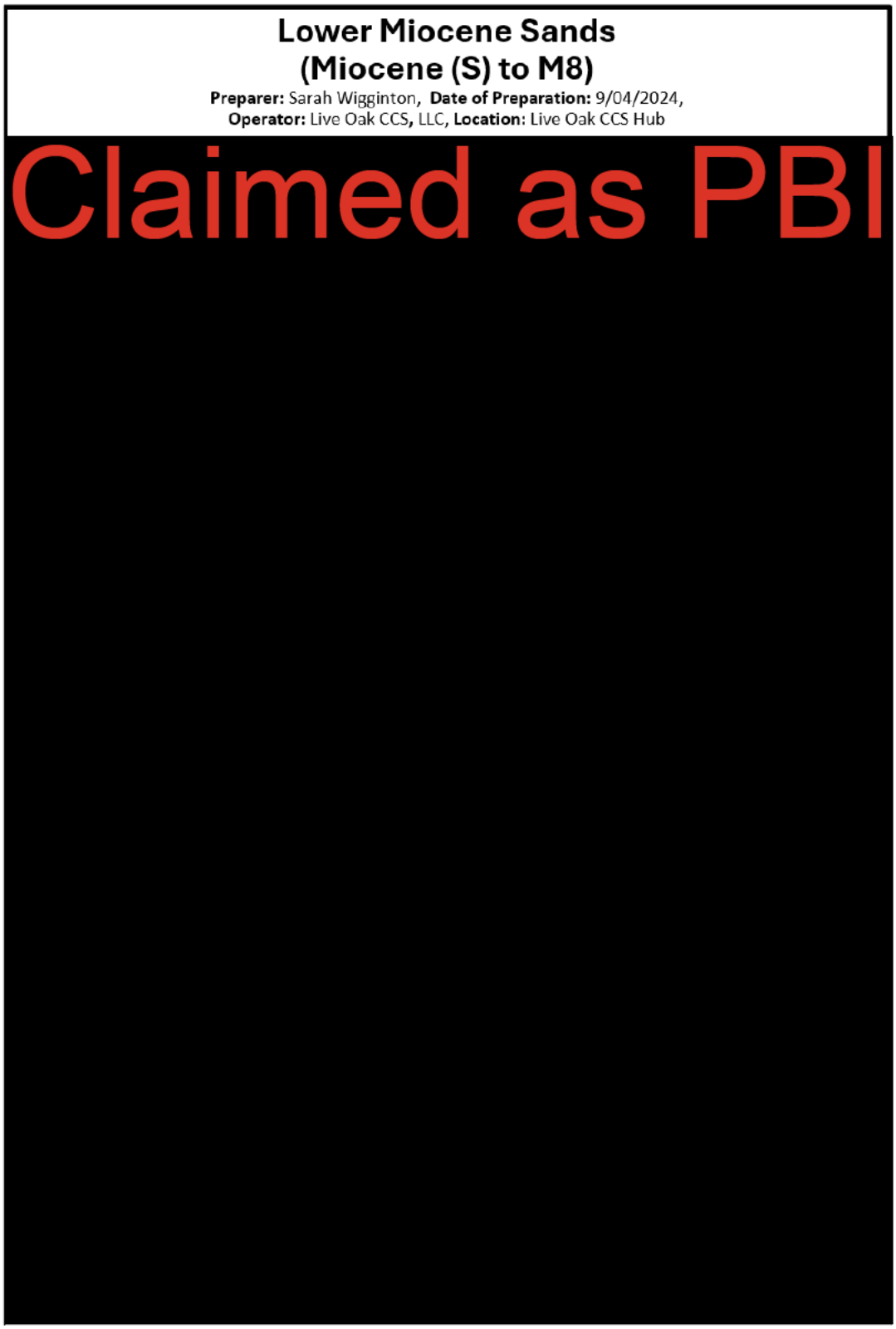

Figure 62: Top structure (top) and isochore (bottom) of the Lower Miocene Sand (structure C.I. = 250'; depths SSTVD; Isochore C.I. = 100') with the six potential LMIC injection sites shown. See information for LMIC petrophysical wells in Figure 20 and Table 2.

Lower Miocene sediments are composed of mostly fine-grained sand, silt, and shale with continental alluvial deposits containing some coarse quartz and chert (John et al., 1992). They have good to excellent reservoir quality with published regional porosity values ranging from 22% to 35% with a most likely value of 28%, and a wide range of permeability from 20 mD to 8,000 mD with a most-likely value of 500 mD (Nehring Associates Inc., 2010). Goddard (2015) indicates reservoir porosities of 22% to 30% and 100 mD to 2,500 mD of permeability for the Lower Miocene Sands in southern Louisiana.

Well logs for twenty wells underwent petrophysical analysis to calculate porosity from acoustic, neutron and density logs. Vshale was derived from a simple correlation among spontaneous potential (SP), gamma ray logs (GR), and resistivity logs, and from this process a volume of shale/net sand flag was created. Results for the Claimed as PBI (API No. Claimed as PBI) are shown in Figure 58.

Figure 63A shows the Porosity-Permeability transform for fifteen wells with Lower Miocene Sand core. Descriptions of Lower Miocene Sands indicate that samples with permeability less than 100 mD are described as silty and or shaly sand while values in the 100 mD to 1,000 mD range have some amount of silt and shale. These descriptions also indicate that neither porosity nor permeability vary with depth, and that permeability is inversely related to the percentage of silt and clay in the sand. The cross-plot relationship in Figure 63 was then used to calibrate the calculated porosity logs and assign a constant low permeability value to intervals flagged as shale.

The remainder of this page intentionally left blank.

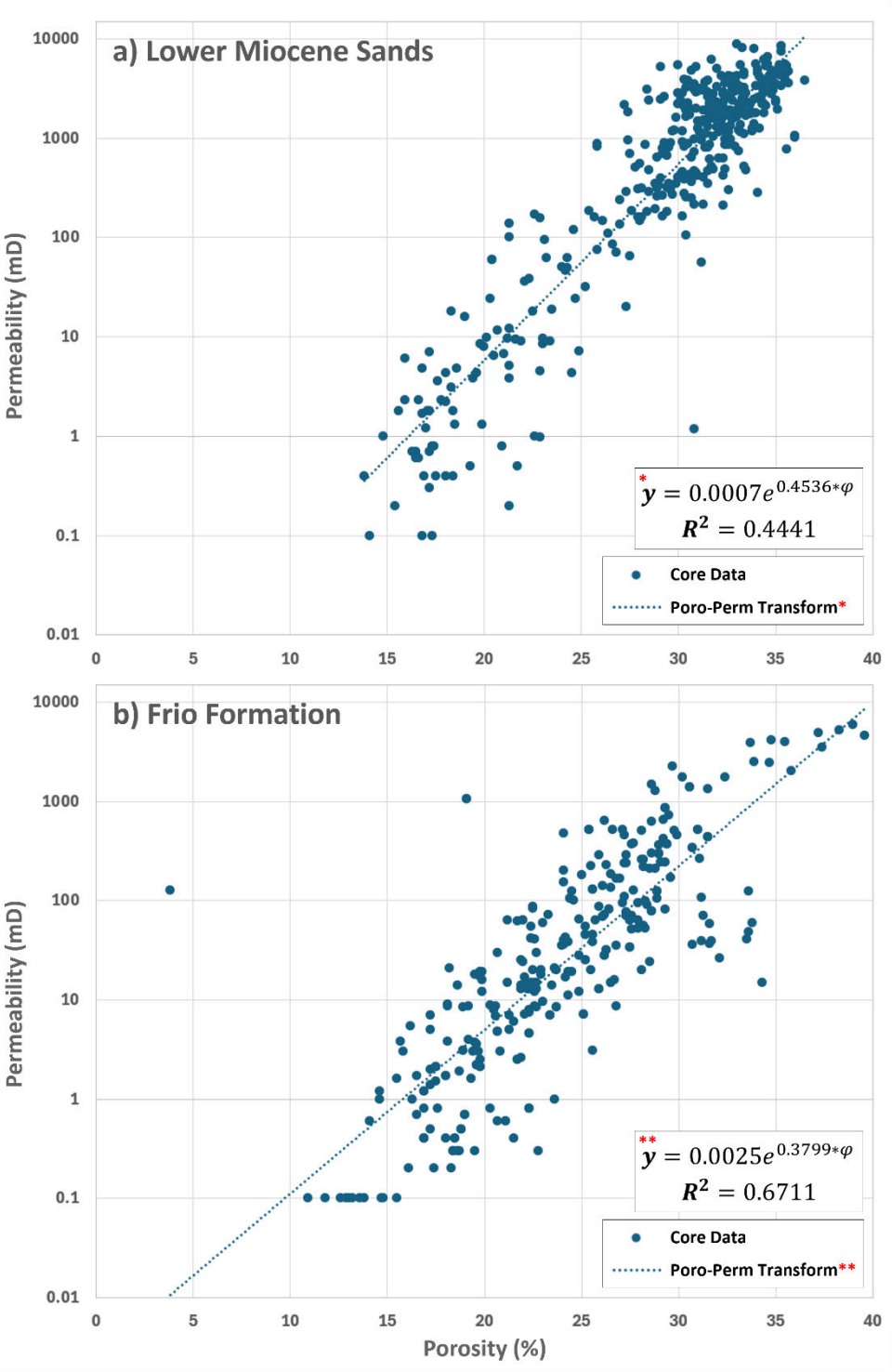

Figure 63: Porosity (%) versus permeability (mD) cross-plot for 15 wells per zone with core data and poro-perm correlations separated into (a) Lower Miocene Sand and (b) Frio Formation. Both formations have high porosity and permeability in the sand, while zones with higher shale content have lesser reservoir quality. Combined 30 wells in the Ascension, East Baton Rouge, Iberville, St. John

The Baptist, St. Martin, and West Baton Rouge parishes have publicly available porosity and permeability from core data (see Table 2 in subsection 2.1.13.4. for API No. and location data).

The Waste Disposal 8 well (API No. 1709588008, see well no. 5 in Figure 22 and Table 2) has XRD data for both major components and clay speciation, presented in Table 7.

Table 7: Summary of XRD data for the Waste Disposal 8 well (API No. 1709588008) in St. John the Baptist parish, LA.

Depth (Feet)	Quartz (%)	Feldspar (%)	Plagioclase (%)	Calcite (%)	Pyrite (%)	Total Clay (%)	Kaolinite (%)	Chlorite (%)	Illite (%)	Mixed layer Illite/Smectite (%)
7977	93	4	2	--	--	1	24	4	44	28
7989	92	4	1	--	--	3	24	4	32	40
8020	99	--	--	--	--	1	20	4	33	43
8051	88	4	3	--	--	5	18	4	13	65
8070	91	5	2	--	--	2	23	5	22	50
8140	96	3	--	--	--	1	11	8	24	57
8196	88	4	--	2	--	6	16	2	18	64
8220	96	--	--	--	1	3	24	5	20	51
Average	92.875	4	2	2	1	2.75	20	4.5	25.75	49.75

-- Too small to measure

Samples average 93% quartz with approximately 6% Plagioclase and Feldspar. Total clay percentage averages less than 3%. Half of the clay mineral fraction is kaolinite, illite, and chlorite, while the other half is mixed-layer illite-smectite.

Illite and kaolinite help stabilize an injection plume by adsorbing and fixing it in place. Smectite will as well, except in some specific cases described in subsection 2.4.1.1 above.

2.4.1.3. LMIC Lower Confining Zone: Anahuac Formation

The Anahuac Formation is a transgressive marine shale deposited by rising sea levels in Oligocene time and is composed of shale at the base with increasing limey shale, limey sandstones, and limestone upward in its strata (Galloway et al., 2000; John et al., 1992). The Heterostegina Lime, or Het Lime, near the top of this interval in the project area contains the maximum transgression at approximately 25 Ma (Figure 54; Galloway et al., 2000). There are no formal members of the Anahuac, but John et al. (1992) have divided it into three depositional systems; proximal delta, distal delta, and slope environments based on sand/shale ratio and reservoir geometry to describe its oil and gas production capacity.

The Anahuac Formation is the most carbonate-rich Cenozoic age formation in the Gulf of Mexico region, containing reef and detrital limestone along with calcareous sand and shale (John et al., 1992; Meyerhoff, 1968). It is a light to dark greenish gray colored shale with increasing calcareous content from southwest Louisiana eastward, containing thin calcareous sands and limestone beds that increase in frequency eastward, where there are few siliciclastics and carbonate lithologies are dominant (John et al., 1992).

In Cameron, Jefferson Davis, Vermillion, Acadia, St Landry, Lafayette, St. Martin, Iberia, Iberville, Assumption, and Ascension parishes south and west of the project area, the Anahuac Formation contains oil and gas productive deltaic and slope sand reservoirs below open marine calcareous sandstones (John et al., 1992; Goddard et al., 2005).

Anahuac Formation thicknesses are usually hundreds of feet but locally approach 1,000 feet and average 750 feet in southern Louisianna (Roberts-Ashbey et al., 2014; Goddard et al., 2005). Figure 64 shows approximately 2,500 feet in the project area, approximately 1,000 feet of which is the Anahuac Formation (Swanson et al., 2013; John et al., 1992; Goddard et al., 2005).

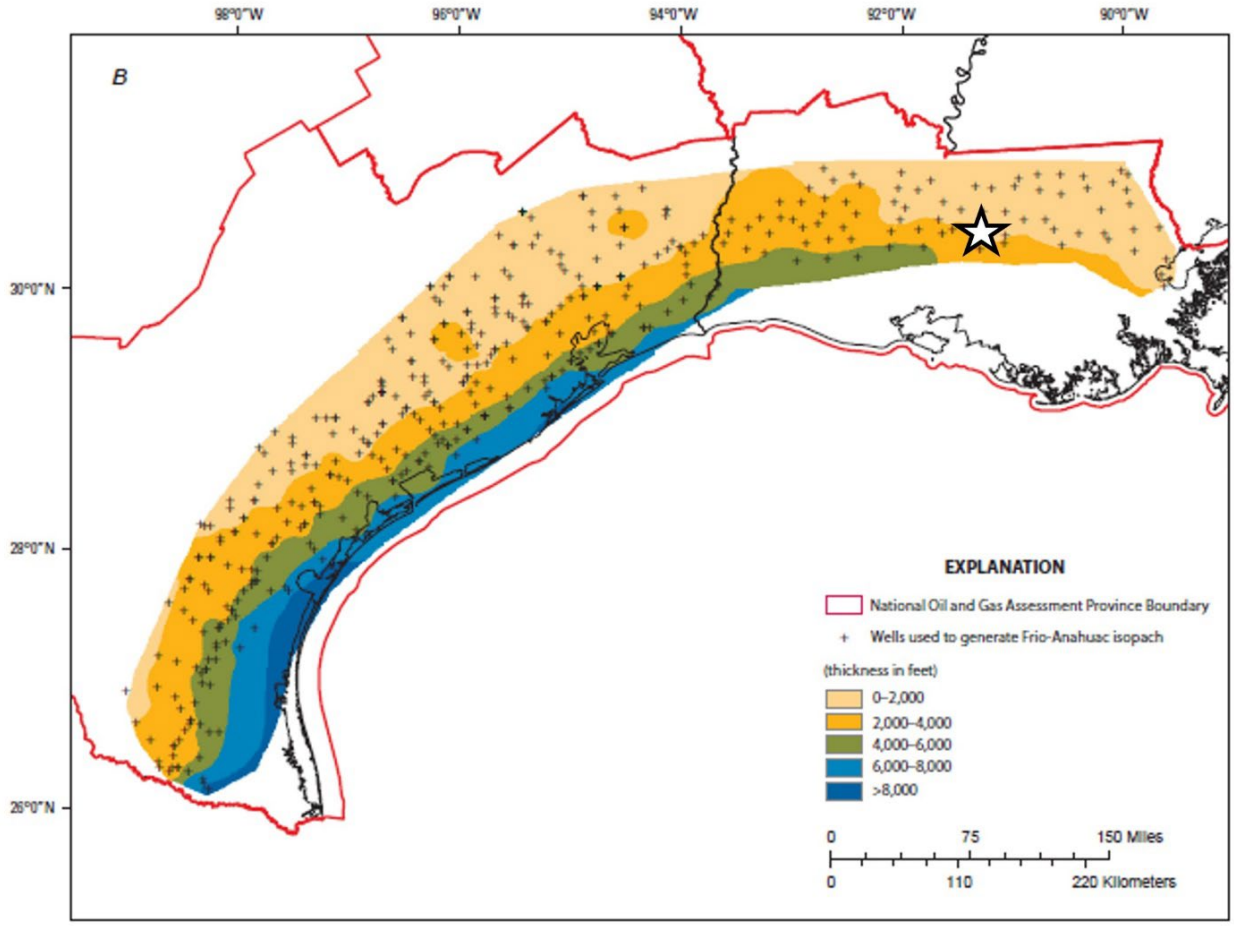

Figure 64: Total isopach thickness for the combined Anahuac and Frio Formations. The star indicates the approximate location of the project area. Modified from Swanson et al., 2013.

Structural mapping of the top Anahuac Formation (Figure 65) shows it dipping gently south into the Gulf of Mexico. The estimated Anahuac Formation top from this regional work is ~8,000 feet (Figure 65; Swanson et al., 2013; Bebout and Gutierrez, 1982 and 1983; Dodge and Posey, 1981).

The remainder of this page intentionally left blank.

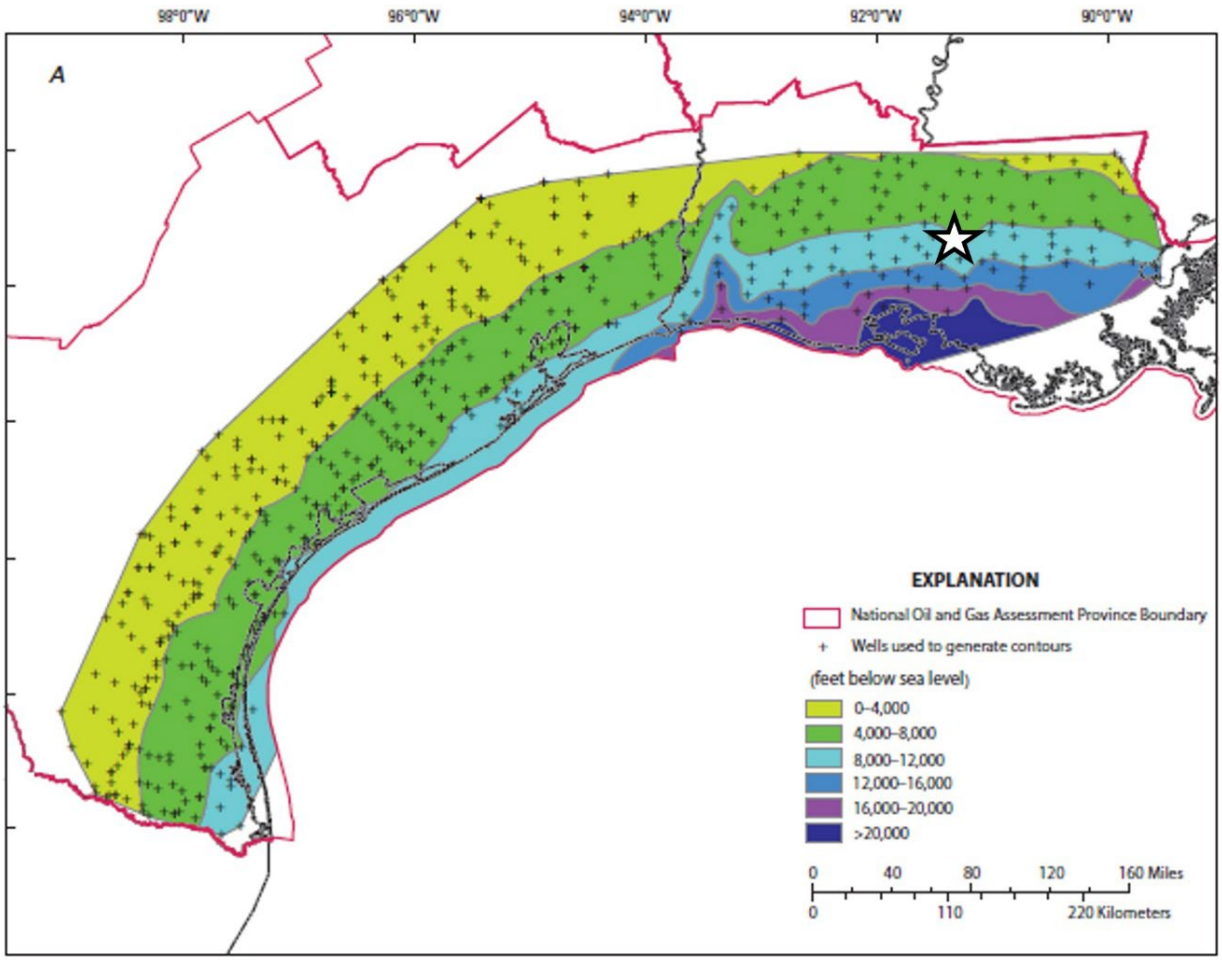

Figure 65: Regional top Anahuac Formation structural contours in subsea true vertical depth. Surface elevation is < 20' in the project area. The star is the approximate location of the project area. Structural contours are modified utilizing work by Bebout and Gutierrez, 1982 and 1983; Dodge and Posey, 1981.

A cross-section from Port Allen south to Lobdell Field illustrates the Anahuac Formation that will be encountered in the project area (Figure 66). Goddard et al. (2005) describe the Anahuac in and near the project area as pro-delta shales with calcareous sandstone interbeds overlain by shallow marine calcareous sandstones and limestones with increasing limestone upward to the Het Lime. The depth to the top of the Anahuac is anticipated to be 7,000 to 8,000 feet, and it is approximately 800 feet thick, with no oil and gas production in these fields or the surrounding area in the project area (Goddard et al., 2005). Anticipated formation sands produce oil and gas from fault-controlled structural closures in Lobdell and Port Allen Fields. These are conventional oil and gas accumulations and do not impact the viability of the Frio Formation to be a CO_2 injection zone, as will be discussed in subsection 2.4.2.2 below.

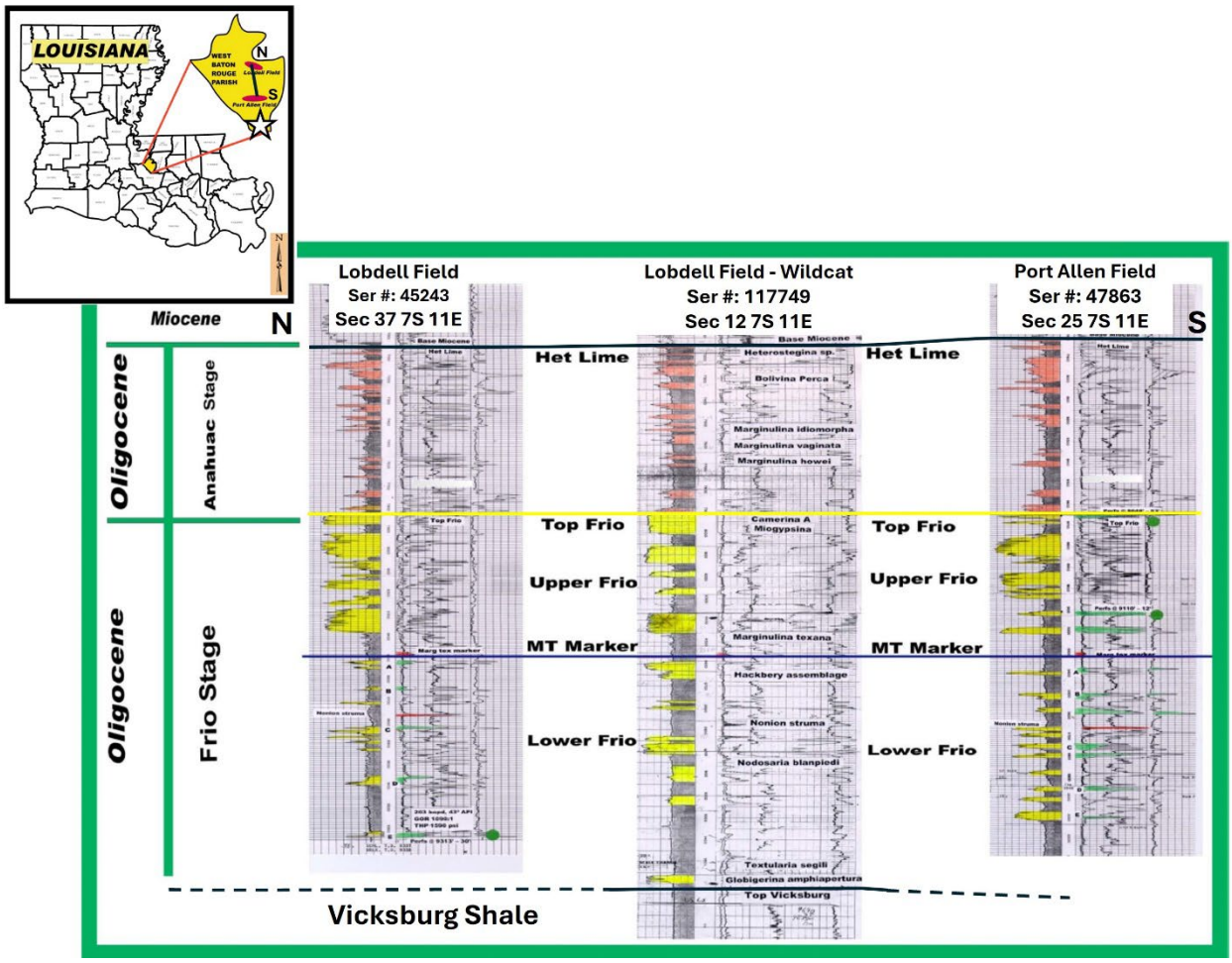

Figure 66: Stratigraphic cross-section showing the shaly and limey Anahuac Formation upper confining zone in central West Baton Rouge parish north of the project area which is identified with a star on the location map. The Frio Formation injection interval, and the top of the Vicksburg Shale lower confining zone are also shown. The stratigraphic datum is the MT Marker within the Marginulina texana paleontological interval. Modified from Goddard et al., 2005.

A published cross-section from West Addis Field in West Baton Rouge and Iberville parishes west of the project area indicates approximately 1,000 feet of Anahuac Formation slightly deeper at approximately 8,500-8,600 feet (Figure 67; Krueger Jr., 1967). There is no oil and gas production from the Anahuac Formation at West Addis Field. As in Figure 64, Figure 65 shows the continuity of the Anahuac and the Frio Formations near the project area. The West Addis Field oil and gas accumulation is also a faulted closure and not indicative of continuous hydrocarbon production from the Frio Formation (Krueger Jr., 1967).

The remainder of this page intentionally left blank.

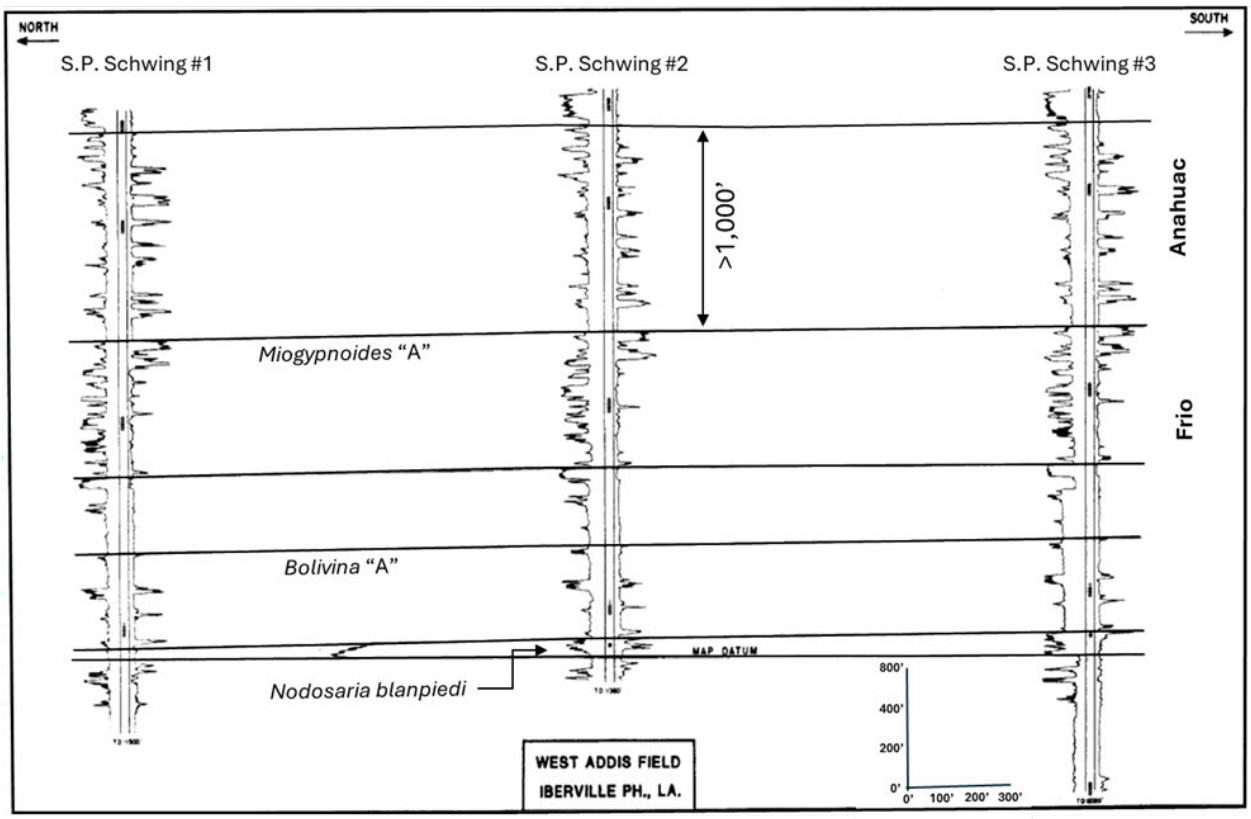

Figure 67: Published cross section from West Addis field in Iberville and West Baton Rouge parishes showing the continued shaley properties of the Anahuac Formation to the west of the project area and south of the Lobdell and Port Allen field areas. Modified from Krueger Jr., 1967.

The Anahuac Formation in East Feliciana parish and in the Florida parish area north and east of the project area is described as a 200 to 600-foot-thick section of limestone interbedded with calcareous sandstones and shale (Goddard and Zimmerman, 2003).

Figure 68 shows the local structure and isopach map for the Anahuac Formation in the project area. The Anahuac Formation is anticipated to be encountered at an average true vertical depth of approximately 8,580 feet and will average 955 feet in thickness.

The remainder of this page intentionally left blank.

Figure 68: Top structure (left) and isochore (right) of the Anahuac Formation (structure C.I. = 150'; depths SSTVD; Isochore C.I. = 200') with the three potential OFIC injection sites shown. See information for OFIC petrophysical wells in Figure 21 and Table 2.

There are two main lines of evidence indicating the effectiveness of the Anahuac Formation as an upper confining zone. The most direct evidence is that it is its own seal for oil and gas reservoirs where production exists. In the greater area, the Anahuac Formation along with Frio Formation internal shales are also a recognized seal for Frio Formation reservoirs in southern Louisiana (Galloway et al., 1982, 1983 and 2000). In West Baton Rouge and Iberville parishes, the Anahuac Formation is the seal above the Frio Formation at Bayou Choctaw field south of the project area. The Frio Formation is gas charged to the base of the Anahuac Formation in some wells in Port Allen field north of the project area (Neal et al., 1993; Goddard et al., 2005).

The second line of evidence also comes from published literature. The majority of CO_2 confining zones meeting the U.S. Geological Survey criteria for long-term effective sealing zones are marine shales found on the open shelf or in a basinal setting because they are regionally extensive, have low permeability, and are homogenous (Merril, 2013). The U.S. Geological Survey's Geologic Framework for the National Assessment of Carbon Dioxide Storage Resources-U.S.-Gulf Coast identifies that the fine-grained marine shales of the Anahuac Formation are an effective confining zone for the Frio Vicksburg Storage Assessment Unit due to its shaley composition and great thickness (Roberts-Ashby et al., 2014).

The closest available mineralogical composition data for the Anahuac Formation is from the Frio Brine Study conducted by the Gulf Coast Carbon Center (GCCC) (Hovorka et al., 2008) which was conducted in Texas state waters near the Louisiana border. Bulk and clay mineralogy are presented in Table 8 below.

Table 8: Bulk mineralogy and clay species for the Anahuac Formation from the Frio Brine pilot project area.

Anahuac Shale Character	
	Mineralogy
Bulk	28% Quartz
	20% Calcite
	12% Other
	41% Clay
Clay % (Total to 100%)	75% Illite/smectite
	11% Illite
	11% Kaolinite
	3% Chlorite

Porosity and permeability for the Anahuac Formation from the Frio Brine Pilot project show porosity ranging from 11% to 17% (average 13%) while permeability ranges from 0.082 mD to 2.74 mD (average 0.97 mD).

Bulk mineralogy, as seen in Table 8, is mostly unreactive to CO_2 injection except for the clay minerals, particularly the mixed-layer illite/smectite, which makes up 75% of the total clay. Illite and kaolinite help stabilize an injection plume by adsorbing and fixing it in place. As previously discussed, smectite will as well, except in some specific cases (Busch et al., 2016).). Busch et al. (2016) and Martin et al. (2022) stress the importance of understanding confining zone mineralogy,

particularly clay mineralogy. Live Oak CCS, LLC plans to conduct site-specific assessment of mineralogy during pre-operational testing.

The values in Table 8 can be generally applied across the area with the caveat that the project area is to the north and east and may contain higher percentages of calcite (John et al., 1992; Goddard and Zimmerman, 2003). Literature also states that the dominant provenance for Oligocene sediment contains volcaniclastic sediments entering the Gulf of Mexico from the west (Galloway et al., 2000; Galloway, 2008; Swanson et al., 2013; and Snedden et al., 2020). Due to greater distance from the source area, Oligocene rocks in central and eastern Louisiana have a lower percentage of these sediments. These depositional trends will be discussed more thoroughly for the Frio Formation injection zone in subsection 2.4.2.2 below.

2.4.2 CCS System 2: The Oligocene Frio Injection Complex (OFIC)

In the project area, the Oligocene storage complex is composed from top to bottom of the Anahuac Formation upper confining zone, Frio Formation injection zone, and the Vicksburg Shale as the lower confining zone. These confining and injection zones extend throughout the Gulf of Mexico, and their properties in the project area make them an effective CO_2 storage complex (Figure 53, Figure 54). The Oligocene age designation for this storage interval is asserted by many authors, including but not limited to Galloway et al. (1991), Galloway et al. (2000), Dubiel et al. (2007), Galloway (2008), Swanson et al. (2013), Roberts-Ashby et al. (2014), Goddard (2015), and Goddard and Zimmerman (2003).

2.4.2.1. OFIC Upper Confining Zone: Anahuac Formation

The Anahuac Formation is the upper confining zone for the OFIC and the lower confining zone for the LMIC. It is discussed in detail in subsection 2.4.1.3 above with evidence that it is a robust upper confining zone for the OFIC.

2.4.2.2. OFIC Injection Zone: Frio Formation

The Frio Formation comprises late Oligocene age deltaic, marine, and marginal-marine sands and interstitial shales (Swanson et al., 2013; Galloway et al., 2000). Age-equivalent strata include continental siliciclastic sediments of the Catahoula Formation and mixed siliciclastic-carbonate and shallow water carbonates of the Paynes lower Hammock Formation and the Chickasawhay (Galloway et al., 1982 and 1991). There are no formally recognized members of the Frio Formation, but many authors break it into Upper and Lower sandstone intervals and include a Middle Frio as well (Figure 53; Swanson et al., 2013; Goddard et al., 2005; Krueger Jr., 1967).

Regionally, the Frio Formation was deposited in a wide variety of marine, near-shore, deltaic, and continental environments (Galloway et al., 2000; Galloway et al., 2008). Galloway et al. (2000) created depositional diagrams for the combined Frio Formation/Vicksburg Shale, as shown in Figure 13 in subsection 2.1.9 of this Application Narrative. The greatest coarse sediment load for early Oligocene Vicksburg deposition took place in the western Gulf of Mexico in the Norma and Noria wave-dominated deltaic systems on the Texas Coast along the Rio Grande sediment dispersal axis (RG). The Louisiana coast received much less sediment through the initially much smaller Central Mississippi dispersal axis (CM), promoting Vicksburg marine shale deposition (Galloway et al., 2000). Later, during Frio Formation deposition, sedimentary input from the RG

lessened, and the dominant axis became the Houston Delta (HD) area. Eventually, the Mississippi Valley river-dominated delta system of Central Louisiana deposited Frio Formation sand in southern Louisiana (Figure 13; Galloway, 2008; Galloway et al., 2000; Galloway et al., 1982; Combes, 1993). High volcanic input, including recycled volcanic ash, was introduced into depocenters most proximally in the western Gulf of Mexico, while less clastic input was deposited overall in the eastern Gulf of Mexico (Galloway et al., 2000).

Figure 66 shows top Frio Formation depths as greater than 8,600 feet TVD in the Port Allen field, and Figure 67 shows this top in West Addis Field at approximately 9,700 feet TVD (Goddard et al., 2005; Krueger Jr., 1967). The anticipated top of the Frio Formation in the project area is approximately 10,770 feet TVD (Figure 53).

Regionally, the Frio-Vicksburg combined thickness ranges between 1,100 and 2,700 feet (Roberts-Ashby et al., 2014). Figure 66 from the Lobdell Field area in West Baton Rouge parish shows 1,500 feet of Frio Formation, as does Figure 67 from the West Addis Field in West Baton Rouge and Iberville parishes (Goddard et al., 2005; Krueger Jr., 1967).

Southwest of the project area in southwest Louisiana and adjacent counties in Texas, the Frio Formation contains a large area of up to 3,000 feet of sediments composed of submarine channel-fill and submarine fans called the Hackberry trend (Swanson et al., 2013). This feature formed when Jurassic Louann Salt mobilized, causing a continental shelf collapse during middle Frio deposition and creating areas of sand fault-block fill and channel fill (Ogiesoba and Hammes, 2012; Galloway et al., 2000). Figure 69 shows a schematic cross-section of the Hackberry Trend and the different Frio strata it created within each bio-stratigraphic zone.

The remainder of this page intentionally left blank.

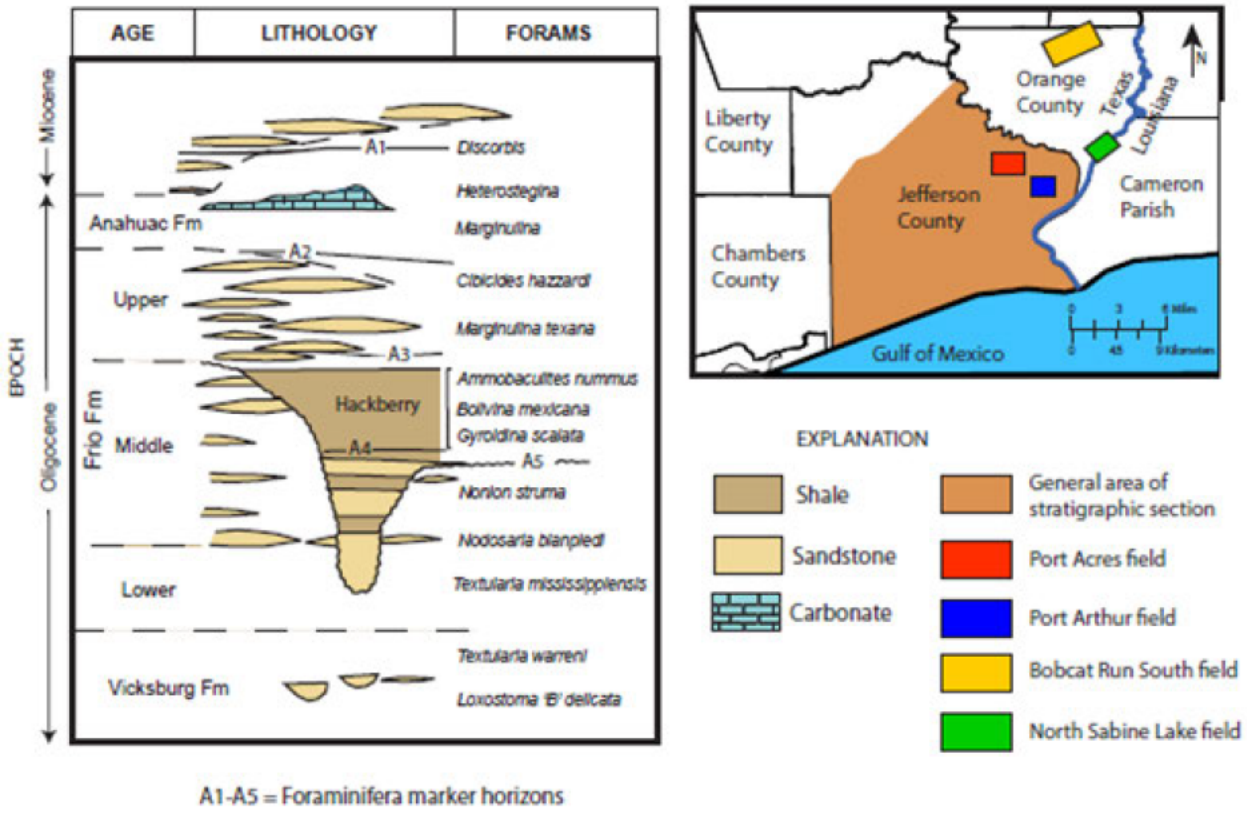

Figure 69: Schematic showing Frio Formation deposition in the Hackberry Trend area southwest of the project area. Modified from Swanson et al., 2013.

Growth faults during Vicksburg Shale and Frio Formation deposition created areas of increased thickness in small subbasins and rollover structural traps against the faults that formed them. The project area is within a more stable area with minimal thickening due to fault movement and radical increases in thickness unlikely (Swanson et al., 2013). Faulting near the project area is seen in the West Addis, Port Allen, and Lobdell fields and is addressed in subsection 2.3 of this Application Narrative.

Reservoir quality in the Frio Formation increases from west to east as the percentage of quartz increases, while volcanic and carbonate rock fragments decrease (Loucks et al., 1984). Preservation of the primary porosity contributes to more porous and permeable shallow Frio sands, while secondary porosity formation is important for maintaining porosity and permeability in deep Frio sands (Loucks, 2005). Overall, reservoir quality is ideal with average porosity ranging from 20% to 35% (average 27%) while permeabilities range from 50 mD to 2,500 mD with an average of 685 mD (Swanson et al., 2013). Other sources indicate permeabilities of 0.1 mD to 3,000 mD with 200 mD as the most likely value for the Frio Formation and Vicksburg Shale combined (Nehring and Associates Inc., 2010). In southern Louisiana, the Frio Formation has 15% to 33% porosity and 100 mD to 2,500 mD of permeability (Goddard, 2015). Frio Sand in the Claimed as PBI [redacted] well (API No. Claimed as PBI [redacted]) in West Baton Rouge parish has 20% to 30% porosity and 300 mD to 2,610 mD of permeability.

Figure 63 shows the Poro-Perm transform for Frio Formation for 30 wells with publicly available core data in Ascension, East Baton Rouge, Iberville, St. John the Batist, St. Martin, and West Baton Rouge parishes. Frio Formation have overall good to very good reservoir quality and exhibit the same degradation of permeability with increasing silt and clay content. Table 2 in subsection 2.1.13.4. shows API numbers and locations of wells included in Figure 63.

2.4.2.3. OFIC in the Project Area

The lower part of the Frio Formation in West Baton Rouge and Iberville parishes is composed of 10 to 30 feet thick sandstone reservoirs separated by 100 to 200 feet thick shales, while the upper part of the Frio Formation contains massive sands separated by thinner shales (Goddard et al., 2005; Krueger Jr., 1967). These mostly shallow water marine sands are interpreted as marine bars, barrier bars, and delta-front distributary mouth bars consistent with their location in the Central Mississippi delta axis of deposition (Figure 13; Goddard et al., 2005; Krueger Jr., 1967; Galloway, 2000).

The Frio Formation in the Florida parishes of eastern Louisiana is 1,000 to 1,800 feet thick and made up of sandstone interbedded with shale deposited conformably above the Vicksburg Shale (Goddard and Zimmerman, 2003). The interpreted depositional environment is shallow marine, and sand is deposited in barrier bars and stacked distributary mouth bars.

Well logs for an overlapping set of twelve wells that underwent petrophysical analysis for the Lower Miocene Sand were also used to evaluate the Frio Formation. As with the Lower Miocene Sand, Frio Formation porosity logs were calculated as were Vshale curves and Vshale flags. Figure 63B shows the porosity-permeability transform for fifteen wells with core in the Frio Formation.

In the West Baton Rouge parish portion of the project area, sands in the Frio Formation in the [redacted] well core (API No. Claimed as PBI; see location in Figure 22 and Table 2) are described as mostly fine to very fine-grained sand, commonly silty to occasionally very silty and shaley. Silty intervals are very shaly and slightly calcareous. Silty and shaley sands are calcareous to very calcareous.

Table 9 summarizes the core data available for this well. The Frio Formation shows the same inverse relationship between percentage silt and shale and permeability that was observed in the Lower Miocene Sand. The porosity-permeability cross-plot relationship from Figure 63 was used to calibrate porosity logs and assign a constant permeability value to intervals flagged as shale in the Frio Formation as was done in the Lower Miocene Sand interval.

The remainder of this page intentionally left blank.

Table 9: Summary of core analysis for the Claimed as PBI well (API No. Claimed as PBI) in Green Lake Field, West Baton Rouge parish.

Claimed as PBI	**Frio Reservoir Summary**	
UWI#: Claimed as PBI	**Green Lake Field**	
Location: Claimed as PBI		
Top Oligocene: 7,900'	**Base Oligocene**: >10,800'	
Core Depths included: 9,444-9,685		
Core Data Summary		
	Average	Range
Core Perm: Sand (mD)	592	2.9-2,610
Core Phi: Sand (%)	25%	19-30%
% Silt & Clay: Sand	33%	11-61%
Core Perm: Silt (mD)	0.7	0.6-0.8
Core Phi: Silt (%)	17%	16.4-17.1%
% Silt & Clay: Silt	82.50%	82-85%
Note there are only 2 Silt data points		

Mapping in the immediate project area shows an average gross thickness of 925 feet for the Frio Formation injection interval and less than 25% sand in the formation. There is an average of 317 feet of sand at the injection well locations (Figure 70).

The remainder of this page intentionally left blank.

Figure 70: Top structure (left) and isochore (right) of the Frio Formation (structure C.I. = 500'; depths SSTVD; Isochore C.I. = 100') with the three potential OFIC injection sites shown. See information for OFIC petrophysical wells in Figure 21 and Table 2.

There is no compositional analysis data for the Frio Formation in this area. Loucks et al. (1984) discusses changes in clay content regionally in the Frio Formation, and Galloway et al. (2000) and Swanson et al. (2013) discuss lower percentages of volcaniclastic rock and reworked clays encountered in the Oligocene from west to east in the Gulf of Mexico. If there are high percentages of interlayered illite/smectite in the Frio Formation clay mineral fraction, it could present complications for CO_2 sequestration as previously discussed in subsection 2.4.1.3 above.

2.4.2.4. OFIC Lower Confining Zone: Vicksburg Shale

The lower confining zone for the OFIC is the Vicksburg Shale (Galloway et al., 1982, 1983, and 2000; Goddard and Zimmerman, 2003). Figure 13 shows early Oligocene Vicksburg Shale and Frio Formation in one diagram. Galloway et al. (2000) describe changes within the Vicksburg Shale from west to east. Sand deposition occurred primarily in the western Gulf of Mexico on the Texas side while shale was deposited in Louisiana due to a low volume, muddy sediment load transmitted down the Central Mississippi delta system in the early Oligocene. This depositional pattern created a wide, muddy continental shelf in West Baton Rouge and the surrounding parishes (Galloway et al., 2000; Galloway, 2008). In southern Louisiana, the Vicksburg Shale is composed of shelf mud and marl with no oil and gas production (Galloway, 2008; Goddard, 2015). At Bayou Choctaw field in Iberville Parish, the Vicksburg Shale is overlain by deepwater marine Frio Formation shale beneath Lower Frio Formation sand reservoirs (Goddard and Zimmerman, 2003; Neal et al., 1993).

A schematic structural cross section from east central West Baton Rouge parish shows the continuity of the Vicksburg Shale from the Lobdell Field through Port Allen Field and an approximate thickness of 500 feet (Figure 46; Goddard et al., 2005).

The Vicksburg Shale is an effective lower confining zone for the OFIC. There are overpressured zones within this shaly zone that do not extend upward at Bayou Choctaw field indicating a lack of vertical communication (Neal et al., 1993). The Vicksburg Group (Howe, 1962), in combination with the Jackson Group (Howe, 1962), forms the stratigraphic top-seal for Cockfield Sand reservoirs at Opelousas field in St. Landry parish, Louisiana (Paine et al., 1968).

Goddard et al. (2005) reported that the Kern County Land Co. Martin J Kahao #1 well was used to determine the area stratigraphy for the wells in Lobdell and Port Allen fields (Figure 46). No publicly available data or published information could be located to confirm the mineralogy, sealing properties, or mechanical strength of the Vicksburg Shale lower confining zone.

2.4.3 Regional Estimated Injection Zone Storage Capacity

Prospective storage resource estimates for the project were calculated for the sandstone reservoirs using the methodology detailed in Goodman et al. (2011) and Goodman et al. (2016) for saline formations. This methodology generates storage resource estimates using equations 3 and 4 (from Goodman et al. (2016)):

$$G_{CO2} = A_t h_g \emptyset_{total} \rho_{CO2} E_{Saline} \quad \text{..... Eq 3,}$$

where E_{saline} is the CO_2 storage efficiency factor that reflects a fraction of the total pore volume that is filled by CO_2,

$$E_{Saline} = E_A E_h E_\emptyset E_V E_d \quad \text{Eq 4,}$$

where A is area, h is thickness, Ø is porosity, V is volumetric displacement, and d is microscopic displacement.

Prospective storage resource estimates were calculated using average properties across all reservoir formations within the project area in the DOE-NETL CO2 SCREEN tool. Sandstone intervals were isolated for the Lower Miocene Sand and Frio Formations, and average physical characteristics were calculated for a resource estimate. All physical inputs, storage efficiencies, and assumptions are shown in Table 10. The resource estimate suggests that all reservoir formations may be able to store between 173 (P10) to 914 (P90) MMT of CO_2. Table 11 details the results of the prospective storage resource calculations.

Table 10: Parameters used for Calculating Storage Resource Estimates for Reservoir Formations. Note: CO_2 density is based on reservoir conditions using regional gradients. Efficiency values obtained from 2024 version of NETL CO2 Screen Tool for respective depositional environment.

Resource Estimate Inputs			
Attribute		**LMIC**	**OFIC**
Mean Sand Thickness (m)		553	278
Mean Porosity (%)		27.7	28
Area (Km^2)		74.4	
Depositional Environment		Shallow Marine	Shallow Marine
Saline Storage Efficiency	**P10**	2.01	0.69
	P50	4.97	1.92
	P90	8.63	4.15

Table 11: Cumulative and probabilistic scenarios for prospective storage resource estimates for all reservoir formations based on the SEM values. 30 years of injected volume was calculated using Storage Efficiency Factors Type CO2BRA (2022).

Reservoir	**Total CO_2 (MMT)**			**Total CO_2 (MMT/$mile^2$)**		
	P10	**P50**	**P90**	**P10**	**P50**	**P90**
Lower Miocene Injection Complex	146	378	739	5.10	13.17	25.76
Oligocene Frio Injection Complex	27	76	174	0.93	2.63	6.07
Total Summed Storage	**173**	**454**	**914**	**6.03**	**15.80**	**31.83**

2.5. Geomechanical, Petrophysical, and Rock Physics Information

Petrophysical data evaluation was conducted using well logs from 20 well locations. Porosities were calculated using a combination of acoustic, neutron, and density logs. Thirty wells, 15 in the LMIC and 15 in the OFIC, with core and well log data were used to determine the porosity-

permeability correlations in the area of interest as listed in Table 2. Each injection zone (Lower Miocene Sand and Frio Formation) was assigned a unique porosity and permeability correlation (Figure 63). Porosity correlations were focused and calibrated using the volume of shale (Vshale) flag to apply only on the sandstones. Vshale was determined using a simple correlation among gamma ray, spontaneous potential, and resistivity logs creating a volume of shale/net sand flag. The shales from the Vshale flag were assigned permeability values based on a constant value or distribution as available.

Geomechanics and rock physics analyses were determined using data from 5 well logs from which rock properties were determined using empirical relationships and will be detailed in subsection 2.5.6 of this Application Narrative.

Initial observations indicate that both the Lower Miocene Sand and Frio Formation are suitable for CO_2 storage, but the Lower Miocene Sand is likely capable of storing more CO_2 due to its higher porosity and permeability, as well as its cleaner composition with less silt and clay content. The Lower Miocene Sand and Frio Formation exhibit notable differences in their petrophysical properties (Table 12). The Lower Miocene Sand has a gross mean porosity (PHIT) of 0.261 while the Frio Formation has a gross mean porosity of 0.13. Lower Miocene Sand sand volume (VSAND) is 0.767, compared to 0.485 in the Frio Formation, suggesting better permeability and fluid flow. The Lower Miocene Sand also has lower silt (VSILT) and clay (VCLAY) volumes, 0.059 and 0.134 respectively, compared to 0.303 and 0.157 in the Frio Formation, indicating a cleaner and more favorable formation for CO_2 injection. The lime volume (VLIME) is slightly higher in the Lower Miocene Sand, which could impact its mechanical properties.

Table 12: Table of Petrophysical Properties for Injecting Zones from the Claimed as PBI well (API No. Claimed as PBI; see location for Well No. 34 in Figure 20, Well No. 54 in Figure 21, and Table 2).

Formation	Depth (ft)	PHIT (Mean)	VSAND (Mean)	VSILT (Mean)	VCLAY (Mean)	VLIME (Mean)
Lower Miocene Sand	7991.5 - 8342.5	0.261	0.767	0.059	0.134	0.033
Frio Formation	10259.5 - 10367	0.13	0.485	0.303	0.157	0.031

2.5.1 Middle Miocene Upper Confining Zone Petrophysical Analysis

The Middle Miocene Confining Zone porosity was evaluated using neutron-density and sonic logs, calibrated to core porosity and permeability data (Figure 71). The porosity model includes only the net sand intervals, which are essential for understanding the seal integrity. The stratigraphic horizons for the Top Miocene and Miocene (S), the top and the base of the Middle Miocene Confining Zone, respectively, are interpreted to be laterally continuous throughout the project area and were used to assess the sealing capacity of the Middle Miocene Confining Zone, ensuring that the zone can effectively trap CO_2 and prevent upward migration.

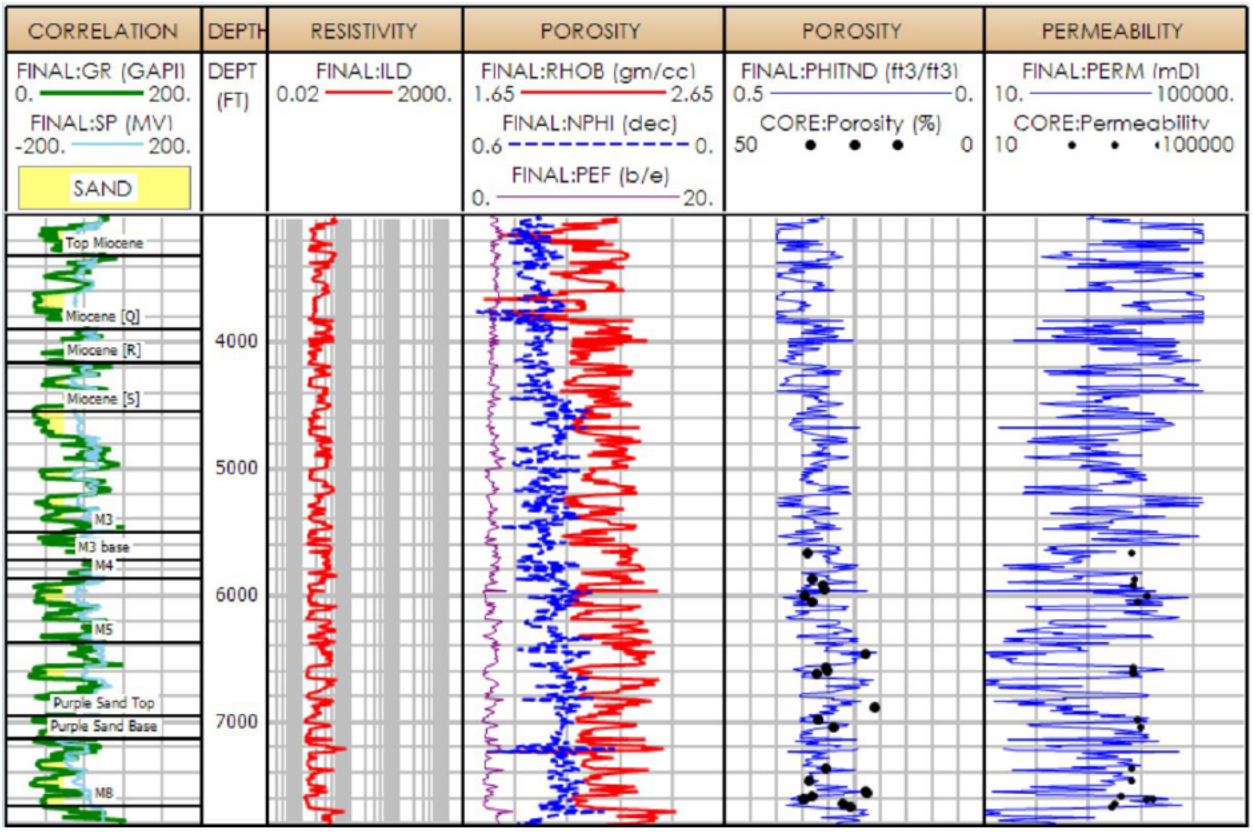

Figure 71: Representative log section through the Lower Miocene Injection Complex showing the vertical variability and locations of core points used in the petrophysical modeling. The log display shows the gamma ray and spontaneous potential logs (far left), the depth track in feet measured depth, the porosity curves, the calculated porosity curve with core data points, and the calculated permeability curve with core data points (far right). Data from API No. Claimed as PBI (see well No. 1 in Figure 20 and Table 2).

2.5.2 Lower Miocene Injection Complex Petrophysical Analysis

Existing data on the LMIC, with the injection zone being represented by the Lower Miocene Sand, indicates a depth of 7,991.5 to 8,342.5 feet. This sandstone exhibits an average porosity (PHIT) of 0.261, with a maximum of 0.41, indicating a high storage capacity. The sand volume (VSAND) is significantly high, averaging 0.767, which suggests excellent permeability. The silt volume (VSILT) and clay volume (VCLAY) are 0.059 and 0.134 on average, respectively, indicating a relatively cleaner sand with less fine-grained material that could impede fluid flow. The lime volume (VLIME) is low, averaging 0.033, typical for sandstones and beneficial for maintaining mechanical stability. This data is summarized in Table 12, and a representative section of the Lower Miocene Sand injection zone can be seen in Figure 71.

2.5.3 Anahuac Upper Confining Zone Petrophysical Analysis

The Anahuac confining zone was analyzed for its confining properties and potential to act as a barrier to vertical CO_2 migration. The petrophysical analysis focused on average porosity values, which suggest good sealing capacity (Figure 72). The clay content in this zone is also higher, which

when paired with the low porosity values, indicates an effective seal which is crucial for trapping CO_2 within the injection zones and preventing vertical migration into overlying formations.

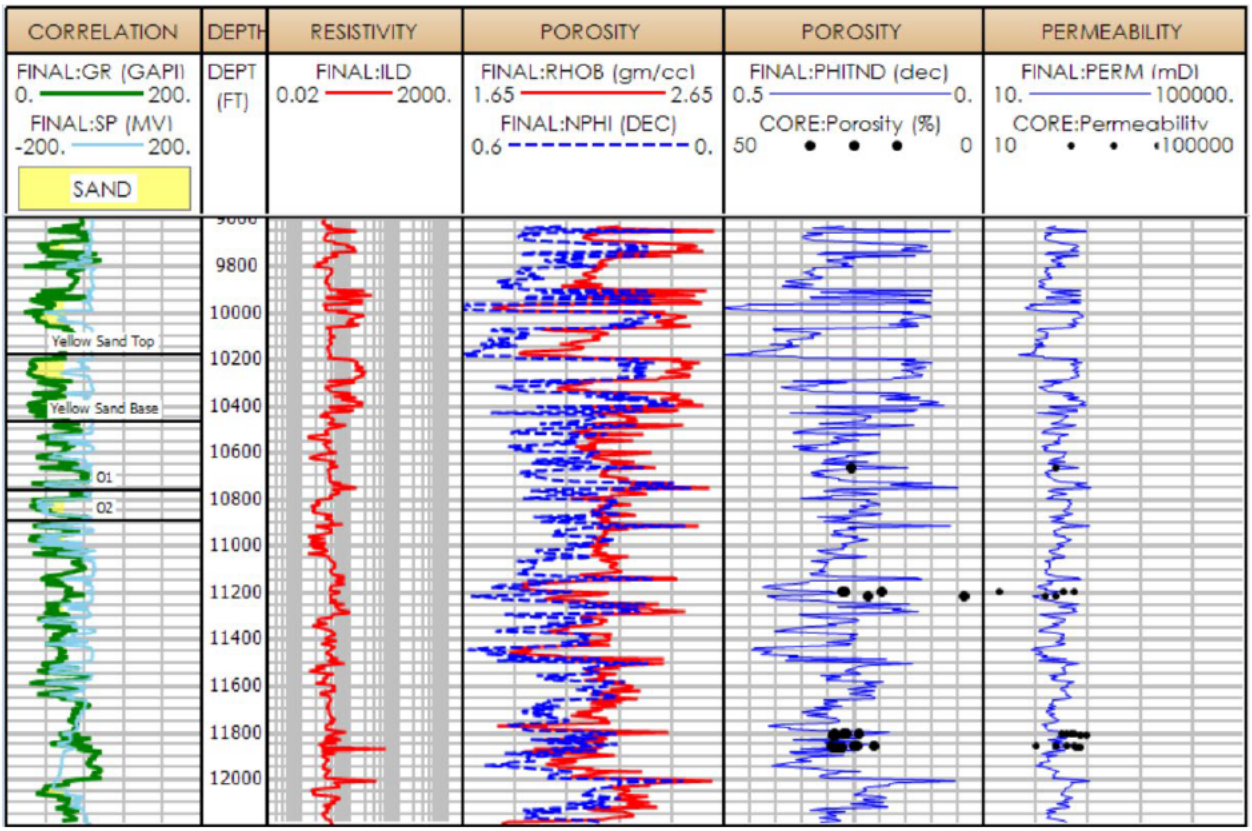

Figure 72: Representative log section through the Oligocene Frio Injection Complex showing the vertical variability and locations of core points used in the petrophysical modeling. The log display shows the gamma ray and spontaneous potential logs (far left), the depth track in feet measured depth, the porosity curves, the calculated porosity curve with core data points, and the calculated permeability curve with core data points (far right). Data from API No. Claimed as PBI (see well No. 16 in Figure 21 and Table 2).

2.5.4 Oligocene Frio Injection Complex Petrophysical Analysis

Existing data on the OFIC, with the injection zone being represented by the Frio Formation, was analyzed for its petrophysical properties. This sandstone lies at a depth of 10,259.5 to 10,367 feet MD. The gross average porosity (PHIT) is 0.13, with a minimum of 0 and a maximum of 0.275, indicating variable storage capacity across the formation. The sand volume (VSAND) averages 0.485, with a maximum of 0.91, suggesting a moderate to high presence of sand which is beneficial for permeability. The silt volume (VSILT) averages 0.303, and the clay volume (VCLAY) is 0.157 on average, indicating a mixed composition that could affect fluid flow. The lime volume (VLIME) is relatively low, averaging 0.031, which is typical for sandstones but can affect the mechanical properties of the rock. This data is summarized in Table 12, and a representative section of the Frio Formation injection zone can be seen in Figure 72.

2.5.5 Vicksburg Shale Zone Petrophysical Analysis

There is limited publicly available or published data for the Vicksburg Shale formation geomechanics and petrophysics within the project area. Site-specific data for all injection and confining zones in the project area will be obtained during pre-operational testing (see the Pre-Operational Testing Program for details). Information on injection and confining zone composition, mechanical strength, porosity and permeability and ultimately water chemistry and formation pressures will be gathered during pre-operational testing. Additionally, due to the buoyancy of CO_2, vertical migration away from the Vicksburg Shale zone within the injection complex is expected.

2.5.6 Geomechanics

A geomechanical evaluation reviewed data from five wells: Claimed as PBI (API No. Claimed as PBI), Claimed as PBI (API No. Claimed as PBI), Claimed as PBI (API No. Claimed as PBI), Claimed as PBI (API No. Claimed as PBI), and Claimed as PBI (API No. Claimed as PBI; see well locations in Figure 20, Figure 21 and Table 2). The analysis aimed to assess data quality, pore pressure, fracture pressure, and rock brittleness in the LMIC and OFIC upper confining zones and the LMIC lower confining zone. The OFIC lower confining zone has no data in the project area. Data quality issues were identified, including the absence of shallow density data crucial for pore pressure analysis and the lack of shear sonic data needed for brittleness proxies. The data quality varied, with resistivity logs being the most reliable and density logs often the worst due to washouts, possibly from underbalanced drilling. The Oligocene lithology was noted as questionable, affecting data reliability. The use of synthetic data increased error margins compared to measured logs. For density editing and synthesis, shale-sand trends were fitted using GR or SP logs. The density was reconstructed from a combination of compressional sonic (DTC) and GR log data, with specific adjustments for carbonate presence based on log responses.

Pore pressure analysis used Eaton's formula, incorporating hydrostatic and overburden pressures (Eaton, 1969). The normal pressure trend was established, and overpressure was indicated by deviations in the DTC log, particularly below 9,000 feet in Claimed as PBI 1 (API No. Claimed as PBI; see Well No. 40 location in Figure 20 and Table 2). The modeled pore pressure in the OFIC was slightly higher than hydrostatic, around 0.5-0.6 psi/ft. Fracture pressure was calculated at approximately 0.9 psi/ft, and overburden stress was about 1 psi/ft. Shear synthesis, using the Greenberg-Castagna model, provided estimates of various elastic properties, including P-impedance, S-impedance, and moduli like bulk modulus, shear modulus, and Young's modulus (Figure 73, Figure 74, and Figure 75). These properties are essential for understanding rock behavior under stress. Brittleness proxies were evaluated using the Modified Rickman method and Voigt-Reuss bounds . The Modified Rickman method uses Young's modulus and Poisson's ratio to assess brittleness, ductility, and rock strength, while Voigt-Reuss bounds consider theoretical bounds in bulk density versus P-wave velocity space (Figure 76, Figure 77, and Figure 78).

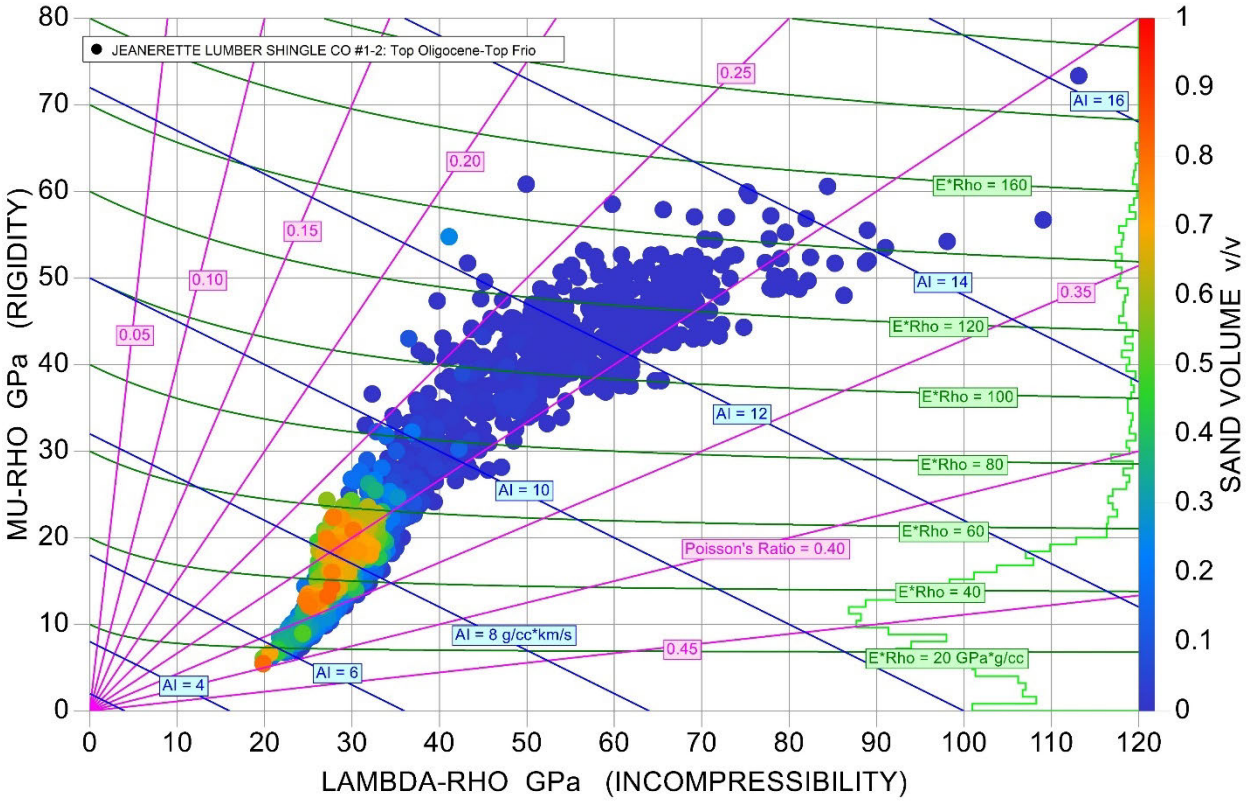

Figure 73: Incompressibility vs Rigidity - Sand. An example from the Top Oligocene to Top Frio confining zone interval for the sand volume fraction colored from 0 (cool colors) to 1(warm colors) (see right axis) vs Lambda-Rho (incompressibility) from 0 to 120 GPa (see bottom axis) vs Mu-Rho (rigidity) from 0 to 80 GPa (see left axis). The P-wave impedance (Al) is plotted in blue from 0 to 16 g/cc*km/s, Poisson's Ratio is plotted in magenta ranging from 0 to 0.5, Youngs Modulus (E)*Rho is plotted in green ranging from 0 to 200 GPa*g/cc. Note that the majority of the high sand volume fraction samples have both a low incompressibility and low rigidity, suggesting that the high sand fraction is relatively compressible and ductile.

The remainder of this page intentionally left blank.

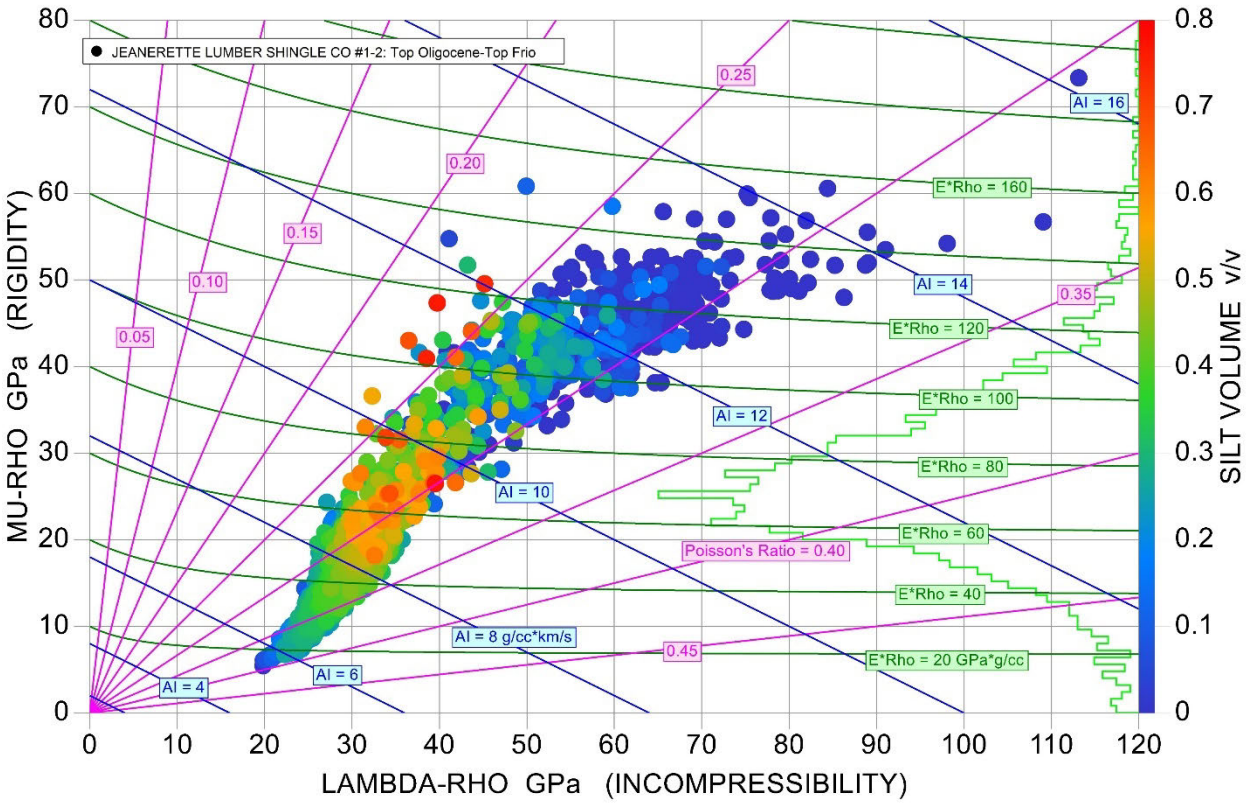

Figure 74: Incompressibility vs Rigidity - Silt. An example from the Top Oligocene to Top Frio confining zone interval for the silt volume fraction colored from 0 (cool colors) to 1 (warm colors) (see right axis) vs Lambda-Rho (incompressibility) from 0 to 120 GPa (see bottom axis) vs Mu-Rho (rigidity) from 0 to 80 GPa (see left axis). The P-wave impedance (Al) is plotted in blue from 0 to 16 g/cc*km/s, Poisson's Ratio is plotted in magenta ranging from 0 to 0.5, Youngs Modulus (E)*Rho is plotted in green ranging from 0 to 200 GPa*g/cc.

The remainder of this page intentionally left blank.

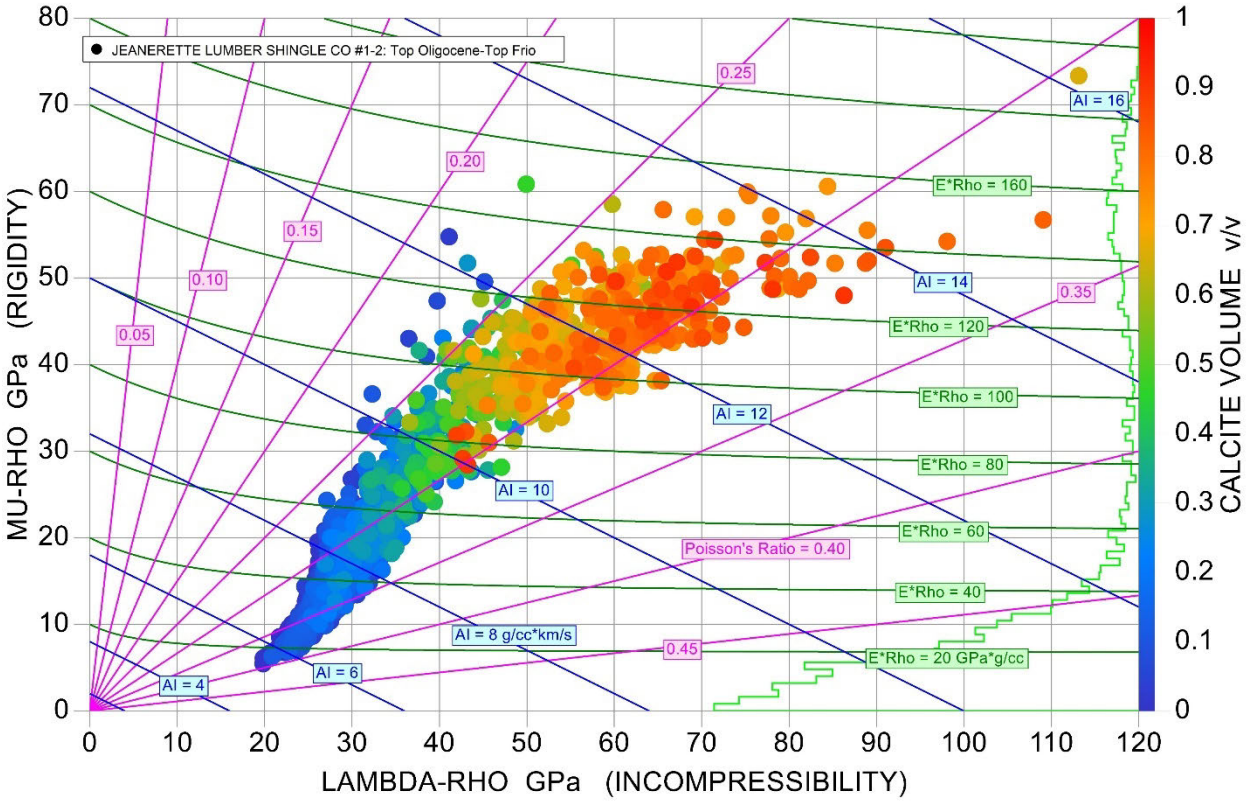

Figure 75: Incompressibility vs Rigidity – Calcite (limestone). An example from the Top Oligocene to Top Frio confining zone interval for the calcite volume fraction colored from 0 (cool colors) to 1(warm colors) (see right axis) vs Lambda-Rho (incompressibility) from 0 to 120 GPa (see bottom axis) vs Mu-Rho (rigidity) from 0 to 80 GPa (see left axis). The P-wave impedance (AI) is plotted in blue from 0 to 16 g/cc*km/s, Poisson's Ratio is plotted in magenta ranging from 0 to 0.5, Youngs Modulus (E)*Rho is plotted in green ranging from 0 to 200 GPa*g/cc. Note that the majority of the high calcite volume fraction samples have both a high incompressibility and high rigidity, suggesting that the high calcite fraction (limestones) are relatively incompressible and rigid.

The remainder of this page intentionally left blank.

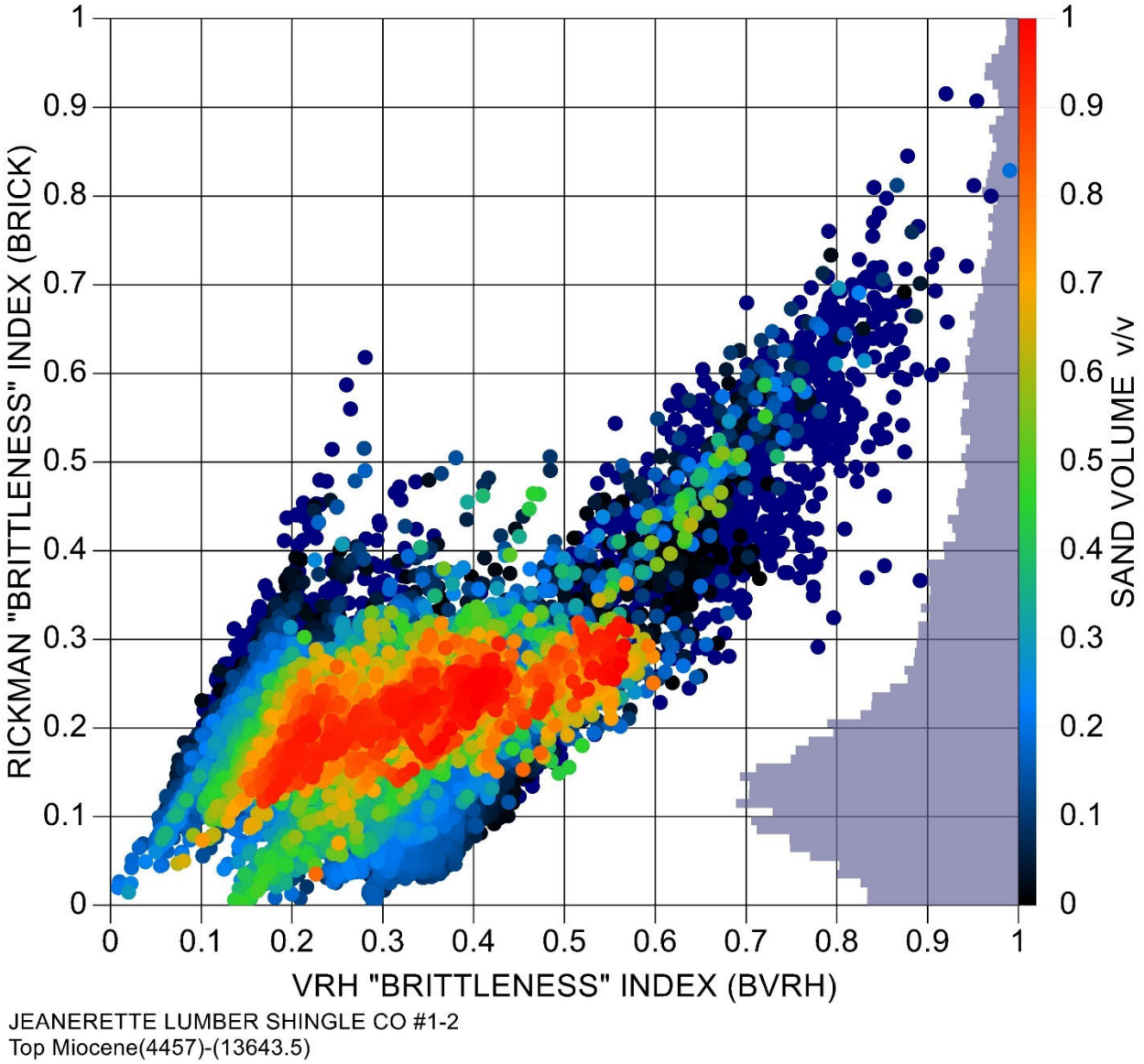

Figure 76: Voigt-Reuss vs Rickman Brittleness Indices – Sand. An example from the Top Miocene (4,457 ft) to Oligocene (13,643.5 ft) section for the sand volume fraction from 0 to 1 (right axis) vs Voigt-Reuss Bounds (VRH) 'brittleness' index (BVRH) from 0 to 1 (bottom axis) vs Rickman "brittleness" index (BRICK) from 0 to 1. The data points are colored by the sand volume fraction with warmer colors representing higher sand volume fraction vs cooler colors representing lower sand volume fraction. Note that the majority of the high sand volume fraction samples have a low "brittleness" index, suggesting that they are relatively compressible and ductile.

The remainder of this page intentionally left blank.

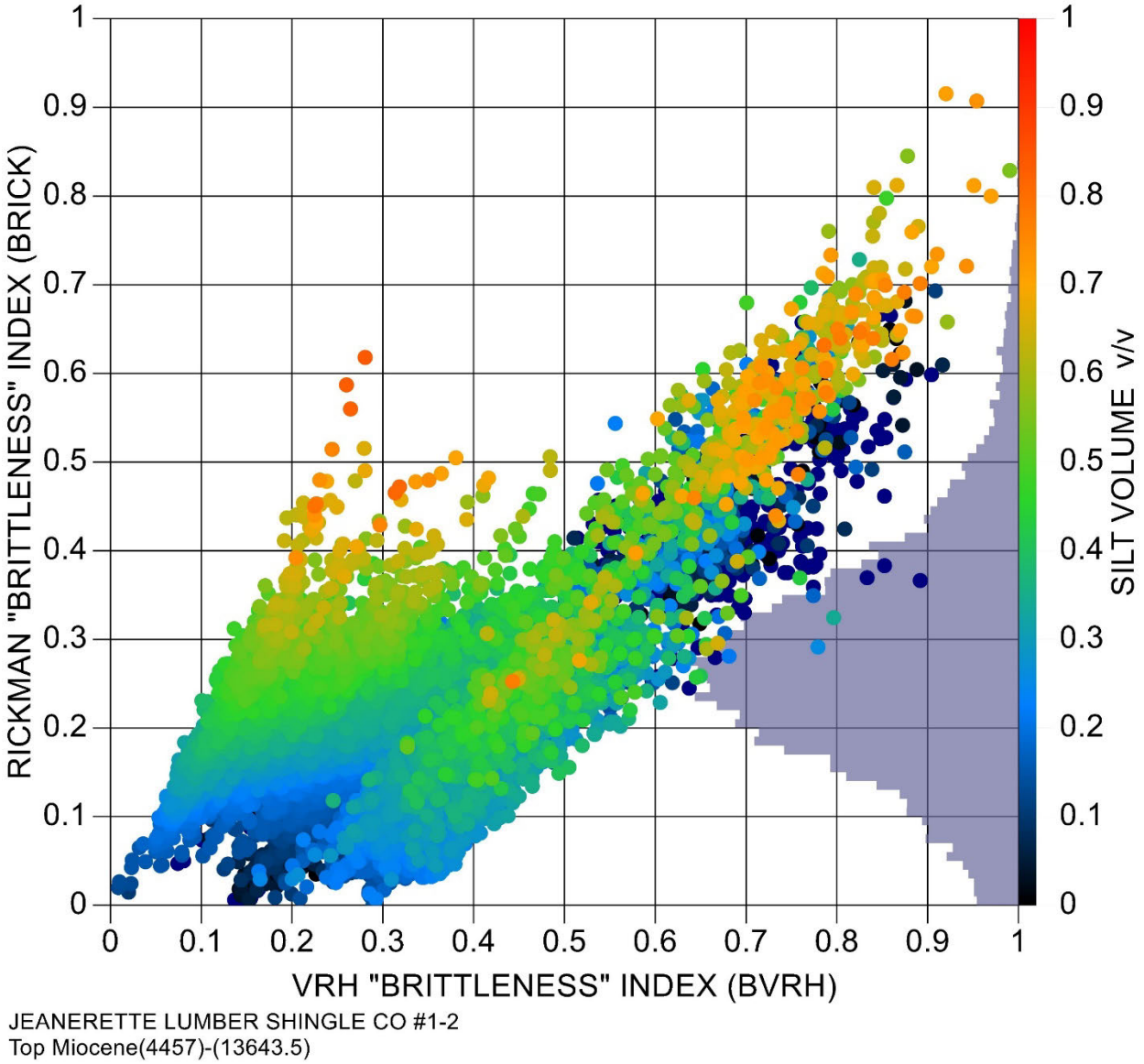

Figure 77: Voigt-Reuss vs Rickman Brittleness Indices – Silt. An example from the Top Miocene (4,457 ft) to Oligocene (13,643.5 ft) section for the silt volume fraction from 0 to 1 (right axis) vs Voigt-Reuss Bounds (VRH) 'brittleness' index (BVRH) from 0 to 1 (bottom axis) vs Rickman "brittleness" index (BRICK) from 0 to1. The data points are colored by the silt volume fraction with warmer colors representing higher silt volume fraction vs cooler colors representing lower silt volume fraction.

The remainder of this page intentionally left blank.

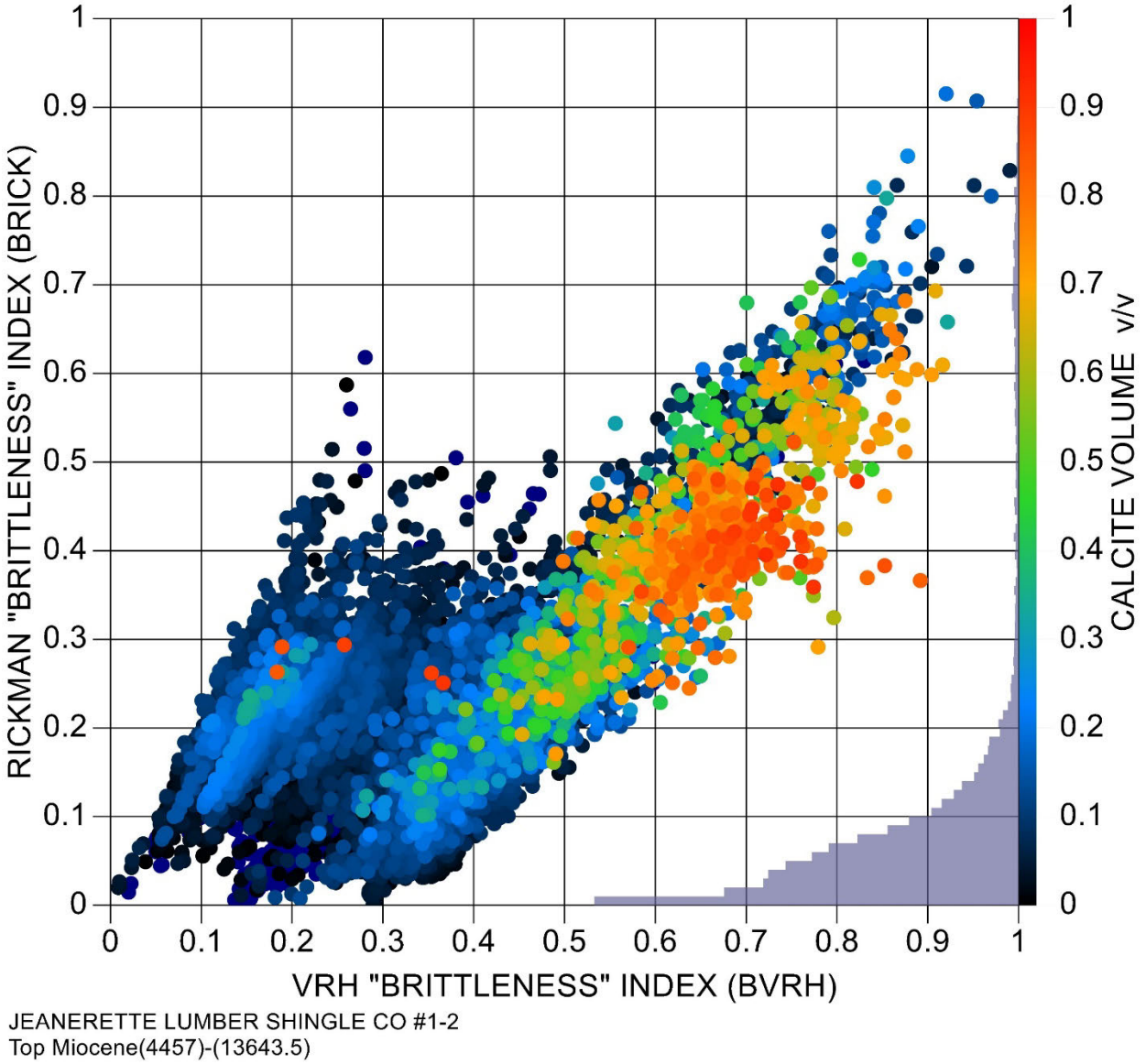

Figure 78: Voigt-Reuss vs Rickman Brittleness Indices – Calcite (limestone). An example from the Top Miocene (4,457 ft) to Oligocene (13,643.5 ft) section for the calcite volume fraction from 0 to 1 (right axis) vs Voigt-Reuss Bounds (VRH) 'brittleness' index (BVRH) from 0 to 1 (bottom axis) vs Rickman "brittleness" index (BRICK) from 0 to1. The data points are colored by the calcite volume fraction with warmer colors representing higher calcite volume fraction vs cooler colors representing lower calcite volume fraction. Note that the majority of the high calcite volume fraction samples have both a high Voit-Reuss and Rickman "brittleness" index, suggesting that the high calcite fraction (limestones) are relatively brittle compared to quartz fractions.

The remainder of this page intentionally left blank.

In summary, the geomechanical evaluation of the project provided a comprehensive analysis of well data, focusing on pressure trends, fracture pressure, and rock brittleness. The results, despite data limitations, offer a robust foundation for planning and executing the project effectively.

2.5.6.1. Proposed Geomechanical Studies

Proposed geomechanical studies include in-situ stress analysis and fracture pressure analysis, which are to be completed as part of the data collection program in the Pre-Operation Testing Program. The in-situ stress analysis aims to determine the stress state of the reservoir and overlying formations, providing insights into the mechanical stability of the confining zones. Fracture pressure analysis will evaluate the maximum pressure that can be applied without fracturing the confining zones, ensuring that the injection process does not compromise the integrity of the storage formations.

2.5.7 Rock Physics

Rock physics analysis involved the use of AVO (Amplitude Versus Offset) synthetics to model the elastic properties of the sands and their response to CO_2 substitution (Figure 79). This analysis is crucial for understanding how the rock formations will behave under different saturation states and pressures, which is essential for effective CO_2 sequestration. The in-situ brine saturation models represent the baseline state with full water saturation (Sw = 1), providing a reference point for comparing changes induced by CO_2 injection. In contrast, the CO_2 substitution models represent different levels of CO_2 saturation: Sw = 0.97 (3% CO_2) and bulk volume water (BVW) = 0.03 (97% CO_2). These models simulate how the presence of CO_2 affects the rock's properties, offering insights into the feasibility and efficiency of CO_2 storage in the formations.

The results from these models indicate notable changes in the properties of the Lower Miocene Sand when CO_2 is substituted. This sandstone exhibits notable alterations in elastic properties such as P-sonic velocity (P-wave velocity), bulk density, and Poisson’s ratio (Figure 79). These changes are particularly pronounced in the Lower Miocene Sand, suggesting it is highly responsive to CO_2 injection. Higher sensitivity to CO_2 indicates that the rock's physical properties, such as its ability to compact and accommodate CO_2, are very well suited for sequestration purposes. The Frio Formation still has all of the hallmarks of a viable injection target; however, it sees less change in these properties under similar conditions, indicating a lower sensitivity to CO_2 injection. The high porosity and sand volume, coupled with lower silt and clay content in the Lower Miocene Sand, provide a favorable environment for CO_2 storage. These petrophysical properties enhance permeability and fluid flow, ensuring more efficient CO_2 injection and retention.

The remainder of this page intentionally left blank.

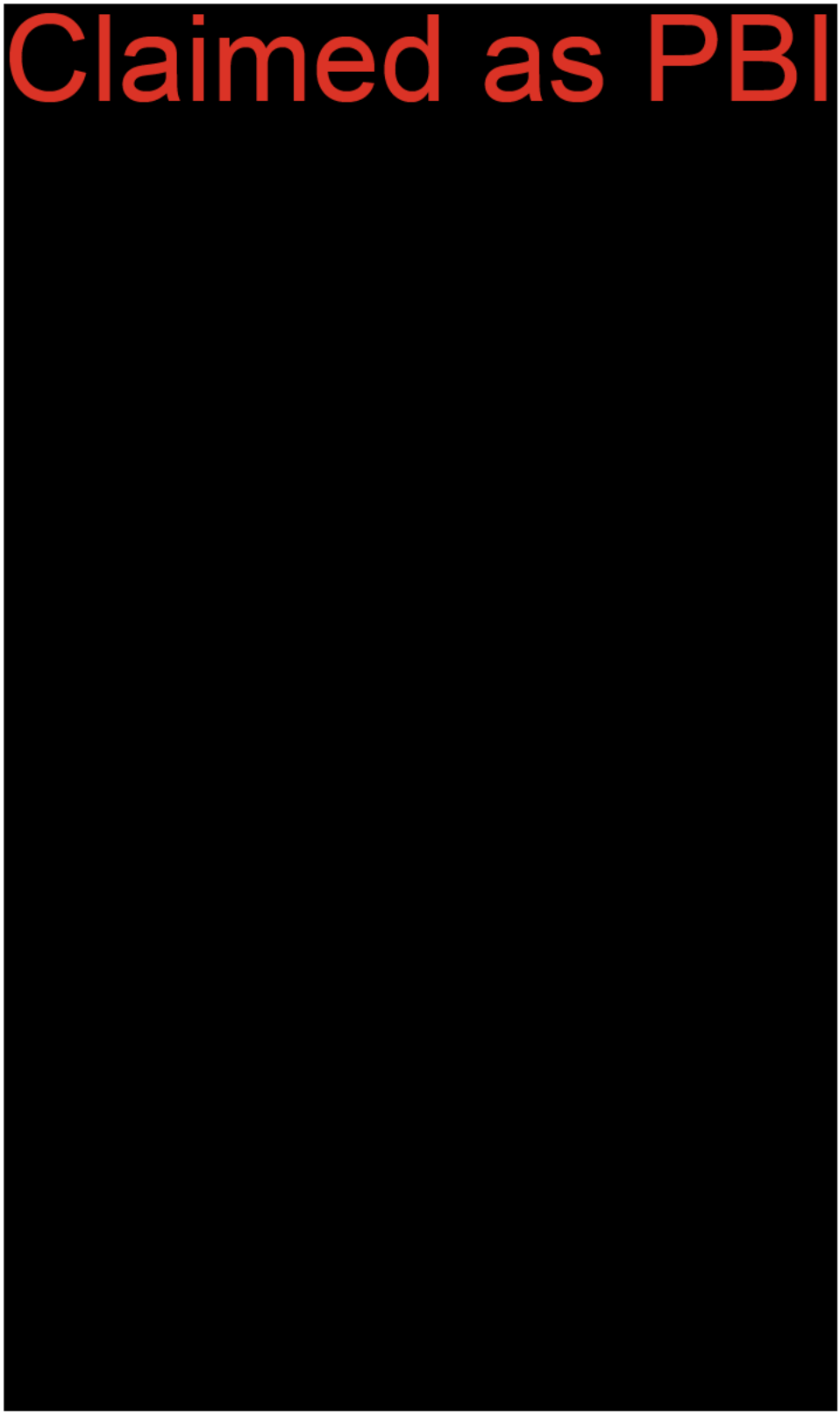

Figure 79: CO_2-Substitution Cross plots. In-Situ / SWE = 0.97 / BVWE = 0.03 cases (Lower Miocene Sand cross plot on the left and Frio Formation cross plot on the right).

2.6. Seismic History

The USGS Advanced National Seismic System (ANSS) Comprehensive Earthquake Catalog was used to provide the historical seismicity record for the AoR on local and regional scales (USGS, 2024). The catalog indicates two earthquakes with a magnitude greater than 2.5 have occurred in the last 40 years (from February 2024 to February 1984) within a 100-mile radius of the project area (Figure 80, Table 13). The closest seismic event in the last 40 years was approximately 40 miles from the AoR.

The remainder of this page intentionally left blank.

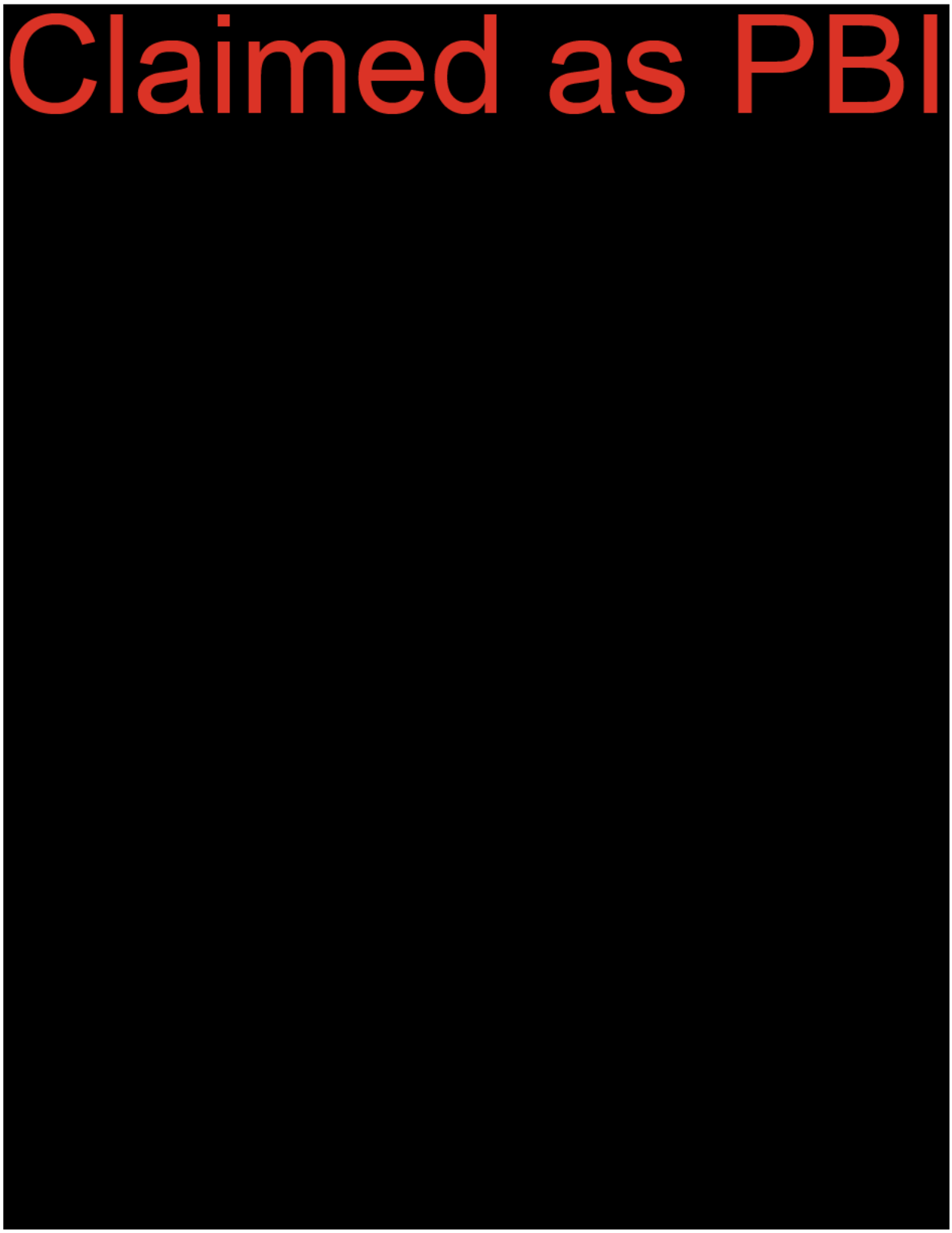

Figure 80: Map of seismic events and fault lines, search radius of 50 miles, and AoR "center point".

The project area is located in a region of very low observed seismicity. The AoR is located at the northern edge of the Gulf of Mexico Basin (Snedden et al., (2020) and is generally considered to be low risk for damaging earthquake shaking. The USGS National Seismic Hazard map (Petersen et al., 2023) shows that the AoR lies within an area with a 5-25% chance in 100 years of earthquake shaking equivalent to a Modified Mercalli Intensity (MMI) level VI or higher event. (Figure 81). An MMI VI event is "Felt by all, many frightened. Some heavy furniture moved; a few instances of fallen plaster. Damage slight." (Petersen et al., 2023). The USGS National Seismic Hazard model used to estimate the risk of earthquake shaking predicts peak horizontal acceleration of no more than 0.08g ($g = 9.8 m/s^2$) with a 2% probability for exceedance in 50 years for the AoR (Figure 82A), corresponding to MMI V shaking (Figure 82B).

The remainder of this page intentionally left blank.

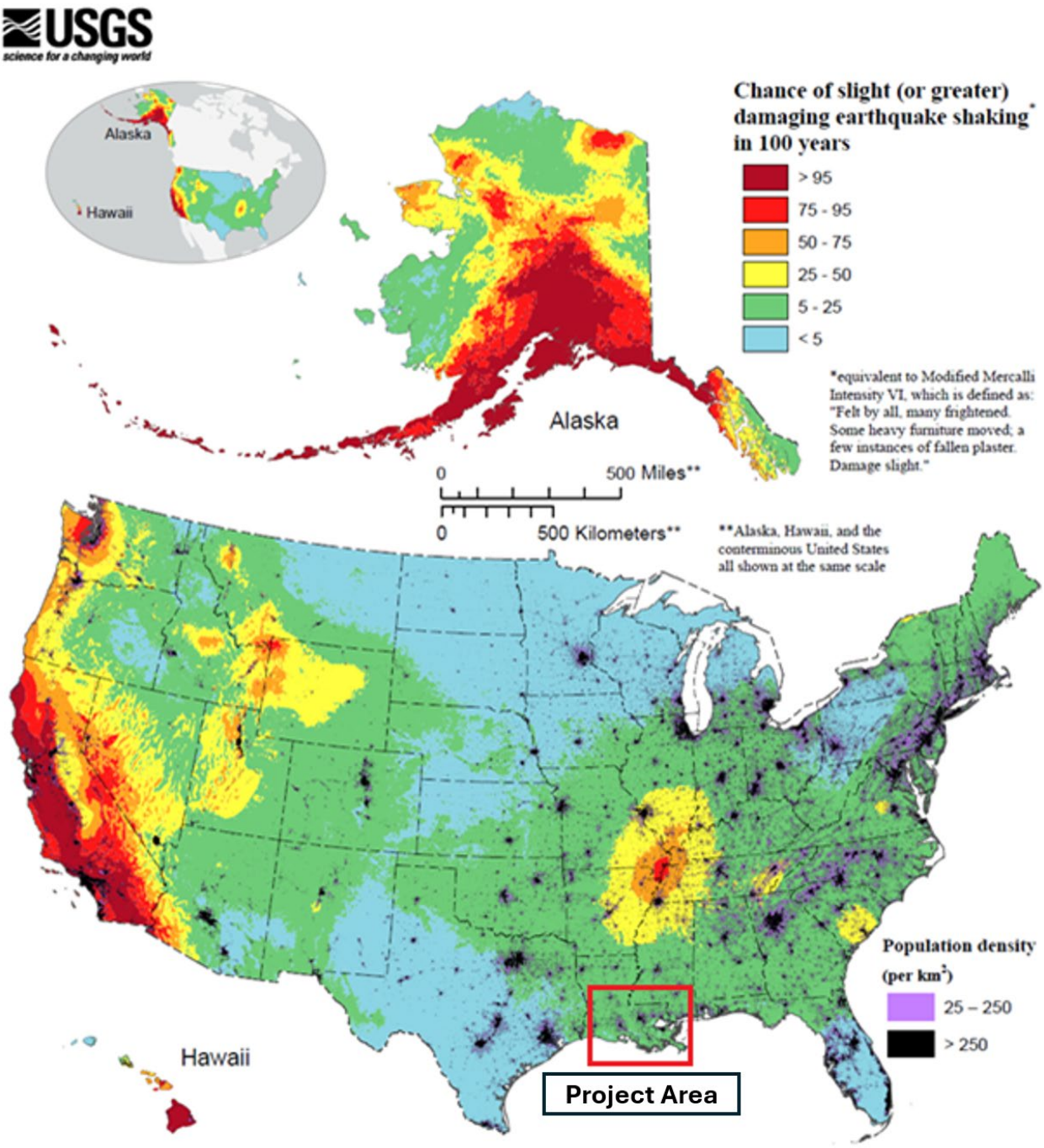

Figure 81: USGS National Seismic Hazard map showing percent chance of Modified Mercalli Intensity VI shaking in 100 years.

The remainder of this page intentionally left blank.

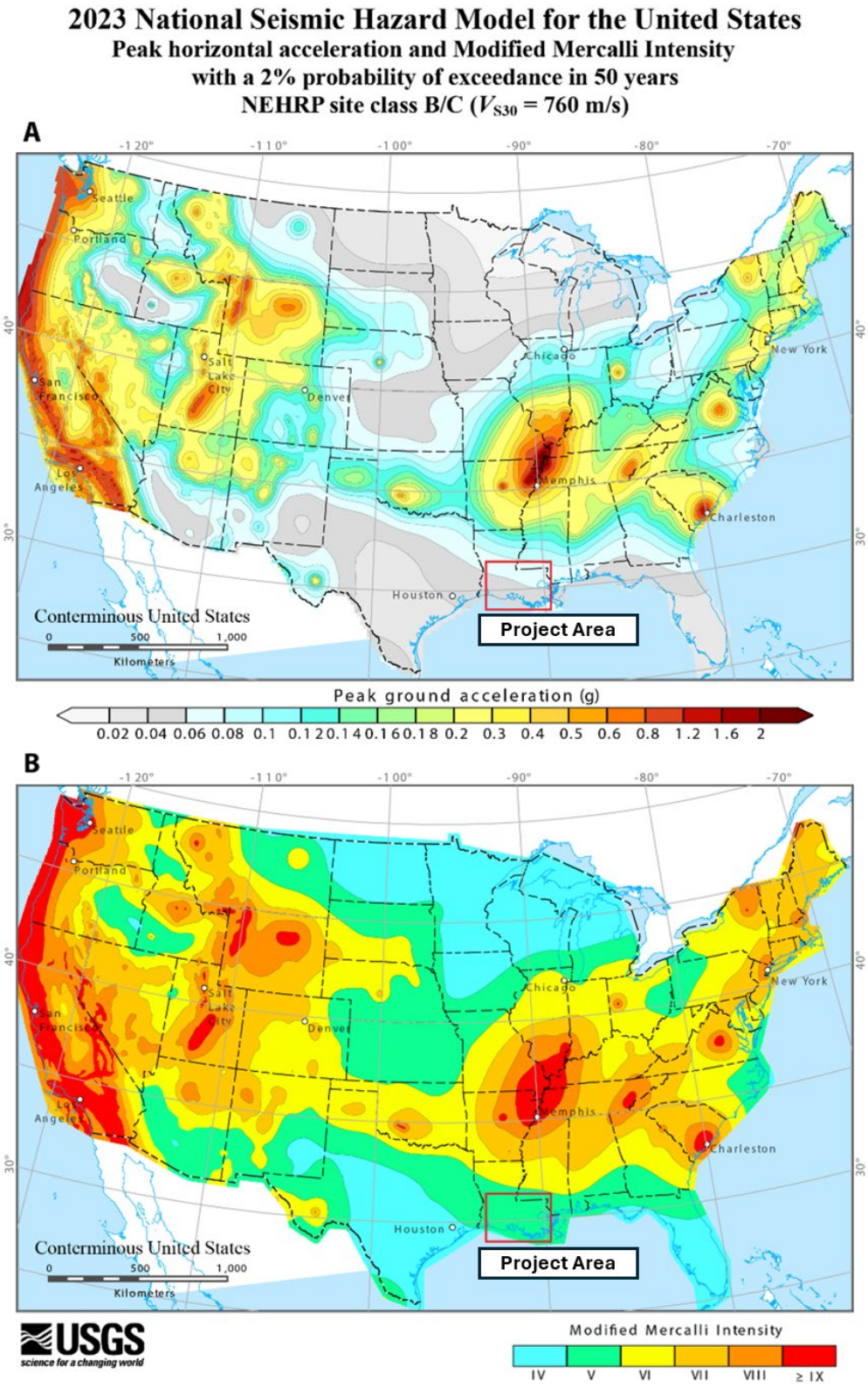

Figure 82: USGS National Seismic Hazard Map showing A) peak predicted ground acceleration and B) corresponding Modified Mercalli Intensity shaking. Study area shown in red rectangle. (Figure adapted from Petersen et at., 2003)

Regionally, predicted peak ground acceleration increases towards the New Madrid Seismic zone near the Missouri – Tennessee border but remains below 0.10g within a 100-mile radius of the AoR (Figure 82A) or MMI VI (Figure 82B). The New Madrid Seismic zone is the most significant source of historical seismicity in the broader region, with a 95% chance of an MMI VI or higher event in 100 years (Figure 81). This high-risk zone is confined to an area >600 miles from the AoR. Overall, the seismic history and earthquake shaking risk assessments modeled by the USGS indicate that the AoR has a relatively low risk of damaging earthquake activity.

More locally, the two earthquakes recorded in the last 40 years were M 3.0 events with felt shaking but no reported damage (MMI = IV) (USGS). Tectonically, the northern Gulf of Mexico basin is characterized as a passive margin and generally regarded as seismically quiescent. However, the Gulf Coast region is situated within a gravitationally-driven deformation system where Cenozoic sediments accumulated at the passive margin are gradually sliding basin-ward (downslope) along weak detachment layers associated with underlying salt (e.g. Peel et al., 1995; Gagliano et al., 2003b, Hudec et al., 2013; Figure 82). Louisiana and the AoR lie at the up-slope limit of this system where the sediments are under extension, resulting in the development of growth faults, which are observed in seismic and well data and mapped at the surface (Figure 16; McCulloh and Heinrich, 2013). Growth faults are a subset of normal faults that are characterized by steeply dipping fault traces at the near-surface that curve to low dip angles as they root into weak detachment layers parallel to stratigraphy (see subsection 2.3 in this Application Narrative), in this case the Jurassic Louann Salt (Figure 16). In general, the sedimentary section involved in growth faulting along the Gulf Coast is considered too weak to accumulate the strains associated with damaging earthquakes, but surficial and near-surface observations (e.g., fault scarps) indicate that these faults have been gradually slipping at low rates since being re-activated during the Quaternary (Gagliano, 2005; McCulloh and Heinrich, 2012).

Of the two earthquakes within the 100-mile search radius of the AoR, the 2005 M 3.0 event near the town of French Settlement was spatially coincident with the Baton Rouge Fault zone (Figure 80). The 5 km depth of the 2005 earthquake (Table 13) would place it near the base of the Baton Rouge Fault zone, where the growth faults merge into the Jurassic Louann Salt regional detachment surface (Figure 16). However, the very low level of historic seismic activity and the gradual nature of slip on the growth fault systems suggest they represent a limited seismic hazard.

Table 13: Earthquakes recorded from 2/1984 – 2/2024 within 100-mile radius of AoR (USGS, 2024).

Date	Latitude	Longitude	Depth (ft)	Magnitude (mblg)
8/2/2010	30.815	-90.854	1,312	3.0
12/20/2005	30.258	-90.708	16,404	3.0

2.7. Hydrologic and Hydrogeologic Information

The primary regulatory focus of the injection well program is protection of human health and the environment, including protection of potential underground sources of drinking water (USDWs). A USDW, as defined in LAC 43:XVII.3601, means an aquifer or its portion:

(1) Which supplies any public water system; or

(2) Which contains a sufficient quantity of groundwater to supply a public water system; and

(a) Currently supplies drinking water for human consumption; or

(b) Contains fewer than 10,000 mg/l total dissolved solids (TDS); and which is not an exempted aquifer.

The following subsections detail the regional and local hydrogeology and hydrostratigraphy in and near the project area.

2.7.1 Regional Hydrogeology

In August 2019, the Council on Watershed Management agreed to use eight watershed regions within Louisiana designated as the "Louisiana Watershed Initiative". Watersheds are geographic areas that have drainage patterns to specific waterbodies. The watersheds for Louisiana are presented in Figure 83, with a focus on Regions 5 and 6 where the project area is located. The associated river basins are also presented. River basins in the project area are Atchafalaya, Terrebonne, Mississippi, and Pontchartrain.

The remainder of this page intentionally left blank.

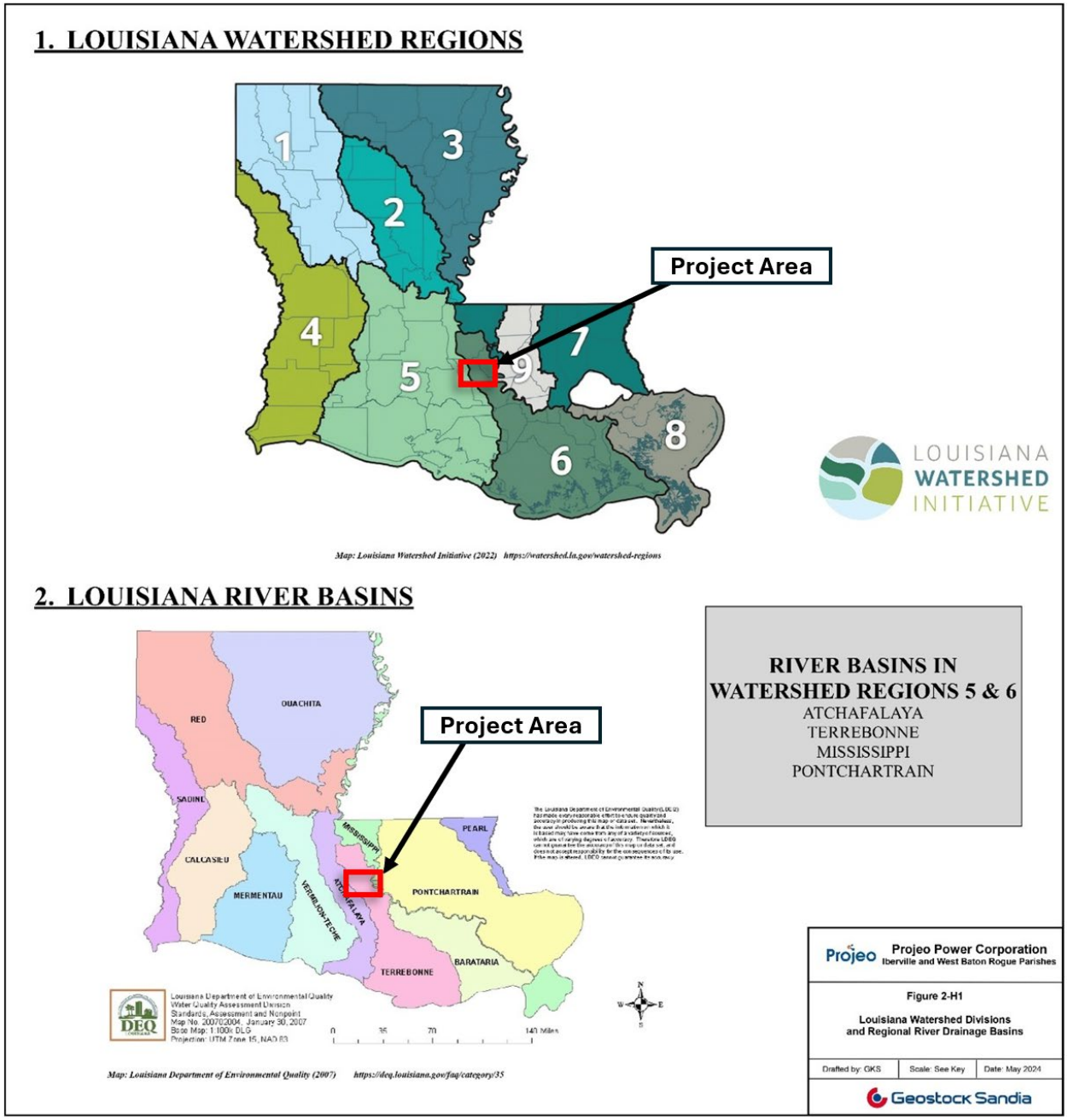

Figure 83: Major watersheds and river basins of Louisiana. The red box shows the project area. (Figure adapted from Louisiana Department of Environmental Quality, 2007)

The predominant aquifers of Louisiana by location, presented in Figure 84, occur within Paleocene and younger formations and contain usable quality water (<3,000 milligrams per liter (mg/L) TDS). These aquifer systems regionally crop out in bands parallel to the Mississippi Embayment and dip and thicken towards the southeast.

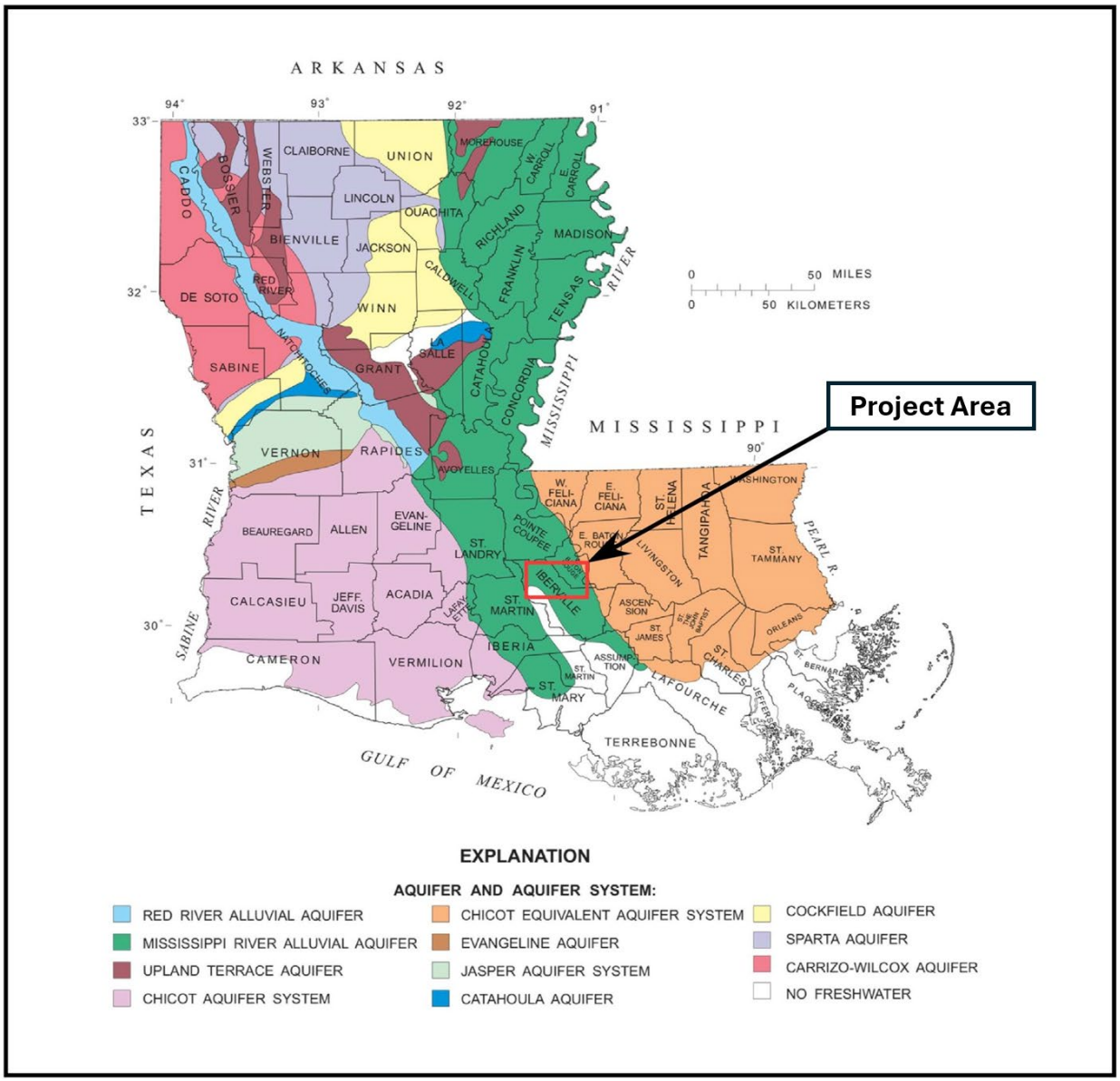

Figure 84: Principal aquifer systems of Louisiana. (In Purpera et al., (2020) modified from Stuart et al., (1994)).

As recognized by the USGS, there are four major regional aquifer systems of importance in Louisiana (Figure 85):

- Sparta Aquifer
- Mississippi River Alluvial Aquifer
- Chicot Aquifer System
- Southern Hills Aquifer System

The project area is in the Mississippi River Alluvial Aquifer System and Southern Hills Aquifer System.

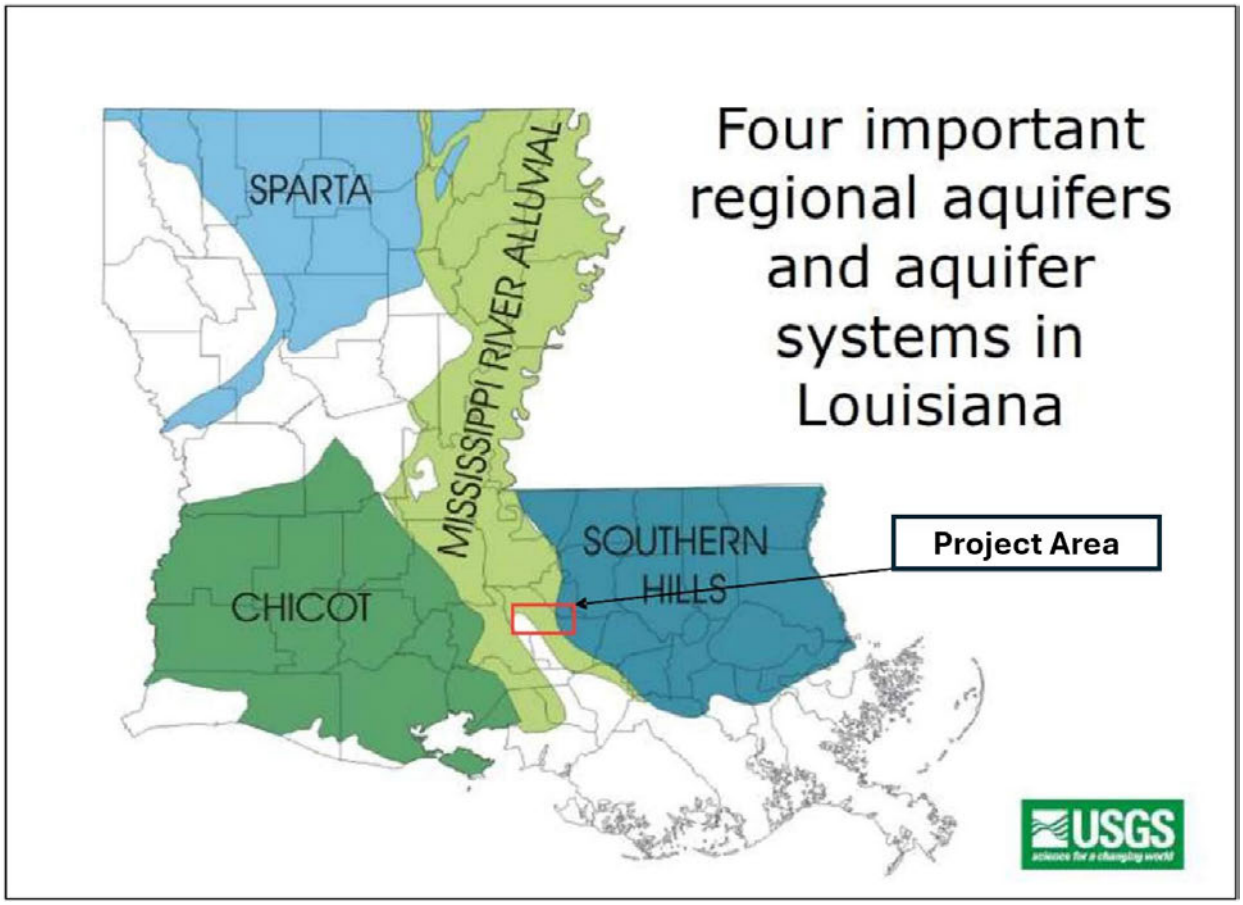

Figure 85: Major regional aquifers and aquifer systems in Louisiana. Lovelace (2009) with USGS contributions prepared for Louisiana Groundwater Resources Commission

Figure 86 contains a hydro-stratigraphic column for the State of Louisiana. The columns on Figure 84 denote the aquifer units for regions in the state. The central and southeastern portions of the state have been highlighted (red box outline) as this provides the regional context applicable to this project.

The remainder of this page intentionally left blank.

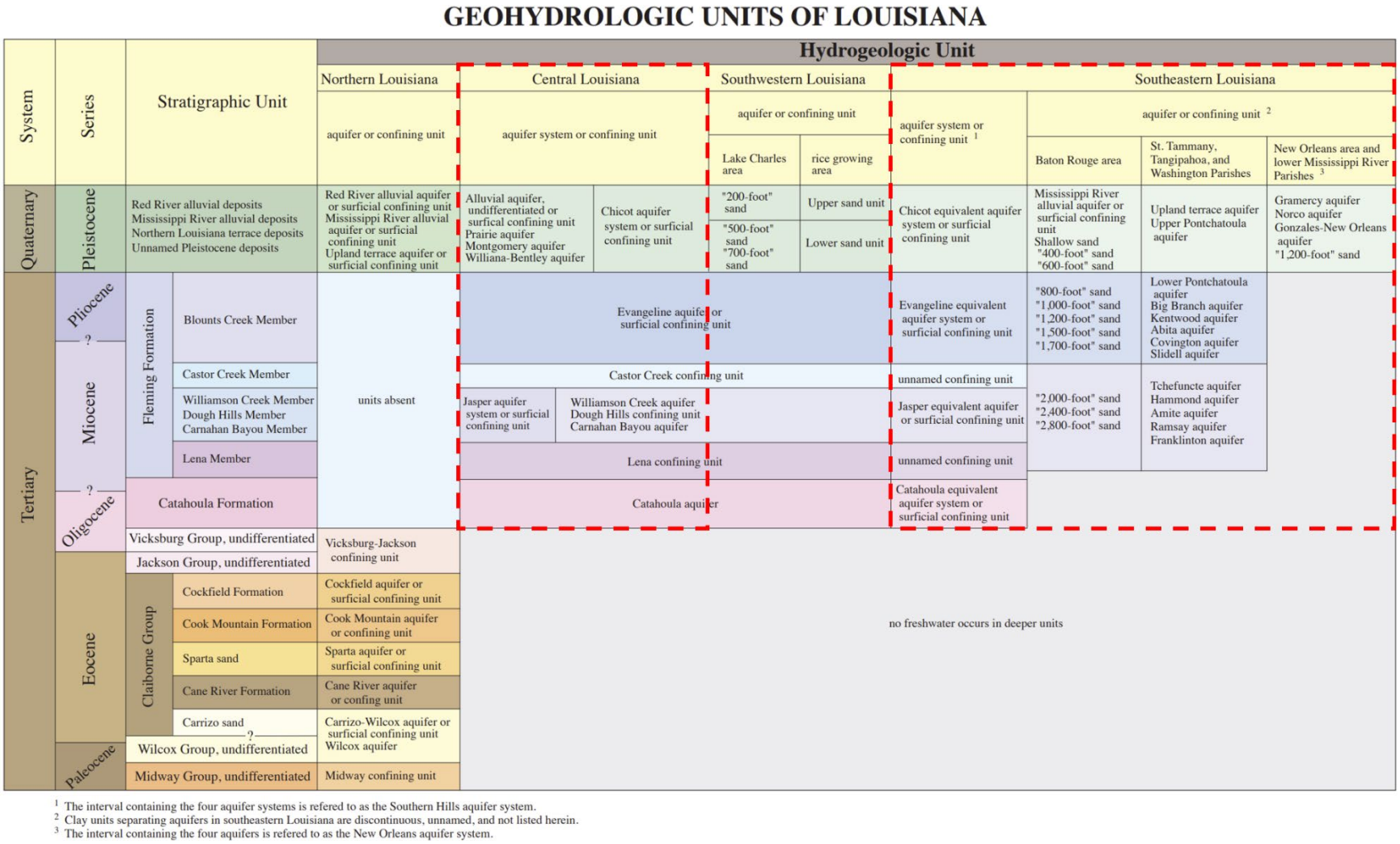

Figure 86: Hydrostratigraphic column for the state of Louisiana from the United States Geological Survey. The red box outlines Central and Southeastern Louisiana, where the project area is located. Modified from Buono (1983).

Groundwater moves through aquifer systems from areas of high hydraulic head to areas of lower hydraulic head. Regional uses from industry and the public water systems have some impacts on diverting the direction of flow. Published potentiometric maps for the regional aquifers are provided and discussed in the subsections below.

2.7.1.1. Mississippi River Alluvial Aquifer

The Mississippi River Alluvial (MRA) Aquifer is the main regional aquifer system of interest for the project area. This system is comprised of Pleistocene and Holocene-aged sediments. The Pleistocene deposits are of two general types: an approximately coastwise, gulfward thickening wedge of deltaic sediments and the relatively thin, veneer-like deposits which form the stream terraces and alluvial valley fill (Rollo, 1960). The system contains gravel to coarse-grained sand at the base and fines upwards into clays. In some localized areas, the surface is covered with impermeable clays.

It is a major source of freshwater in the north-northeastern part of Louisiana and into the Mississippi River. Recharge to the Mississippi River alluvial aquifer is primarily from precipitation and, to a lesser degree, by leakage from underlying sediments such as the Cockfield aquifer (Prakken, et al., 2014). The MRA Aquifer discharge and recharge is also controlled by surface water features that may cross the strata, such as rivers and lakes. This aquifer system can be separated into two hydrogeologic units, an upper confining unit of silt, clay, and fine sand that impedes the downward movement of water into a lower coarse sand and gravel aquifer unit (Martin and Whiteman, 1985). The aquifer ranges in depth from 60 to 260 feet in the areas it contains freshwater.

The MRA Aquifer is used as a primary aquifer in twenty-seven parishes in central Louisiana, and runs north to south, mimicking the Mississippi River (Figure 84). The MRA Aquifer is hydraulically connected to the Mississippi River and flows from high to low hydraulic head. For the MRA Aquifer, hydraulic conductivity generally varies between 10 to 530 feet per day (feet/d). In 2015, withdrawals from the MRA Aquifer totaled 384.60 Mgal/d (Collier and Sargent, 2015) with the majority of the usage for rice irrigation and industry. A potentiometric surface map published by the USGS in 2016 (McGuire et al., 2019) is presented in Figure 87.

The remainder of this page intentionally left blank.

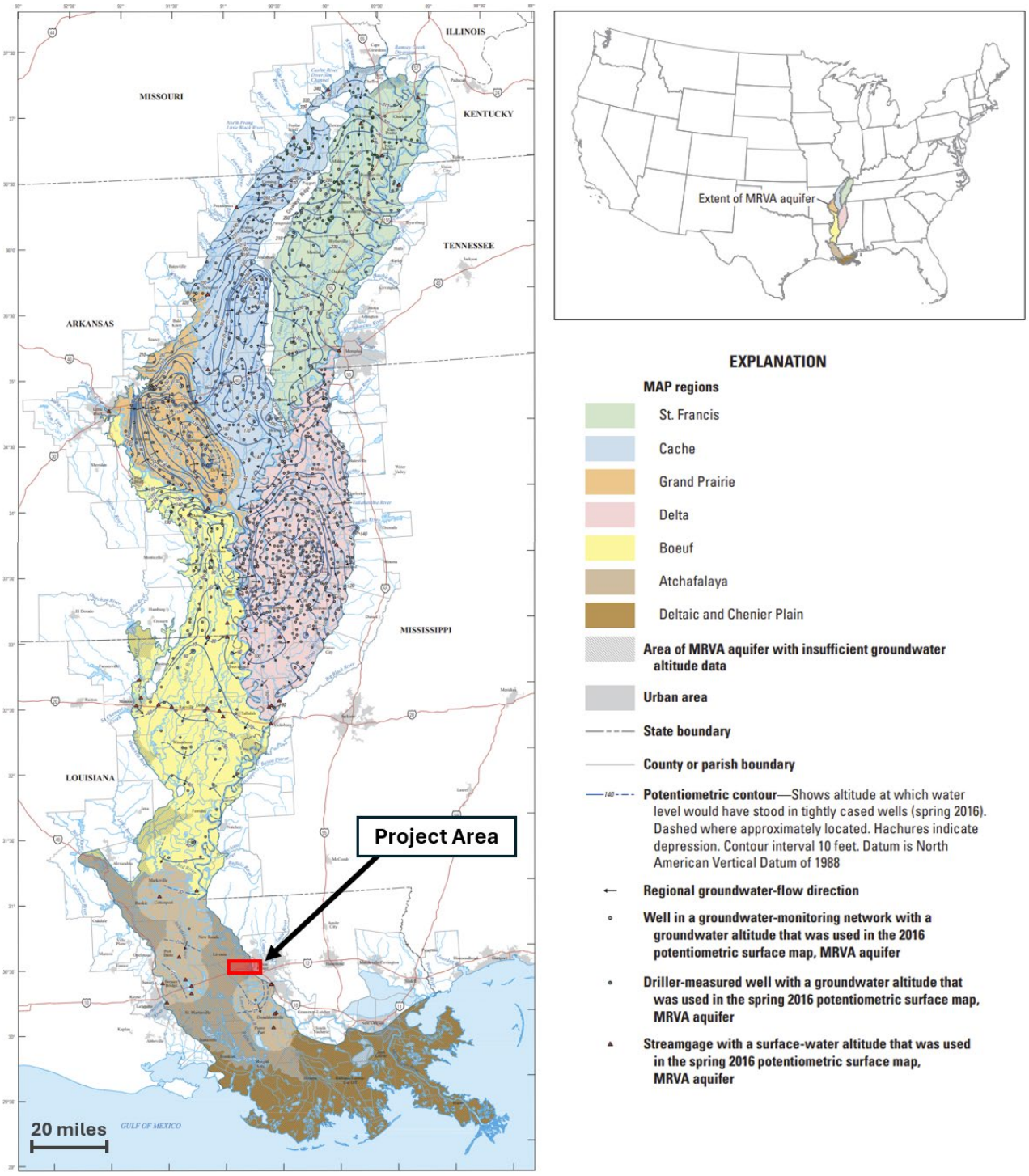

Figure 87: 2016 Potentiometric surface map of the MRV Aquifer. (Figure from McGuire et al., 2019)

2.7.1.2. Chicot Aquifer System

The Chicot Aquifer System is the main regional aquifer system that provides usable groundwater for southwestern Louisiana. These Pleistocene-aged sands are predominately comprised of

unconsolidated to loosely consolidated gravels and coarse graded sands. These gravel, sand, silt, and clay assemblages fine upwards and dip and thicken towards the Gulf of Mexico, thin to the west (towards Texas), and thicken to the east (towards Mississippi) (Nyman, 1984).

In southwestern Louisiana and southeastern Texas, the Chicot Aquifer is subdivided into three sub-units that are separated by confining layers (Sargent, 2011). The principal sand units within the aquifer are the 400-Foot sand and 600-Foot sand. In the northeastern portion of Calcasieu parish, these sands merge and the unit contains undifferentiated sands that are conducted hydraulically. Freshwater in the lower subsections of the Chicot deteriorates in quality with depth (Griffith, 2003).

In Cameron parish, the upper sand section contains freshwater underlain by saltwater (Nyman, 1984), except along the southeastern coast where no freshwater is present (Smoot, 1988). A freshwater to saline interface is driven northwards from the coast by water production for public supply, rice irrigation, and aquaculture (Sargent, 2011). Towards northwestern portions of Acadia parish, there is saltwater present near the base of the lower sand at depths ranging from 700 to 800 feet below ground (Nyman, 1989).

Recharge to the Chicot Aquifer System in Louisiana occurs where the Chicot outcrops in southern Rapides and Vernon parishes, and in northern Allen, Beauregard, and Evangeline parishes. There is also minimal recharge to the system via vertical leakage from the shallow overlying alluvial deposits (Stuart et al., 1994).

A map of the potentiometric surface for the Chicot Aquifer System (Figure 88) shows the direction of groundwater flow. Lovelace et al. (2004) indicated that the flow direction is towards major pumping areas such as Lake Charles in Calcasieu parish and the northern part of Acadia parish and south Evangeline parish, where there is heavy pumping for industrial and irrigation uses.

The remainder of this page intentionally left blank.

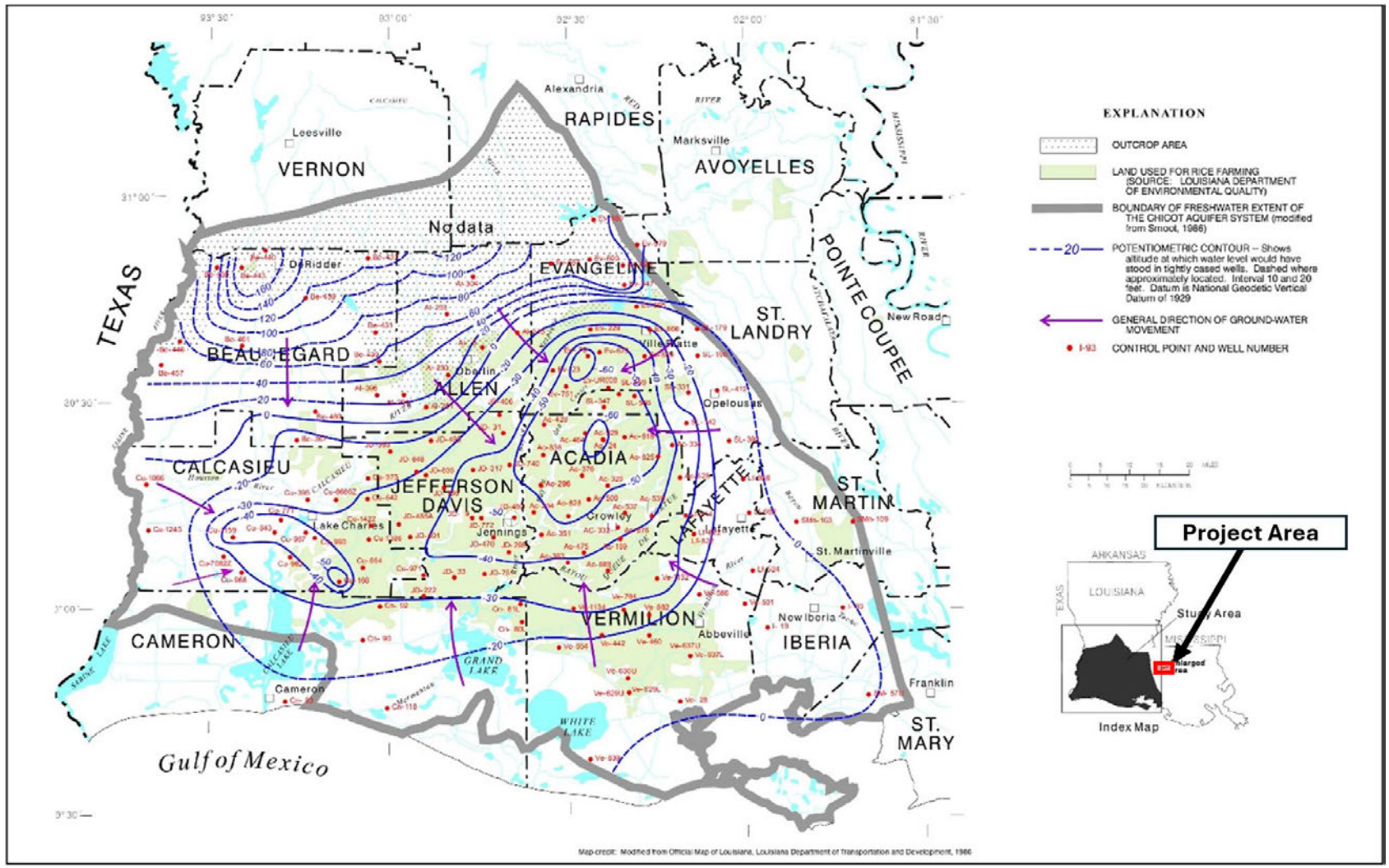

Figure 88: Potentiometric surface of the massive, upper, and 200-foot sands of the Chicot Aquifer System in southwestern Louisiana, January 2003. (Figure from Lovelace et al., 2004)

The Chicot Aquifer System yields the highest amount of groundwater for the state of Louisiana and is the primary source of water for Acadia, Calcasieu, Cameron, and Jefferson Davis parishes. As the aquifer nears the coast, the lower units become saline due to saltwater encroachment, and only the upper portions of the aquifer are used as a source of groundwater. Approximately 849.90 Mgal/d are produced from the entire aquifer based on data from the USGS Fact sheet for Calcasieu parish. The largest withdrawal is associated with rice irrigation and aquaculture (such as the industry of crawfish harvesting), which are seasonal. The Chicot Aquifer System also provides the largest public water supply for the region at 95.60 Mgal/day (Sargent, 2011) and supports large cities such as Lake Charles.

The Chicot Equivalent is comprised of subdivided sand units within the shallow subsurface. The sand units provide freshwater to parishes north of the Baton Rouge fault and are geologically similar to those of the Chicot System of southwestern Louisiana.

2.7.1.3. Southern Hills Aquifer System (SHAS)

The SHAS is a designated Sole Source Aquifer by EPA. Regionally, this system extends from the Gulf of Mexico in southeastern Louisiana and into southwestern Mississippi. The system is largely composed of three main aquifers referred to as the Chicot Equivalent Aquifer, the Evangeline Equivalent Aquifer, and the Jasper Equivalent Aquifer (White, 2017). The Pleistocene-aged SHAS sands are predominately comprised of unconsolidated to loosely consolidated gravels and coarse graded sands (Martin and Whiteman, 1985). These gravel, sand, silt, and clay assemblages fine upwards, and dip and thicken towards the Gulf of Mexico, thin to the west (towards Texas), and thicken to the east (towards Mississippi) (Aronow and Wesselman, 1971).

The SHAS is the primary source of freshwater water for Pointe Coupee, West and East Feliciana, St. Helena, Tangipahoa, Washington, St. Tammany, Livingston, and West and East Baton Rouge parishes. As the aquifer nears the coast, the system becomes saline due to saltwater encroachment, and the boundary of freshwater to saltwater coincides with the Baton Rouge Fault zone (White, 2017). North of the fault is freshwater, and south of the fault is saltwater. Sediment compaction and offset of sedimentary strata across the fault system reduce the lateral hydraulic connectivity of the aquifers; this acts to impede horizontal groundwater flow that creates substantial changes in groundwater level and quality across the Baton Rouge Fault zone (Griffith, 2003). It is noted, however, that in the shallow subsurface, there is some leakage updip (north), through the Baton Rouge Fault zone (Griffith, 2003). Large groundwater withdrawals in the Baton Rouge area have induced the northward encroachment of saltwater across the Baton Rouge Fault zone and into freshwater aquifers in some locations (Griffith, 2003).

Recharge to the system is from southwestern Mississippi and the Louisiana parishes that border the Mississippi state line (Pointe Coupee, West and East Feliciana, St. Helena, Tangipahoa, and Washington parishes). Approximately 293 Mgal/d is produced from the aquifer for the 10-parish area (White, 2017). A potentiometric surface map from the USGS (1980) is provided for the combined aquifers within the Pleistocene-aged formations in southern Louisiana (Figure 89). Main groundwater withdrawal areas from the SHAS are Baton Rouge and New Orleans.

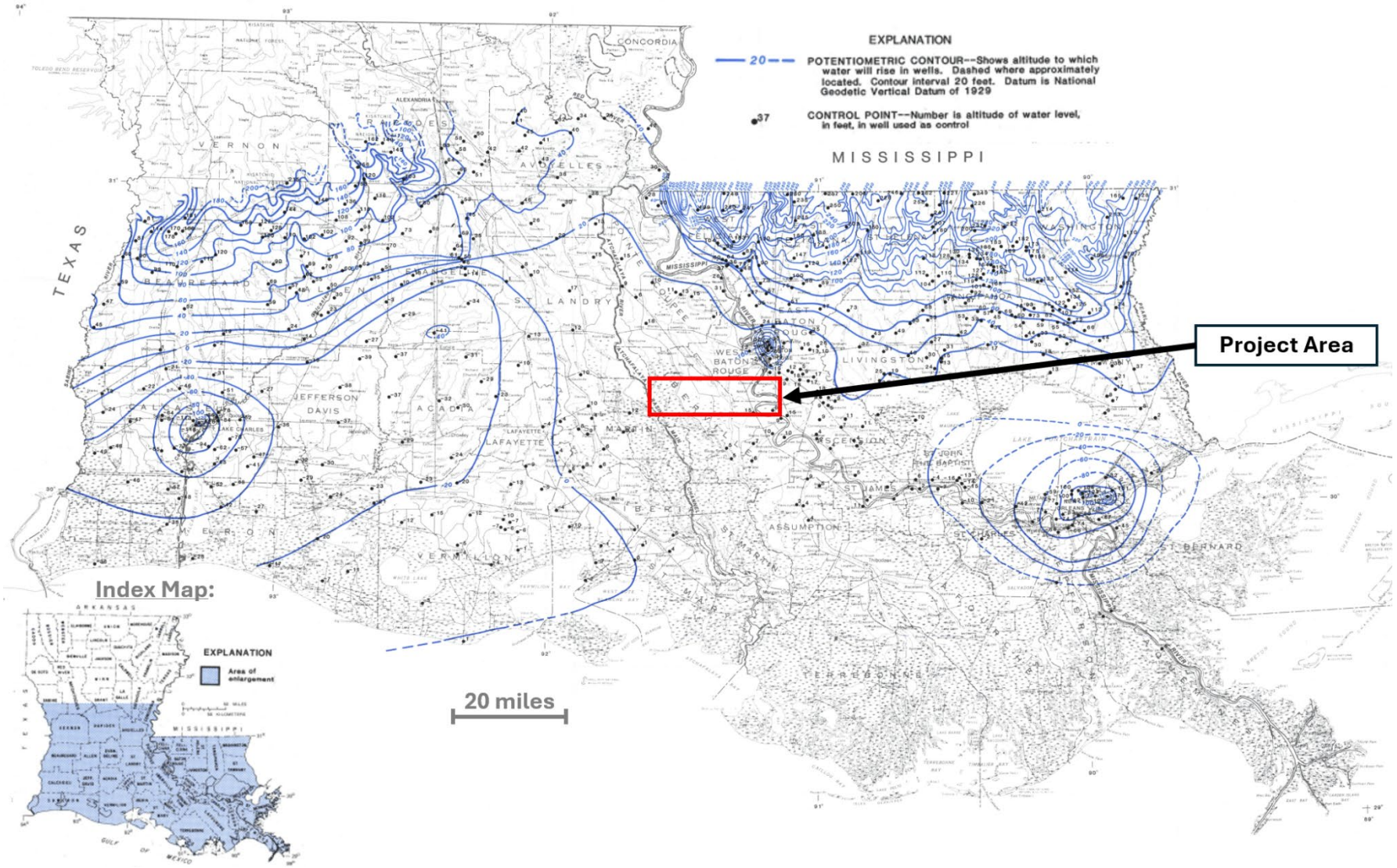

Figure 89: General potentiometric surface of Pleistocene-aged aquifers. The red box shows the project area of interest within the Southern Hills Aquifer System. (From USGS, 1980)

2.7.2 Local Hydrogeology

The project area is located within the MRA Aquifer (Figure 90). The MRA Aquifer marks the transition zone between the Chicot Aquifer System, Evangeline Aquifer System, and Jasper Aquifer System to the west and the Chicot Equivalent Aquifer System, Evangeline Equivalent Aquifer System, and Jasper Equivalent Aquifer System to the east (Smoot, 1988). Additionally, these sub-systems have multiple alternating sand aquifers and shale confining units. These subsets are shown in Figure 91. Hydrostratigraphic units of local importance for Iberville and West Baton Rouge parishes include in descending order (Table 14).

Table 14: Local aquifers and associated hydrostratigraphic sand units.

Aquifer	Sand Units
Mississippi River Alluvium Aquifer	n/a
Chicot Equivalent Aquifer System	400-foot sand
Chicot Equivalent Aquifer System	600-foot sand
Evangeline Equivalent Aquifer System	800-foot sand
Evangeline Equivalent Aquifer System	1,000-foot sand
Evangeline Equivalent Aquifer System	1,200-foot sand
Evangeline Equivalent Aquifer System	1,500-foot sand
Evangeline Equivalent Aquifer System	1,700-foot sand
Jasper Equivalent Aquifer System	2,000-foot sand
Jasper Equivalent Aquifer System	2,400-foot sand
Jasper Equivalent Aquifer System	2,800-foot sand

The remainder of this page intentionally left blank.

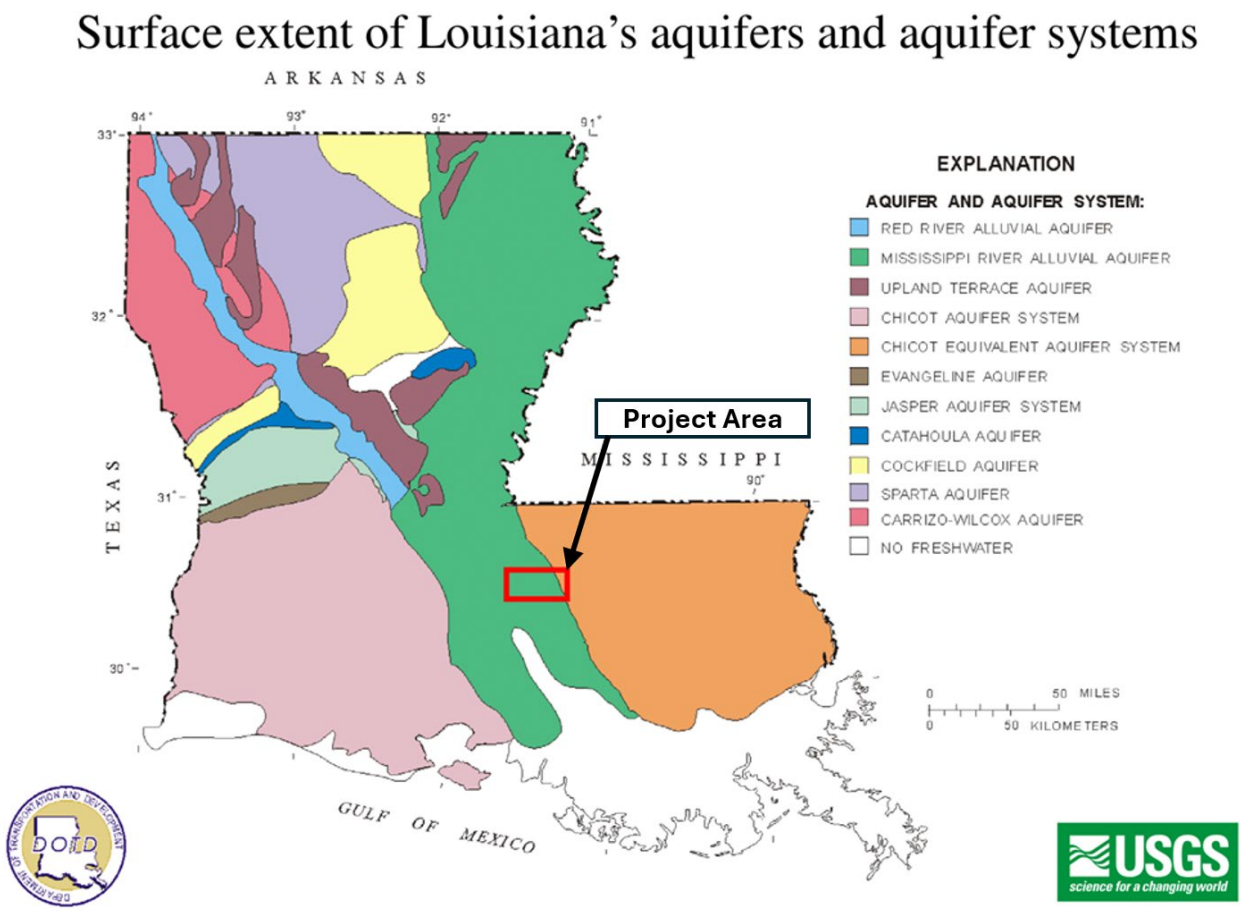

Figure 90: Aquifer systems of Louisiana (USGS: https://www.dnr.louisiana.gov/assets/OC/env_div/gw_res/LA.Aquifer.Map.pdf).

The remainder of this page intentionally left blank.

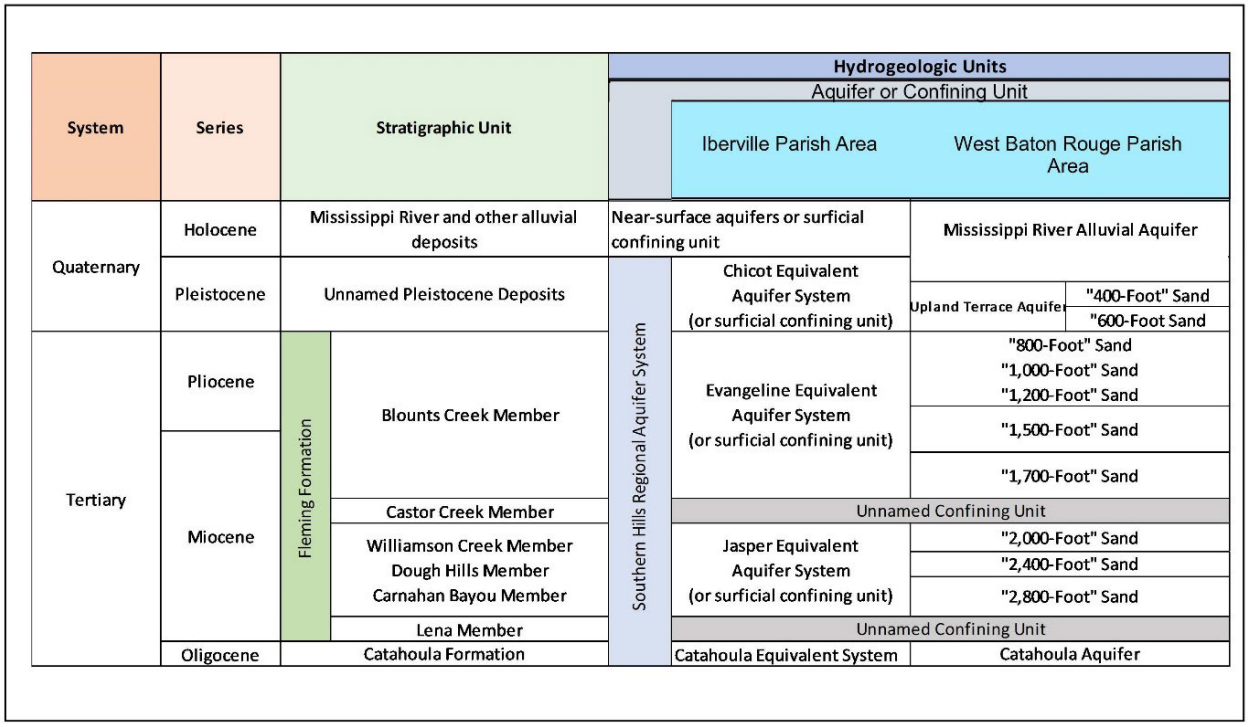

Figure 91: Localized hydrogeologic stratigraphic column for the Mississippi River Alluvial Aquifer System for Iberville and West Baton Rouge parishes. (Figure adapted from Nyman and Fayard, 1978; Buono, 1983; and Prakken, 2004)

For Iberville and West Baton Rouge parishes, these aquifers contain groundwater ranging from freshwater (<500 mg/L TDS) down to the lowermost USDW (standard of 10,000 mg/L TDS) in isolated sands that dip to the south, which are separated by alternating clay layers (Stuart, Knochenmus, and McGee, 1994 and White and Prakken 2016). Figure 92 through Figure 95 are published distribution maps and cross sections illustrating the distribution of the aquifers located above the base of the lowermost USDW. The cross-sections illustrate how the individual sands are discontinuous and not laterally extensive (along strike and dip), suggesting no regional hydrological communication among these isolated sands (Figure 93 and Figure 95).

The remainder of this page intentionally left blank.

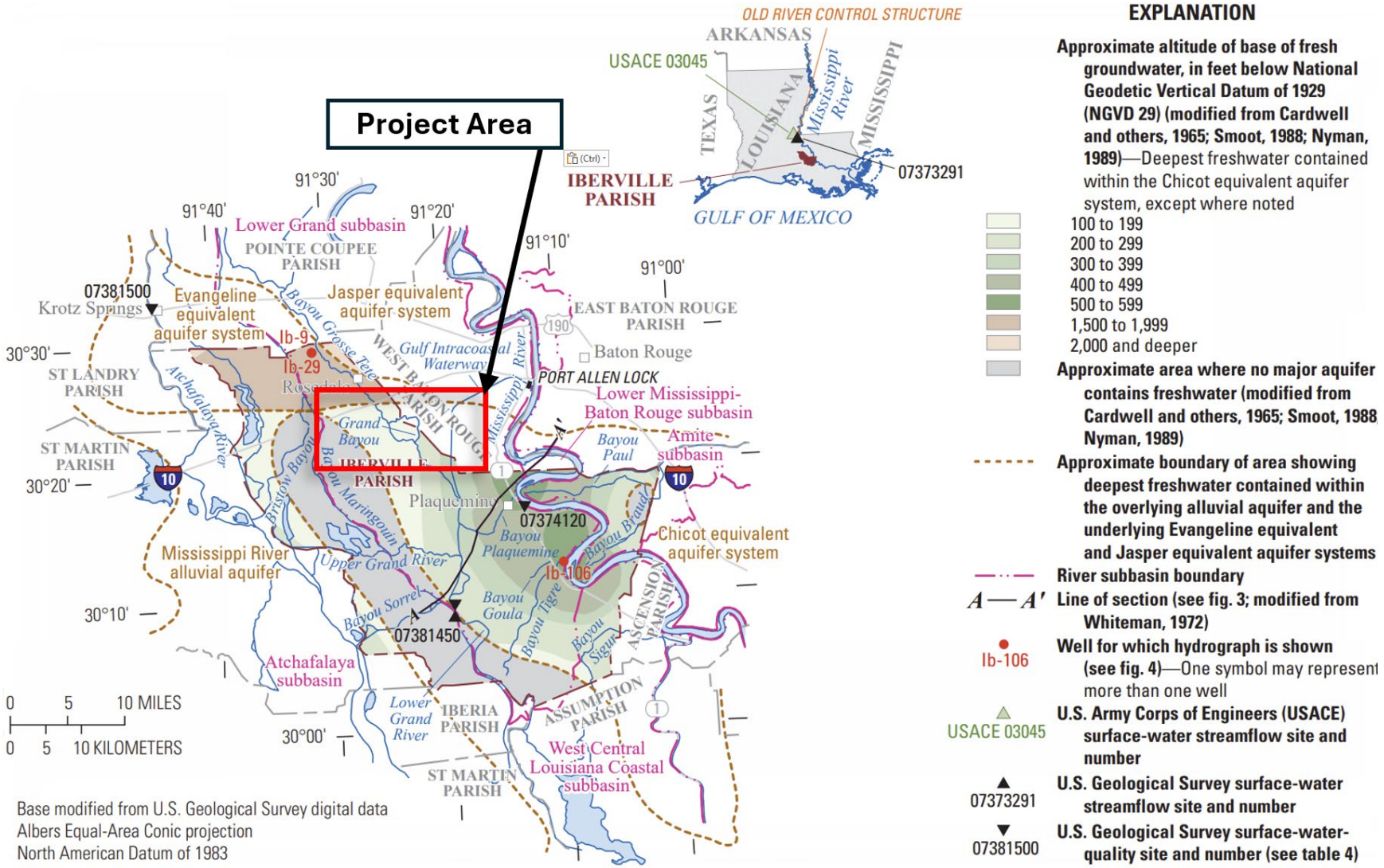

Figure 92: Map for idealized west-to-east hydrogeologic section through Iberville parish, Louisiana, showing aquifers and generalized clay and sand intervals. (Figure adapted from Lindaman and White, 2021)

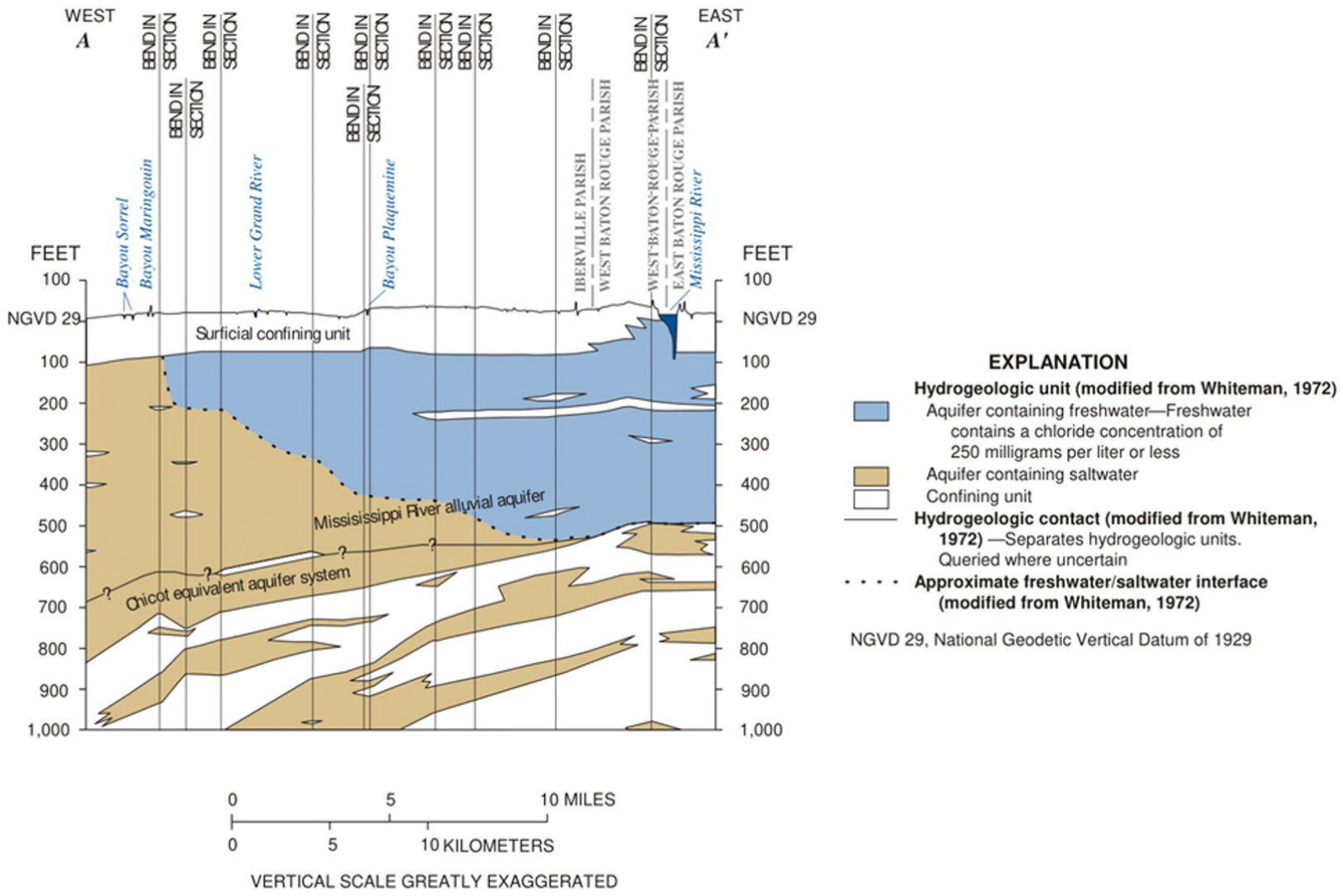

Figure 93: Map for idealized west-to-east hydrogeologic section through Iberville parish, Louisiana, showing aquifers and generalized clay and sand intervals. (Figure adapted from Lindaman and White, 2021)

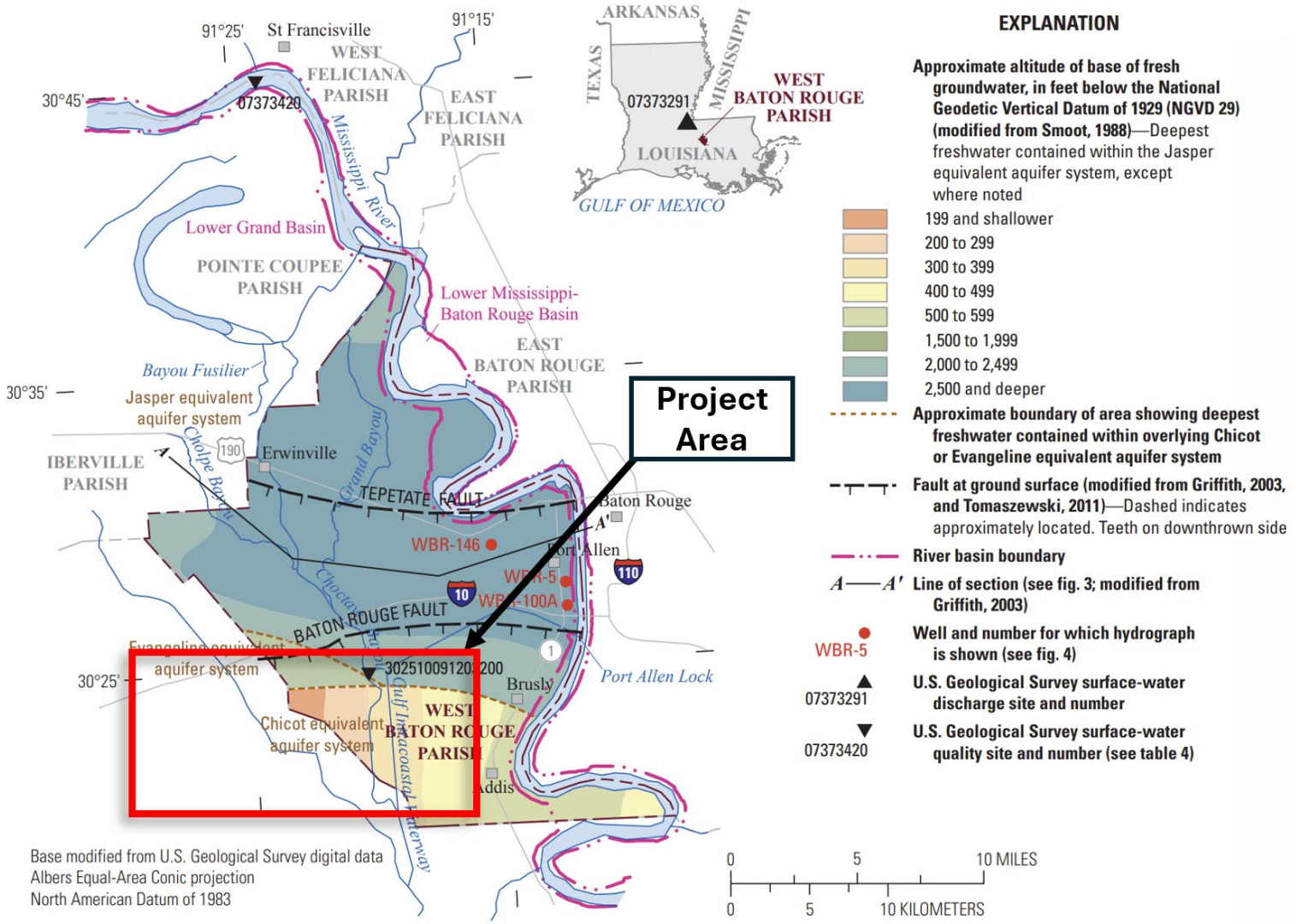

Figure 94: West-to-east hydrogeologic section through West Baton Rouge parish, Louisiana. (Figure adapted from White and Prakken, 2016)

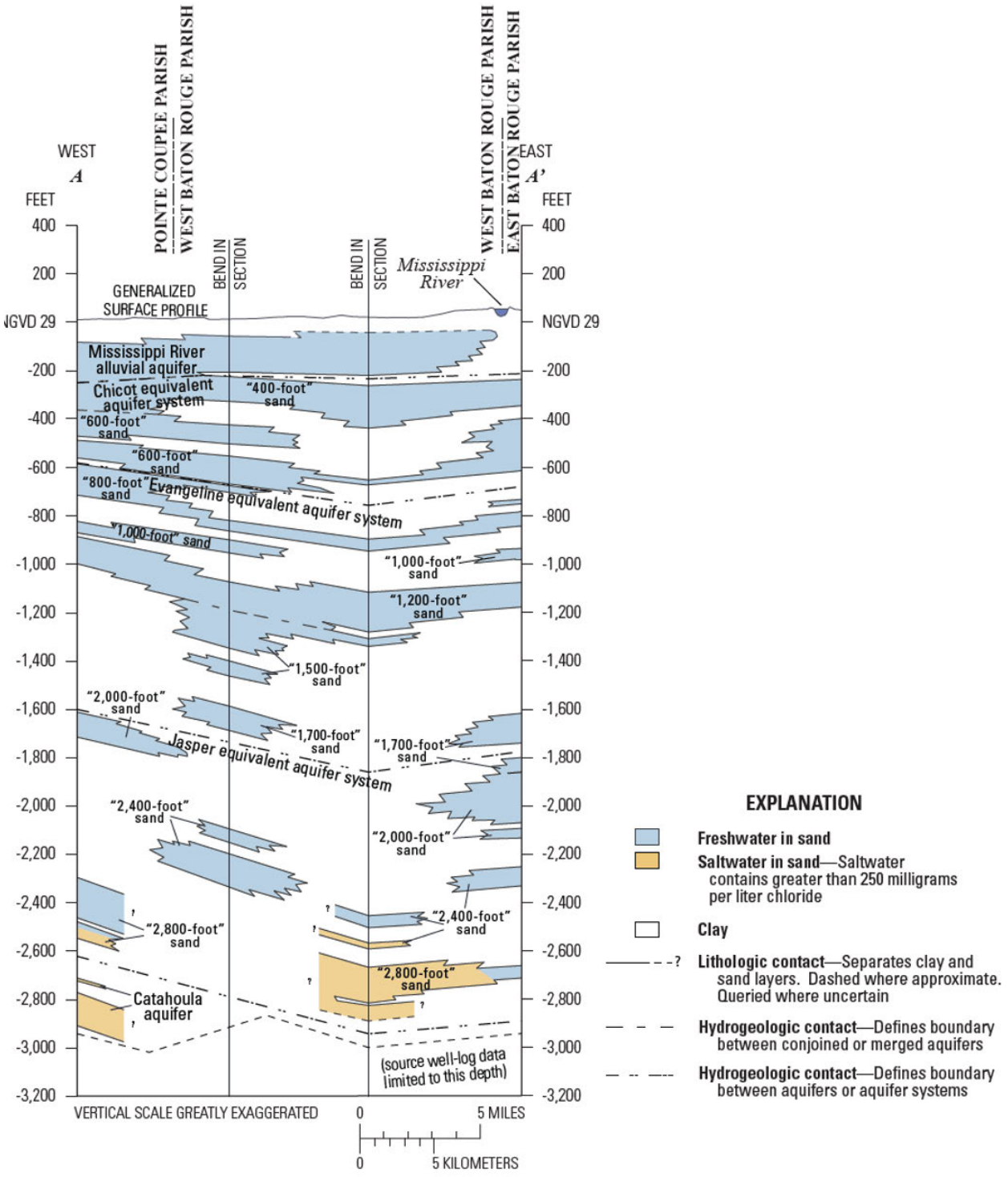

Figure 95: West-to-east hydrogeologic section through West Baton Rouge parish, Louisiana. (Figure adapted from White and Prakken, 2016)

The Chicot Equivalent Aquifer System in Iberville and West Baton Rouge parishes comprises the Lower MRA Aquifer and the Upland Terrace Aquifer, which contains the local 400-foot and 600-foot systems, with the following characteristics (White, 2017; Griffith, 2003):

- A broad, discontinuous, near-surface aquifer;
- Present throughout parishes;
- Extends westward into East Feliciana parish, eastward into Tangipahoa parish, and northward into Mississippi;
- Generally, dips south to southwest at a rate of 10–30 feet per mile;
- Near the southern parish line, the Upland terrace aquifer correlates with the 400-foot and 600-foot sands of the Baton Rouge area;
- Sediments range in grain size from clay through silt and sand to gravel and can be over 300 feet thick. The aquifer is composed primarily of medium- to coarse-grained sand; and
- The water flows in a southerly direction in the parishes (Figure 96).

The remainder of this page intentionally left blank.

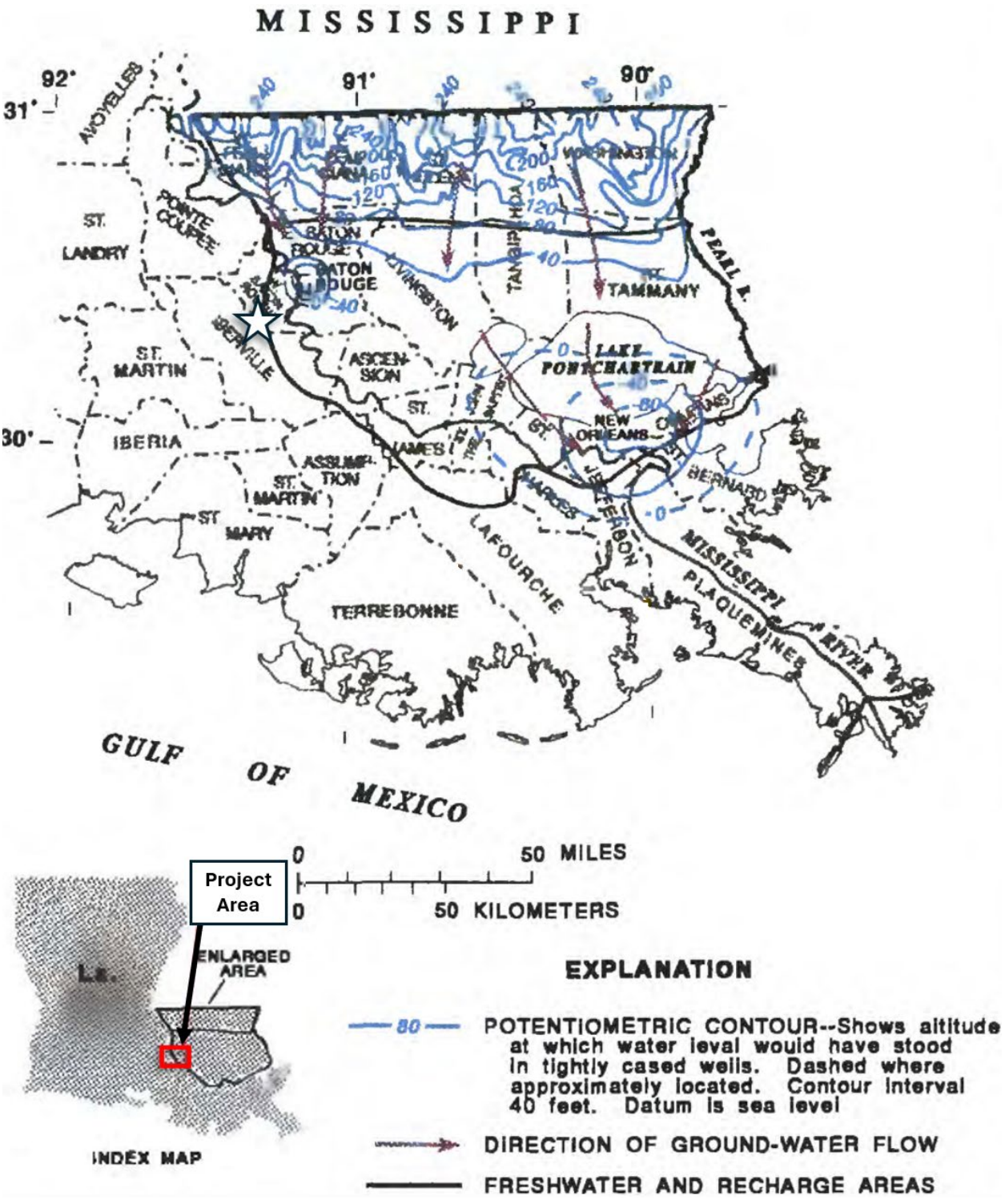

Figure 96: Potentiometric surface and direction of water movement in the Chicot equivalent aquifer system. (Figure adapted from Stuart et al., 1994)

The Evangeline Equivalent Aquifer System in Iberville and West Baton Rouge parishes is comprised of the 800-foot, 1,000-foot, 1,200-foot, 1,500-foot, and 1,700-foot aquifers (White and Prakken, 2016; Griffith, 2003), with the following characteristics:

- Aquifers are generally fine- to coarse-grained sand, with layers of clay usually separating the individual sands. Note that some sands merge with overlying and underlying sands;
- Aquifers contain freshwater (Chloride concentration ≤ 250 mg/L); and
- Groundwater flow direction is generally southwards (Figure 97).

The remainder of this page intentionally left blank.

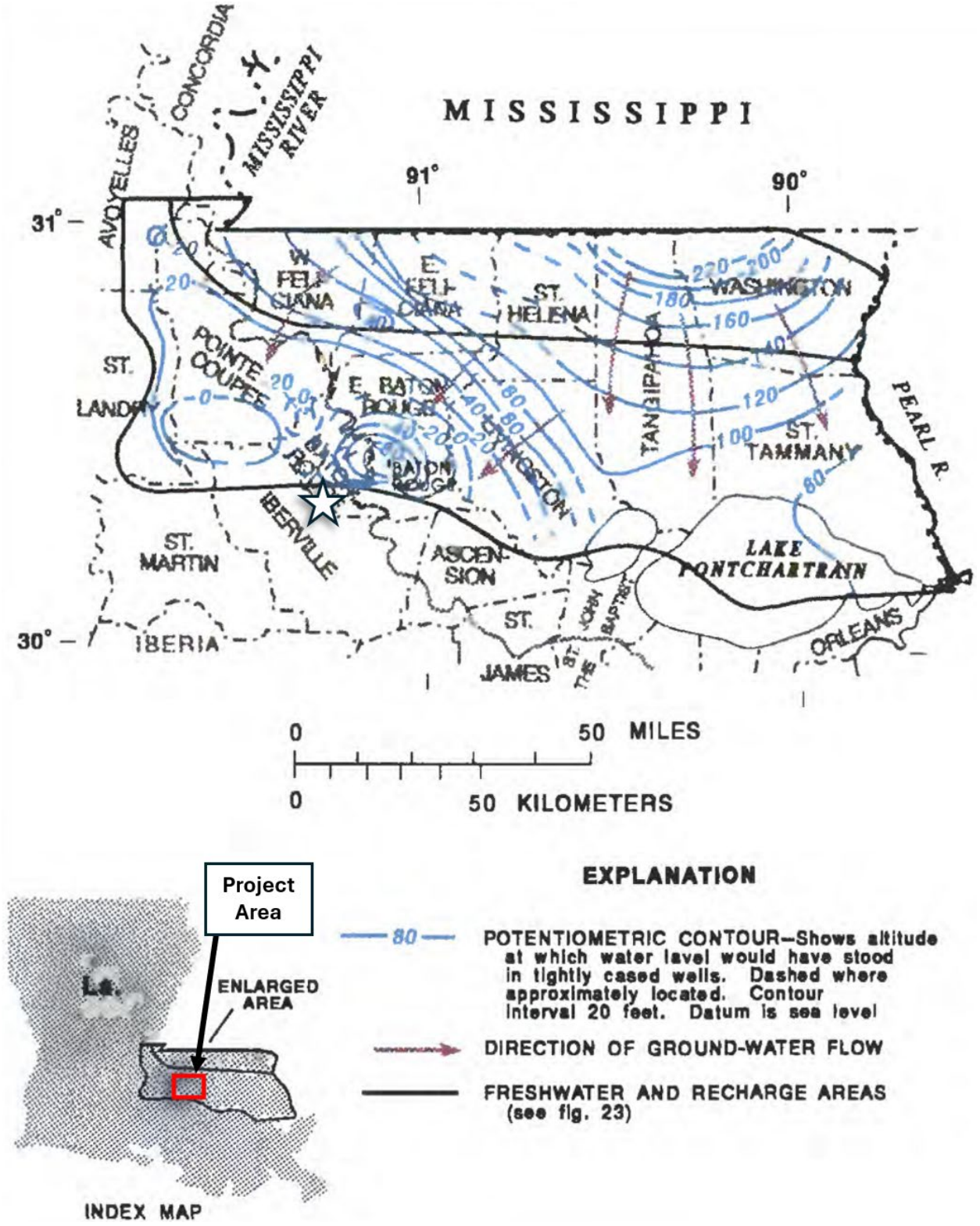

Figure 97: Potentiometric surface and direction of water movement in the Evangeline equivalent aquifer system. (Figure adapted from Stuart et al., 1994)

The Jasper Equivalent Aquifer System in Iberville and West Baton Rouge parishes is comprised of the 2,000-foot, 2,400-foot, and 2,800-foot aquifers (White and Prakken, 2016; Griffith, 2003), with the following characteristics:

- Aquifers are generally fine- to coarse-grained sand, with layers of clay usually separating the individual sands. Note that some sands merge with overlying and underlying sands;
- Jasper Equivalent Aquifer System has a TDS of ~213 PPM (White, 2017);
- Aquifers generally contain freshwater (Chloride concentration ≤ 250 mg/L); and
- The general groundwater flow direction in the Jasper Equivalent Aquifer System in West Baton Rouge parish is in the southward direction (Figure 98).

The remainder of this page intentionally left blank.

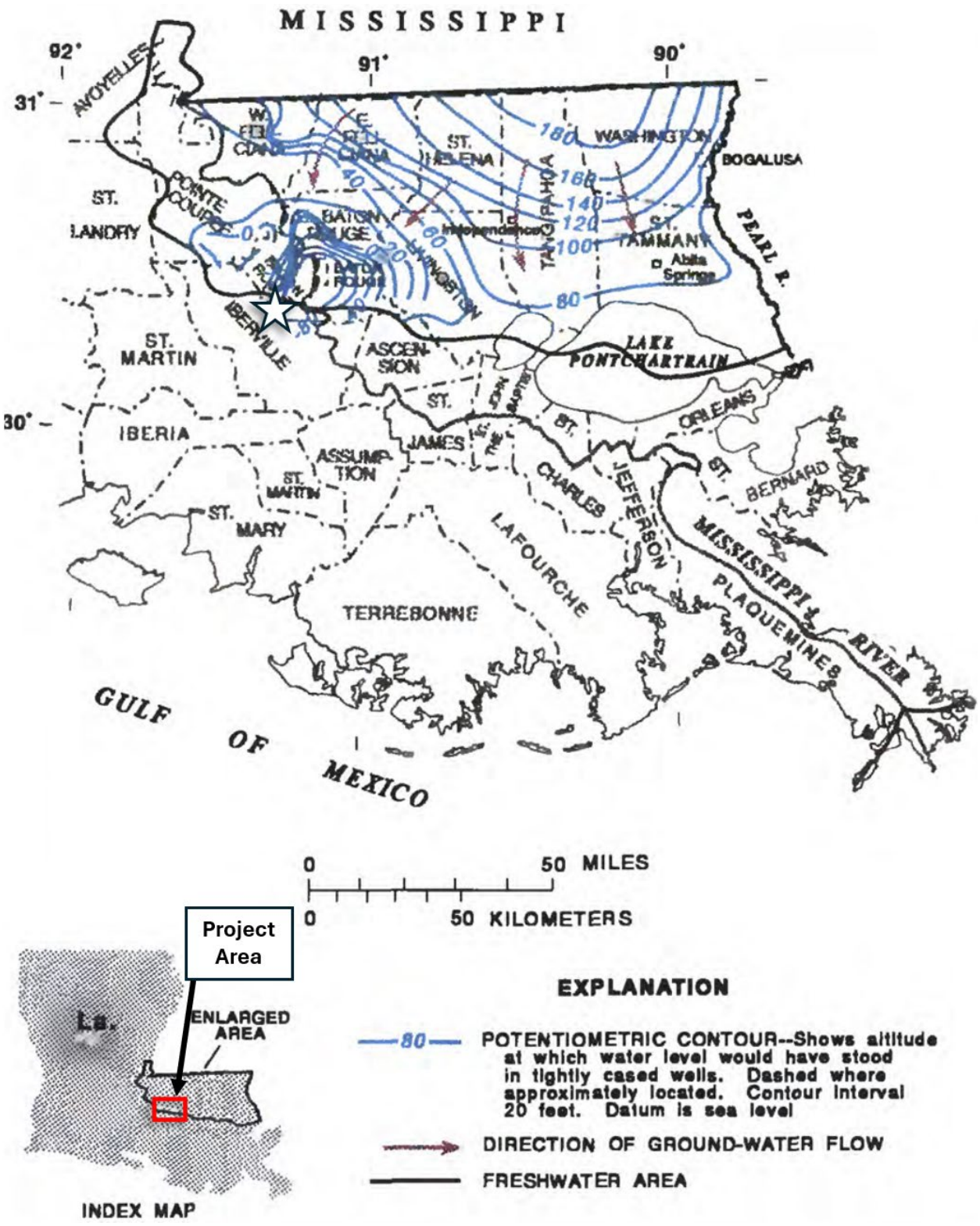

Figure 98: Potentiometric surface and direction of water movement in the Jasper Equivalent Aquifer System. (Figure adapted from Stuart et al., 1994)

Within Iberville or West Baton Rouge parishes, there are no aquifers that are used as sources of groundwater below the Jasper Equivalent Aquifer System.

2.7.3 Baton Rouge Fault

The aquifers contained in the area's Baton Rouge Fault are generally part of the SHAS and include the MRA aquifer, the 400-foot sand, 600-foot sand, 800-foot sand, 1,000-foot sand, 1,200-foot sand, 1,500-foot sand, 1,700-foot sand, 2,000-foot sand, 2,400-foot sand, 2,800-foot sand, and the Catahoula aquifer. The aquifers are separated by confining units from solid clay to sandy and silty clay, which limits vertical groundwater movement. The aquifers and the confining units dip south and southwest towards the Gulf of Mexico, forming a wedge that pinches out northwards. The Baton Rouge Fault dips to the south at an angle between 65 and 70 degrees (Durham and Peeples, 1956). Although there are observations of the Baton Rouge Fault zone sealing in the subsurface, especially in deeper, more compacted stratigraphic units (see subsection 2.3. for detailed discussion), there are also observations that indicate fluid movement across the fault in the shallower, less compacted stratigraphic sections that contain the freshwater aquifers (Griffith, 2003).

The displacement of the sedimentary layers along the fault limits the communication between the layers horizontally and causes significant changes in water levels and quality across the fault (Heywood and Griffith, 2013). This causes the base of the lowermost USDW to be substantially deeper north of the fault than on the south side of the fault. Freshwater flowed southwards to the fault prior to ground water withdrawal north of the fault. The aquifers south of the fault generally contain saltwater, and as withdrawal of water north of the fault began, this created a gradient that allowed the movement of saltwater from south of the fault into the freshwater areas north of the fault (Griffith, 2003).

With the exception of the 2,800-foot sand and the Catahoula aquifers, most of the saltwater located north of the fault is a result of movement from south to north in response to ground water withdrawal north of the fault (Lovelace, 2007). Due to the limited availability of sufficient quality groundwater supply for the public, Iberville parish obtains water from wells in West Baton Rouge parish.

2.7.4 Determination of the Base of the Lowermost USDW

In order to determine the base of the lowermost USDW, available USDW values were exported from the Louisiana Department of Energy and Natural Resources (LDENR) SONRIS database (https://www.sonris.com/) within a radius of approximately 10 miles from the proposed injection wells. To validate the exported USDW values from the SONRIS database, the following two approaches based on the use of data from open-hole geophysical well logs were used:

- Determination of lowermost USDW values were verified from shallow open-hole geophysical logs across the project area with LDENR's Injection and Mining Division's approach (identified below) on determining the base of the lowermost USDW using an electric log. These values are used to verify the SONRIS reported values.

- The resistivity/spontaneous potential methodologies which are described in detail and tabulation of the calculation of sodium chloride content are presented in Appendix C. The "Spontaneous Potential Method" derives the formation fluid resistivity from the resistivity of the mud filtrate and the magnitude of the deflection of the spontaneous potential response (SP) of the formation (the electrical potential produced by the interaction of the formation water, the drilling fluid, and the shale content of the formations). The "Resistivity Method" determines formation fluid resistivity from the resistivity of the formation (Rt) and the formation resistivity factor (F), which is related to formation porosity and a cementation factor (Schlumberger, 1987).

Using the resistivity method, it was calculated that sands with a formation resistivity of greater than 2.0 ohm-m would be considered USDWs. This site-specific calculation is in agreement with LDENR guidance (http://www.dnr.louisiana.gov/assets/OC/im_div/uic_workshop/2_USDW.pdf), which determines the lowermost USDW using the following:

- Ground surface to 1,000 feet: 3 ohms or greater is considered USDW;
- 1,000 feet to 2,000 feet: 2 ½ ohms or greater is considered USDW; or
- 2,000 feet and deeper: 2 ohms or greater is considered USDW.

Adopting a conservative approach, the base of the lowermost USDW across the evaluated logs is placed at the base of the deepest sand with a deep resistivity at 2 ohms. The comparison of the calculated depths with SONRIS reported depths show good alignment.

2.7.5 Base of the Lowermost USDW

The lowermost USDW is defined by the sudden decrease of resistivity at the base of the last sand with an isolating shale below. For the project area, the base of the lowermost USDW is located at a depth ranging from 2,300 to 2,500 feet below ground level (corresponds to sands within the Jasper Equivalent Aquifer System) as shown in the type log (Appendix D). The base of the USDW deepens southwards towards the Gulf of Mexico.

Within a 5-mile radius of the proposed injection wells, the separation between the base of the lowermost USDW and the top of the shallowest Miocene injection zone is approximately 5,204 feet. Multiple alternating permeable sands and clay/shales (aquitards or 'containment shales') are present between the lowermost USDW and the top of the shallowest Miocene injection zone. These alternating sand/shale sequences between the lowermost USDW and the top of the shallowest Miocene injection zone allow for pressure and fluid bleed-off prior to reaching any USDW, if a loss of containment were ever to occur. Collectively, these buffer saline intervals above the shallowest Miocene injection zone have at least two additional laterally extensive shale confining units.

2.7.6 Water Well Data Sets

Water well data was gathered open-source from the SONRIS database (https://www.sonris.com) in May 2024. Water well locations within the AoR are shown on Figure 99. A total of 37 wells are identified with details (e.g., well number identifier well depth, well status, use and aquifer description) keyed to Table 15, in adherence to LAC 43:XVII.3607(C)(1)(a)(iv). Note that well

depths range from 20 to 2,400 feet below ground level, with the majority of wells (92 percent) having a depth of less than or equal to 200 feet (Figure 99).

Out of the 37 identified water wells, 23 wells are currently active, and 14 wells are plugged and abandoned. Of the 23 active wells, 12 wells are used for domestic water supply, 8 wells are used for industrial or irrigation purposes, and 3 wells are used as piezometers or monitoring wells.

The remainder of this page intentionally left blank.

Figure 99: Water well data overview within AoR. Wells are referenced to first column of Table 15.

Table 15: Water well data overview.

#	Record Number	State	Parish	Total Depth (ft, MD)	Water Level (ft, MD)	Completion Date	Geologic Unit	Use Description	Well Status	Longitude (WGS 84)	Latitude (WGS 84)
[redacted]											

#	Record Number	State	Parish	Total Depth (ft, MD)	Water Level (ft, MD)	Completion Date	Geologic Unit	Use Description	Well Status	Longitude (WGS 84)	Latitude (WGS 84)
[redacted]											

The remainder of this page intentionally left blank.

2.7.6.1. Baseline Groundwater Chemistry Sampling Results

In adherence to LAC 43:XVII.3607(C)(1)(a)(iv), water samples were collected and analyzed from four freshwater wells within the project area. The water samples were collected from active pumping wells, following a standard sampling procedure. Analyses were completed at a laboratory accredited under the Louisiana Environmental Laboratory Accreditation Program and met minimum requirements of chlorides, TDS, and pH measurements (Figure 100, Table 16). A detailed report of the water sampling and analysis procedures along with a full data report is provided Appendix E.

The remainder of this page intentionally left blank.

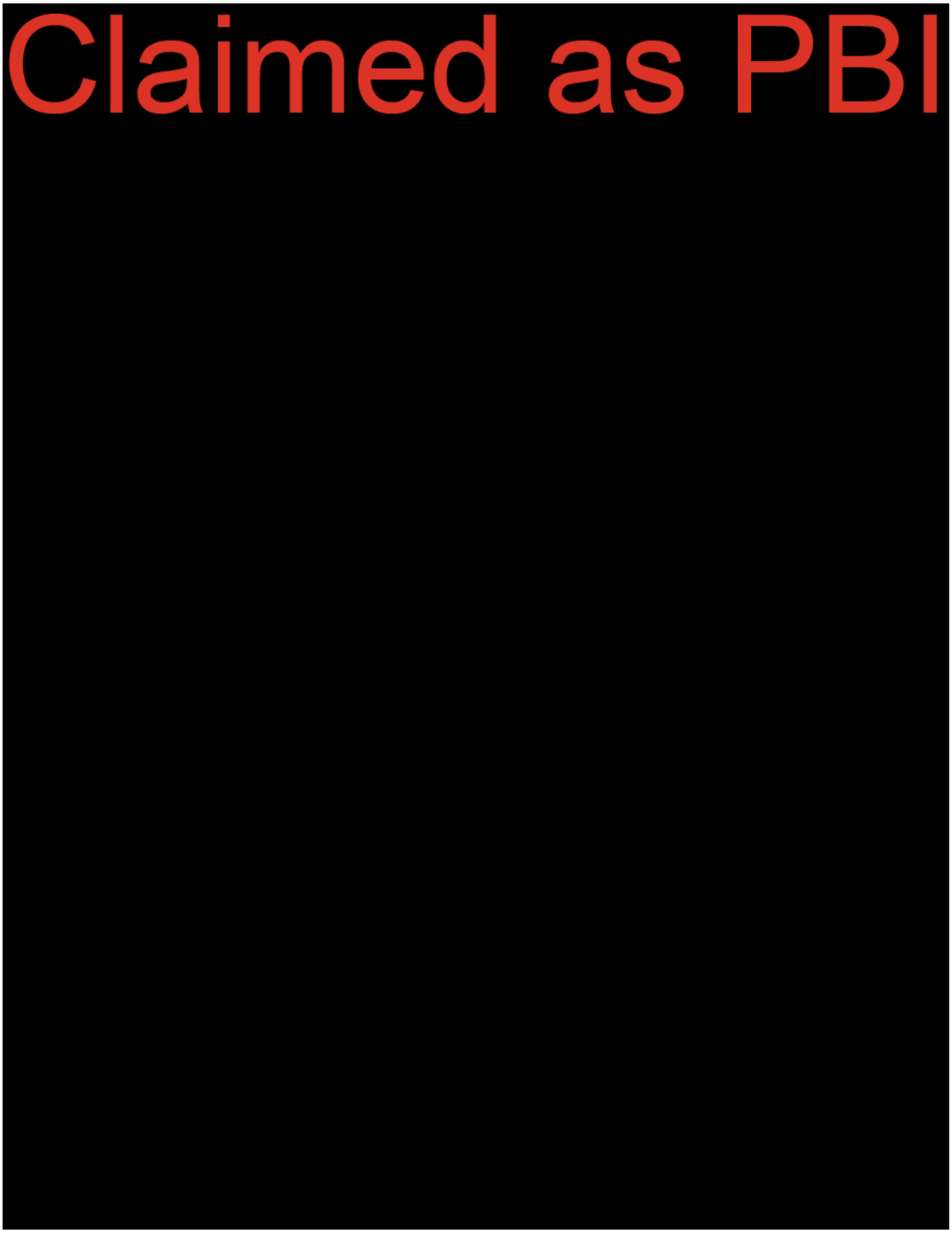

Figure 100: Map of groundwater sampling wells (blue), AoR (red), and injection and observation wells. See Table 16 for further information.

Table 16: Results of freshwater well sampling from the project area. Reporting Limit (RL) noted for each analysis.

Analyte	Unit of Measure	Analytical Report Results									
		Well #1		Well #2		Well #3		Well #4		Blind Duplicate[1]	
		Result	*RL*	*Result*	*RL*	*Result*	*RL*	*Result*	*RL*	*Result*	*RL*
Alkalinity, Total	mg/L	290	1.0	350	1.0	290	1.0	270	1.0	350	1.0
Specific Conductance	umhos/cm	910	10.0	1,300	10.0	850	10.0	1,600	10.0	1,300	10.0
Total Dissolved Solids	mg/L	510	5.0	640	10.0	310	5.0	970	10.0	730	10.0
Density	g/mL	0.9996		0.9997		0.9982		1.0017		0.9982	
Carbon Dioxide	mg/L	280	1.3	340	1.3	270	1.3	260	1.3	340	1.3
Carbon Dioxide, Free	mg/L	23	0.37	28	0.37	18	0.37	21	0.37	28	0.37
pH	SU	7.4		7.4		7.5		7.4		7.4	
Temperature	Degree C	23.6		23.5		23.5		23.7		23.9	

[1]Blind duplicate completed on samples from Well #2 with results showing less than a 5% difference for all parameters except total dissolved solids.

The remainder of this page intentionally left blank.

2.7.7 Local Water Usage

In Iberville parish, with a population of approximately 30,210 people (per 2022 census), the main source of drinking water comes from water wells in West Baton Rouge parish.

The USGS in cooperation with the Louisiana Department of Transportation and Development (LaDOTD), produced a "Water Resources of Iberville Parish" fact sheet with data up until 2020 (Lindaman and White, 2021). The dominant water usage is supplied by surface water (95 percent). The 2014 statistics showed that 30.86 Mgal/d were withdrawn from groundwater supply from the following aquifers:

- Chicot Equivalent provided 3.68 Mgal/d (~ 12%),
- MRA Aquifer provided 26.72 Mgal/d (~87 %), and
- Jasper Equivalent Aquifer System provided 0.46 Mgal/d (~ 1 %).

In West Baton Rouge parish, with a population of approximately 27,377 people (per 2022 census), the main source of drinking water comes from the MRA Aquifer and the Chicot, Evangeline, and Jasper equivalent aquifer systems (listed from shallowest to deepest). Precipitation in southeastern Louisiana and southwestern Mississippi is the primary source of recharge for the Chicot, Evangeline, and Jasper equivalent aquifer systems. The MRA Aquifer system is recharged through precipitation that infiltrates the surface clays; flow from the alluvial aquifer from the north, adjacent, and underlying aquifers; and flow from the Mississippi River. East Baton Rouge parish is where the greatest withdrawal rates from the Chicot, Evangeline, and Jasper equivalent aquifers occur.

The USGS, in cooperation with the LaDOTD, produced a "Water Resources of West Baton Rouge Parish" fact sheet with data up to 2016 (White and Prakken, 2016). The dominant water usage is supplied by groundwater (93 percent). The 2010 statistics showed that 10.2 Mgal/d were withdrawn from groundwater supply from the following aquifers:

- MRA Aquifer provided 2.88 Mgal/d (~28 %),
- Chicot Equivalent provided 0.01 Mgal/d (~ 0.1%),
- Evangeline Equivalent provided 7.31 Mgal/d (~ 72 %) and
- Jasper Equivalent Aquifer System provided 0.01 Mgal/d (~ 0.1 %).

2.7.8 Injection Depth Waiver

The proposed injection zones are deeper than the base of the lowermost USDW (2,300 feet) as shown in Appendix D. An injection depth waiver is not required or requested for this project.

2.8. Geochemistry

2.8.1 Baseline Fluid Chemistry

Average salinity was calculated and initial fluid chemistry data were collected from the USGS Produced Water Database for the USDWs, the injection zones, and the confining zones and are shown in Table 17 and Table 18 (Blondes et al., 2023). The database was filtered to include data only from Louisiana (Figure 101). Anomalous and outlier data points were investigated to determine validity, and in some cases these data points were removed from the dataset due to their high uncertainty. Fluid samples will be acquired during the construction of injection and observation wells as part of the Pre-Operational Testing Program to validate or update these data.

The regional USGS sampling data indicate that the Lower Miocene Sand (LMIC injection zone) has an average TDS of 113,046 mg/L, whereas the Middle Miocene Confining Zone (LMIC upper confining zone) averages 89,894 mg/L. The calculated average TDS of the Frio Formation (OFIC injection zone) is 80,241 mg/L, whereas the Anahuac Formation (LMIC lower confining zone, OFIC upper confining zone) is 107,926 mg/L (Table 17). No data was available for the Vicksburg Shale. The brines of the intended injection complexes are predominantly Na^+ and Cl^- with secondary Ba^{2+}, HCO_3^-, Ca^{2+}, K^+, Mg^{2+}, and SO_4^{2-}. For reference, initial fluid chemistry data collected from the USGS National Produced Waters Geochemical Database for the USDWs, the injection zones, and the confining zones are shown in Table 18.

Additional data was utilized in the local project area to determine appropriate TDS values for reservoir simulation. The LMIC data showed a reasonable TDS value to be 190,000 mg/L, including input data from the Claimed as PBI (API No. Claimed as PBI), Claimed as PBI (API No. Claimed as PBI), and Claimed as PBI (API No. Claimed as PBI) wells. The OFIC data showed a reasonable TDS value to be 150,000 mg/L, including input data from Claimed as PBI (API No. Claimed as PBI; Subsurface Inc., 2013a and Subsurface Inc., 2013b), Claimed as PBI (API No. Claimed as PBI and API No. Claimed as PBI; Geostock Sandia, LLC, 2020a and Geostock Sandia, LLC 2020b), DuPont / Denka Pontchartrain (Sandia Technologies, LLC, 2013), and Innophos Geismar (WSP, 2017) projects (Table 17 and Figure 101).

Table 17: Regional Total Dissolved Solids data for the injection complexes. There is no data for the Vicksburg Shale or USDW zone. NA indicates data not available.

Total Dissolved Solids				
Formation Type	Formation	TDS (mg/L)		n =
		Average	Range	
Confining Zone	Middle Miocene Confining Zone	89,984	34,068 – 135,636	10
Injection Zone	Lower Miocene Sands	113,046	12,158 – 274,000	194
Confining Zone	Anahuac Formation	107,926	44,656 – 235,998	13
Injection Zone	Frio Formation	80,241	10,120 – 337,932	131
Confining Zone	Vicksburg Shale	NA	NA	0
USDW	Quaternary / Pliocene Undif.	NA	NA	0

Figure 101: Location map of regional baseline fluid chemistry data from the USGS National Produced Waters Geochemical Database (2023). Wells used for local salinity study for the LMIC and OFIC injection zones shown with API values.

Table 18: Regional Baseline Fluid Chemistry data for the injection complexes from USGS (National Produced Waters Geochemical Database, 2023).

Baseline Fluid Chemistry					
Parameter/Constituent	Units	LMIC		OFIC	
		Middle Miocene Confining Zone	Lower Miocene	Anahuac	Frio Formation
pH	Standard Units	6.8	6.6	5.7	6.7
Ba^{2+}	mg / L	177.0	92.4	32.1	33.6
HCO^{3-}		589.0	269.3	462.9	508.4
Ca^{2+}		2,047.6	2,269.5	2,738.5	2,837.4
Cl^{-}		54,321.4	5,7141.7	50,997.0	44,625.0
K^{+}		264.0	223.8	228.0	365.0
Mg^{2+}		450.7	571.3	474.2	489.4
Na^{+}		32,494.0	33,160.4	29,290.4	25,467.6
SO_4^{2-}		9.7	44.4	176.9	101.6

2.8.2 Fluid-Rock Interactions

A literature review was conducted to evaluate the potential for reactivity between the fluid and solid phases during injection into the LMIC and OFIC.

2.8.2.1. Lower Miocene Injection Complex

There are currently no studies that could be found regarding the fluid-rock reactivity of the Lower Miocene Injection Complex. XRD data were available for the Miocene from a disposal well in St. John the Baptist Parish to the east. Samples averaged 93% quartz, 6% Feldspars and <3% total clay. Of the clay content, ~%50 consisted of illite and chlorite while the other 50% contained illite-smectite. In a geochemical study on CO_2 interactions with clay, Busch et al. (2012) modeled cases where CO_2 had adverse effects on smectite clays. Depending on the hydration of the smectite, CO_2 can either cause the smectite to collapse or swell, in either case forming fractures. However, in the case of the Miocene, even though half of the clay content is smectite, the overall total rock content is very low and would have negligible effects.

2.8.2.2. Oligocene Frio Injection Complex

A regional U.S. Gulf Coast study on fluid-rock reactivity injected 1,600 tons of CO_2 into the Frio Formation over a span of ten days. Chemical changes were observed as the CO_2 reached the observation well, including a drop in pH, an increase in alkalinity, and major increases in dissolved iron, manganese and calcium. Rapid dissolution of calcium occurred at CO_2 breakthrough and could have implications towards creating pathways for leakage in the seal rock or casing cement (Kharaka, 2006).

2.8.3 Planned Testing and Modeling

The data utilized for evaluating geochemical interactions within the Frio siliciclastic reservoirs are regional and not specific to the project area. Consequently, following the completion of pre-operational testing and logging and data collection, it will be determined if reactive transport modeling should be conducted.

Whole core and sidewall core samples will be acquired from the proposed injection zones to determine the petrophysical and mineralogical properties of the LMIC and OFIC (see Pre-Operational Testing Program). Mineralogical analysis will determine the type percent composition of potentially reactive minerals within the OFIC and LMIC at the proposed injection locations.

Fluid sampling from the injection zone and shallower zones is planned to establish a baseline geochemical description of reservoir fluids. Collected fluid samples are planned to be used to develop synthetic brine compositions to run core flooding studies to assess possible interactions between injected CO_2, reservoir matrix, and in-situ brine. Fluid samples will allow pre- and post-CO_2 injection analysis to determine the changes in brine chemistry, which can be compared with reservoir samples subjected to geochemical testing to assess changes in the rock matrix. If testing concludes that geochemical changes to reservoir rock or fluids are, a reactive transport model can be built and coupled with the current reservoir model to assess long term fate of injected CO_2 as it is related to mineralogical changes in the reservoir.

2.9. Site Suitability

Based on all available data and research presented in this Application Narrative, the project area meets the suitability requirement outlined in the regulations for CO_2 injection. The LMIC consists of the Middle Miocene Confining Zone as the upper confining zone, the Lower Miocene Sand as the injection target, and the Anahuac Formation which acts as the lower confining unit for the Lower Miocene Sand and the upper confining unit for the OFIC. The remainder of the OFIC consists of the Frio Formation as the injection target and the Vicksburg Shale as the lower confining unit.

The LMIC is a package of interbedded sand, shale, and silt measuring approximately 4,450 feet in thickness, and is a stratigraphically variable sequence containing sands that range from less than 10 feet to upwards of ~350 feet thick with an average of 1,707 feet of cumulative net reservoir separated by approximately 10 feet to upwards of 500 feet thick shales. The LMIC is composed of fluvial deltaic, marine shoreline, and shoreface sandstones with interstitial shales (Rainwater, 1964; John et al., 1992). During the Miocene, the predominant source of sedimentation shifted from the Rio Grande River system to the Mississippi drainage, causing significant sedimentation. The Lower and Middle Miocene sands present in the project area are separated by marine flooding surfaces offshore and equivalent nearshore marine to brackish fine-grained deposits closer to shore. Each episode contains repeated stacked parasequences containing distinct facies in order: continental sediments including massive sands with little to no shale, alternating nearshore and shallow marine sands and near shore marine shale, then moderately deep marine deposits containing offshore sand, silt, and shale including deep marine shales (Galloway et al., 2000; Rainwater, 1964; Limes and Stipe, 1959). The reservoir quality is noted as good to excellent and is linked to deposition facies, which results in a reported range of porosity from 22% to 35% and

permeabilities of 20 mD to 8,000 mD (Nehring Associates Inc., 2010). Wireline logs, core, and petrophysical evaluation from wells in the nearby subsurface resulted in an average model porosity of ~27% and an average permeability of ~472 mD in the net reservoir.

The OFIC is primarily composed of sandstone and shale, with minor siltstones and carbonates measuring approximately 2,300 feet in thickness. The OFIC is a stratigraphically variable sequence containing sands that range from less than 10 feet to upwards of 200 feet thick with an average of 271 feet net reservoir separated by approximately 10 feet to 250 feet thick shales. The sands are mostly shallow water marine sands interpreted as marine bars, barrier bars, and delta-front distributary mouth bars deposited along the Central Mississippi delta axis of deposition (Goddard et al., 2005; Krueger Jr., 1967; Galloway, 2000). Preservation of primary porosity contributes to more porous and permeable shallow Frio sands; secondary porosity formation is important for maintaining porosity and permeability in the deep Frio sands (Loucks, 2005). Variability within the OFIC results in reported ranges of porosity from 15% to 33% and permeabilities of 100 mD to 2,500 mD. Wireline logs, core, and petrophysical evaluation from wells in the nearby subsurface resulted in an average model porosity of ~27.7% and an average permeability of ~108 mD in the net reservoir.

Static earth modeling and simulation of the project area resulted in a total injection volume of 337.5 MMt CO_2 in the LMIC and 42 MMt CO_2 in the OFIC for the potential injection locations over 30 years. Due to the relatively high porosity and permeability in the LMIC and the offset Baton Rouge Fault system, the plume size and distribution is limited to the project AoR through injection management in the individual sand zones over the 30-year injection period and 50-year PISC period. Using the US-DOE-NETL methods, it was calculated that the LMIC has the potential to be able to sequester P10: 146, P50: 378, P90: 739 MMt of CO_2. The OFIC has the potential to be able to sequester P10: 27, P50: 76, P90: 174 MMt of CO_2. Data collection from pre-operational testing will narrow the uncertainty range prior to injection.

Literature review and regional well log analysis indicate that the project's confining zones will provide long-term containment of CO_2. The LMIC upper confining zone, the Middle Miocene Confining Zone, consists of laterally extensive marine shales that are a cumulative 100 feet to 400 feet thick (Goddard and Zimmerman, 2003). There is evidence supporting the Middle Miocene Confining Zone as an effective long-term seal from CO_2 injection. As previously mentioned, Goddard and Zimmerman (2003) recognize the Middle Miocene Confining Zone as a regional top-seal for Miocene gas reservoirs in the Florida Parishes area, where it also prevents fresh water in shallow Plio-Pleistocene aquifers above it from mixing with much higher salinity water in the Miocene sandstone reservoirs below. It also satisfies the U.S. Geological Survey requirements as a confining zone for the Lower Miocene Storage Assessment Unit (Roberts-Ashby, 2014). The Middle Miocene Confining Zone is also complemented by multiple shale zones with similar characteristics between the Lower Miocene Sands that are between 2,187 feet to 3,865 feet thick and are laterally continuous with varying thickness throughout the region. The Anahuac Formation, which sits at the top of the OFIC and base of the LMIC, is a laterally continuous unit that consists of shales with greater than 400 feet thickness and less than 0.0015 mD permeability, topped by a carbonate zone of less than 50 feet to 250 feet thickness that is reported as impermeable. Finally, the Vicksburg Shale has a reported thickness of 500 feet, which has not been measured in the project area due to lack of well penetrations, but it has been measured as impermeable, and is laterally continuous across the basin (Goddard et al., 2005). These confining

zones and their historical longevity are robust, indicating that secondary confining zone identification is unnecessary.

The major geologic structural features in the project area are related to salt tectonics (see subsection 2.1.13 of this Application Narrative). The primary structural features adjacent to the injection complexes are two salt diapir structures to the south of the project area and the Baton Rouge fault system to the north of the project area. All mapped and observable structural features, including salt diapirs and normal faults, are located outside of the AoR for all injection and confining zones. Kinematic fault modeling and fault seal analysis of the Baton Rouge Fault system, completed to better understand the geometry and fault-fluid interaction behavior across and along the fault zone, is discussed in subsection 2.3 of this Application Narrative. Overall, fault seal analysis of the Baton Rouge Fault system suggests that one or more of the sealing mechanisms are present and likely adequate for the fault system to act as a barrier to fluid flow. Furthermore, reservoir simulation and modeling efforts demonstrate that neither the pressure nor CO_2 plumes should migrate northward to and interact with the Baton Rouge Fault system as discussed in subsection 1.2 of the Area of Review and Correction Action Plan. There are, however, 22 confirmed legacy wells that penetrate the caprock within the AoR as seen in Figure 74 of subsection 3.2 in the Area of Review and Corrective Action Plan. These wells are addressed in the plan, along with those wells without depth data, to ensure that the legacy wells are not conduits for potential leakage. Literature review of the fluid chemistry, injection and confining zone mineralogy, and analogs for the injection complexes suggest that the siliciclastic intervals will have minimal reaction with the injected CO_2. Laboratory analysis of CO_2 interaction with smectite clays suggest the potential risk for adverse impacts due to interactions. However, this is seen as a low risk due to the low concentration of smectite clay within the LMIC and OFIC. The rate and magnitude of these reactions will be evaluated when gathering site-specific data for the project area during pre-operational testing. Surface and well infrastructure materials are being designed using CO_2 compatible materials and techniques, and the proposed CO_2 stream is dry (95 CO_2); thus, no adverse interactions are anticipated. Corrosion testing prior to construction will take place to confirm material compatibility.

3. Summary of Other Plans

3.1. Area of Review and Corrective Action Plan

The information and files submitted in the Area of Review and Corrective Action Plan satisfy the requirements of LAC 43:XVII.3615. This plan addresses how the project AoR is delineated and uses corrective action techniques to address all deficient artificial penetrations and other features that compromise the integrity of the confining zone above the injection zone. The AoR encompasses the entire region surrounding the project's injection wells where USDWs may be endangered by injection activity.

The computational models describe modeling of the subsurface injection of CO_2 into the LMIC and OFIC at the project injection wellsites. The STOMPX-CO2 (LMIC) and REVEAL (OFIC) simulators were used to assess the development of the CO_2 plume, the pressure front, and the long-term outcome of the injected CO_2. Simulation indicates for the LMIC and OFIC that both the CO_2 plume and pressure front will define the maximum extent of the AoR over the lifetime of the project. Therefore, the AoR for the project is defined as the maximum extent of the CO_2 plume for

both the LMIC and OFIC, and the maximum extent of the threshold pressure for the LMIC (95.6 psi) and OFIC (123 psi) which occurs at the end of injection for both injection complexes. This plan details the computational modeling, assumptions that were made, and site characterization data that the model was based on to satisfy the requirement of LAC 43:XVII.3615(3).

There are records for 22 existing oil and gas wellbores and 37 water wells within the AoR. Per LAC 43:XVII.3607(C)(2)(d), wells that penetrate the injection or confining zones within the AoR must be tabulated. None of the water wells penetrates the injection or confining zones, but there are up to 22 oil and gas wellbores that may penetrate the primary confining unit within the AoR, 3 of which records of depth are not available. Live Oak CCS, LLC proposes to conduct a magnetometer survey to identify any wells without records in the AoR and a sequential corrective action strategy based on temporal evolution of the threshold pressure boundary, beginning prior to injection and ending in the 30th year of injection.

Live Oak CCS, LLC will review the AoR annually during the injection phase and once every five years during the post-injection phase to ensure the initial model predictions are adequate for predicting the extent of the CO_2 plume and pressure front.

AoR and Corrective Action GSDT Submissions

GSDT Module: AoR and Corrective Action
Tab(s): All applicable tabs

Please use the checkbox(es) to verify the following information was submitted to the GSDT:
☐ Tabulation of all wells within AoR that penetrate confining zone ***[40 CFR 146.82(a)(4)]***
☐ AoR and Corrective Action Plan ***[40 CFR 146.82(a)(13) and 146.84(b)]***
☐ Computational modeling details ***[40 CFR 146.84(c)]***

3.2. Financial Responsibility

Live Oak CCS, LLC has prepared the Financial Assurance Demonstration to comply with requirements at LAC 43:XVII.3609(C). The plan estimates costs of project activities and provides information on financial instruments that Live Oak CCS, LLC will use to demonstrate Financial Assurance for the following activities: (1) Corrective Action; (2) Injection Well Plugging; (3) Post-Injection Site Care and Site Closure; and (4) Emergency and Remedial Response. The estimated costs of each of these activities are presented in Table 19 below.

Table 19: Cost Estimates for Activities to be Covered by Financial Responsibility.

Activity	Total Cost ($)	Timeline of Coverage
Corrective Action	$9,902,200	2027-2058
Plugging Injection Wells	$6,660,360	2063
Post-Injection Site Care and Site Closure	$17,597,000	2058-2107
Emergency and Remedial Response	$17,900,638	2028-2058

Live Oak CCS, LLC will execute a combination of financial instruments prior to construction of the injection wells. These financial instruments will cover the costs of one emergency leakage event as discussed in the Emergency and Remedial Response Plan, all of the costs of injection well plugging as discussed in the Injection Well Plugging Plan, all of the costs of corrective action as discussed in the Area of Review and Corrective Action Plan, and all of the costs of 50 years of post-injection site care and site closure as discussed in the Post-Injection Site Care and Site Closure Plan.

Financial Responsibility GSDT Submissions
GSDT Module: Financial Responsibility Demonstration ***Tab(s):*** Cost Estimate tab and all applicable financial instrument tabs Please use the checkbox(es) to verify the following information was submitted to the GSDT: ☐ Demonstration of financial responsibility ***[40 CFR 146.82(a)(14) and 146.85]***

3.3. Injection Well Construction

The project's injection wells, LO-01 M, LO-01 F, LO-02 M, LO-03 M, LO-04 F-M, LO-05 M, LO-06 M, and LO-06 F will be newly drilled and are designed to accommodate the mass of CO_2 that will be delivered to the project and the subsurface characteristics of the CO_2 injection intervals. Injection well construction is further described in the following plans that are part of this application: (1) Stimulation Program and (2) Construction Details for each injection well.

3.3.1 Proposed Stimulation Program [LAC 43:XVII.3607(C)(2)(h)]

The Stimulation Program describes the stimulation measures that the project may use to mitigate drilling-induced damage near the wellbore without interfering with containment. It is expected to effectively clear the perforated interval of fines, perforation charge residue, and debris from cement or casing. Additionally, stimulation serves to eliminate drilling mud filtrate and dissolved minerals present in the formation. This process is common, as the untreated presence of these elements can lead to elevated downhole injection pressures and diminished injectivity, underscoring the significance of thorough treatment.

Data from offset wells in the region indicate a possibility of formation sand entering the wellbore during interruptions in CO_2 injection in the LMIC. Sand control screens to limit sand infiltration are proposed for wells injecting in the LMIC (i.e., LO-1 M, LO-2 M, LO-3 M, LO-5 M, and LO-06 M). A resin control system in the Miocene formation without the need of screens is proposed for LO-04 F-M which injects into both the LMIC and OFIC.

Specific stimulation fluids, additives, and diverters will be based on injection well site conditions after completion of the pre-operational testing program and determination that stimulation is needed. Prior to conducting stimulation activities on any of the injection wells, Live Oak CCS, LLC will obtain a written work authorization by submitting Form UIC-17 to the OC with details on the purpose of stimulation, procedures, and stimulation fluids to be used and their anticipated volumes and concentrations.

3.3.2 Construction Procedures [LAC 43:XVII.3617(A)]

Construction Details for each injection well describes the analysis conducted and proposed designs for injection wells LO-01 M, LO-01 F, LO-02 M, LO-03 M, LO-04 F-M, LO-05 M, LO-06 M, and LO-06 F that ensure the prevention of the movement of fluids into or between USDWs, that allow the use of testing devices and workover tools, and that allow continuous monitoring of the annulus space between the injection tubing and long string casing.

LO-01 M, LO-02 M, LO-03 M, LO-05 M and LO-06 M well designs propose a 7-inch outer diameter (OD) tubing tapered down to 5.5-inch OD, a maximum wellhead pressure of 2,220 psig and maximum injection rate of 3.5 MMt/y into the LMIC. The design involves multiple casing strings at varying depths, including a 20-inch diameter conductor casing set at a depth of approximately 200 ft BGS, a 13.375-inch diameter surface casing set at around 2,800 ft BGS inside a 17.5-inch borehole, and a 9.625-inch long string casing inside a 12.25-inch borehole set at varying depths for all the wells. Long string casing will be equipped with a cement differential valve (DV) tool, BakerWrap XP^{TM} wrap-on-pipe open-hole stand-alone screens, and open-hole permanent packers to isolate Miocene injection intervals. Tubing will be equipped with retrievable packers and sliding sleeves to allow selective injection of CO_2. Surface casing will be cemented from casing shoe to the surface, while long string casing will be cemented from DV tool to the surface. Section of the long string casing below the DV tool will not be cemented. The proposed well schematics for LO-01 M, LO-02 M, LO-03 M, LO-05 M and LO-06 M are in Figure 9 and Figure 10 of the Construction Details of each respective well.

LO-01 F and LO-06 F well designs propose a 7-inch OD tubing tapered down to 5.5-inch OD and then further tapered down to 3.5-inch OD, a maximum wellhead pressure of 2,220 psig and maximum injection rate of 1.5 MMt/y into the OFIC. The design involves multiple casing strings at varying depths, including a 20-inch diameter conductor casing set at a depth of approximately 200 ft BGS, a 13.375-inch diameter surface casing set at around 2,800 ft BGS inside a 17.5-inch borehole, a 9.625-inch long string casing inside a 12.25-inch borehole, and a 7.625-inch liner inside a 9.125-inch borehole set at varying depths for both the injection wells. Liner will be overlapped inside the bottom of the long string casing, and tubing will be equipped with a retrievable packer to isolate the injection interval from the annulus. All casing strings will be cemented to the surface except liner which will be cemented to the liner hanger packer. The proposed well schematics for LO-01 F and LO-06 F are in Figure 12 and Figure 13 of the Construction Details of each respective well.

LO-04 F-M well design proposes a 7-inch OD tubing tapered down to 5.5-inch OD, a maximum wellhead pressure of 2,220 psig, maximum injection rate of 3.5 MMt/y into the LMIC and 1.5 MMt/y into the OFIC. The design involves multiple casing strings at varying depths, including a 20-inch diameter conductor casing set at a depth of approximately 200 ft BGS, a 13.375-inch diameter surface casing set at around 2,800 ft BGS inside a 17.5-inch borehole, a 9.625-inch long string casing inside a 12.25-inch borehole set at around 9,890 ft, and a 7.625-inch liner inside a 9.125-inch borehole set at around 11,900 ft. Liner will be overlapped inside the bottom of the long string casing. Tubing will be equipped with packers to isolate all four injection intervals (three in LMIC and one in OFIC), and sliding sleeves will be utilized to inject CO_2 into one or more intervals simultaneously. All casing strings will be cemented to the surface except liner which will

be cemented to the liner hanger packer. The proposed well schematic for LO-04 F-M is in Figure 12 and Figure 13 of the Construction Details.

The borehole diameters are considered conventional for the sizes of casing that will be used and should allow ample clearance between the outside of the casing and the borehole wall. Proposed casing, liner, and tubing sizes should also allow the use of appropriate testing devices and workover tools. While specific alloy compositions, weights, grades, and connections may change due to availability, construction of the well will utilize corrosion resistant alloys such as 22Cr or higher for CO_2 + H_2O wetted sections and adhere to mechanical specifications consistent with design inputs presented herein. Final alloy selection at procurement will be based on the most current applicable materials testing results from API, AMPP, or other standard bodies currently focused on CCS.

Summaries of the casing program for LO-01 M, LO-02 M, LO-03 M, LO-05 M, and LO-06 M are in Table 6 and for LO-01 F, LO-04 F-M, and LO-06 F are in Table 7 of the Construction Details for each respective well. Properties of casing and tubing materials for LO-01 M, LO-02 M, LO-03 M, LO-05 M, and LO-06 M are in Table 7 and for LO-01 F, LO-04 F-M, and LO-06 F are in Table 8 of the Construction Details for each respective well. Packer specifications for LO-01 M, LO-02 M, LO-03 M, LO-05 M, and LO-06 M are in Table 9 and Table 10 and for LO-01 F, LO-04 F-M, and LO-06 F are in Table 10 and Table 11 of the Construction Details for each respective well. Measures are in place to prevent exceeding fracture gradients or mandated injection pressures. Adjustments may be made based on future reservoir characterization. The final nodal analysis recommends a tubing configuration and operational parameters to ensure pressure and rate limitations are met while considering factors such as zonal isolation and well integrity.

3.4. Pre-Operational Testing Plan

The Pre-Operational Testing Program is designed to meet the requirements of LAC 43:XVII.3617(B) and 3619, including the establishment of an accurate baseline dataset of pre-injection site conditions, verification of depths and physical characteristics of the injection and confining zones, and assurance of conformance with injection well construction requirements in LAC 43:XVII.3617(A). The pre-operational formation testing program will be implemented at all injection wells to verify the chemical and physical characteristics of the injection zones and confining zones.

The pre-operational testing program will include a combination of wireline logging and whole and side-wall coring. In addition, formation geohydrologic testing will be completed to verify injectivity of the storage formation. Fracture pressure will be determined using the formation testing tool and minifrac tests in the observation wells, which help limit borehole rugosity and provide the highest probability of achieving a mechanically sound cement installation in the injection wells. The pre-operational testing program will determine or verify the depth, thickness, mineralogy, lithology, porosity, permeability, and geomechanical information of the Middle Miocene Upper Confining Zone (confining zone), the Lower Miocene Sand (upper injection zone), the Anahuac Formation (confining zone), the Frio Formation (lower injection zone), the Vicksburg Shale (basal confining zone), and other relevant geologic formations. In addition, formation fluid characteristics will be obtained from the Lower Miocene Sand and Frio Formation to establish baseline data against which future measurements may be compared. Reports detailing the results

and interpretations of all testing operations will be provided to the OC following conclusion of analysis and before the start of CO_2 injection operations. Cement bond, variable density, and temperature logs will be run after long string casing is cemented in place to verify the quality of the cement job in injection wells. Additionally, mechanical integrity tests, including annular pressure tests will be conducted to ensure the safe injection of CO_2 once the injection wells are put into operation.

Pre-Operational Logging and Testing GSDT Submissions
GSDT Module: Pre-Operational Testing ***Tab(s):*** Welcome tab Please use the checkbox(es) to verify the following information was submitted to the GSDT: ☐ Proposed pre-operational testing program ***[40 CFR 146.82(a)(8) and 146.87]***

3.5. Well Operation

The Summary of Requirements – Class VI Operating and Reporting Conditions describes the operational design developed to adhere to LAC 43:XVII.3621 and provides a plan for safe injection into LO-01 M, LO-01 F, LO-02 M, LO-03 M, LO-04 F-M, LO-05 M, LO-06 M, and LO-06 F.

Live Oak CCS, LLC seeks to safely inject CO_2 in eight injection wells: five in the Miocene formation, denoted as M; three in the Frio formation, denoted as F; and one well perforated into both the Miocene and Frio formations, denoted as F-M. Table 1 of the Summary of Requirements summarizes the proposed operational parameters for all the injection wells. These parameters are expected to remain constant throughout the injection period. However, some variability in operational parameters may stem from variations in volume from the CO_2 sources, which may impact injection volumes during limited periods of time. The injection rate values were modeled using Petroleum Experts' PROSPER software, and the nodal analysis results can be found in subsection 2.1 of the Construction Details for each injection well.

Using average annual and maximum instantaneous CO_2 injection rates, injection tubing string sizes were selected for injection wells to meet the project requirements. Expected wellhead pressures during injection operations were calculated using the average reservoir pressure during a 30-year injection period, as derived from the reservoir model. Maximum wellhead pressures for injection wells were calculated based on the hydraulic fracture gradient and 90% of hydraulic fracture pressure at the top depth in the LMIC. However, pipeline specifications for CO_2 transport limit the maximum wellhead pressure to 2,220 psig, which is lower than the calculated fracture pressures.

Each injection well will be monitored to ensure safe operations, in compliance with LAC 43:XVII.3621(A)(6)(a). Operational safety monitoring includes continuous monitoring of the injection pressure at the wellhead and bottomhole, continuous monitoring of flow rate, volume and/or mass, and temperature of CO_2 stream, continuous monitoring of the pressurized annulus, continuous fiber optic temperature monitoring along the well, and corrosion coupon monitoring to identify and monitor corrosion of materials used in construction of compression equipment, pipeline, and wells which encounter CO_2. In compliance with LAC 43:XVII.3621(A)(6)(b), all the

continuous monitoring data will be digitally recorded, and instruments will be weatherproof or housed in weatherproof enclosures when located in areas exposed to climatic conditions. The proposed monitoring requirements can be found in subsection 2.4 of the Summary of Requirements for all the injection wells.

In adherence to LAC 43:XVII.3621(A)(5), Live Oak CCS, LLC will monitor and maintain mechanical integrity of each injection well at all times during operation. Well maintenance and workovers will be part of normal operations to keep each injection well in a safe operating condition. Procedures for well maintenance will vary depending on the nature of the procedure. All maintenance and workover operations will be monitored to ensure there is not a loss of mechanical integrity.

For injection shutdowns occurring under routine conditions (e.g., for well workovers), Live Oak CCS, LLC will reduce CO_2 injection at a rate of up to 200,000 metric tons per day over a maximum of 2 days to ensure protection of health, safety, and the environment.

The CO_2 will be captured from industrial facilities and power plants located in the industrial corridor surrounding the Mississippi River south of Baton Rouge and transported by pipeline to the Live Oak CCS Hub. The CO_2 will be in the liquid phase as it enters the wellhead and will transition to a supercritical phase in the wellbore. The injectate stream composition coming into the storage field will vary throughout the injection phase of the project. To account for this, Live Oak CCS, LLC plans to continuously monitor the CO_2 stream chemical composition to ensure it meets minimum composition specifications that will be refined when sources are finalized, and capture equipment is operational. Due to the anticipated low water content within the CO_2 stream, CO_2-induced corrosion affecting well components is not likely - as noted by the U.S. EPA well construction guidance (US EPA, 2012). Live Oak CCS, LLC will monitor for potential corrosion induced by the injectate as outlined in Section 4.0 of the Testing and Monitoring Plan. Live Oak CCS, LLC will submit quarterly reports to the OC during the injection period. Reporting requirements are detailed in Section 6 of the Summary of Requirements.

3.6. Testing and Monitoring Plan

The Testing and Monitoring Plan describes how Live Oak CCS, LLC will monitor the project to verify that it is not endangering USDWs, pursuant to LAC 43:XVII.3625. Additionally, the monitoring and testing data will be used to track the CO_2 plume and pressure front, validate and refine geological models and simulations used to forecast the distribution of the CO_2 within the storage zones, support AoR re-evaluations, and demonstrate non-endangerment. The Quality Assurance and Surveillance Plan meeting the requirement of LAC 43:XVII.3625(A)(11) is provided as an Appendix to the Testing and Monitoring Plan.

In addition to monitoring the injection wells, Live Oak CCS, LLC plans to drill and monitor up to fourteen observation wells for the project: seven in-zone observation wells in the Lower Miocene Sand and Frio Formation, three above-zone observation wells in the Middle Miocene Sands, three lowermost USDW observation wells in the Jasper Equivalent Aquifer System, and one shallow USDW well in the Chicot Aquifer System. A summary of these wells and their approximate depths is in Table 1 of the Testing and Monitoring Plan. Proposed monitoring activities and frequencies for these wells are summarized in Table 2 of the Testing and Monitoring Plan.

The Testing and Monitoring Plan will utilize direct and indirect monitoring technologies that will monitor:

- Injectate composition detailed in Section 2.0 of the Testing and Monitoring Plan (LAC 43:XVII.3625(A)(1));
- Operational parameters detailed in Section 3.0 of the Testing and Monitoring Plan (LAC 43:XVII.3625(A)(2));
- Corrosion of well materials and components detailed in Section 4.0 of the Testing and Monitoring Plan (LAC 43:XVII.3625(A)(3));
- Any migration of CO_2 or brine above the confining zone, including formation water quality monitoring, detailed in Section 5.0 of the Testing and Monitoring Plan (LAC 43:XVII.3625(A)(4));
- Well integrity over the injection phase of the project detailed in Section 6.0 of the Testing and Monitoring Plan (LAC 43:XVII.3625(A)(5));
- Near well-bore environment using pressure fall-off testing detailed in Section 7.0 of the Testing and Monitoring Plan (LAC 43:XVII.3625(A)(6)); and
- Development of the CO_2 plume and pressure front in the storage formation over time detailed in Section 8.0 of the Testing and Monitoring Plan (LAC 43:XVII.3625(A)(7)).

Testing and Monitoring GSDT Submissions

GSDT Module: Project Plan Submissions
Tab(s): Testing and Monitoring tab

Please use the checkbox(es) to verify the following information was submitted to the GSDT:
☐ Testing and Monitoring Plan ***[40 CFR 146.82(a)(15) and 146.90]***

3.7. Injection Well Plugging

The Injection Well Plugging Plans for each injection well describe the process Live Oak CCS, LLC proposes to plug injection wells LO-01 M, LO-01 F, LO-02 M, LO-03 M, LO-04 F-M, LO-05 M, LO-06 M, and LO-06 F in conformance with requirements set forth in LAC 43:XVII.3631(A). Plugging activities will begin following the cessation of CO_2 injection. Live Oak CCS, LLC may postpone plugging the injection well to use it to monitor in-zone reservoir conditions post-injection. The Post-Injection Site Care and Site Closure Plan and Financial Responsibility Demonstration assume that each injection well will be used as an observation well for the first 5 years after injection ceases then plugged in accordance with this plan.

During both injection and post-injection phases, industry-standard downhole pressure gauges will measure and record bottom-hole pressure (BHP). These gauges will be installed in the injection tubing, enabling continuous real-time surface readout of pressure data. After cessation of injection activities and any post-injection monitoring period, these gauges will be used to obtain the final BHP of the injection interval. In the event originally installed gauges are not functioning properly, BHP will be recorded using a wireline deployed pressure gauge. Following the determination of BHP, a buffered fluid (brine) will be employed to flush and fill the well, ensuring pressure control. The measured BHP will guide the selection of the appropriate weight of brine to stabilize the well

and may inform decisions regarding the blend of cement needed to plug the well and address considerations such as preventing leak-off or premature setting. An external MIT will be conducted before plugging. If mechanical integrity is compromised, repairs will be made before proceeding with plugging operations.

Live Oak CCS, LLC will submit Form UIC-17 to the OC with the procedure to plug and abandon each injection well and receive written approval before beginning actual well plugging operations. Within 30 days of plugging each injection well, Live Oak CCS, LLC will submit a well plugging and abandonment report to the OC for the respective well as detailed in subsection 5.1 of the Injection Well Plugging Plan for each well.

Injection Well Plugging GSDT Submissions

GSDT Module: Project Plan Submissions
Tab(s): Injection Well Plugging tab

Please use the checkbox(es) to verify the following information was submitted to the GSDT:
☐ Injection Well Plugging Plan ***[40 CFR 146.82(a)(16) and 146.92(b)]***

3.8. Post-Injection Site Care (PISC) and Site Closure

The Post-Injection Site Care and Site Closure Plan describes the activities that Live Oak CCS, LLC will perform to meet the requirements of LAC 43:XVII.3633. The Post-Injection Site Care (PISC) timeframe will begin when all CO_2 injection ceases and ends with site closure. Live Oak CCS, LLC provides a plan demonstrating a 50-year PISC timeframe as discussed in the Area of Review and Corrective Action Plan. No alternative PISC timeframe is requested at this time. Live Oak CCS, LLC will monitor groundwater quality and track the position of the CO_2 plume and pressure front after the end of injection operations. Live Oak CCS, LLC may not cease post-injection monitoring until a demonstration of non-endangerment of USDWs has been approved by the OC pursuant to LAC 43:XVII.3633(2)(c). Following approval for site closure, Live Oak CCS, LLC will plug all observation wells, restore the site to its original condition, and submit a site closure report and associated documentation. The Site Closure Plan is detailed in Section 5 of the Post-Injection Site Care and Site Closure Plan.

The PISC plan includes groundwater quality monitoring and plume and pressure front tracking during the post-injection phase. Data collected during the post-injection phase will be used as evidence for protection of groundwater resources, pressure front stabilization, and CO_2 plume stabilization in the non-endangerment demonstration required for site closure. These, along with other activities described in the plan, will meet the requirements of LAC 43:XVII.3633(2)(a). Details of proposed post-injection monitoring are in Tables 4, 5, and 6 of the Post-Injection Site Care and Site Closure Plan. The results of all post-injection phase testing and monitoring will be submitted to the OC and EPA in semi-annual reports with data from January through June submitted by the end of July, and data from July to December submitted by the end of January (LAC 43:XVII.3629(A)(1)(a)).

PISC and Site Closure GSDT Submissions
GSDT Module: Project Plan Submissions ***Tab(s):*** PISC and Site Closure tab Please use the checkbox(es) to verify the following information was submitted to the GSDT: ☐ PISC and Site Closure Plan ***[40 CFR 146.82(a)(17) and 146.93(a)]***

3.9. Emergency and Remedial Response Plan

The Emergency and Remedial Response Plan (ERRP) describes actions that Live Oak CCS, LLC will take to address an emergency in the AoR that may cause movement of the injection fluid or formation fluid in a manner that may endanger an USDW during the construction, operation, or post-injection site care periods, pursuant to LAC 43:XVII.3623. Live Oak CCS, LLC will work with Iberville and West Baton Rouge parishes to seek approval of this ERRP.

Examples of potential risks include: (1) injection or observation well integrity failure, (2) injection well monitoring and/or surface equipment failure, (3) natural disaster, (4) fluid leakage into a USDW, (5) CO_2 leakage to USDW or land surface, or (6) an induced seismic event. In the case of one of the listed risks, site personnel, project personnel, and local authorities will be relied upon to implement this ERRP. Live Oak CCS, LLC will work with Iberville and West Baton Rouge parishes to establish a community notification system that includes coordination with emergency preparedness and response agencies and public notification in the event of an emergency. Coordination with local agencies will include conducting a tabletop exercise that simulates emergency situations and responses prior to the project beginning operation.

If Live Oak CCS, LLC obtains evidence that the injected CO_2 stream and/or associated pressure front may cause an endangerment to a USDW, Live Oak CCS, LLC will perform the following actions:

1. Initiate shutdown plan for the injection well(s).
2. Immediately notify the Project Manager during construction or Operations Manager during operations.
3. Take all steps reasonably necessary to identify and characterize any release.
4. Notify the 24-hour Emergency Contact (Appendix B of the ERRP) followed by the OC within 24 hours of the emergency event, per LAC 43:XVII.3623(2)(c).
5. Implement applicable portions of the approved ERRP.

The emergency contact list in Appendix B of the ERRP will be updated annually at a minimum, and the ERRP will be reviewed at least once every five years following its approval as well as within one year of an AoR reevaluation and following any significant changes to the injection process or the injection facility or an emergency event. Periodic training will be provided, not less than annually, to construction personnel, well operators, project safety personnel, environmental personnel, the operations manager, and corporate communications. The training plan will record that the necessary personnel have been trained and possess the required skills to perform their relevant emergency response activities described in the ERRP.

Emergency and Remedial Response GSDT Submissions
GSDT Module: Project Plan Submissions ***Tab(s):*** Emergency and Remedial Response tab Please use the checkbox(es) to verify the following information was submitted to the GSDT: ☐ Emergency and Remedial Response Plan ***[40 CFR 146.82(a)(19) and 146.94(a)]***

3.10. Injection Depth Waiver and Aquifer Exemption Expansion

No injection depth waiver or aquifer exemption expansion is being requested in this application.

3.11. Optional Additional Project Information

The project's drilling program schedule is included in Appendix F, showing the estimated spud dates of each proposed well within the project. Also, expanded size versions of figures within the Application Narrative that may be hard to read are included in Appendix G.

3.12. Other Information

3.12.1. Form UIC-60 CCS

Pursuant to LAC 43:XVII.3607(B)(1), Class VI Well Permit Application Form UIC-60 CCS has been provided for each injection well proposed in this application: LO-01 M, LO-01 F, LO-02 M, LO-03 M, LO-04 F-M, LO-05 M, LO-06 M, and LO-06 F. Each form includes one original Certified Location Plat that complies with the requirements of the IMD-GS-10 Policy and results of groundwater sampling in four water wells within the AoR.

3.12.2. Environmental Justice Plan

At the request of the OC, an Environmental Justice Plan for the project has been provided. This plan provides an environmental justice assessment for the AoR and describes project benefits and disbenefits. The project's Stakeholder Engagement Strategy is detailed as well as progress to date on implementing the plan.

3.12.3. Environmental Analysis

Live Oak CCS, LLC will prepare an Environmental Analysis for the project pursuant to LRS 30:1104.1 and submit it to the OC during the technical review period of the permit application.

The remainder of this page intentionally left blank.

4. References

Allan, U.S., 1989. Model for hydrocarbon migration and entrapment within faulted structures. AAPG Bulletin, 73(7), pp.803-811.

Anderson, E. G. (1979) Basic Mesozoic study in Louisiana: The northern coastal region and the Gulf Basin Province. Louisiana Geological Series Folio Series 3, 58 p.

Aronow, S. and Wesselman, J. B., 1971, Groundwater Resources of Chambers and Jefferson Counties, Texas: Texas Water Development Board Report No. 133.

Barker, C. E., Biewick, L. R. H., Warwick, P. D., & SanFilipo, J. R. (2000). Preliminary Gulf Coast Coalbed Methane Exploration Maps: Depth to Wilcox, Apparent Wilcox Thickness and Vitrinite Reflectance Open-File Report (Open-File Report 2000–113; Open-File Report, p. 4). U.S. Geological Survey. https://pubs.usgs.gov/of/2000/ofr-00-0113/

BeBout, D. G,. (1992). Introduction to Paleocene-Eocene Plays. In D. G. Bedout, W. A. White, C. M. Garrett, & T. F. Hentz (Eds.), Atlas of Major Central and Eastern Gulf Coast Gas Reservoirs. (p. 36). The University of Texas at Austin, Bureau of Economic Geology. https://store.beg.utexas.edu/atlases-of-major-oil-and-gas-reservoirs/3012-at0005.html

Bebout, D. G., & Gutiérrez, D. R. (1983). Regional Cross Sections, Louisiana Gulf Coast Eastern Part (Folio Series No. 6; p. 10). Louisiana Geological Survey.

BeBout, D. G,. (1992). Introduction to Paleocene-Eocene Plays. In D. G. Bedout, W. A. White, C. M. Garrett, & T. F. Hentz (Eds.), Atlas of Major Central and Eastern Gulf Coast Gas Reservoirs. (p. 36). The University of Texas at Austin, Bureau of Economic Geology. https://store.beg.utexas.edu/atlases-of-major-oil-and-gas-reservoirs/3012-at0005.html

Berggren, W. A., Kent, D. V., Swisher, C. C., III, & Aubry, M.-P. (1995). A Revised Cenozoic Geochronology and Chronostratigraphy. In W. A. Berggren, D. V. Kent, M.-P. Aubry, & J. Hardenbol (Eds.), Geochronology, Time Scales and Global Stratigraphic Correlation (Vol. 54, p. 0). SEPM Society for Sedimentary Geology. https://doi.org/10.2110/pec.95.04.0129

Blondes, M. S., Brennan, S. T., Merrill, M. D., Buursink, M. L., Warwick, P. D., Cahan, S. M., Corum, M. D., Cook, T. A., Craddock, W. H., DeVera, C. A., Drake II, R. M., Drew, L. J., Freeman, P. A., Lohr, C. D., Olea, R. A., Roberts-Ashby, T. L., Slucher, E. R., & Varela, B. A. (2013). National assessment of geologic carbon dioxide storage resources: Methodology implementation. In Open-File Report (Open File Report 2013–1055). U.S. Geological Survey. https://doi.org/10.3133/ofr20131055

Blondes, M.S., Knierim, K.J., Croke, M.R., Freeman, P.A., Doolan, C., Herzberg, A.S., and Shelton, J.L., (2023), U.S. Geological Survey National Produced Waters Geochemical Database (ver. 3.0, December 2023): U.S. Geological Survey data release, https://doi.org/10.5066/P9DSRCZJ.

Brennan, S. T., Burruss, R. C., Merrill, M. D., Freeman, P. A., & Ruppert, L. F. (2010). A Probabilistic Assessment Methodology for the Evaluation of Geologic Carbon Dioxide Storage

(Open File Report 2010–1127; p. 31). U. S. Geological Survey. https://pubs.usgs.gov/of/2010/1127/

Buono, A. (1983). The Southern Hills regional aquifer system of southeastern Louisiana and southwestern Mississippi (Water Resources Investigation Report 83–4189; p. 44). United States Department of the Interior and United States Geological Survey in cooperation with the U.S. Environmental Protection Agency. https://doi.org/10.3133/wri834189

Burruss, R. C., Brennan, S. T., Freeman, P. A., Merrill, M. D., Ruppert, L. F., Becker, M. F., Herkelrath, W. N., Kharaka, Y. K., Neuzil, C. E., Swanson, S. M., Cook, T. A., Klett, T. R., Nelson, P. H., & Schenk, C. J. (2009). Development of a Probabilistic Assessment Methodology for Evaluation of Carbon Dioxide Storage (Open File Report 2009–1035; p. 89). U. S. Geological Survey. https://pubs.usgs.gov/of/2009/1035/

Busch, A., Bertier, P., Gensterblum, Y., Rother, G., Spiers, C. J., Zhang, M., & Wentinck, H. M. (2016). On sorption and swelling of CO2 in clays. Geomechanics and Geophysics for Geo-Energy and Geo-Resources, 2(2), 111–130. https://doi.org/10.1007/s40948-016-0024-4

Childs, C., Manzocchi, T., Nell, P.A.R., Walsh, J.J., Strand, J.A., Heath, A.E. and Lygren, T.H., 2002. Geological implications of a large pressure difference across a small fault in the Viking Graben. Norwegian Petroleum Society Special Publications, 11, pp.187-201.

Childs, C., Manzocchi, T., Walsh, J.J., Bonson, C.G., Nicol, A. & Schopfer, M.P.J. 2009. A geometric model of fault zone and fault rock thickness variations. Journal of Structural Geology, 31, 117–127, https://doi.org/10.1016/j.jsg.2008.08.009

Collier, A.L. and Sargent, B.P., 2015, Water Use in Louisiana, 2015, Department of Transportation and Development, Water Resources Special Report No. 18

Combes, J. M. (1993). The Vicksburg Formation of Texas: Depositional systems distribution, sequence stratigraphy, and petroleum geology. AAPG Bulletin (American Association of Petroleum Geologists); (United States), 77:11. https://www.osti.gov/biblio/5467085

Cook, C.E., Darrow salt dome, Ascension Parish, Louisiana, AAPG Bulletin, v. 22, n. 10, pp. 1412 – 1422

DeCelles, P. G., 2004, Late Jurassic to Eocene evolution of the Cordilleran thrust belt and foreland basin system, western U.S.A.: American Journal of Science, v. 304, no. 2, p. 105–168, doi:10.2475/ajs.304.2.105.

Diegel, F. A., Schuster, D. C., Karlo, J. F., Shoup, R. C., & Tauvers, P. R. (1995). Cenozoic Structural Evolution and Tectono-Stratigraphic Framework of the Northern Gulf Coast Continental Margin. In M. P. A. Jackson, D. G. Roberts, & S. Snelson, Salt Tectonics (pp. 109–151). American Association of Petroleum Geologists.

Dodge, M. M., & Posey, J. S. (1981). Structural Cross Sections, Tertiary Formations, Gulf Coast. PDF (p. 6) [Structural Cross Sections]. Bureau of Economic Geology, The University of Texas at Austin. https://store.beg.utexas.edu/cross-sections/2717-cs0002.html

Dokka, R. K., Sella, G. F., & Dixon, T. H. (2006). Tectonic control of subsidence and southward displacement of southeast Louisiana with respect to stable North America. Geophysical Research Letters, 33(23), 5. https://doi.org/10.1029/2006GL027250

Dubiel, R. F., Coleman, J. L., Hackley, P. C., Hayba, D. O., Karlsen, A. W., Pearson, O. N., Pitman, J. K., Swanson, S. M., & Warwick, P. D. (2007). Assessment of Undiscovered Oil and Gas Resources in Tertiary Strata of the Gulf Coast, 2007 (Fact Sheet 2007–3066; Fact Sheet, p. 4). U.S. Geological Survey. https://pubs.usgs.gov/fs/2007/3066/pdf/FS07-3066_508.pdf

Durham, C. O., and Peeples, E. M., 1956, Pleistocene fault zone in southeastern Louisiana: Gulf Coast Association of Geological Societies Transactions, v. 6, p. 65–66.

Eaton, B. A. (1969). Fracture Gradient Prediction and Its Application in Oilfield Operations. Journal of Petroleum Technology, 21(10), 1353–1360. https://doi.org/10.2118/2163-PA

Feng, J. (1995). Post mid-Cretaceous seismic stratigraphy and depositional history, deep Gulf of Mexico [PhD Dissertation, University of Texas at Austin]. http://hdl.handle.net/2152/44093

Filina, I., J. Austin, T. Dore, E. Johnson, D. Minguez, I. Norton, J. Snedden, and R.J. Stern, 2022, Opening of the Gulf of Mexico: What we know, what questions remain, and how me might answer them, Tectonophysics, v. 822, doi: 10.1016/j.tecto.2021.229150.

Frank, J.P., 2017, Evidence of fault movement during the Holocene in southern Louisiana: integrating 3-D seismic data with shallow high resolution seismic data, University of New Orleans Theses and Dissertations, 2321, 83 p.

Gagliano, S.M., 2005, Effects of Earthquakes, Faults Movements, and Subsidence on the South Lousiana Landscape, The Louisana Civil Engineer, Journal of the Louisana Section of The American Society of Civil Engineers, v. 13, n. 2, p. 5 – 7, 19-22.

Gagliano, S.M., Kemp, E.B., III, Wicker, K.M., and Wiltenmuth, K.S., 2003a, Active Geological Faults and Land Change in Southeastern Louisiana: A Study of the Contribution of Faulting to Relative Subsidence Rates, Land Loss, and Resulting Effects on Flood Control, Navigation, Hurricane Protection and Coastal Restoration Projects: Report prepared for U.S. Army Corps of Engineers, New Orleans District by Coastal Environments, Inc., under contract DACW 29-00-C-0034, 178 p.

Gagliano, S.M., Kemp, E.B., III, Wicker, K.M., Wiltenmuth, K.S., and Sabate, R.W., 2003b, Neo-tectonic framework of southeast Louisiana and applications to coastal restoration: Gulf Coast Association of Geological Societies Transactions, v. 53, p. 262–276.

Galloway, W. E. (1986). Depositional and Structural Framework of the Distal Frio Formation, Texas Coastal Zone and Shelf. Geological Circular, 86–8, 16. https://doi.org/doi.org/10.23867/gc8608

Galloway, W. E. (1989). Genetic Stratigraphic Sequences in Basin Analysis II: Application to Northwest Gulf of Mexico Cenozoic Basin1. AAPG Bulletin, 73(2), 143–154. https://doi.org/10.1306/703C9AFA-1707-11D7-8645000102C1865D

Galloway, W. E., Bebout, D. G., Fisher, W. L., Dunlap, J. B., Jr., Cabrera-Castro, R., Lugo-Rivera, J. E., & Scott, T. M. (1991). Cenozoic. In A. Salvador (Ed.), The Gulf of Mexico Basin: Vol. J (p. 0). Geological Society of America. https://doi.org/10.1130/DNAG-GNA-J.245

Galloway, W. E., Ewing, T. E., Garrett, C. M., Tyler, N., & Bebout, D. G. (1983). Atlas of major Texas oil reservoirs (p. 139). University of Texas at Austin, Bureau of Economic Geology. https://store.beg.utexas.edu/atlases-of-major-oil-and-gas-reservoirs/1779-at0002.html

Galloway, W. E., Ganey-Curry, P. E., Li, X., & Buffler, R. T. (2000). Cenozoic Depositional History of the Gulf of Mexico Basin. AAPG Bulletin, 84(11), 1743–1774.

Galloway, W. E., Hobday, D. K., & Magara, K. (1982). Frio Formation of Texas Gulf Coastal Plain: Depositional Systems, Structural Framework, and Hydrocarbon Distribution1. AAPG Bulletin, 66(6), 649–688. https://doi.org/10.1306/03B5A2F5-16D1-11D7-8645000102C1865D

Galloway, W. E., T. L. Whiteaker, and P. E. Ganey-Curry, 2011, History of Cenozoic North American drainage basin evolution, sediment yield, and accumulation in the Gulf of Mexico basin: Geosphere, v. 7, no. 4, p. 938–973, doi: 10.1130/GES00647.1.

Galloway, W.E., 2008, Depositional evolution of the Gulf of Mexico sedimentary basin, in A. D. Miall, ed., Sedimentary basins of the world: The sedimentary basins of the United States and Canada, v. 5: The Netherlands, Elsevier, 505–549.

Geostock Sandia, LLC (2020a). 2020 EPA No Migration Petition Reissuance, Rubicon LLC Geismar Louisiana Facility – Section 3 Flow and Containment Modeling: Houston, Texas.

Geostock Sandia, LLC (2020b). 2020 EPA No Migration Petition Request Injection Well No. 6, Rubicon LLC Geismar Louisiana Facility – Section 3 Flow and Containment Modeling: Houston, Texas.

Goddard, D. A. (2015). Quick Look Handbook Onshore Louisiana Petroleum Producing Formations (p. 43). Louisiana State University Center for Energy Studies. https://www.lsu.edu/ces/publications/2001/quick_look.pdf

Goddard, D. A., Zimmerman, R. K., & Meeks, C. M. (2005). Remaining Hydrocarbon Potential in Oligocene Reservoirs of Mature Fields, West Baton Rouge Parish, Louisiana. Gulf Coast Association of Geological Societies Transactions, 55, 251–267.

Goddard, D. A., & Zimmerman, R. K. (2003). Shallow Miocene and Oligocene Gas Potential: Southeastern Louisiana's Florida Parishes. Gulf Coast Association of Geological Societies Transactions, 53, 287–301.

Goodman, A., Hakala, A., Bromhal, G., Deel, D., Rodosta, T., Frailey, S., Small, M., Allen, D., Romanov, V., Fazio, J., Huerta, N., McIntrye, D., Kutchko, B., Guthrie, G. (2011). U.S.DOE Methodology for the development of geologic storage potential for carbon dioxide at the national and regional scale. International Journal of Greenhouse Gas Control, 5(4). 952-965. https://doi.org/10.1016/j.ijggc.2011.03.010

Goodman, A., Sanguinito, S., Levine, J.S. (2016). Prospective CO2 saline resource estimation methodology: Refinement of existing US-DOE-NETL methods based on data availability, International Journal of Greenhouse Gas Control. V.54 (1). 242-249. https://doi.org/10.1016/j.ijggc.2016.09.009.

Griffith, J.M., 2003, Hydrogeologic framework of southeastern Louisiana: Louisiana Department of Transportation and Development Water Resources Technical Report no. 72, 21 p., 18 pls.
Hanor, J.S., 1982, Reactivation of fault movement, Tepetate fault zone, south central Louisiana: Gulf Coast Association of Geological Societies Transactions, v. 32, p. 237–245.

Heywood, C. E., & Griffith, J. M. (2013). Simulation of Groundwater Flow in the "1,500-Foot" Sand and "2,000-Foot" Sand and Movement of Saltwater in the "2,000-Foot" Sand of the Baton Rouge Area, Louisiana (Open-File Report 2013–1153; p. 87). United States Department of the Interior United State Geological Survey. https://pubs.usgs.gov/of/2013/1153/OFR_2013-1153.pdf

Hovorka, S., Collins, D., Benson, S., Myer, L., Bryer, C., & Cohen, K. (2008). Update on the Frio Brine Pilot: Frio Final Technical Report (p. 500). Gulf Coast Carbon Center. https://www.osti.gov/servlets/purl/990448

Howe, H. J. (1962). Subsurface geology of St. Helena, Tangipahoa, Washington and St. Tammany Parishes, Louisiana: Gulf Coast Association of Geologists Societies Transactions, 12, 121–155.

Hudec, M.R. and M.P.A. Jackson, 2007, Terra infirma: Understanding salt tectonics, Earth Science Reviews, v. 82, p. 1 – 28, doi: 10.1016/j.earscirev.2007.01.001.

Hudec, M.R., M.P.A. Jackson, and F.J. Peel, 2013a, Influence of deep Louann structure on the evolution of the Gulf of Mexico, AAPG Bulletin, v. 97, n. 10, p. 1711 – 1435, doi: 10.1306/04011312074.

Hudec, M.R., I.O. Norton, M.P.A. Jackson, and F.J. Peel, 2013b, Jurassic evolution of the Gulf of Mexico salt basin, AAPG Bulletin, v. 97, n. 10, p. 1683 – 1710, doi: 10.1306/04011312073.

Hulsey, J.D., 2016, Applying modern interpretation techniques to old hydrocarbon fields to find new reserves: A case study in the onshore Gulf of Mexico, U.S.A., University of New Orleans Theses and Dissertations, 2160, 52 p.

Jackson, M., T. Dooley, M. Hudec, and A. McDonnell, 2011, The pillow fold belt: A key subsalt structural province in the northern Gulf of Mexico: AAPG Search and Discovery article 10329, 23 p., http://www.searchanddiscovery.com/documents/2011/10329jackson/ndx_jackson.pdf.

John, C. J., Jones, B. L., Pope, D. E., & Silva, M. E. (1992). Anahuac Sandstone-Louisiana Gulf Coast. In D. G. Bedout, W. A. White, C. M. Garrett Jr., & T. F. Hentz (Eds.), Atlas of Major Central & Eastern Gulf Coast Gas Reservoirs (pp. 25–27). Bureau of Economic Geology. https://store.beg.utexas.edu/atlases-of-major-oil-and-gas-reservoirs/147-at0005.html

Kharaka, Y.M., Cole, D.M., Hovorka, S.D., Gunter, W.D., Knauss, K.G., and Freifeld, B.M., (2006), Gas-water-rock interactions in Frio Formation following CO2 injection: Implications for the storage of greenhouse gases in sedimentary basins, Geology, v.34, n. 7, p. 577-580.

Knipe, R. J., Jones, G. and Fisher, Q. J. 1998. Faulting, fault sealing and fluid flow in hydrocarbon reservoirs: an introduction. In: Jones, G., Fisher, Q. J. and Knipe, R. J. (eds) Faulting, Fault Sealing and Fluid Flow in Hydrocarbon Reservoirs. Geological Society, London, Special Publications, 147, vii-xxi.

Krueger, Jr., W. C. (1967). West Addis Field: Iberville and West Baton Rouge Parishes, Louisiana. In Oil and Gas Fields of Southeast Louisiana (Vol. 2, pp. 119–123). New Orleans Geological Society. https://archives.datapages.com/data/nogs/data/002/002002/0119.htm

Limes, L. L., & Stipe, J. C. (1959). Occurrence of Miocene Oil in South Louisiana. Gulf Coast Association of Geological Societies Transactions, 9. http://archives.datapages.com/data/gcags/data/009/009001/0077.htm

Lindsay, N.G., Murray, F.C., Walsh, J.J. &Watterson, J. 1993. Outcrop studies of shale smears on fault surfaces. In: Flint, S.S. & Bryant, I.D. (eds) The Geological Modelling of Hydrocarbon Reservoirs and Outcrop Analogues. International Association of Sedimentologists, Special Publications, 15, 113–123, https://doi.org/10.1002/9781444303957.ch6

Lopez, J.A., Penland, S., and Williams, J., 1997, Confirmation of active geologic faults in Lake Pontchartrain in southeast Louisiana: Gulf Coast Association of Geological Societies Transactions, v. 47, p. 299–303.

Loucks, R. G., Dodge, M. M., & Galloway, W. E. (1984). Regional Controls on Diagenesis and Reservoir Quality in Lower Tertiary Sandstones along the Texas Gulf Coast. In D. A. McDonald & R. C. Surdam (Eds.), Clastic Diagenesis (Vol. 37, p. 0). American Association of Petroleum Geologists. https://doi.org/10.1306/M37435C2

Lovelace, J.K., 2007, Chloride Concentrations in Ground Water in East and West Baton Rouge Parishes Louisiana 2004-05: US Geological Society Scientific Investigations Report, p. 2007–5069.

Lovelace, J. K., Fontenot, J. W., & Frederick, C. P. (2004). Withdrawals, Water Levels, and Specific Conductance in the Chicot Aquifer System in Southwestern Louisiana, 2000-03 (Scientific Investigations Report 2004–5212; Scientific Investigations Report, p. 61). U.S. Department of the Interior U.S. Geological Survey. https://wise.er.usgs.gov/dp/pdfs/SIR_2004-5212.pdf

Lovelace, J. (2009, December 2). *The Southern Hills Aquifer System Outlook and Sustainability*. Ground Water Resources Commission Meeting, DNR Office of Conservation. https://www.dnr.louisiana.gov/assets/docs/conservation/documents/20091202-presentation.pdf

Lu, J., Carr, D. L., Trevino, R. H., Rhatigan, J. T., & Fifariz, R. (2017). Evaluation of Lower Miocene Confining Units for CO2 Storage, Offshore Texas State Waters, Northern Gulf of

Mexico, USA. In Geological CO2 Sequestration Atlas of Miocene Strata, Offshore Texas State Waters (pp. 14–25). Bureau of Economic Geology.

Mancini, E.A., J. C. Llinás, W.C. Parcell, M.Aurell, B. Bádenas, R. R. Leinfelder, and D. J. Benson, 2004, Upper Jurassic thrombolite reservoir play, northeastern Gulf of Mexico: AAPG Bulletin, v. 88, no. 11, p. 1573–1602, doi:10.1306/06210404017.

Martin, A. Jr and Whiteman, C.D., Jr. 1985, Generalized Potentiometric Surface of Aquifers of Pleistocene Age, Southern Louisiana, 1980.S. Geological Survey Water-Resources Investigation Report 84-4331, Sheet

Martín, D., Aparicio, P., García, S., & Maroto-Valer, M. M. (2022). Mixed-Layer Illite-Smectite Illitization under Supercritical CO2 Conditions. Applied Sciences, 12(22), Article 22. https://doi.org/10.3390/app122211477

McBride, B.C., 1998, The evolution of allochthonous salt along a megaregional profile across the northern Gulf of Mexico basin, AAPG Bulletin, v. 82, n. 5B, p. 1037 – 1054.

McCulloh, R.P., and Heinrich, P.V., 2012, Surface faults of the south Louisiana growth-fault province, in Cox, R.T., Tuttle, M.P., Boyd, O.S., and Locat, J., eds., Recent Advances in North American Paleoseismology and Neotectonics East of the Rockies: Geological Society of America Special Paper 493, p. 37–49, doi:10.1130/2012.2493(03).

McFarlan, E., Jr., & Menes, L. S. (1991). Lower Cretaceous. In A. Salvador (Ed.), The Gulf of Mexico Basin: Vol. J (pp. 181–204). Geological Society of America. https://doi.org/10.1130/DNAG-GNA-J.181

McGuire, V. L., Seanor, R. C., Asquith, W. H., Kress, W., & Strauch, K. R. (2019). Potentiometric surface of the Mississippi River Valley alluvial aquifer, spring 2016. In *Scientific Investigations Map* (Scientific Investigations Map 3439; p. 14 pgs, 5 sheets). U.S. Geological Survey. https://doi.org/10.3133/sim3439

Merrill, M. (2013). Depositional Environment as an Indicator of Favorable Regional Sequestration Targets: Examples from the USGS CO2 Storage Resource Assessment. Energy Procedia, 37, 4975–4981. https://doi.org/doi: 10.1016/j.egypro.2013.06.410

Meyerhoff, A. A. (Ed.). (1968). Geology of natural gas in South Louisiana. In Natural gases of North America: American Association of Petroleum Geologists Memoir (pp. 376–581). American Association of Petroleum Geologists.

Morton, R. A., & Walter B. Ayers, J. (1992). Plio-Pleistocene Genetic Sequences of the Southwestern Louisiana Continental Shelf and Slope: Geologic Framework, Sedimentary Facies, and Hydrocarbon Distribution (Report on Investigations 210; p. 77). University of Texas at Austin, Bureau of Economic Geology. https://www.beg.utexas.edu/publications/plio-pleistocene-genetic-sequences-southwestern-louisiana-continental-shelf-and-slope

Nasreen, M. (2003). *The Effect of Faults upon Ground Water Flow in the Baton Rouge Fault System* [Thesis, University of New Orleans]. https://biotech.law.lsu.edu/blog/The-Effect-of-Faults-upon-Ground-Water-Flow-in-the-Baton-Rouge-Fa.pdf

Neal, J. T., Magorian, T. R., Byrne, K. O., & Denzler, S. (1993). Strategic Petroleum Reserve (SPR) additional geologic site characterization studies, Bayou Choctaw salt dome, Louisiana (DOE Contract Report SAND-92-2284; p. 95). Sandia National Lab. (SNL-NM), Albuquerque, NM (United States). https://doi.org/10.2172/10190133

Nehring Associates Inc. (2010). The significant oil and gas fields of the United States (data current as of December 2008) [dataset].https://doi.org/10.1130/DNAG-GNA-J.245

Nyman, D. J., & Fayard, L. D. (1978). Ground-water resources of Tangipahoa and St. Tammany Parishes, southeastern Louisiana (Technical Report 15; Louisiana Department of Transportation and Development, Office of Public Works Water Resources Technical Report, p. 76). Louisiana Department of Transportation and Development, Office of Public Works Water Resources.

Nyman, D. J., 1984, The occurrence of high concentrations of chloride in the Chicot aquifer system in southwestern Louisiana, 200 03: US Geological Survey Scientific Investigations Report 2004-5212, 56 p.

Nyman, D. J., 1989. Quality of Water in Freshwater Aquifers in Southwestern Louisiana. Louisiana Department of Transportation and Development, Water Resources Technical Report 42, p. 29.

Ogiesoba, O., & Hammes, U. (2012). Seismic interpretation of mass-transport deposits within the upper Oligocene Frio Formation, south Texas Gulf Coast. AAPG Bulletin, 96, 845–868. https://doi.org/10.1306/09191110205

Ogilvie, S. R., Dee, S. J., Wilson, R.W. & Bailey, W. R. (eds) 2020. Integrated Fault Seal Analysis. Geological Society, London, Special Publications, 496, 1–8.

Olariu, M. I., DeAngelo, M., Dunlap, D., & Treviño, R. H. (2019). High frequency (4th order) sequence stratigraphy of Early Miocene deltaic shorelines, offshore Texas and Louisiana. Marine and Petroleum Geology, 110, 575–586. https://doi.org/10.1016/j.marpetgeo.2019.07.040

Paine, W. R., Spillers, J. P., Waters, K. M., Andrews, D. I., Baysinger, E. M., Borland, A. M., Cotton, J., Cristina, Jr., S. T., Hall, Jr., Justin P., Kimmey, B. W., McDougall, J. E., Meyerhoff, A. A., Munchrath, M. A., Paffett, D. L., Raspberry, F. L., Rockwood, D. N., Roederer, Jr., Edward P., Stipe, J. C., & Woodbury, H. O. (1968). Geology of Natural Gas in South Louisiana. In B. Warren Beebe (Ed.), Natural Gases of North America, Volumes 1 & 2 (Vol. 9, pp. 376–581). American Association of Petroleum Geologists. https://doi.org/10.1306/M9363C29

Peel, F. J., Travis, C. J., & Hossack, J. R. (1995). Genetic Structural Provinces and Salt Tectonics of the Cenozoic Offshore U.S. Gulf of Mexico: A Preliminary Analysis. In M. P. A. Jackson, D. G. Roberts, & S. Snelson (Eds.), Salt Tectonics: A Global Perspective (Vol. 65, p. 0). American Association of Petroleum Geologists.

Petersen, M.D., Shumway, A.M., Powers, P.M., Field, E.H., Moschetti, M.P., Jaiswal, K.S., Milner, K.R., Rezaeian, S., Frankel, A.D., Llenos, A.L., Michael, A.J., Altekruse, J.M., Ahdi, S.K., Withers, K.B., Mueller, C.S., Zeng, Y., Chase, R.E., Salditch, L.M., Luco, N., Rukstales, K.S., Herrick, J.A., Girot, D.L., Aagaard, B.T., Bender, A.M., Blanpied, M.L., Briggs, R.W., Boyd, O.S., Clayton, B.S., DuRoss, C.B., Evans, E.L., Haeussler, P.J., Hatem, A.E., Haynie, K.L., Hearn, E.H., Johnson, K.M., Kortum, Z.A., Kwong, N.S., Makdisi, A.J., Mason, H.B., McNamara, D.E., McPhillips, D.F., Okubo, P.G., Page, M.T., Pollitz, F.F., Rubinstein, J.L., Shaw, B.E., Shen, Z.K., Shiro, B.R., Smith, J.A., Stephenson, W.J., Thompson, E.M., Thompson Jobe, J.A., Wirth, E.A., and Witter, R.C., 2023, Data Release for the 2023 U.S. 50-State National Seismic Hazard Model - Overview: U.S. Geological Survey data release, https://doi.org/10.5066/P9GNPCOD.

Prakken, L. B. (2004). *Louisiana ground-water map no. 17: Generalized potentiometric surface of the Kentwood aquifer system and the "1,500-foot" and "1,700-foot" sands of the Baton Rouge area in southeastern Louisiana, March–April 2003* (2862; U.S. Geological Survey Scientific Investigations Map, p. 2 Sheets). U.S. Geological Survey and Louisiana Department of Transportation and Development, Office of Public Works and Intermodal Public Works and Water Resources Division. https://wise.er.usgs.gov/dp/pdfs/SIM_2862.pdf

Prakken, L., White, V., and Lovelace, J. 2014, Water Resources of Sabine Parish, Louisiana. Reston, VA: U. S. Geological Survey, Reston, VA, United States. doi:10.3133/fs20143040Purpera, D. G., Edmonson, N. B., & LeBlanc, K. (2020). *Louisiana's Management of Water Resources* (Performance Audit Services, p. 110) [Agency Audit]. Louisiana Legislative Auditor. https://app.lla.state.la.us/PublicReports.nsf/0/7AE69DA84B7F7E89862585040079C762/$FILE/LMWR.pdf

Rainwater, E. H. (1964). Regional Stratigraphy of the Gulf Coast Miocene. Gulf Coast Association of Geological Societies Transactions, 14, 81–124.

Rautman, C.A. and J.S. Stein, 2004, Conversion of the Bayou Choctaw geological site characterization report to a three-dimensional model, Sandia Report SAND2003-3299, Sandia National Laboratories, Albuquerque, N.M., 52 p.

Rautman, C.A., K.M. Looff, K.M. Looff, 2010, A three-dimensional geometric model of the Bayou Choctaw salt down, southern Louisiana, using 3-D seismic data, Sandia Report SAND2010-1900C, Sandia National Laboratories, Albuquerque, N.M., 23 p.

Roberts-Ashby, T. L., Brennan, S. T., Buursink, M. L., Covault, J. A., Craddock, W. H., Drake II, R. M., Merrill, M. D., Slucher, E. R., Warwick, P. D., Blondes, M. S., Gosai, M. A., Freeman, P. A., Cahan, S. M., DeVera, C. A., & Lohr, C. D. (2014). Geologic Framework for the National Assessment of Carbon Dioxide Storage Resources—U.S. Gulf Coast (Open-File Report 2012-1024-H; Open-File Report, p. 85). U. S. Department of the Interior U. S. Geological Survey. https://pubs.usgs.gov/of/2012/1024/h/pdf/ofr2012-1024h.pdf

Rollo, J.R., 1960, Ground water in Louisiana: Louisiana Department of Conservation and Department of Public Works, Water Resources Bulletin 1, 84 p.

Salvador, A. (1991). Triassic-Jurassic. In A. Salvador (Ed.), The Gulf of Mexico Basin: Vol. J (pp. 131–180). Geological Society of America. https://doi.org/10.1130/DNAG-GNA-J.131

Sandia Technologies, LLC (2013). EPA Petition Reissuance Application for Injection Well No. 4 (SN970113)), Injection Well No. 7 (SN970909), and Injection Well No. 8 (SN971914) – E. I du Pont de Nemours & Company, Pontchartrain Works – Section 3 Flow and Containment Modeling: Houston Texas.

Sargent, B. P., 2011, Water use in Louisiana, 2010: Louisiana Department of Transportation and Development Water Resources Special Report no. 17, 135 p.

Sawyer, D. S., Buffler, R. T., & Pilger, R. H., Jr. (1991). The crust under the Gulf of Mexico basin. In A. Salvador (Ed.), The Gulf of Mexico Basin: Vol. J (pp. 53–72). Geological Society of America. https://doi.org/10.1130/DNAG-GNA-J.53

Schlumberger, 1987, Log Interpretation Principles/Applications, Schlumberger Educational Services, Houston, Texas, p. 198.

Shreveport Petroleum Data Association. (n.d.). *Shreveport Petroleum Data Association*. Shreveport Petroleum Data Association. Retrieved August 26, 2024, from https://www.spdalogs.org/data

Smoot, C.W., 1988, Louisiana hydraulic atlas map No. 3: Altitude of the base of the Freshwater in Louisiana: U.S. Geological Survey Water-Resources Investigation Report 86-4314, 1 sheet, http://pubs.er.usgs.gov/publication/wri864314

Snedden, J., R.C. Cunningham, and J.W. Virdell, 2020, The northern Gulf of Mexico offshore super basin: Reservoirs, source rocks, seals, traps, and successes, AAPG Bulletin, v. 104, no. 12, pp. 2603 – 2642, doi:10.1306/09092020054.

Snedden, J. W., and W. E. Galloway, 2019, The Gulf of Mexico sedimentary basin: Depositional evolution and practical applications: Cambridge, United Kingdom, Cambridge University Press, 344 p., doi:10.1017/9781108292795.

Sohl, N. F., Martínez R., E., Salmerón-Ureña, P., & Soto-Jaramillo, F. (1991). Upper Cretaceous. In A. Salvador (Ed.), The Gulf of Mexico Basin: Vol. J (pp. 205–244). Geological Society of America. https://doi.org/10.1130/DNAG-GNA-J.205

Stern, R.J., Dickinson, W.R., 2010. The Gulf of Mexico is a Jurassic backarc basin. Geosphere 6 (6), 739–754, doi: 0.1130/GES00585.1

Stern, R. J, E. Y. Anthony, M. Ren, B. E. Lock, I. Norton, J. I. Kimura, T. Miyazaki, T. Hanyu, Q. Chang, and Y. Hirahara, 2011, Southern Louisiana salt dome xenoliths: First glimpse of Jurassic (ca. 160 Ma) Gulf of Mexico crust: Geology, v. 39, p. 315–318, doi: 10.1130/G31635.

Stuart, C. G., Knochenmus, D., & McGee, B. D. (1994). Guide to Louisiana's Ground-Water Resources (Water Resources Investigation Report 94–4085; p. 60). U.S. Geological Survey and

Louisiana Department of Transportation and Development. https://pubs.usgs.gov/wri/1994/4085/report.pdf

Subsurface Technology, Inc. (2013a). Completion Report for Waste Disposal Well No. 1 – Mosaic Fertilizer, LLC, Uncle Sam, Louisiana: Baton Rouge Louisiana, 53 p.

Subsurface Technology, Inc. (2013b). Completion Report for Waste Disposal Well No. 2 – Mosaic Fertilizer, LLC, Uncle Sam, Louisiana: Baton Rouge Louisiana, 47 p.

Swanson, B. F. (1981). A Simple Correlation Between Permeabilities and Mercury Capillary Pressures. Journal of Petroleum Technology, 33(12), 2498–2504. https://doi.org/10.2118/8234-PA

Swanson, S. M., Karlsen, A. W., & Valentine, B. J. (2013). Geologic assessment of undiscovered oil and gas resources: Oligocene Frio and Anahuac Formations, United States Gulf of Mexico coastal plain and State waters. In *Open-File Report* (Open-File Report 2013–1257). U.S. Geological Survey. https://doi.org/10.3133/ofr20131257

Tomaszewski, D. J. (1996). *Distribution and movement of saltwater in aquifers in the Baton Rouge Area, Louisiana, 1990-1992* (Water Resources Technical Report 59; p. 50). U.S Geological Survey. https://wise.er.usgs.gov/dp/pdfs/TR59.pdf

Treviño, R. H., & Meckel, T. (2019). Offshore CO2 storage resource assessment of the northern Gulf of Mexico (Texas-Louisiana) (p. 151) [Final Scientific and Technical Report]. The University of Texas at Austin Bureau of Economic geology. https://www.beg.utexas.edu/files/publications/contract-reports/CR2019-Trevino-1.pdf

Trevino, R. H., Meckel T. A., Olariu, M., Dunlap, D., Deangelo, M. V., Lu, J., Sabbagh, R., & Klokov, A. (2018). Offshore CO2 Storage Resource Assessment of the Northwest Gulf of Mexico Inner Continental Shelf, Upper Texas – Western Louisiana Coast. Search and Discovery, 80630, 27.

U.S. Geological Survey, Earthquake Hazards Program, 2024, Search Earthquake Catalog, accessed February, 2024 at URL https://earthquake.usgs.gov/earthquakes/search/

U.S. Geological Survey, Water Resources of West Baton Rouge Parish, Louisiana, 2016, accessed August, 2024 at URL https://pubs.usgs.gov/fs/2016/3068/fs20163068.pdf

White, V.E., 2017, Water resources of the Southern Hills regional aquifer system, southeastern Louisiana: U.S. Geological Survey Fact Sheet 2017–3010, 6 p., https://doi.org/10.3133/fs20173010

White, V. E., & Prakken, L. B. (2016). Water resources of St. Helena Parish, Louisiana. In Fact Sheet (Fact Sheet 2016–3047; p. 6). U.S. Geological Survey. https://doi.org/10.3133/fs20163047

Whiteman Jr., C. D. (1979). *Saltwater encroachment in the "600-foot" and "1,500-foot" sands of the Baton Rouge area, Louisiana, 1966-78, including a discussion of saltwater in other sands*

(Water Resources Technical Report 19; p. 49). Louisiana Department of Transportation and Development, Office of Public Works.

Winker, C. D., & Buffler, R. T. (1988). Paleogeographic evolution of early deep-water Gulf of Mexico and margins, Jurassic to middle Cretaceous (Comanchean). AAPG Bull.; (United States), 72:3. https://www.osti.gov/biblio/6595794

Worrall, D. M., & Snelson, S. (1989). Evolution of the northern Gulf of Mexico, with emphasis on Cenozoic growth faulting and the role of salt. In A. W. Bally & A. R. Palmer (Eds.), The Geology of North America—An Overview: Vol. A (p. 0). Geological Society of America. https://doi.org/10.1130/DNAG-GNA-A.97

WSP (2017). Completion Report – Innophos Inc., DW Well Nos. 1 & 2 – Serial Nos. 975071 & 975072, Geismar Louisiana, Ascension Parish: Baton Rouge, Louisiana.

Yielding, G., Bretan, P. and Freeman, B., 2010. Fault seal calibration: a brief review. Geological Society, London, Special Publications, 347(1), pp.243-255.

Yielding, G., Freeman, B. & Needham, T. 1997. Quantitative fault seal prediction. AAPG Bulletin, 81, 897–917, https://doi.org/10.1306/522B498D-1727-11D7-8645000102C1865D

Zulqarnain, M., Sears, S. O., Zeidouni, M., Hughes, R. G., Carlson, D., & Rivera, C. F. (2023). GCS site selection in saline Miocene formations in South Louisiana. International Journal of Greenhouse Gas Control, 122, 103818. https://doi.org/10.1016/j.ijggc.2022.103818

Appendix A: Cross-Section Well Details

Serial Number	API	Well Name	Operator Name	Elevation (KB, ft)	Perforated Intervals (MD, ft)	Well TD (MD, ft)	Well Status
[redacted]							